Exceptional Preservation of Cells in Phosphate and the Early Evolution of the Biosphere



Leila Battison

Department of Earth Sciences

University of Oxford

A thesis submitted for the degree of

Doctor of Philosophy

Trinity 2012

For my parents,
who always know when to say the right thing.
And for my friend Lynn,
who always knew when to say the wrong thing.

Acknowledgements

Four years is a long time to spend in one place, doing one thing, but it is made a joy by those people who touch your life in the process. More people deserve thanks for putting up with me and my thesis, than would fit in the thesis itself, so a simple few must suffice to fill this space. First, I must thank my supervisor, Martin Brasier. We have worked together through the joys and the trials, and I have appreciated his quiet faith in me over the years. I thank him for opening doors for me, and for sharing in some special friendships. My affection and thanks also go to our friend and colleague Lynn Margulis, who touched my life and will never be forgotten. I wouldn't be the scientist I am today if it wasn't for the advice and mentoring, generously given, of my peers and my superiors. I am thankful for the support of the entire Early Life consortia, and in particular Stephan Bengtson, Charles Wellman, Paul Strother, Nora Noffke, and Emmanuelle Javaux, for their time and patience. Advice often crosses over into practical help, and I have had the great fortune to collaborate with, and work alongside, some of the most wonderful people. Nicola McLoughlin, David Wacey, Sean McMahon and Richard Matthewman have helped to motivate me with new and interesting research techniques. I thank them for the inspiration and for the new research directions we have explored together. I am also deeply grateful for the unerring support of Jeremy Hyde, Owen Green, and Norman Charnley, who have weathered through my many requests and catastrophies. Company, assistance and guidance in the field made four years in Scotland a bearable prospect, so thanks to Richard Callow, Kate Hibbert, and various Masters students. The Department of Earth Sciences in Oxford has been like a home to me for the last eight years, and it will always contain a group of people of whom I am inordinately fond. This last year, more so than ever, I have enjoyed the companionship and tough love of my palaeo-family, so I thank Russell Garwood, Latha Menon, Emma Jude, Laura Soul, Sam Giles, Graeme Lloyd, Alex Liu, Matt Friedman and Jack Matthews, for

at least pretending to take me seriously. Thanks also to those within the fallout zone of the Thesis, Ana Heureux, Katie Bray, and the rest of L1, you've been so very lovely. Outside the world of geology, my friends have used a combination of tea, alcohol and alternative pursuits to help to keep me sane. Thanks to Hannah Hogben for unstopppable cheer and the perfect cup of tea. Thanks to Jo Eberhardt for being a girl in a time of crisis, and for being a rational sounding board for emotions and spelling errors. Thanks (again) to Sam Giles for never, ever, taking me seriously. And thanks to Tim Funnell, for being much better at not distracting me than I was in his situation. Oxford has many delights, but none so great as those of the Morris Men, who will not only keep me in beer, but also in good company. The last two years have been a pleasure, and it is thanks to them, for making me feel welcomed and loved. So to Stan, Sam, and Sveta, Duncan, Dave and Dicky, Jo, Gerard and Graham, Mark, Mark, Mac, and Melissa, and everyone else in the OUMM and OCMM: Thank You. Words cannot express how much I owe to my mummy and daddy. For seeing me through the ups and downs, for knowing me better than anyone else can, and for never, ever doubting me. I did this for myself, but I couldn't have done it without them. So with love I offer my greatest, most hugest thanks to them.

Abstract

The Proterozoic period saw some of the most fundamental revolutions in the biological and geological world. During this period, life diversified and set the stage for the radiation of multicellular life, altering the face of the planet in the process. The fossil record of this time is not yet fully understood, and a revisitation of a historically reported fossil deposit in the 1 Ga Torridon rocks of northwest Scotland shows that they host the fossils of the earliest non-marine eukaryotes, as well as a full and diverse fossil assemblage preserved in sedimentary phosphates and shales. Fine scale sedimentology of the fluvio-lacustrine rocks of the Torridon Group reveals them to be laid down in a laterally variable basin with distinctly different palaeoenvironments. The resident biota is seen to be similarly variable between lithofacies. New criteria for classifying taphonomic effects are presented, and used to characterise assemblages from different palaeoenvironments, with broader applications beyond this study. The Torridon rocks are also host to macrostructures on the surfaces and soles of beds, and these are interpreted as of likely biological origin, with their variability mapped between different lithofacies. High-resolution studies of both the preserved biota and the mineralogy of the preserving medium reveal in detail not only the fine scale structure of the fossil organisms, but also the reasons for their exceptional preservation. Phosphate is analysed in detail to explain its enigmatic occurrence in Proterozoic lakes. To place the Torridon deposits in context, both older and younger rocks were examined in comparison, from the 2 Ga Gunflint Formation of Ontario, Canada, and the Precambrian-Cambrian successions of eastern Newfoundland respectively. New finds of phosphate in these rocks help to reveal biochemical interactions and evolution on the early Earth, with implications for further understanding life on our own planet and elsewhere.

Long Abstract

The palaeobiology of the Proterozoic is classically poorly understood, owing to its microscopic fossil record, and the advanced age of deposits. But after over a century of exploration into some of the oldest rocks on Earth, knowledge and understanding has grown, and studies of Precambrian rocks and fossils are beginning to answer questions about our origins and early evolution, with implication for astrobiological investigations.

The Proterozoic, dating from 2500 to 542 Ma, was a time of major change in the physical and biological environments on earth. The time period saw the assembly and subsequent breakup of Rodinia, the first well understood supercontinent, while stepwise oxygenation of the atmosphere was reflected in chemical sediments and isotopic fractionations. Atmospheric conditions and global temperature remained stable for much of the Proterozoic, yet major glaciations are seen after around 730 Ma, suggested by some to be global 'snowball' events.

Since the origin of life at least 3.5 Ga ago, major revolutions in the biosphere took place before the appearance of animals. The appearance of oxygenic photosynthesis, eukaryotes, sexual reproduction, and multicellularity can be traced with microfossil evidence as well as organic biomarkers, isotope signatures, and phylogenetic divergence estimates.

Yet while data on Proterozoic deposits continue to grow, some biases towards younger, aquatic, marine rocks and their constituent assemblages remain. Searches for terrestrial or non-marine fossils in deep time will help to redress the balance, and will enrich a better understanding of evolutionary histories and future perspectives for life on Earth and elsewhere.

The Torridon rocks of northwest Scotland, dating to approximately 1 Ga, have been reported to contain microfossils preserved in shales and phosphatic nodules, from a fluvio-lacustrine setting, but studies of the geology, microbiota and associated structures have been somewhat lacking. This study examines the Torridon assemblage in detail for the first time, examining fossil diversity and preservation, as well as petrological information and associated macroscopic structures. Fossiliferous rocks of the Torridon Group are compared to older and younger successions from Ontario, Canada, and eastern Newfoundland respectively.

The Torridon group, outcropping in the northwest of Scotland, comprises red fluvial

sandstones and grey lacustrine shales, dating to around 950 Ma. A non-marine environment is demonstrable, through examination of large-scale structural information, and characteristic sedimentological features such as small wavelength ripples marks, plane-to plane alternation in ripple strike, and desiccation without evaporites.
Sedimentological data were collected from all accessible outcrops of the lowermost Diabaig Formation, as well as from the uppermost Cailleach Head Formation, and comparable sediments from the Sleat Group on Skye. Reconstructing palaeoenvironment from sedimentary successions shows that the Diabaig lake basin was very laterally variable, with lithofacies representing deep distal waters, energetic delta tops, and desiccating muddy shorelines. This is the first time a variable lake basin has been resolved in such detail in ancient rocks. Sedimentary rocks of the Cailleach Head Formation record a larger, periodically deepening and infilling basin. Similarity of sedimentary features between the Diabaig Formation of the Torridon Group, and the Kinloch Formation of the Sleat Group, allow correlation of the previously unconstrained Sleat Group.

Following the establishment of precise lacustrine lithofacies within the Torridon Group, the constituent microbiota may be approached with a fuller understanding of depositional environment. Although microfossils have previously been reported from acid macerates of the shales, the phosphate-hosted biota has been somewhat neglected since preliminary reports in the early 20th Century. This study seeks to redress this issue by providing a comprehensive description of fossils from both shale and phosphate.
As with any new Proterozoic microfossil discovery, biogenicity and antiquity must be proven. This is achieved in the Torridon rocks by the observation of coherent membrane-bound structures that are completely occluded by phosphate, amongst other features.
In order to compare the overall morphological diversity without reference to formal Proterozoic taxa, an informal taxonomic scheme is erected, which classifies eight morphotypes on the basis of their characteristic shape and wall structure. These morphotypes are then used in statistical analysis of the assemblage through objective data collection.
Most analysis is carried out by optical microscopy with transmitted light, but several modern high-resolution techniques and analytical methods are employed to further resolve Torridon taxonomy. Imaging by secondary electron SEM (SE-SEM), Raman spectroscopy and mapping, FIB-TEM analysis with elemental mapping and serial

FIB-SEM sectioning and FIB-SEM-EDX characteristation reveals fine scale details of the fossil walls and preservational details.
Torridon morphotypes are systematically described to allow comparisons of diversity between Proterozoic assemblages. 25 species are identified, from 17 genera, of which 8 are newly described but unnamed.

The varied lithofacies within the basins of the Torridon group are testament to different depositional environments. The constituent assemblages of different settings can thus be compared to assess the amount of ecological variation between them. The objective, informal taxonomic scheme detailed previously is used in comparing diversity, but the exceptional preservation in phosphate also permits an assessment of taphonomic alteration within the assemblage.
To objectively compare taphonomy between different environments within the Torridon and between it and other assemblages, an objective classification is required that is applicable to all organic-walled microfossils. Degradation is thus assessed by ordinal, qualitative observations in the physical, chemical, and biological domains, that can be visualised in a three-dimensional 'taphospace' plot.
The variation between lithofacies of the Diabaig Formation is first assessed. Diversity and taphonomic information suggests changing ecological dominance in response to local water stresses and nutrient inputs. Material of the Diabaig and Cailleach Head Formations is similarly compared to illustrate differences between structurally different basins.
Differences between the assemblages of the shale-hosted and phosphate-hosted biota are assessed by applying the same metrics, measuring first the effect of maceration on assemblage richness to appreciate information loss by this preparation method. Acid macerates of phosphatic and siliciclastic material are subsequently compared for the Cailleach Head and Diabaig Formations, showing complex relationships that are likely related to ecology and preservation, and interactions between them.

In association with the phosphate- and shale-hosted microbiota, the Diabaig Formation also hosts abundant macroscopic traces on the surfaces and soles of siliciclastic beds. Following justification of their biogenicity using comparative petrographical and morphological data, these features may be classified as microbially-induced sedimentary structures, caused by colonising microbial mats modifying the sediment surface and subsurface.
Classification of these wrinkle structures structures permits better assessment of their

distribution and modes of growth. Nine broad morphologies are identified, grouped into ordered structures, disordered structures, and modifications of sedimentary features. Sedimentary modification is reflected by sharpening or multicresting of wave ripples, and the occurrence of synaeresis cracks. Ordered structures comprise reticulate networks of varying size and shape, variously described as networks and ladders, as well as regularly spaced simple or stellate nodes, and parallel ridges and grooves comparable with the Ediacaran taxon 'Arumberia'. Flat-bottomed pits and protrusions also rarely occur in dense, non-overlapping colonies.
These differing macroscopic features are formed by a combination of sculpted mat growth, subsequent modification of the mat or local sediment by physical processes, and changes in morphology during preservation of these features.
Differences in the appearance and diversity of these macroscopic structures are compared between several different lithofacies of the Diabaig Formation, revealing possible palaeoenvironmental controls on the type of wrinkle structure seen, and the characteristic morphology of that structure. For example, tufted mats that form reticulate networks and ladders are absent from deeper water sediments, indicating a light requirement for these forms. Further identification and classification of these features beyond the Torridon will help to further constrain these palaeoenvironmental variables.

The occurrence of fossils within the Torridon phosphates is a rare, if not unique occurrence, and the presence of phosphates themselves in the lacustrine environment may be considered enigmatic. As such, it is of interest to analyse and characterise the microstructure and mineralogical associations of the Torridon phosphates to better understand its mode of formation.
Different scales of observation, using differing techniques, are employed to best resolve all available information. Sedimentological field observations are combined with optical microscopy, followed by characterisation of textures by backscattered electron SEM imaging (SEM-BSE) and energy-dispersive x-ray spectroscopy (SEM-EDX). In addition, Raman spectroscopy, FIB-TEM and FIB-SEM-EDX are used to map the fine-scale structure and elemental composition of phosphates.
These combined methods reveal phosphate in the Torridon to be intimately associated with iron-bearing mineral phases, in particular an iron-rich clay mineral. In places, these clay minerals show zonation within and around microfossils, whereas in others phosphates and clays are intimately intermixed in a cryptoctrystalline matrix.
Comparison of the phosphate occurrences between different lithofacies of the Diabaig

Formation, and Cailleach Head Formation highlights general similarities and localised differences that are presumably related to differing microenvironments of formation. The maturity of the environment with respect to biological material seems to have a strong control: 'granular' phosphate forming in areas with disseminated carbon, and 'pure' phosphate forming in more pristine, microfossil-bearing environments.
A mode of formation for these phosphates is proposed, that involves supersaturation of phosphate ions driven by biological accumulation and release in combination with redox-controlled iron pump and shuttle. Precipitation occurs within the seston layer or just below the sediment-water interface.

To place the microbiological and phosphate discoveries of the Torridon in context with the rest of the Proterozoic, comparative material from older and younger strata were sought. For an older succession, the 2 Ga Gunflint chert of Ontario, Canada was chosen, as it contains a diverse assemblage of microfossils that can be compared taphonomically, and the predominantly chemical sediments represent major sedimentological differences of this earlier time.
Fine scale sedimentological data were collected from a wide range of localities and lithofacies within the Gunflint Formation, ranging from deep-water volcaniclastics, through sub wave-base chert-carbonates, to intertidal stromatolitic cherts. These data are used to reconstruct a modified basin model that incorporates an ephemeral grainstone bar that supplies sediment to deep and shallow waters.
Microfossils were recovered from cherts within three different lithofacies, representing a limited subsample of the previously described diversity. Taphonomic alteration of these assemblages is visualised through taphospace plots, and compared between localities. Microfossils show generally high grades of chemical alteration consistent with the granular appearance of most microfossils. Macroscopic surficial structures of putative biological origin, distinct from stromatolites, are analysed for biogenicity and variability between different lithofacies.
Phosphate was recovered from four Gunflint lithofacies for the first time. Characterisation by field observation, ammonium molybdate testing, optical microscopy and SEM-BSE and SEM-EDX techniques reveal the differing habits of these small scale deposits. Within these deposits, the close association of phosphate with disseminated carbonaceous material or biological surficial structures indicates an active biological role in concentration and precipitation of these minor deposits.

Younger comparative successions for the Torridon rocks were chosen in the terminal Neoproterozoic Avalonian succession, and Precambrian-Cambrian boundary Placentian series of eastern Newfoundland. These successions offer opportunity to directly study biological and chemical revolutions at the end of the Proterozoic.
No organic-walled microfossils were recovered from thin sections of these siliciclastic rocks, precluding direct diversity or taphonomic comparison. Two putatively biological microscopic features are discussed, however, with respect to their likely biogenicity. Uniserial or densely multiserial pyrite strings are found in phosphatic shales, and starburst-like associations of hollow tubular forms, interpreted as ambient inclusion trails (AITs), are observed in nodular phosphates of the Avalonian succession.
Sedimentary phosphate from these deposits is described in detail for the first time. Combining field sedimentological observations with optical microscopy and SEM-BSE and SEM-EDX characterisation reveals phosphatic textures that are in some ways similar to the Torridon phosphates. Findings made at three localities of the Avalonian succession, and two environments in the Placentian, reveal likely chemical changes that took place at the beginning of the Cambrian. A characteristically 'Proterozoic' mode of phosphate formation, involving concentration of phosphate ions by biological degradational release and redox-driven liberation of iron-bound phosphates, is replaced by phosphogenesis that is rarer, occurring only in significant periods of hiatus, and subsequently reworked. Such changes are consistent with inferred chemical revolutions caused by the advent of Cambrian bioturbation and oxygenation of the water column.

Using the detailed observations of the microfossil, macrostructural, and phosphatic material of the Torridon Group, in combination with the investigations and discoveries made in the older Gunflint Formation and younger Precambrian-Cambrian boundary successions of eastern Newfoundland, it is possible to place these new findings in context with the rest of the Proterozoic.
Fossil affinities of the Torridon microbiota can be establised to some extent, using high resolution imaging, and some forms may be assigned a eukaryotic affinity, making these the earliest reported non-marine eukaryotes. The overall assemblage contains prokaryotic and eukaryotic, autotrophic and heterotrophic forms. Diversity of the Torridon assemblage is moderate, but notable morphotyptes characteristic of this time period are missing from the lacustrine environment. This absence may be due to physical inhibitors to lake colonisation, or could reflect the time needed to make such a move.

Taphonomy has been assessed objectively for the first time within and between individual deposits, and the newly devised taphospace plots offer further opportunity for assessing degradation in organic-walled microfossils. Further data will allow characterisation of different taphonomic environments, as well as a reassessment of Proterozoic taxa that are diagnosed on the basis of taphonomic artefacts.

The exceptional preservation of microfossils within the Torridon phosphates and shales is likely due to the presence of iron-rich clays in these rocks, corroborated by their absence, and corresponding absence of microfossils, in other phosphates of Proterozoic and Cambrian age. Layering of clays around organic vesicles protects them from further decay, before occlusion by phosphate. It is likely that the unique lake chemistry of the Torridon basin permitted the authigenic growth of these clays in abundance.

Through three newly described occurrences of phosphate, it is possible to put the evolution of phosphogenesis in some context. In Proterozoic siliciclastic settings, such as the Torridon Group and the Avalonian succession, concentration and precipitation of phosphate is controlled by biological release and biologically induced iron desorption. In chemical sediments of the Gunflint, iron oxides are absent and so phosphate can only be concentrated in small amounts by the resident biota. Following the appearance of vertical burrowing in the Cambrian, phosphogenesis is forced downwards in the sediment and occurs much more rarely, during hiatuses.

The fuller understanding of the Proterozoic that these microbial assemblages and petrological associations affords is also of use in astrobiological investigations. Understanding evolution and preservation in a variety of early earth environments guides where and how astrobiological searches may be conducted.

While addressing many unresolved questions, this study of the Torridon Group and associated Proterozoic units also raises subjects for future investigation. Better understanding of the stratrigraphically lower, and likely lagoonal setting of the Stoer Group may put the Torridon in further perspective, and search and discovery of more lacustrine deposits in the Proterozoic will inform on non-marine biological evolution at this time. Microbiological studies can be supported by modern experimental approaches, and supporting evidence may be sought from isotope or biomarker studies, and renewed search for macroscopic structures can help to constrain their formation and distribution. Finally, non-economic deposits of phosphate can reveal much about chemical evolution in the Proterozoic and elsewhere, and should be actively sought.

Contents

1 Introduction **1**

1.1 Proterozoic Geology 1

1.1.1 Tectonics 1

1.1.2 Atmospheric Evolution and Temperature 2

1.2 Proterozoic Biota 3

1.2.1 Evidence for life 5

1.2.1.1 Body fossils 5

1.2.1.2 Molecular fossils 5

1.2.1.3 Molecular clocks 6

1.2.1.4 Isotopes 6

1.2.2 Biotic Revolutions 7

1.2.2.1 Oxygenic photosynthesis 7

1.2.2.2 Eukaryotes 8

1.2.2.3 Sex 9

1.2.2.4 Multicellularity 10

1.3 Epistemology 11

1.4 Understanding the Proterozoic Fossil Record 12

1.4.1 Evolutionary histories 13

1.4.2 Astrobiological implications 13

1.5 The Torridon approach 14

2 Geology of the Torridon Group **17**

2.1 Introduction 17

2.2 Geological Setting and Stratigraphy 18

2.3 A non-marine environment 20

2.3.1 Large scale structural information 21

2.3.2 Small wavelength wave ripples 21

2.3.3 Changes in plane-to-plane wave ripple direction 22

2.3.4 Rapid facies changes . . . 22
2.3.5 Abundant desiccation without evaporites or carbonates . . . 23
2.4 Reconstructing ancient palaeoenvironments . . . 24
2.4.1 Torridon Group . . . 24
2.4.1.1 Diabaig Formation . . . 24
2.4.1.2 Cailleach Head Formation . . . 41
2.4.1.3 Sleat Group . . . 43
2.5 Reassessing a classic stratigraphy . . . 46
2.5.1 The Diabaig basin . . . 46
2.5.2 Relationships of the Sleat Group . . . 47

3 Taxonomy of Torridon microfossils 50
3.1 Overview and previous reports . . . 50
3.2 Justifying biogenicity . . . 51
3.2.1 Organic structures are autochthonous to the rock . . . 51
3.2.2 Organic structures are formed by biogenic processes . . . 53
3.2.3 Microfossils preserve original morphology . . . 55
3.3 A preliminary form taxonomy . . . 56
3.4 A new assemblage through new methods . . . 69
3.4.1 Secondary electron SEM . . . 69
3.4.2 Raman spectroscopy . . . 74
3.4.3 FIB-TEM analysis . . . 80
3.4.4 FIB-SEM and FIB-SEM-EDX analysis . . . 83
3.5 Formal Taxonomy . . . 87

4 Comparison of Torridon microfossils 105
4.1 Taphonomy . . . 105
4.1.1 Introducing taphospace and data collection . . . 105
4.1.1.1 Physical . . . 106
4.1.1.2 Chemical . . . 107
4.1.1.3 Biological . . . 108
4.1.2 Construction of a taphospace . . . 110
4.2 Variation between palaeoenvironments . . . 113
4.2.1 Variation within the Diabaig Formation . . . 114
4.2.1.1 Lower Diabaig . . . 114
4.2.1.2 Badachro . . . 116
4.2.1.3 Fladday . . . 116

4.2.1.4 North Shieldaig (Fish Farm) . . . 117
4.2.2 Variation between Diabaig and Cailleach Head Formations . . 120
4.3 Comparing the phosphate-hosted and shale-hosted biotas 123
4.3.1 The effect of maceration on diversity and taphonomy 125
4.3.2 Differences between macerated phosphate and shale 127

5 Torridon macrostructures 132
5.1 Introduction . . . 132
5.2 Justifying Biogenicity . . . 134
5.3 Classifying structures . . . 135
5.3.1 Modification of Sedimentary Features . . . 135
5.3.1.1 Sharpening of ripple crests and multi-crested ripples 135
5.3.1.2 Synaeresis cracks . . . 136
5.3.2 Ordered Surficial Structures . . . 137
5.3.2.1 'Arumberia' . . . 137
5.3.2.2 Networks . . . 137
5.3.2.3 Ladders . . . 138
5.3.2.4 Nodes . . . 138
5.3.2.5 Flat bottomed pits and protrusions . . . 140
5.3.3 Disordered Surficial Structures . . . 140
5.3.3.1 Microreticulate network . . . 141
5.3.3.2 Pustulae and pitting . . . 142
5.4 Possible mode of formation . . . 142
5.4.1 Growth of mats . . . 142
5.4.2 Modification of mats and sediment . . . 143
5.4.3 Preservation of mats . . . 144
5.5 Variation between environments . . . 146
5.5.1 Shieldaig Bay and Peninsula . . . 146
5.5.2 North Shieldaig (Fish Farm) . . . 148
5.5.3 Balgay River and Shore . . . 149
5.5.4 Upper Diabaig . . . 150
5.5.5 Lower Diabaig . . . 151
5.5.6 Badachro . . . 153
5.5.7 Brochel Castle . . . 154
5.5.8 Brochel Sheilings . . . 155
5.6 Summary . . . 157

6 Torridon phosphates **160**
6.1 Previously reported phosphate in Torridon 160
6.2 Description of phosphate and associated minerals 161
6.2.1 Large scale sedimentology 161
6.2.2 Optical microscopy 162
6.2.3 SEM BSE and EDX analyses 162
6.2.4 Raman 165
6.2.5 FIB-TEM 165
6.2.6 FIB-SEM-EDX 167
6.3 Variation of phosphate between environments 168
6.3.1 Lower Diabaig 169
6.3.2 North Shieldaig (Fish Farm) 171
6.3.3 Shieldaig Peninsula 171
6.3.4 Fladday 173
6.3.5 Brochel Castle 176
6.3.6 Badachro 176
6.3.7 Cailleach Head 178
6.4 Potential sources, sinks, and modes of formation 182
6.4.1 Sources 182
6.4.2 Sinks 183
6.4.3 Mode of Formation 184

7 Deeper in the Proterozoic: the Gunflint Formation **188**
7.1 Global Proterozoic Context 188
7.2 Geology 190
7.2.1 Background 190
7.2.2 Sedimentological study 191
7.2.2.1 Schreiber Channel 192
7.2.2.2 Frustration Bay 196
7.2.2.3 Pass Lake 198
7.2.2.4 Centennial Park 200
7.2.2.5 Boulevard Lake 203
7.2.2.6 Kakabeka Road Cut 207
7.2.2.7 Kakabeka Car Park 209
7.2.2.8 Kaministiquia River Eastern Shore 210
7.2.2.9 Kaministiquia River Western Shore 212

7.2.3 Revised palaeoenvironmental interpretations 212
7.3 Microbiota 215
7.3.1 Background 215
7.3.2 Fossil recovery and biogenicity 216
7.3.2.1 Identifiable fossils 217
7.3.2.2 Biogenicity 217
7.3.3 Applying taphospace 221
7.4 Macroscopic Structures 223
7.4.1 Stromatolites and stratiform lamination 223
7.4.2 Non-stromatolitic macroscopic structures 225
7.4.2.1 Kaministiquia River Eastern Shore 225
7.4.2.2 Centennial Park 227
7.4.2.3 Boulevard Lake 229
7.5 Phosphate 230
7.5.1 Previous work 230
7.5.2 Phosphate in the Gunflint Formation 230
7.5.2.1 New findings 231
7.5.2.2 Environments of phosphogenesis 236
7.5.3 Phosphatisation and Biota 239
7.6 Summary 240

8 Major transitions: the End-Proterozoic in Newfoundland 242
8.1 Introduction 242
8.2 Global context 243
8.3 Geology 244
8.3.1 Avalonian Succession 244
8.3.2 Placentian Series 247
8.4 Microbiota 249
8.4.1 Introduction 249
8.4.2 Organic-Walled Microfossils 250
8.4.3 Pyrite Strings 250
8.4.4 Ambient Inclusion Trails 252
8.5 Phosphate 255
8.5.1 Previous reports 255
8.5.2 New Findings 256
8.5.2.1 Spaniards Bay South 256

8.5.2.2 Silos Cove . . . 258
8.5.2.3 Ferrylands Head . . . 260
8.5.2.4 Grand Bank Head . . . 260
8.5.2.5 Little Dantzic Cove . . . 262
8.6 Modes of Formation and Perspective . . . 265

9 Context and Perspectives **267**
9.1 Microbiota . . . 267
9.1.1 Fossil Affinities . . . 267
9.1.2 Diversity . . . 269
9.1.3 Taphonomy . . . 271
9.2 Phosphate . . . 273
9.2.1 Preservation in Phosphate . . . 273
9.2.2 Phosphate in context . . . 275
9.2.2.1 Torridon . . . 276
9.2.2.2 Gunflint Formation . . . 278
9.2.2.3 Newfoundland . . . 279
9.3 Astrobiology . . . 281

10 Future directions **283**
10.1 Geology . . . 283
10.2 Microbiota . . . 284
10.3 Microbially induced macrostructures . . . 285
10.4 Phosphate . . . 285

Bibliography **287**

A Methods **315**
A.1 Preparation . . . 315
A.1.1 Ammonium molybdate . . . 315
A.1.2 Thin Section . . . 315
A.1.3 Acid Maceration . . . 316
A.1.4 FIB extraction of ultrathin TEM lamellae . . . 316
A.2 Imaging and Analysis . . . 317
A.2.1 Optical Microscopy . . . 317
A.2.2 SEM-BSE, SE and EDX . . . 317
A.2.3 Raman spectroscopy . . . 318

A.2.4 TEM analysis of FIB-milled wafers 318
A.2.5 FIB-SEM nano-tomography 318
A.2.6 3D volume rendering 319

B Materials **321**

C Publications **330**

D Atlas of Proterozoic Microfossils **333**

List of Figures

1.1 Events of the Proterozoic 4

2.1 Location, stratigraphy and simplified geological map of the Torridon of northwest Scotland 19
2.2 Plate illustrating characteristically lacustrine features of the Diabaig Formation 22
2.3 Key to sedimentary logs 25
2.4 Sedimentary log of Diabaig Formation at Lower Diabaig 26
2.5 Sedimentary log of Diabaig Formation at Upper Diabaig 27
2.6 Sedimentary log of part of the succession of Diabaig Formation at Balgay Shore 29
2.7 Sedimentary log of Diabaig Formation at Shieldaig Peninsula 31
2.8 Sedimentary log of Diabaig Formation at North Shieldaig 33
2.9 Sedimentary log of Diabaig Formation at Sheildaig Bay 34
2.10 Sedimentary log of Diabaig Formation at Badachro 36
2.11 Sedimentary log of Diabaig Formation at Fladday 38
2.12 Sedimentary log of part of the exposure of Diabaig Formation at Brochel 39
2.13 Sedimentary log of part of the exposure of Cailleach Head Formation at Cailleach Head 42
2.14 Sedimentary log of Kinloch Formation, Sleat Group at Sleat Peninsula West 44
2.15 Sedimentary log of Kinloch Formation, Sleat Group at Kyle of Lochalsh 45
2.16 Schematic reconstruction of the Diabaig basin 48

3.1 Plate illustrating eight informally defined microfossil morphotypes of the Torridon Group 59
3.2 Total abundance of informal morphotypes in the Torridon Group . . 60
3.3 Histogram illustrating the distribution of coccoid diameters from microfossil survey 61

3.4 Scatter chart showing the relationship between cluster size and constituent cell size, with reference to the number of cells in cluster . . . 62
3.5 Histogram illustrating the distribution of filament diameters from microfossil survey . . . 63
3.6 Photomicrographs illustrating microfossils of note . . . 65
3.7 Various modes of degradation and decay of microfossils from the Torridonian phosphate . . . 68
3.8 Microfossils imaged and analysed by secondary electron SEM . . . 71
3.9 Evidence of bacterial heterotrophy in secondary electron SEM images 73
3.10 Laser raman maps of a large, dark-walled fossil . . . 77
3.11 Laser raman maps of two small, light-walled microfossil . . . 78
3.12 FIB-TEM image and element maps of a small, thin-walled vesicle . . 82
3.13 Serial FIB-SEM images through a compressed cluster of thin-walled vesicles, and slice-based three-dimensional reconstruction of two select cells . . . 84
3.14 FIB-SEM-EDX imaging and elemental mapping of a large, dark-walled fossil . . . 86
3.15 Formally described taxa from the Torridon Group . . . 91
3.16 Formally described taxa from the Torridon Group . . . 92
3.17 Formally described taxa from the Torridon Group . . . 95

4.1 Plate illustrating examples of each taphonomic grade. . . . 111
4.2 Construction of 'taphospace' plot . . . 113
4.3 Assemblage data for Lower Diabaig . . . 115
4.4 Assemblage data for Badachro . . . 117
4.5 Assemblage data for Fladday . . . 118
4.6 Assemblage data for North Shieldaig . . . 119
4.7 Comparison of ecosystem dominance between palaeoenvironments . . 121
4.8 Comparison of the assemblages of the Diabaig Formation and the Cailleach Head formation. . . . 122
4.9 Comparison of morphotype abundances in phosphates prepared by thin section and by acid maceration in the Cailleach Head Formation, and Diabaig Formation . . . 125
4.10 Comparison between the taphospace plots for phosphate-hosted microfossils prepared by thin section and acid maceration in the Diabaig Formation and Cailleach Head Formation . . . 126

4.11 Comparison of morphotype abundances in macerated phosphates and shales from the Cailleach Head Formation, and Diabaig Formation . . 128
4.12 Comparison between the taphospace plots of microfossils macerated from the shales and the phosphates from Diabaig Formation, and Cailleach Head Formation 129

5.1 Microbial modification of sedimentary features 136
5.2 Ordered microbial macrostructures 139
5.3 Disordered microbial macrostructures 141
5.4 Schematic mode of formation of microbially induced wrinkle structures 144
5.5 Microbially induced macrostructures from Sheildaig Bay and Peninsula 147
5.6 Microbially induced macrostructures from North Sheildaig 148
5.7 Microbially induced macrostructures from Balgay River and Shore . . 149
5.8 Microbially induced macrostructures from Upper Diabaig 151
5.9 Microbially induced macrostructures from Lower Diabaig 152
5.10 Microbially induced macrostructures from Badachro 154
5.11 Microbially induced macrostructures from Brochel Castle and Sheilings 156
5.12 Location of wrinkle structures within the idealised Diabaig Basin . . 158

6.1 Textural and chemical differences between 'pure' phosphate and 'granular' phosphate from the Torridon Group 163
6.2 Application of high resolution techniques to studying phosphate in the Torridon Group 166
6.3 Phosphate sedimentology, petrology and mineralogy at Lower Diabaig 170
6.4 Phosphate sedimentology, petrology and mineralogy at North Sheildaig 172
6.5 Phosphate sedimentology, petrology and mineralogy at Sheildaig Peninsula 173
6.6 Phosphate sedimentology, petrology and mineralogy at Fladday . . . 175
6.7 Phosphate sedimentology, petrology and mineralogy Brochel Castle . 177
6.8 Phosphate sedimentology, petrology and mineralogy at Badachro . . . 179
6.9 Phosphate sedimentology, petrology and mineralogy at Cailleach Head 180
6.10 Proposed mode of formation of phosphate in the Torridon Group . . 185

7.1 Outcrop map of the Gunflint Formation 193
7.2 Summary of sedimentological structures at Schreiber Channel 194
7.3 Summary of sedimentological structures at Frustration Bay 196
7.4 Summary of sedimentological structures at Pass Lake 199

7.5 Summary of sedimentological structures throughout Centennial Park outcrops 201
7.6 Summary of sedimentological structures at Boulevard Lake 204
7.7 Summary of sedimentological structures at the Kakabeka Road Cut outcrop 208
7.8 Summary of sedimentological structures at the Kakabeka Car Park outcrop 209
7.9 Summary of sedimentological structures at outcropping on the shore of the Kaministiquia River 211
7.10 Schematic reconstruction of an idealised depositional basin for the Gunflint Formation lithofacies 214
7.11 Organic walled microfossils identified from resampled cherts of the Gunflint Formation 218
7.12 Carbon-containing carbonate microspheres, identified here as pseudofossils 220
7.13 Taphospace plots for organic-walled microfossils recovered from three Gunflint lithofacies 221
7.14 Summary of stromatolitic structures in various Gunflint lithofacies . . 224
7.15 Candidate microbially induced macrostructures in various Gunflint lithofacies 228
7.16 Plate illustrating phosphate occurrence in the ferruginous banded chert-carbonate at the parking lot of Kakabeka falls 232
7.17 Plate illustrating phosphate occurrence in the grainy and banded chart-carbonates at Frustration Bay 233
7.18 Plate illustrating phosphate occurrence in the volcaniclastic shale upstream of Kakabeka Falls 235
7.19 Plate illustrating phosphate occurrence in the ferruginous phosphatic chert-carbonate at Boulevard Lake 237
7.20 Likely loci of phosphogenesis within Gunflint sediments 238

8.1 Map of the Avalon and Burin Peninsulas, eastern Newfoundland . . . 245
8.2 Generalised stratigraphy of the Avalonian and Pacentian successions . 248
8.3 Pseudofossils or fossils from the Avalonian of eastern Newfoundland . 253
8.4 Phosphate sedimentology, petrology and mineralogy at Spaniards Bay South 257
8.5 Phosphate sedimentology, petrology and mineralogy at Silos Cove . . 259

8.6 Phosphate sedimentology, petrology and mineralogy at Ferrylands Head Formation 261
8.7 Phosphate sedimentology, petrology and mineralogy at Grand Bank Head 263
8.8 Phosphate sedimentology, petrology and mineralogy at Little Dantzic Cove 264

9.1 Schematic illustrating the hypothesised mode of preservation for the Torridon fossils 274
9.2 Profiles through microbial mats 280

Chapter 1

Introduction

The field of palaeontology, much advanced since its Victorian heyday, is today concerned with big questions in evolution, fossil preservation, and interactions between life and the physical environment. Fossil deposits continue to be sought to address these questions, and well known deposits are revisited with brand new techniques to reveal more about life's four billion-year heritage.

While the fossil record of the Phanerozoic has received much academic attention, due to its abundant macroscopic fossil record, much remains to be learnt about the Proterozoic. A time of biotic, climatic and geological revolution, it holds the key to understanding some of the most fundamental steps in the evolution of life, contained within enigmatic microfossil remains. Understanding them can help to unlock the secrets of the Proterozoic, and with it, a better understanding of where we came from and where we are going.

1.1 Proterozoic Geology

The Proterozoic spans from the end of the Archaean 2500 Ma ago, through to the beginning of the Cambrian and of the Phanerozoic, at 542 $\pm$ 0.3 Ma ago. During this time, sedimentary, igneous, and metamorphic rocks were deposited or emplaced, and are now found on every major continent.

1.1.1 Tectonics

Tectonics in the Proterozoic were dominated by the assembly and subsequent breakup of Rodinia in the Mesoproterozoic and Neoproterozoic respectively (Li et al. 2008). Assembly took place during the Grenville orogeny, between around 1.3 and 1.1 Ga,

from fragments of the supposed early supercontinent Columbia, which broke up around 1.8 Ga ago (Zhao et al. 2002, 2004). The Grenville orogeny resulted in vast folded mountain belts that are today exposed in Newfoundland and elsewhere (Tollo et al. 2004). The latitudinal position of the Proterozoic continent is unresolved, but various reconstructions place it straddling the equator (Torsvik 2003) or located primarily in the southern hemisphere (Scotese 2001). Following its breakup around 550 Ma, the rocks deposited at this time were later deformed and metamorphosed in the Caledonian orogeny during the Silurian and the Ordovician (Cocks & Torsvik 2006, Jones & Blake 2003, McKerrow et al. 2000).

1.1.2 Atmospheric Evolution and Temperature

The long period of time represented by the Proterozoic period is occupied by the major changes in atmospheric and ocean composition, as well as climate, that altered the planet from a hot, noxious world, to the habitable environment of the Phanerozoic and today.

Dominating this period is the Great Oxidation Event, or Oxygen Catastrophe; weathering profiles and shifts in mineralogical deposition record a jump in oxygen concentrations in the atmosphere around 2.4 Ga (Holland 2006) that was accompanied by a stepwise increase in oxygenation of the oceans (Scott et al. 2008).

Considerable evidence is building to support the idea that oxygenation of the oceans was delayed, or instead more complex than previously thought, being instead dominantly sulphidic from around 1.8 Ga (Poulton et al. 2004). The first great jump in oxygenation seen at 2.4 Ga is presumed to be intimately associated with the evolution of oxygenic photosynthesis, although the cause-correlation relation has yet to be resolved. Some authors (Dutkiewicz et al. 2006) argue that the event was a delayed response to the evolution much earlier of oxygenic photosynthesis, while others (Kopp et al. 2005) argue for an alternative cause but suggest that the abiogenic oxygen rise promoted the rise of photosynthetic organisms at this time. Sulphur isotope evidence from the Torridon of northwest Scotland has recently hinted at the oxygenation of terrestrial regimes by 1.2 Ga ago (Parnell et al. 2010). Following this change in atmospheric composition early in the Proterozoic, conditions appear to have been remarkably stable, prompting some to term the period from 2 Ga to 1 Ga the 'Boring Billion' (Holland 2006). Not only did oxygen levels remain relatively constant, but the availability of nutrients remained stable and low, as revealed by isotopic values

and weathering profiles (Brasier & Lindsay 1998, Lindsay & Brasier 2000). It is likely that the stability of pre-Rodinian conditions contributed to this low variability, and a view is emerging that the evolution and diversification of sulphur-oxidizing microbes also contributed to the stability (Johnston et al. 2009). Such a view is concordant with the emerging understanding of sulphur-based metabolisms at this time (Wacey et al. 2011).

Temperature profiles throughout the Proterozoic are partly related to changes in atmospheric composition. Throughout the 'Boring Billion', it seems temperature remained relatively constant with warm greenhouse conditions, although evidence is limited to the absence of glacial tillites, and extrapolated oxygen isotope data (Knauth 2005, Schopf & Klein 1992). Where evidence of glaciation does occur, it does so on a large scale, leading some to suggest extensive 'Snowball' glaciation at various stages throughout the Proterozoic (Hoffman et al. 1998, Kirschvink et al. 2000). Around 2.2-2.4 Ga, the Huronian glaciation is recorded throughout Canada, and later, at least two snowball-style events are indicated by palaeomagnetic reconstructions of glacial diamictites: the Sturtian around 730-716 Ma (Macdonald et al. 2010), and the Marinoan/Varangian between 560 and 650 Ma (Mawson 1949, Williams et al. 2008). It is likely that these events, regardless of their worldwide extent or otherwise, fundamentally influenced the evolution of life at the time, and may be correlated with the diversification of novel forms like those of the Ediacaran biota at the terminal Proterozoic.

1.2 Proterozoic Biota

In searching for the very earliest traces of life, palaeontological techniques are combined with holistic geological and planetary chemical understandings, as well as explorative prebiotic chemistry. Resolving the earliest form of life and then attempting to discover its fossil record is a complex process and one that is the preoccupation of astrobiological collaboration. It is generally accepted that in order for life as we know it to survive and thrive, the minimum requirements are a liquid solvent—in this case water—and sufficiently low temperatures for organic materials to remain bonded. On Earth, these conditions are thought to have prevailed relatively rapidly after its formation, with water oceans delivered by cometary and asteroidal impact (Dauphas et al. 2000, Delsemme 1999) and continental surfaces cooling relatively rapidly (De Paolo 1981), being only locally affected by the later heavy bombardment

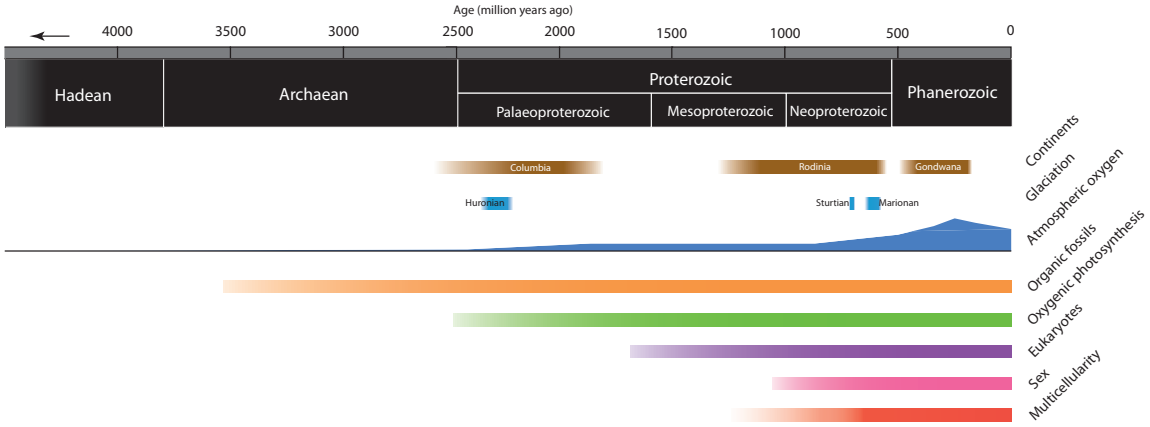


Figure 1.1: Events of the Proterozoic. Geological timescale illustrating timing of various events: existence of supercontinents, periods of major glaciation, atmospheric oxygen levels, organic fossils, appearance of oxygenic photosynthesis, evolution of eukaryotes, origin of sex, and appearance of multicellularity. For detail and references, see text.

(Abramov & Mojzsis 2009). The first potentially sedimentary rocks are found dating to 3.85 Ga, from Akilia, Greenland (Manning et al. 2006), indicating that an active hydrological cycle was present at this time, delivering and renewing nutrients that may be useful to primitive life.

It is amongst the earliest sedimentary rocks, the Strelley Pool Chert in Western Australia, dated at 3.4 Ga, that the earliest putative microfossils have been found (Wacey et al. 2011). Taking the place of the previously disputed fossils of the 3.5 Ga Apex chert (Brasier et al. 2002, 2005, 2006, Schopf 2006, 1993, Schopf et al. 2002), these new forms comprise a low but notable diversity of tubular and coccoid forms, combined with mineralogical and chemical biomarkers that suggest they represent sulphur-oxidizing microbes colonizing beach rock under anoxic conditions. The multiple lines of evidence supporting this find strengthen its claim for biogenicity, but much work remains to be done to verify questions still surrounding the deposit.

Further microfossil deposits of Archaean age are limited, but include putative permineralised microbial colonisations at 3.44 Ga (Westall et al. 2006), and gigantic organic walled microfossils from 3.2 Ga shales of South Africa (Javaux et al. 2010). It is not until the Proterozoic that verifiably biogenic organic-walled microfossils attain a diversity that is informative to the study of early evolution. One of the earliest of

these diverse assemblages in the Proterozoic is the Gunflint microbiota, from the 2 Ga Gunflint chert in Ontario, Canada.

1.2.1 Evidence for life

1.2.1.1 Body fossils

The body fossil record of the Proterozoic is almost exclusively dominated by microscopic organic-walled microfossils, preserved two-dimensionally in shales, or with a degree of three-dimensional structure in cherts. Such preservation is rare in the Phanerozoic and would be considered exceptional preservation, but is commonplace in Precambrian depositional environments, due to the fundamentally differing diagenetic chemistries. As such, microbial structures can be preserved and retained throughout the two-billion year pre-metazoan history of life.

A few exceptions to this organic-walled body fossil record are occasional deposits of mineralized microfossils, whether by encrusting iron minerals or permineralisation by chert, phosphate, or carbonate (e.g. Horodyski & Donaldson 1980, Schelble et al. 2004, Zhang et al. 1998). In many cases, however, these fossils have similar morphology and distribution to organic-walled morphotypes, and so may be considered alongside them, taking into account their special conditions of preservation.

Macroscopic fossils occur infrequently throughout the Proterozoic record, although most macrobiota are concentrated during the terminal Proterozoic Ediacaran period. At this time, three-dimensional casts and moulds of enigmatically constructed organisms are preserved in volcaniclastic and siliciclastic sedimentary rocks, and are the subject of much study (e.g. Brasier & Antcliffe 2009, Hofmann et al. 1990, Xiao & Laflamme 2009). Occasionally, carbonaceous megafossils are preserved parallel to shale laminae in siliciclastic rocks in the Neoproterozoic, with tubular, irregular, or discoidal forms being variously attributed to *Grypania* Walter, Oehler and Oehler, *Beltana* Walcott and *Chuaria* Walcott. It is likely that these represent remains of macroscopic algal thalli that are related to more microscopic forms in the organic-walled microfossil record.

1.2.1.2 Molecular fossils

Molecular fossils, or biomarkers, are the fossil remnants of biochemical compounds, the specificity of which may be a useful indicator of particular kinds of metabolic pro-

cesses and thus of different types of organisms. Many studies have been made into the structural transformations of different types of organic hydrocarbons under typical diagenetic and thermal conditions (e.g. Brocks et al. 2005, Volkman 2003) and a vast library of diagnostic compounds and their functional precursors now exists, linking them to established biological sources (Brocks & Summons 2004, Peters et al. 2005). The chemical recovery of such compounds from ancient rocks can, with appropriate calibration, be taken to indicate the presence of those biological sources, supplying the biochemicals at the time.

The study of these molecular fossils is necessarily complex, and many complicating factors must be accounted for when arguing for ancient metabolisms. For example, the Precambrian rocks that are the subject of study have often experienced multiple stages of burial and exhumation and thus may display an unexpected maturity of chemical material, possible affecting the resolution of certain biochemicals. In addition, a complex geological history combined with modern day exposure usually inherent in the study of candidate rocks offer much opportunity for contamination by modern biochemicals, enhancing, diluting, or providing false signals that complicate the picture. As such, caution is needed in the preparation, analysis, and interpretation of these molecular fossils, but they are nevertheless a powerful tool in combination with other biological indicators.

1.2.1.3 Molecular clocks

In studying the major groups of life, molecular clocks have been used to constrain the timing of their divergence from one another. These methods make use of the genetic differences in conserved genes between differing organisms, in combination with empirically constrained rates of molecular change to deduce divergence dates (Benton & Donoghue 2007, Zukerkandl & Pauling 1962). Although threatened by uncalibrated extrapolation in the early years of its application, the method is continually being honed by additional information on non-constant evolutionary rates, to produce divergence dates for major biological groups that can be calibrated with body fossil and molecular fossil evidence to build a richer picture of early life revolutions (Douzery et al. 2004, Peterson et al. 2004).

1.2.1.4 Isotopes

The fractionations of many stable isotopes are used in a wide variety of geological investigations, and are of great use in understanding biological processes acting to

modify the environment. In particular, light fractionation of ^{13}C isotopes in carbonaceous matter is taken as a strong indication of a biological origin for that material, owing to life's energetic preference for lighter isotopes (Brugnoli & Farquhar 2000). Similar phenomena observed in both $^{33}S/^{32}S$ and $^{34}S/^{32}S$ fractionations are taken as indicators of a strong modifying sulphur oxidising metabolism.

Bulk sampling of organic material and its associated minerals permits analysis of these isotope fractionations in even the most ancient of rocks. Indeed, light fractionation of ^{13}C in the 3.85 Ga metamorphosed rocks of Isua and Akilia, Greenland (Schidlowski 1988) have been taken as evidence of life in these most ancient rocks (Mojzsis et al. 1997). Interpretation of the results must proceed with caution, however, as life is not the only contributing factor to stable isotope fraction. Especially in ancient rocks, where non-uniformitarian processes occur, abiogenic fractionation mechanisms may replicate life in a way unobserved and unexpected in modern environments, such as the Fischer-Tropsch fractionation over catalysing metals, interpreted to be the cause of the light $\delta^{13}C$ seen in the disputed Apex microbiota (Brasier et al. 2004). Yet, in combination with body fossil and biomarker evidence, isotopes preserved within the rock can further reveal the secrets of early Proterozoic evolution.

1.2.2 Biotic Revolutions

By comparing the sparse record of life in the Archaean with the recognizable metazoan-dominated ecosystems of the beginning of the Cambrian, it is clear that a number of biological revolutions occur during the Proterozoic. Such revolutions are necessary to accelerate life from primitive prokaryotic forms to cellular machinery capable of advanced multicellularity and locomotion, but it is not yet fully resolved when and how they took place. Major steps that must have taken place during the Proterozoic are detailed below.

1.2.2.1 Oxygenic photosynthesis

Oxygenic photosynthesis, while representing just one of the many possible metabolisms exploited by microbes, has been fundamentally influential in shaping Earth's atmospheric composition and the later evolution of complex life. Today it is the dominant form of autotrophy, taking place under oxygenic conditions and using carbon dioxide, water, and radiative energy from the sun to create organic molecules to be used in respiration, and oxygen as a byproduct. It is found in all modern plants, and in some

single-celled eukaryotes as well as in the diverse cyanobacteria.

Signatures for the appearance of this metabolism can be sought in the detection of an increase in oxygen content in the atmospheres and oceans, as well as from molecular clock estimates, the identification of fossil organic biomarkers like 2α-methylhopanes (Summons et al. 1999), short chain acyclic isoprenoids (Peters et al. 2005) or stigmastane and 24-ethylcholesterane (Volkman 2003), and the record of verifiable body fossils of photosynthetic organisms (Knoll et al. 2007).

The sudden rise in oxygenic weathering and deposition around 2.4 Ga, at the Great Oxygenation Event (GOE), has been attributed by some to the evolution of oxygenic photosynthesis (Kopp et al. 2005), although biomarker evidence suggests an earlier origin (Brocks et al. 1999, Dutkiewicz et al. 2006), and a time lag in atmospheric oxygen buildup caused by mineralogical oxygen drawdown. Calibrated molecular clock reconstructions estimate the origin of cyanobacteria, the most primitive extant photosynthetic organisms, between 2.04 and 3.08 Ga (Hedges et al. 2001), supporting a possible pre-GOE origin of this metabolism. By the mid-Proterozoic, body fossils interpreted as having cyanobacterial affinity, including those with tentative akinetes and heterocysts, are relatively abundant in marine settings (Tomitani et al. 2006). Thus, the majority of evidence points to a very early Proterozoic, or even late Archaean origin of bacterial oxygenic photosynthesis (Figure 1.1).

1.2.2.2 Eukaryotes

The evolution of eukaryotes—cells with a membrane-bound nucleus and complex sub-cellular machinery from which all multicellular life is descended—from primitive prokaryotes is regarded by some as the most fundamental evolutionary change (Lane 2009). Today it is generally accepted that the transition occurred due to a stepwise acquisition of organelles via pronged symbiosis between prokaryotic and transitional forms, now termed endosymbiogenesis (Sagan 1967). Identifying this transition in the fossil record is somewhat more problematic, however, as many of the changes that occur do so sub-cellularly, and sub-cellular details are almost never preserved even in the best fossil deposits. Some morphological criteria for identifying body fossils of eukaryotes do exist, and in combination with molecular fossil evidence they help to broadly constrain the appearance of complex cells.

While sub-cellular details of cells may not be preserved, certain qualities of a preserved external wall have been shown to be indicators of eukaryocity in fossils, as they may only be produced by mobile cytoskeletal-controlled cytoplasm and enhanced intra-cellular transport afforded by eukaryotic organelles (Knoll et al. 2006). These are generally considered to be the combination of a large size vesicle, greater than 60 μm in diameter, a multi-layered ultrastructure to the cell wall, excystment by median split greater than half the circumference of the equator, and complex ornamentation on the outside of the cell wall (Javaux 2007, Javaux et al. 2003, 2001, Knoll et al. 2006). One of these factors on their own may not necessarily indicate a eukaryotic nature, but the combination of all of them is strong evidence of an organised, mobile cytoplasm only found in eukaryotes. Such combined pieces of evidence are first seen in the Mesoproterozoic, in early assemblages of acritarchs from the Roper Group (Javaux et al. 2003, 2001), indicating that diverse eukaryotic morphotypes were present by the beginning of the Neoproterozoic, 1 Ga ago. This is supported by evidence in the form of fossil steranes in Proterozoic rocks, leading to the conclusion that steroid biosynthesis, characteristic of eukaryotes, was taking place as long ago as 1650 Ma ago (Dutkiewicz et al. 2003, Schopf & Klein 1992, Summons & Walter 1990) (Figure 1.1). Abundances of these biomarkers in Mesoproterozoic rocks are low, which may suggest degradation of the biomarker record or an originally low eukaryotic biomass.

1.2.2.3 Sex

Alongside the appearance of complex eukaryotic cells, the origin of meiotic, sexual reproduction was arguably responsible for genetic mixing that allowed increased evolutionary tempo, morphological diversity, and may have also precipitated the evolution of multicellularity (Butterfield 2000). Biological origins of meiotic reproduction have been investigated (Margulis & Sagan 1986) and some conclude an intimate link between eukaryocity and meiotic sex, through interpretation of molecular phylogenies (Dacks & Roger 1999), but investigation into its early fossil record has thus far been very limited. Similar to the transition from prokaryotic to eukaryotic cells, the transition from mitotic cloning to meiotic sexual reproduction was a change that took place primarily *within* the cells, which is unlikely to be preserved. Instead, proxies for the sexual reproduction process must be sought in individual morphologies of population changes. In particular, the production of meiotic tetrads in the early stages of gametogenesis may leave a fossil record in the form of characteristically ordered structures like the organic walled microfossil *Eotetrahedrion princeps*. This form is found in early Neoproterozoic sedimentary rocks (Schopf & Blacic 1971), placing the

origin of sex to at least 900 Ma (Tappan 1976), although interpretation of this form as a reproductive structure is far from conclusive. Similarly, morphotypes created after fertilisation may be recognised and allied to sexual reproduction. The enigmatic phosphate-permineralised megaspheric coccoids from the 635-551 Ma Doushantuo Formation in China have been claimed as animal embryos (Xiao & Knoll 2000, Xiao et al. 1998), thus implying sexual reproduction by this time. The interpretation of these forms is subject to heated debate however, and their embryonic affinity has been undermined by increasing evidence of giant microbial colonies (Bailey et al. 2006, Donoghue 2007).

It may be predicted that the enhanced genetic mixing that sexual reproduction affords would result in an increase in diversity and evolutionary tempo after its first appearance. Using diversity criteria of acritarchs from the Neoproterozoic, Knoll (1995) showed such an increase, dated around 950 Ma. If this is a valid interpretation of the fossil record, and the changes are indeed due to the advent of sexual reproduction, then this places the revolution around the Mesoproterozoic-Neoproterozoic boundary. Given that the fossil record of this major revolution remains unresolved, it is clear that fossil studies in the Proterozoic have much to reveal to further narrow down the timing, environment and stages involved in 'inventing' sexual reproduction.

1.2.2.4 Multicellularity

The origin of multicellularity and the subsequent appearance of metazoans and macroscopic plants is arguably the transition that has most visibly shaped the Earth over the last 500 million years. At the beginning of the Cambrian, with the appearance of the majority of recognisable animal phyla (Bambach et al. 2007), it is clear that a multicellular way of life is firmly established, but the history of these and other multicellular lineages in the Proterozoic is as yet poorly understood. Macroscopic fossils such as those of the Ediacaran biota are testament to macroscopic organismic architecture, but a lack of cellular preservation in these fossils precludes further interpretation as to their affinity, or even of their multicellularity (Seilacher et al. 2003). Evidence must instead be sought in the exceptional microfossil record deeper in the Proterozoic, and in molecular biomarker and phylogenetic reconstructions.

The earliest microfossil form argued to be truly multicellular is that of the supposed red alga *Bangiomorpha pubescens* Butterfield, which bears a striking resemblance to modern day Bangiophyte algae, and contains differentiated cell types clearly

growing together in vertically oriented algal thalli (Butterfield 2000). This example, dating to around 1.2 Ga, is isolated, and no similar forms are found elsewhere in the record until algal thalli of the Ediacaran period (Xiao et al. 2004), suggesting that such an early origin of multicellularity was likely a biological experiment that did not become dominant until conditions became more favorable. The biomarker record suggests a similarly ancient origin of multicellularity, indicating sponges, the most primitive metazoa, appeared between 1.4 and 1.1 Ga ago (Skorokhod et al. 1999), although the absence of any identifiable fossil record of such structures calls these conclusions into some doubt. Molecular clock estimates of the origin of metazoa vary from over 900 Ma to 573-656 Ma (Peterson et al. 2004), dependent on rate of 'tick' and chosen calibration data. Thus, precise dating of this apparently visible revolution has yet to be achieved, and further examination of the Proterozoic record can potentially assist in enhancing the resolution of mode and timing of this transition.

1.3 Epistemology

Even given the overall exceptional preservation of organic-walled microfossils in the Proterozoic, and the potential for alternative supporting evidence in the form of biomarkers, molecular clock estimates, and isotope fractionations, the fossil record of this time period is far from complete.

Due to the nature of the fossilisation process, certain biases in the record occur, which are notably prevalent within the Phanerozoic, but also apply to the Proterozoic. Firstly, there is an overrepresentation of fossils from aquatic environments, as these are the loci of significant sediment deposition necessary for burial and protection of fossil material before degradation. Terrestrial environments experience net erosion rather than deposition, and so any living organisms on land have little opportunity for preservation *in-situ*.

Secondly, of the aquatic environments, fossils from the marine realm are typically overrepresented at the expense of a non-marine lacustrine or fluvial record. Marine basins are much larger and longer lived than those depositional environments found on land. Lake basins are laterally less extensive, shallower, and receive a much higher mean sediment flux, meaning that they are ephemeral on a geological timescale. Thus their chances of preservation and later exposure are reduced, and any fossil record

they contain is locally limited and easily destroyed.

Finally, there exists a bias towards younger rocks and the more advanced fossil material that they contain, owing to the tectonic alteration and destruction of older basins. In the Proterozoic this a particular issue, as rocks deposited over a billion years ago have been involved in at least three continental assemblies and breakups. The chances of sedimentary fossil-containing material surviving relatively unaltered is diminishingly small, and the rock record, as well as the fossil record, becomes predictably more sparse with increasing antiquity in the Precambrian.

In addition to the biases inherent in the fossil and rock records, the majority of Proterozoic fossil discoveries have been made within fine grained siliciclastic rocks or in microcrystalline chert, and searches for microfossils continue to be dominantly within these lithologies (e.g. Schopf & Klein 1992). While the preservational processes in these depositional environments are relatively well understood, and they are consistently the source of well-preserved informative fossil assemblages, good preservation may not be limited to these rock types, as shown by rare calcium mineralisation (e.g. of the supposed cyanobacterium *Girvanella* (Riding 1975)) or phosphate permineralisation (e.g. of the algal and supposed embryo fossils of the Doushantuo Formation, China (Xiao et al. 1998)). A broader outlook of fossilising media is necessary to gain a full understanding of fossil morphology, preservation, and geobiology.

In order to fill the gaps in our knowledge and understanding of the Proterozoic fossil record, new geological and palaeontological data should be actively sought for ancient terrestrial and non-marine deposits. Within those deposits, and elsewhere within the Precambrian time period, alternative fossilising media should be examined to further inform on distribution of fossil organisms and their biogeochemical interactions.

1.4 Understanding the Proterozoic Fossil Record

The benefits of understanding the Proterozoic fossil record are ample justification for its continued study, and the considerable epistemological gaps in our current knowledge drive and direct geological and palaeontological investigations. A fuller picture of the early stages in life's evolution offer opportunity for not only understanding evolutionary history on Earth, but is also of great value to astrobiological investigations.

1.4.1 Evolutionary histories

A fuller understanding of the Proterozoic will fill in a vast period of Earth history, previously understudied, and still poorly represented in the public consciousness. Two billion years of evolution in the microscopic realm set the stage for the Phanerozoic diversification of macroscopic organisms that are the poster children of palaeontology. This record, although microscopic, offers unique opportunities for tracking the cellular and sub-cellular revolutions that were necessary in the evolution of life. A more complete knowledge of these evolutionary revolutions will permit better communication to non-scientific audiences, and thus alter public perceptions and perspectives.

The body fossil record is also an important factor in constraining various proxies for life and life processes, such as molecular clocks, isotopes and biomarkers. By expanding and enriching the database of organic walled microfossils from the Proterozoic, and by using new techniques to assess their biological affinity, well constrained data can be used to provide precise anchors for extrapolations into deep time. Not only will this enhance the understanding of biospheric processes, but it will improve the precision and accuracy of previously poorly constrained proxies.

Finally, by combining the body fossil record with biological and biogeochemical proxies, the palaeontology of the Proterozoic can be used to synthesise information on biosphere-Earth interactions in an early, non-uniformitarian environment. Observing causation and correlation within geobiological systems can shed light on how the presence and evolution of life shaped the evolution of our planet. Such knowledge may be used for a variety of applications, including harnessing geobiological phenomena for industrial applications (Trent et al. 2010), or the creation and calibration of predictive models of planetary evolution for Earth and other planets (Lammer et al. 2009).

1.4.2 Astrobiological implications

The field of astrobiology today has advanced much since its beginnings 50 years ago. It is now an active field of research, involving close interdisciplinary collaboration between many aspects of the physical and life sciences. Although extra-terrestrial life has yet to be discovered, huge advancements continue to be made in understanding where life came from, where it may be distributed, and how it may differ (e.g. Des Marais & Walter 1999, Lineweaver et al. 2004). In this, early life palaeontology

has an important role to play.

It is generally accepted that any extra-terrestrial life we will be able to find in our solar system will not only be microbial, but will also be fossilized or dormant, owing to the consistent lack of life signs from local planetary bodies. This is likely to be due to the fact that less habitable environments, such as those on the planetary bodies outside the classic 'habitable zone' (Kasting et al 1993), would not provide the optimum conditions for life to thrive, and thus evolution would be stalled. Further, if life was established on other planets early in their history but which later went extinct, there is a good chance of finding their fossilized remnants, either through detection of the fossil organisms themselves, or through interpretation of organic or inorganic biomarkers. As described above, understanding such a fossil record is the preoccupation of Proterozoic palaeontology, and the lessons learned and techniques used may easily be adapted and applied to local astrobiological investigations. Understanding the Proterozoic record can assist in the better understanding of how life was initially established, how it diversified, and how it reacted to or shaped planetary conditions on Earth, with potential comparison to other primitive planetary environments. It will inform as to the environments in which life may have thrived on other planets, given adaptation to non-uniformitarian primate Earth conditions, and therefore shape hypotheses of where to look for extra-terrestrial life. The fossil record of early life on earth gives important information on the modes and processes of preservation involved with microbial organisms, and an exploration of study methodologies shapes the scientific view of how best to look for microbial fossils, both on Earth and on other planets. Finally, a holistic view of biology-Earth interactions allow a better understanding of the capabilities of life, for use in forward modelling or practical applications of space exploration or planetary colonization, amongst others.

1.5 The Torridon approach

The Mesoproterozoic-Neoproterozoic transition, around 1000 Ma, was a critical interval for the evolution of complex eukaryote cells (Knoll et al. 2006). Cellular microfossil Lagerstätten dating from this time are found worldwide in marine sediments, and they can be used to record the appearance and diversification of eukaryotic microfossils. Such remains consist largely of compacted carbonaceous materials in shales, and three dimensional organic structures within cherts. For example, the first widely accepted eukaryotic microfossils appeared in shallow marine to deltaic argillites of the $\sim$1400

Ma Roper Group (Javaux et al. 2001), while later examples of possible red algal affinity have been reported from marine cherts of the ∼1200 Ma Hunting Formation of Arctic Canada (Butterfield 2000).

While such exceptionally preserved remains have been used to chart the diversity of putative eukaryotic cells at this time, various preservational or study biases have limited the documentation of the microbial assemblages. The non-marine Torridonian rocks of northwest Scotland have recently been shown to contain robust evidence for the earliest non-marine eukaryotes (Strother et al. 2011). Phosphatic bands and nodules within the lacustrine sediments have been known to contain a sparsely documented cellular Lagerstätte for over a century (Geikie 1900, Teall 1907). Here the potential of these Lagerstätten deposits is explored, to preserve a varied assemblage of microfossils, including not only the enigmatic eukaryotic forms, but also autotrophic and heterotrophic bacteria, allowing greater insights into ecosystem components at this time.

Previous reports of microfossils from the Torridon rocks have been obtained almost exclusively from acid maceration of grey shales (Cloud & Germs 1971, Downie 1962, 1984, Peat & Diver 1982, Zhang 1982). Such a technique reveals only the more recalcitrant and complete organic structures for study because smaller and more delicate forms may be damaged or lost, resulting in the loss of information. As such, the phosphatic nodules, which preserve the organic structures in virtually uncompressed three dimensional suspension, offer a unique opportunity to study a relatively diverse and well preserved microfossil assemblage.

A large number of morphotypes are preserved in phosphate, and these can range in preservation from almost pristine organic microfossils to extensive carbon dissemination, allowing some assessment of biological degradation processes, as well as an estimation of the relative proportions of eukaryotic and prokaryotic forms in these ambient non-marine assemblages. Some ecological assessment is also made possible within these Torridonian phosphates, owing to the exceptional levels of cellular preservation that the cryptocrystalline mineral structure of the apatite affords. It may also be assisted by the inference of relatively closed ecosystems in these lakes. Phosphatic bands and nodules are found throughout the relatively limited extent of the palaeo-lakes, meaning that microfossils have been recovered across much of

the basin, potentially allowing a wide range of materials and microorganisms to be analysed.

Chapter 2

Geology of the Torridon Group

2.1 Introduction

The Torridon rocks occupy an important revolutionary period in the Proterozoic. Dating to around 1 Ga, they offer the potential to understand much about the biological evolution of oxygenic photosynthesis, eukaryocity, and sexual reproduction. Yet the potential of these ideally dated rocks may only be realised if the rocks themselves are properly understood.

Understanding the original settings of the sedimentary formations is important for putting subsequent fossil finds into context. While the Torridon has been studied with traditional stratigraphic techniques, which reveal the relations between constituent formations in the group (Stewart 2002), little has been done to resolve the intra-formational relationships, especially in the volumetrically small formations (e.g. the Diabaig Formation). Further, metamorphism of sedimentary deposits, disruptive orogenic deformation, or subsequent modern day erosion and contamination can alter or destroy the precious palaeontological records, and thus it is critical to understand the extent of their effect.

Through a combination of large-scale field mapping over the entirety of northwest Scotland, small-scale sedimentological observations at individual outcrops, and high-resolution analysis of collected samples, the depositional conditions and subsequent geological history of parts of the Torridon Group are here revealed in unprecedented detail.

2.2 Geological Setting and Stratigraphy

Rocks of the Torridon Group outcrop along the northwest coast of Scotland, from the Isle of Skye in the south, to Cape Wrath in the north (Figure 2.1). They overlie Archaean to Palaeoproterozoic gneisses of the Lewisian basement, which have a minimum age of 1409 Ma, from K-Ar dating of micas (Fettes et al. 1992). These basement rocks also display a phase of deformation not present in the Torridon, dated between 980 and 999 Ma, indicated by $^{40}Ar/^{39}Ar$ isotopes (Sherlock et al. 2008).

The Torridon Group is divided into four conformable units, from the base upwards, as follows (Figure 2.1): the lowermost Diabaig Formation, dated at 994±48 Ma, using Rb-Sr estimates from the phosphatic nodules (Turnbull et al. 1996); the Applecross Formation; the Aultbea Formation, with a whole rock Rb-Sr age of 977±39 Ma (Turnbull et al. 1996); and the Cailleach Head Formation (Stewart 2002). The whole group reaches a maximum thickness of 6 km onshore, and is unconformably overlain by late Lower Cambrian quartzites of the Eriboll Formation (Cowie & McNamara 1978, Peach et al. 1907).

Around Ullapool and Lochinver (Figure 2.1), the group is underlain by sediments of the Stoer Group (1177±5 Ma from $^{40}Ar/^{39}Ar$ dating on feldspars (Parnell et al. 2011)), which may have equivalents on Skye (Figure 2.1), placed within the Sleat Group (Stewart 2002, Strother et al. 2011). The relationship between these two latter groups remains unresolved because the Sleat Group lies within the Kishorn Nappe on the Isle of Skye which, together with its greater degree of metamorphic alteration, makes understanding its stratigraphic relationship problematic (Stewart 2002).

The Torridon Group as thus defined comprises a wholly clastic sequence of red and grey sandstones and shales that accumulated within a fluvio-lacustrine depositional environment (Park et al. 2003, Parnell et al. 2010, Strother et al. 2011), which is thought to have lain well within the continent of Rodinia, at a latitude of around 42° S, as indicated by palaeomagnetism of haematised magnetite (Buchan et al. 2000). Mineral suites are consistent with a wet temperate environment at this latitude (Stewart 2002).

The Diabaig Formation at the base of the Torridon Group is a well defined lithostratigraphic unit, comprising breccia and coarse sands derived directly from, and

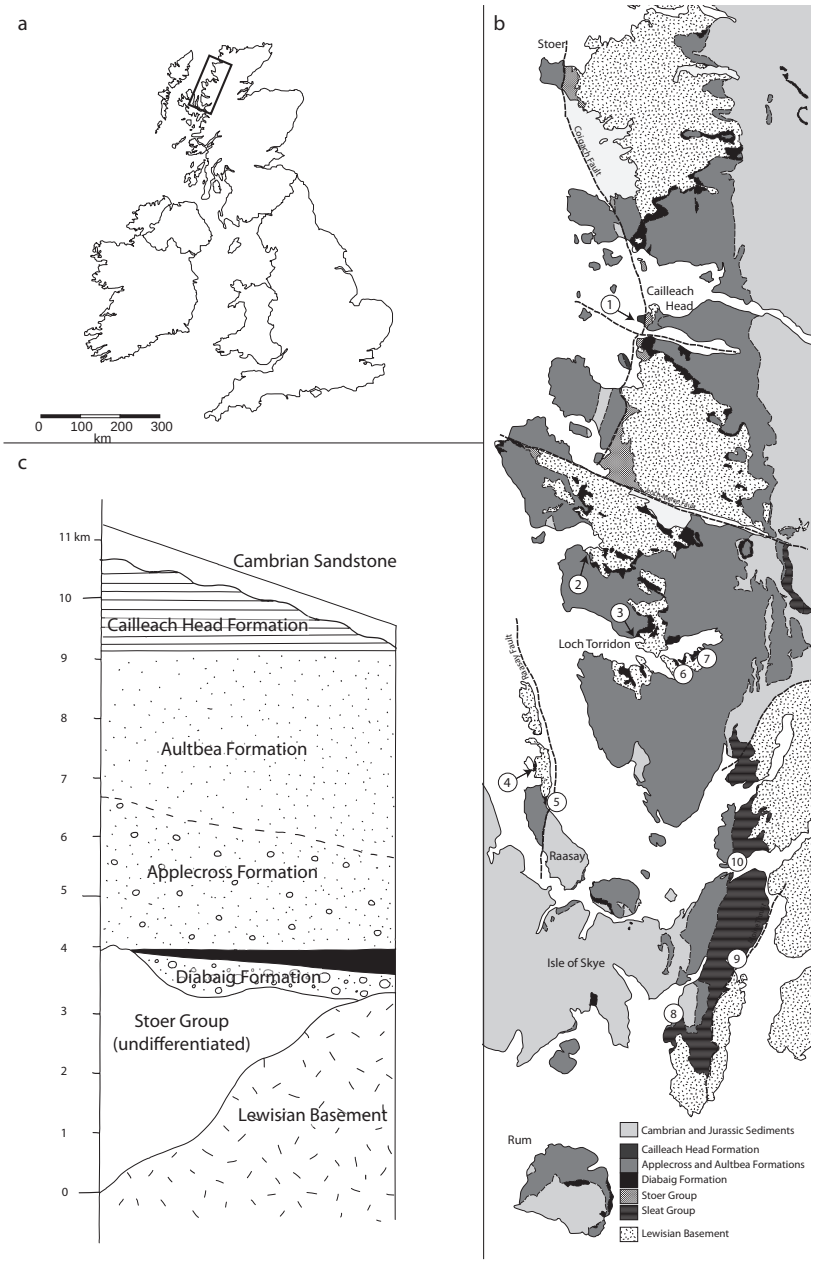


Figure 2.1: Torridon geology. a) Location of the Torridon outcrop with relation to the United Kingdom; b) Simplified geological map of the northwest of Scotland, illustrating formations of the Torridon Group and associated rocks. After (Stewart 2002). Localities studied: 1, Cailleach Head; 2, Badachro; 3, Upper and Lower Diabaig; 4, Fladday; 5, Brochel Castle and Brochel Sheilings; 6, Sheildaig Bay and Peninsula, and North Shieldaig; 7, Balgay River and Shore; 8, Sleat Peninsula West; 9, Kinloch; 10, Kyle of Lochalsh; c) Basic stratigraphy of the Torridon group, showing relationship with underlying Lewisian basement and Stoer Group sediments, and overlying Cambrian sediments. After (Stewart 2002).

infilling large palaeovalleys in the underlying Lewisian gneiss. Upwards within this formation, the sediments become finer grained, culminating in a succession of laterally variable fine red sands and grey shales, rich in phosphatic nodules and bands. The latter unit corresponds to subunit II of the Diabaig Formation *sensu* Stewart (2002). Overall, the Diabaig Formation reaches a maximum thickness of around 115 m, including irregularities above the basal unconformity. The overlying Applecross and Aultbea formations make up the vast bulk of the Torridon Group. The Applecross Formation consists mainly of coarse grained pebbly red sandstone. The overlying Aultbea Formation is finer grained and is mostly lacking in pebbles. Rare argillaceous bands are known to occur in both of these red sandstones. Together, these formations reach a maximum thickness of 5000 m. At the top of the group is the Cailleach Head Formation, which reaches a maximum thickness of around 1800 m and its top is truncated by an angular unconformity beneath Cambrian quartzites of the Eriboll Formation. The Cailleach Head Formation is distinctive for preserving a thick sequence of coarsening upward cyclothems, from grey shales to fine to medium red sandstones. Phosphatic nodules and bands can be found widely within this formation.

Two phases of gentle tilting occurred, first approximately 10 degrees to the west prior to the deposition of the Cambrian quartzites, and afterwards by almost the same amount to the east. As a result, the Torridon rocks today lie more or less vertical, reflecting the position in which they were first deposited nearly a billion years ago (Park et al. 2003).

2.3 A non-marine environment

The majority of sedimentary rocks throughout the entire rock record are derived from marine palaeoenvironments, owing to their great lateral extent, longevity and high sediment flux to these basins. Thus, when encountering a sedimentary succession, it is reasonable to assume it was formed under marine conditions, unless substantial evidence suggests otherwise. This is the case for the Torridon Group of northwest Scotland, making it the earliest verifiable lacustrine basin. The diverse evidence that support such a conclusion is detailed below.

2.3.1 Large scale structural information

The Torridon deposits are rare and especially informative to stratigraphic analysis, in that over the billion years or so since they were deposited, they have undergone very little deformation or regional metamorphosis. Today, we find them in more or less the same stratigraphic and topographic position in which they were first deposited. As a result of this, and the clear landscape unconformity between the Torridon rocks and the underlying Lewisian basement, it should be possible to make reasonable assumptions about the shape and depth of the basin, which may assist in its interpretation as either lacustrine or marine.

It is clear from qualitative mapping of the preserved shape of the basal unconformity (e.g. Stewart 2002) that erosion at the time resulted in a labyrinthine confined water system, as would be seen in an intermontane fluvio-lacustrine system. At this stage, however, interpretation is limited by the western edge of present-day Scotland, where the measurable unconformity disappears beneath the sea. This could be indicative of either sudden sloping away of a land surface onto a terrestrial foreland, or it could reflect a fjord-like setting with narrow valleys linking to the sea across and invaginated coastline, similar to the coastline of Scotland today. While this reconstruction is informative of the local basin geography, which is of use to further palaeoenvironmental reconstructions, it is does not alone provide conclusive evidence of the non-marine nature of the basin. Further, smaller scale sedimentological data are needed.

2.3.2 Small wavelength wave ripples

At several outcrops of the Diabaig Formation and the overlying sandy parts of the transition to the Applecross Formation, symmetrical wave ripples can be found in the sandy and silty lithologies. As well as providing firm evidence for a water depth less than that of the mean wave base, their wavelengths also give some indication of the size of the body of water in which they are formed. Broadly speaking, the wavelength of the ripples depends on the wavelength of the wind-generated wave, which is itself dependent on the fetch across the surface of the water, or the distance they can travel. Wavelengths observed in the Torridon rocks varied from 3 cm to a maximum of 5 cm (Figure 2.2), which is on average smaller than those seen in marine rocks, and can be allied with a small fetch across a correspondingly small body of water. No large waves brought from large marine basins have left their mark on the Torridon sediments.

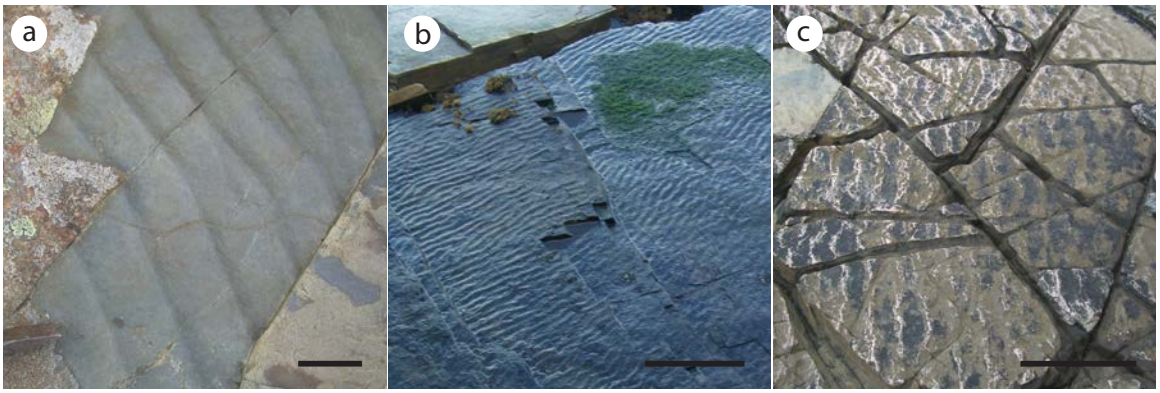


Figure 2.2: Plate illustrating characteristically lacustrine features of the Diabaig Formation. a) Short wavelength wave ripples at Brochel Castle. Scale bar 4 cm; b) Rapidly changing ripple directions at North Shieldaig. Scale bar 50 cm; c) Abundant desiccation cracks with no carbonates or evaporites at Lower Diabaig. Scale bar 20 cm.

2.3.3 Changes in plane-to-plane wave ripple direction

In combination with the above observation that all of the wave ripples seen in the Torridon rocks are small, it must also be noted that the strike, and by extension, the shoaling direction, of these wave ripples sometimes varies substantially between stratigraphically close bedding planes.

For example, in the outcrop at Shieldaig peninsula (Figure 2.2), two bedding planes can be observed: the lower bearing wave ripples that strike NW-SE ; and less than 10 cm above, with ripples striking N-S. Such rapid alternations between strike direction, and therefore wave direction, suggest some factor other than regional and temporally persistent prevailing wind controlling the direction of the waves. It may be that rapid, nearby changes in basin shape result in reflection of waves in differing directions over time, or perhaps variations in the directions of continental winds could cause the observed phenomenon. Either way, the rapid alternation of wave direction from layer to layer is indicative of local influences rather than regional ones, as would be expected for a predominantly continental setting.

2.3.4 Rapid facies changes

Further evidence for the Torridon basin being a confined lacustrine system, though perhaps more circumstantial, is the rapid spatial variation between lithofacies in outcrop. For example, on the isle of Raasay, deep undesiccated mudstones occur at Fladday (Figure 2.1b, locality 4), whereas broad sandy rippled layers are seen at Brochel

(Figure 2.1b, locality 5). Today, these outcrops are less than 2 km apart geographically, and while they may represent slightly diachronous units, there is no major tectonic disturbance between the two facies. Their proximity and the notable differences between their sedimentology, and therefore depositional environment, points towards a small, confined system in which environmental variants are in closer proximity than would be expected for a normal marine shelf environment. Similar juxtapositions of notably different lithofacies are especially visible around the shore of modern day Loch Torridon, with the muddy desiccating shoreline palaeoenvironment of Lower Diabaig closely abutted to coarse sandy deltaic sediments of Shieldaig bay and peninsula.

While these juxtapositions do not necessarily imply a continental setting, they seem to necessitate a confined basin controlled by local geography and devoid of external influences. The facies variations between localities in the Diabaig Formation will be discussed further in this section and Chapter 4.

2.3.5 Abundant desiccation without evaporites or carbonates

One of the most provocative pieces of sedimentological evidence pointing towards a continental setting for the Torridon basin is related to the frequent desiccation found at some of the classic outcrops of the Diabaig Formation. At Lower Diabaig, Shieldaig peninsula and bay, and Brochel, desiccation cracks are common; especially so at Lower Diabaig where cracks are recorded in almost every bedding surface (Stewart 2002). Desiccation is not remarkable in itself, although such a high frequency necessitates a regularly drying environment such as a shoreface. Most notable is the fact that amongst all this desiccation, no evidence of evaporite or carbonate minerals has been found, despite an extensive sedimentological and petrographic search (Figure 2.2). In contrast with this, the unconformably underlying Stoer Group (outcropping around Stoer and Enard Bay in the north of the region; Figure 2.1b) contains extensive carbonate minerals in both desiccating and non-desiccating horizons. This difference is here taken to indicate fundamentally different water chemistry between the two groups: the Torridon lacking the abundant mineral ions that would result in supersaturation-related precipitation of these minerals on desiccation. Such a lack of mineral ions in modern systems would satisfy the requirements for 'fresh water', and so this interpretation is extended to the Proterozoic.

In a similar attempt to assess the water chemistry through mineralogy, Stewart & Parker (1979), measured the boron concentration of authigenic illites of the Stoer

and Torridon Groups. They found concentrations indicative of a non-marine water composition, further corroborating this conclusion.

2.4 Reconstructing ancient palaeoenvironments

Given that sedimentological evidence points towards a fully non-marine setting for the Torridon group, fine-scale sedimentological data were collected in order to better resolve the temporally and spatially variable depositional environments of these rocks. Stratigraphic positions of the formations, and geographical location of the outcrops detailed here can be found in figure 2.1, and are discussed further in Chapter 4.

2.4.1 Torridon Group

Classically, this group, with an onshore thickness of nearly 7 km, has been split into four formations, *sensu* Stewart (2002): the lowermost Diabaig Formation, the Applecross Formation, the Aultbea Formation and the uppermost Cailleach Head Formation. While the broad descriptions of these formations hold in the general case, there is some considerable variation from outcrop to outcrop, and so it is possible to detail variations in non-marine palaeoenvironment. For this study, only and all those outcrops mapped as non-fluvial rocks have been considered, as the primary aim was to map the variation within a lake basin. Considerable variation has been noted between the two lithofacies of the fluvial Applecross and Aultbea Formations (Stewart 2002), but consideration of these environments is beyond the scope of this current study. Localities are detailed below from the lowermost Diabaig Formation, and Uppermost Cailleach Head Formation, as well as the laterally unconstrained Sleat Group.

2.4.1.1 Diabaig Formation

Lower Diabaig Location: N 57° 34' 39.43" W -5° 41' 13.32" to N 57° 34' 40.96" W -5° 41' 21.49" (Figure 2.1, locality 3, Figure 2.4)

On the northern shore of Loch Torridon, just to the north of the hamlet of Lower Diabaig, is a shoreline exposure of fine sedimentary rocks, dipping shallowly (around 10°) to the west. Rocks outcrop for approximately 200 m above the present-day high tide line, exposing around 7.5 m of stratigraphic thickness of the Diabaig formation II *sensu* Stewart (2002).

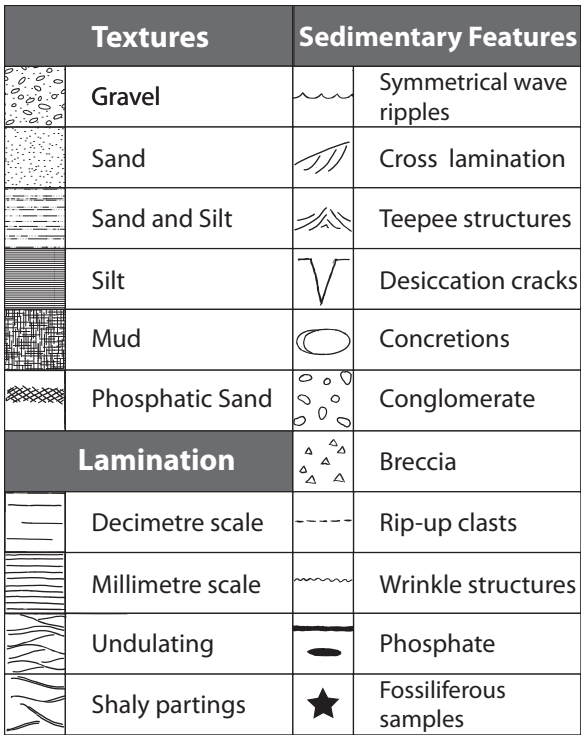


Figure 2.3: Key to sedimentary logs in this chapter.

The outcrop here comprises laminar-bedded fine sands and silts, of a uniform medium grey colour. Occasional decimetre-scale beds of medium sand, with prominent cross-beds also occur. Small wavelength (up to 4 cm) symmetrical wave ripples are abundant, and all units are heavily crosscut by deep and extensive polygonal desiccation cracks. Phosphatic nodules occur in limited areas, as laterally restricted bands and lenses parallel to bedding, near to zones of localised reworking of tabular mud-clasts. Putatively biogenic wrinkle structures occur in abundance in outcrop and in float material; these will be discussed further in Chapter 5.

Such rocks record a quiescent environment with presumably slow deposition of fine, chemically and texturally mature sediment. Sedimentary features are testament to deposition above the fair-weather wave-base, and frequent and periodic subaerial exposure. Such a depositional environment is likely to be found on the shoreline of a lake with fluctuating water levels, possibly related to seasonal changes. Sediment starvation would result in fine sediments settling from suspension, with occasional storms disturbing the sediment and rapidly bringing in beds of coarser, cross-bedded material.

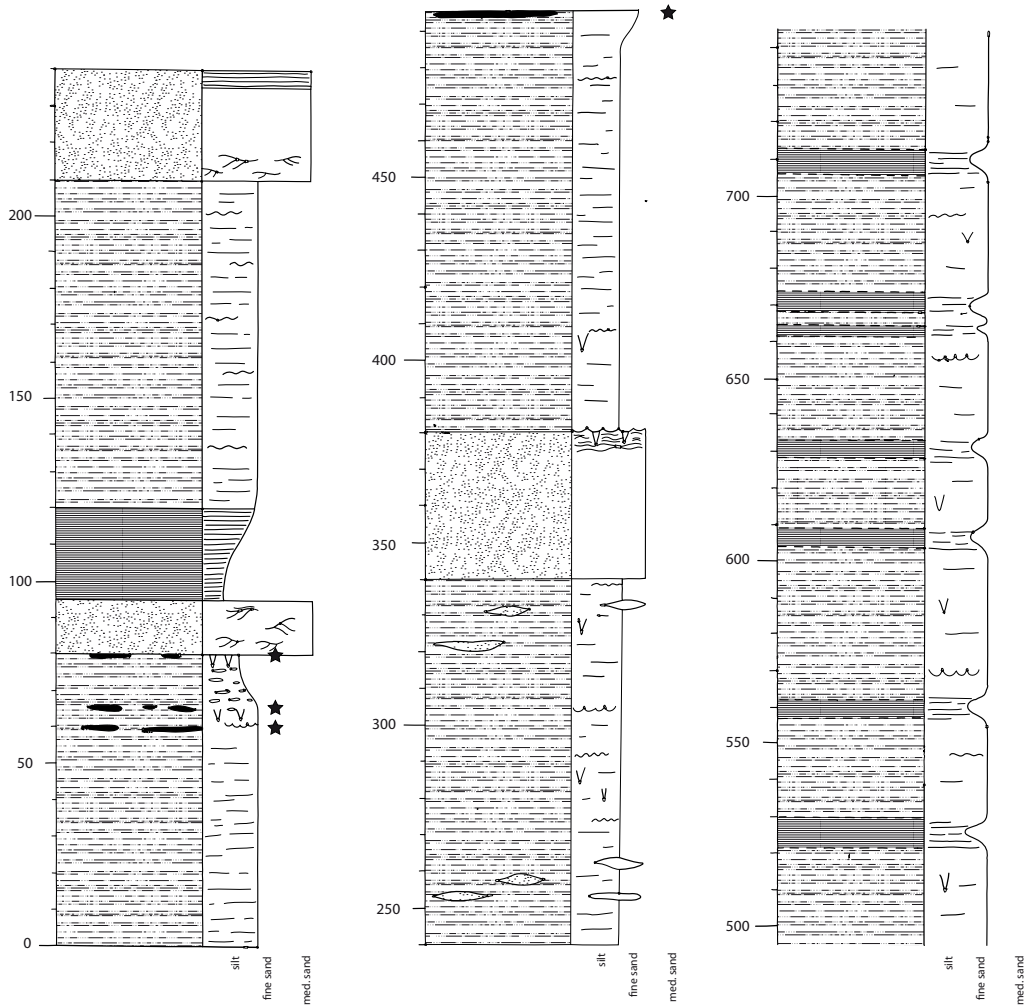


Figure 2.4: Sedimentary log of Diabaig Formation at Lower Diabaig. Height in centimetres.

Upper Diabaig Location: N 57° 34' 43.10", W -5° 38' 55.98" (Figure 2.1, locality 3, Figure 2.5)

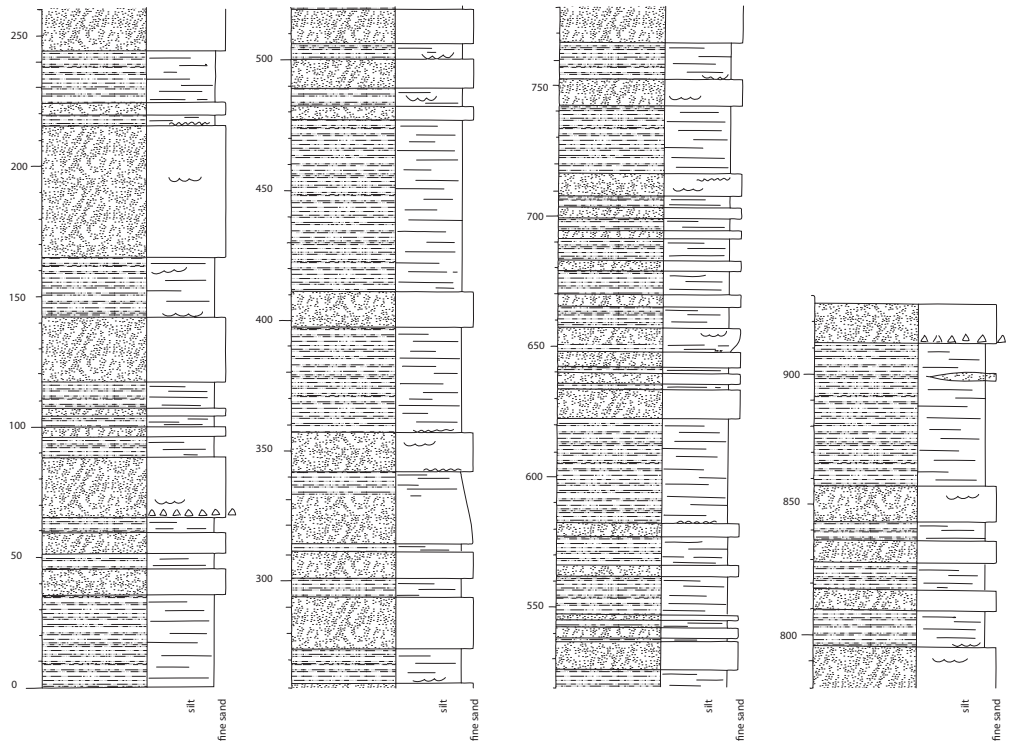


Figure 2.5: Sedimentary log of Diabaig Formation at Upper Diabaig. Height in centimetres.

On the road near the hamlet of Upper Diabaig, at an elevation of around 160 m, at the edge of the freshwater Loch Diabaigas Airde, a cliff exposure of red and grey sandy sedimentary rocks tilts at ∼12 degrees to the west-southwest. These rocks have been mapped as Diabaig Formation II *sensu* Stewart (2002).

The ∼9 m thick section exposes alternating beds of fine sand and silt, forming laterally continuous laminar packages. Centimetre to millimetre-scale laminations are especially apparent in the red silty portions, but greyish sandy units are more or less massive. Sandy units fine upwards, and occasionally coarse gravelly material occurs at their base. Small-wavelength symmetrical wave ripples are abundant; they are observed on bedding plane surfaces and in section. Also notable on the bedding surfaces in specific locations are wrinkle structures of putatively biogenic origin, which are analysed further in Chapter 5. No phosphatic material was recovered from this locality.

Overall grain size here indicates a depositional environment of moderate energy, and sedimentary structures necessitate deposition above the fair weather wave base, but not subaerially exposed. The lateral continuity of beds and lack of current-derived lamination, in combination with the grain size and habit of bedding suggests a zone of relatively low-energy laminar flow. Thus, a general environment of deposition within the mid to distal parts of a clastic delta fan, in shallow water but with moderate sediment input, is proposed for this locality.

Balgy River Location: N 57° 31' 45.51", W -5° 35' 51.90" (Figure 2.1, locality 7, Figure 2.6)

A short river exposure of reddish sandy rocks, on the eastern side of the River Balgy is accessed by footpath from the A896 along the southern shore of Upper Loch Torridon. Exposing almost 4 m of rocks, dipping at 13° to the W, it is mapped as Diabaig Formation II *sensu* Stewart (2002), and is presumed to lie conformably up-section of the shoreline deposit detailed below.

The rocks here are similar in appearance to those seen at Upper Diabaig, but are of slightly coarser grain size. Medium-sandy units fine upwards, are generally massive, and grey in colour. Finer sand beds are red in colour, and contain undulating lamination visible in section, which may be projection of symmetrical wave ripples which are sparsely visible in the few exposed bedding surfaces. Bedding surfaces also display wrinkle structures of putative biological origin that are further discussed in Chapter 5. Petrographically, the rocks are arkosic sandstones, and contain no phosphate minerals.

Overall grain size and the few sedimentological features present suggest a shallow water depositional environment in proximity to a clastic sediment source. Similar to the rocks at Upper Diabaig, these are likely deposited in a mid-fan setting with moderate current energies.

Balgy Shore Location: N 57° 31' 50.5", W -5° 35' 42.82" to N 57° 32' 4.16", W -5° 34' 49.21" (Figure 2.1, locality 7, Figure 2.6)

Stretching along the southern shore of Upper Loch Torridon, from the mouth of the Balgy river to a promontory approximately 1 km to the east, a broken cliff and bedding plane exposure of red sandy rocks occur, which dip shallowly but variably, presumably disturbed by local minor faulting. Approximately 40.5 m stratigraphic

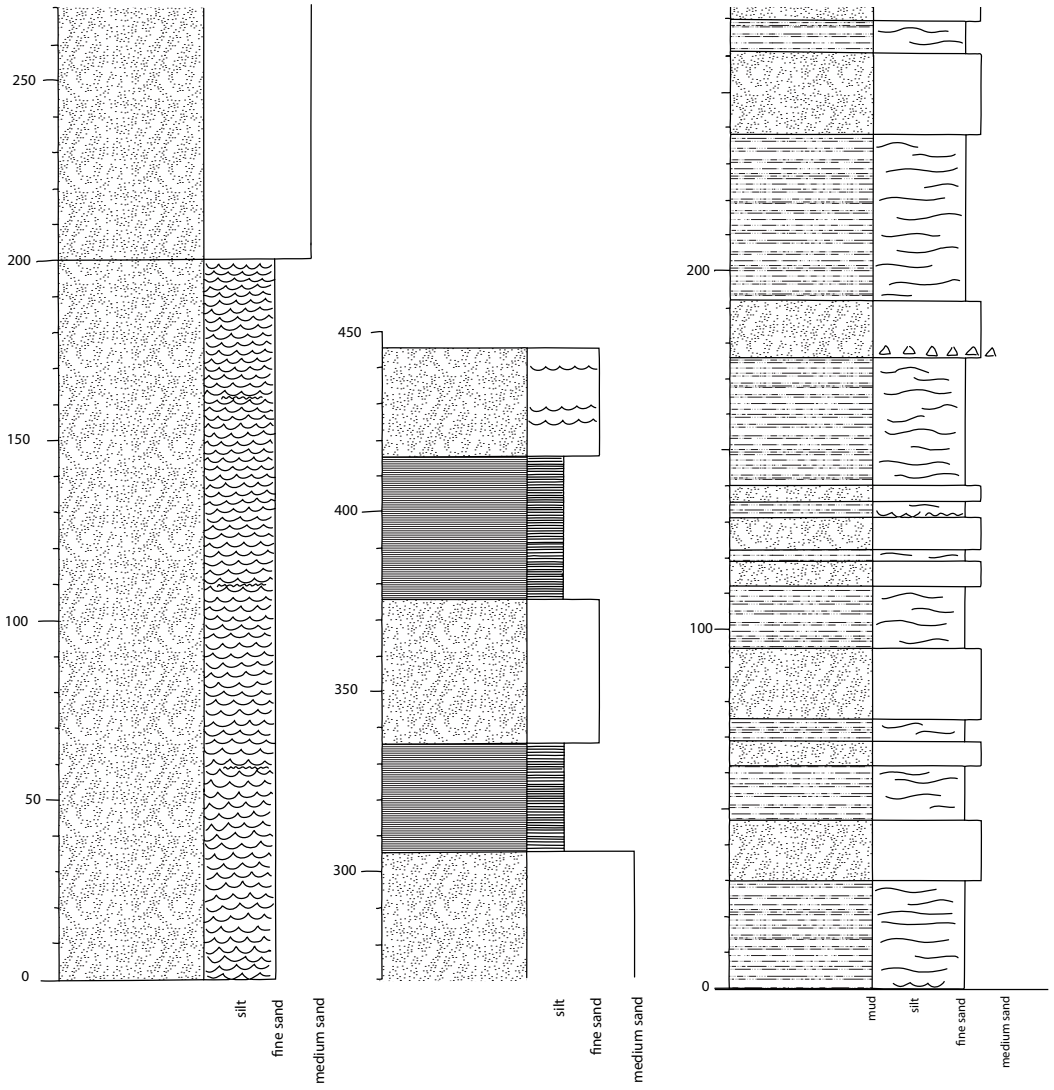


Figure 2.6: Sedimentary log of part of the succession of Diabaig Formation at Balgay Shore. Height in centimetres

thickness of Diabaig Formation *sensu* Stewart (2002) is represented here.

Younging towards the west, the rocks show a broad fining upwards sequence, from coarse cross-bedded red sands at the lowermost, eastern end, through laminar bedded coarse sands, to large units of decimetre-bedded, heavily rippled medium sands with occasional laminar portions and coarser beds. At the westernmost extent, grain sizes drop to fine sand and silt. Sedimentary structures throughout are limited to the extensive symmetrical wave ripples and wrinkle structures of putative biological origin. These wrinkle structures occur predominantly in the fine sediments at the top of the section, and are discussed further in Chapter 5. Chemical composition of the sandstones varies little, comprising arkosic sandstone with a considerable proportion of micas. No phosphatic minerals were found.

The rocks here record a progressive change in depositional regime, from high energy directional currents with input of coarse clastic material, through shallow oscillating wave currents accompanying continued sand input. Upsection, more quiescent conditions permit deposition of finer sediments with low-energy planar lamination. Predominance of wave ripples, combined with the absence of desiccation cracks, indicates an overall submerged depositional setting, which for the most part is above the fair-weather wave base. Upsection variations in grain size and sedimentary textures record a considerable drop in depositional energy, which can be easily allied with increasing water depth and decreasing proximity to a clastic sediment source. The units pass from a current-dominated delta top, through sheet sands, to a quiescent prodelta environment brought about by deepening of the lake basin or migration of the prograding delta.

Shieldaig Peninsula Location: N 57° 31' 46.58", W -5° 37' 17.53" (Figure 2.1, locality 6, Figure 2.7)
On the southern shore of Upper Loch Torridon, to the east of the town of Shieldaig, a small bay is formed by a peninsula stretching from the eastern part of the embayment. On the northern margin of this peninsula, a cliffside outcrop of Diabaig Formation II *sensu* Stewart (2002) exposes around 2.5 m of red sandstones.

Thinly bedded sandstones here consist of laminar units ranging in grain size from coarse to fine, with a noticeable fining or deepening trend. Despite their laminar habit, the coarser sandstone units contain abundant symmetrical wave ripples of

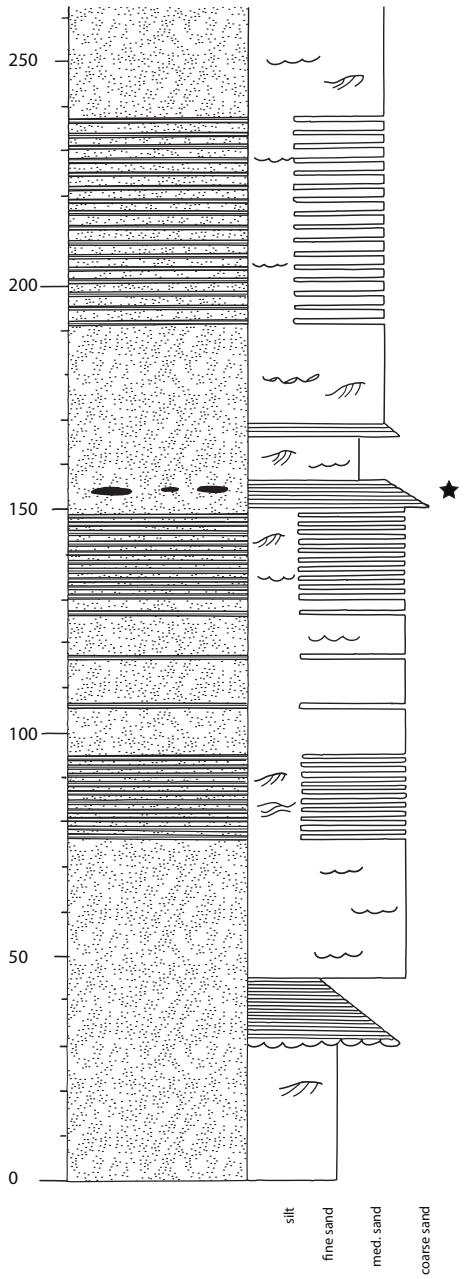


Figure 2.7: Sedimentary log of Diabaig Formation at Shieldaig Peninsula. Height in centimetres.

short wavelength, as well as small-scale cross-bedding; planar lamination is rare but also notably present. Chemically, these rocks are subarkosic arenites. Small lenses of phosphatic material were found in one horizon, confined to the base of a medium grained unit with planar lamination.

The rocks here are testament to an energetic depositional environment above the fair weather wave base with alternating wave-dominated, and current-dominated regimes. Planar lamination in this setting is most likely due to high energy laminar flow. Such a setting may be found in a delta-top, where small scale variations in water level and distributary position bring about rapid changes in depositional regime.

North Shieldaig (Fish Farm) Location: N 57° 31' 54.29", W -5° 36' 44.99" (Figure 2.1, locality 6, Figure 2.8)

To the north of the peninsula described above, on the eastern shore of the embayment in Upper Loch Torridon, a series of bedding plane and cliff section outcrops expose a complex succession of grey-red sandstones and silts, mapped as Diabaig Formation II *sensu* Stewart (2002). Lying conformably beneath the section exposed on the peninsula (described above), around 6 m of more or less horizontally bedded rock is logged in a cliff section, accessed to the northern side of nearby fish farm launch ramp.

At its lowermost extent, the exposure here somewhat resembles that of Shieldaig Peninsula, comprising reddish coarse to fine sandstones with cross-lamination, but at this locality symmetrical wave ripples are lacking. Planar lamination is prevalent and discontinuous bands of coarse sand are frequently interbedded with more massive medium sandstone. Upsection, very coarse jasperitic material occurs in thin horizons, followed by grey-coloured silt units, before massive medium red sand resumes. Chemically, the sediments represented here are more exotic than those seen elsewhere, including abundant feldspathic material and some lithic fragments. Phosphatic bands and lenses occur on several horizons, but are in many places impure, with a rough sandy texture and pale colour.

The predominantly coarse grain size of this outcrop, combined with the channel-like discontinuous beds, indicate a high-energy current-dominated depositional setting, such as a delta top with frequent distributary channel incursions. Planar lami-

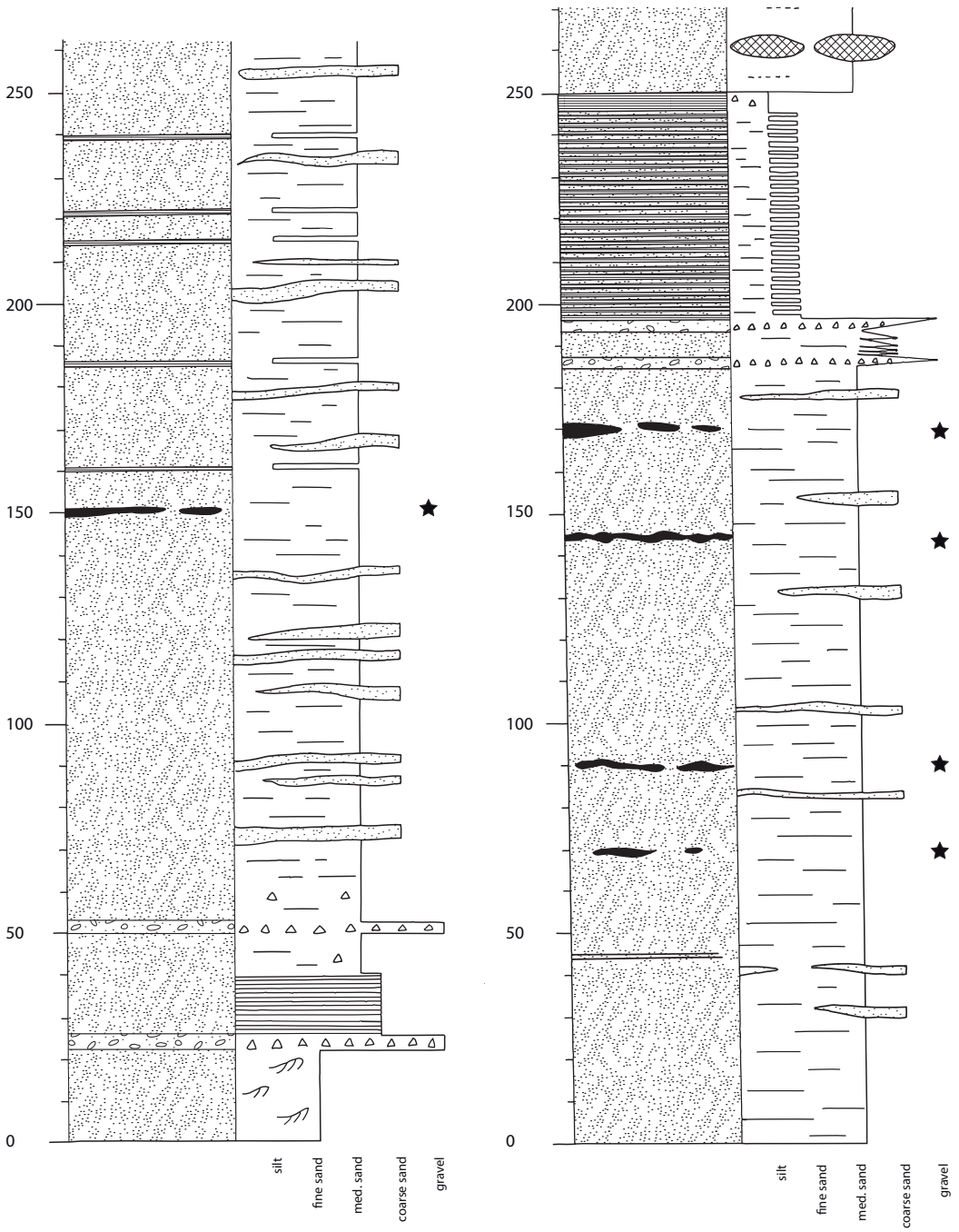


Figure 2.8: Sedimentary log of Diabaig Formation at North Shieldaig. Height in centimetres.

nation here may therefore be a result of high-energy laminar flow, or may represent quiescent periods of slow deposition between channel flows.

Shieldaig Bay Location: N 57° 31' 14.35", W -5° 37' 16.96" (Figure 2.1, locality 6, Figure 2.9)

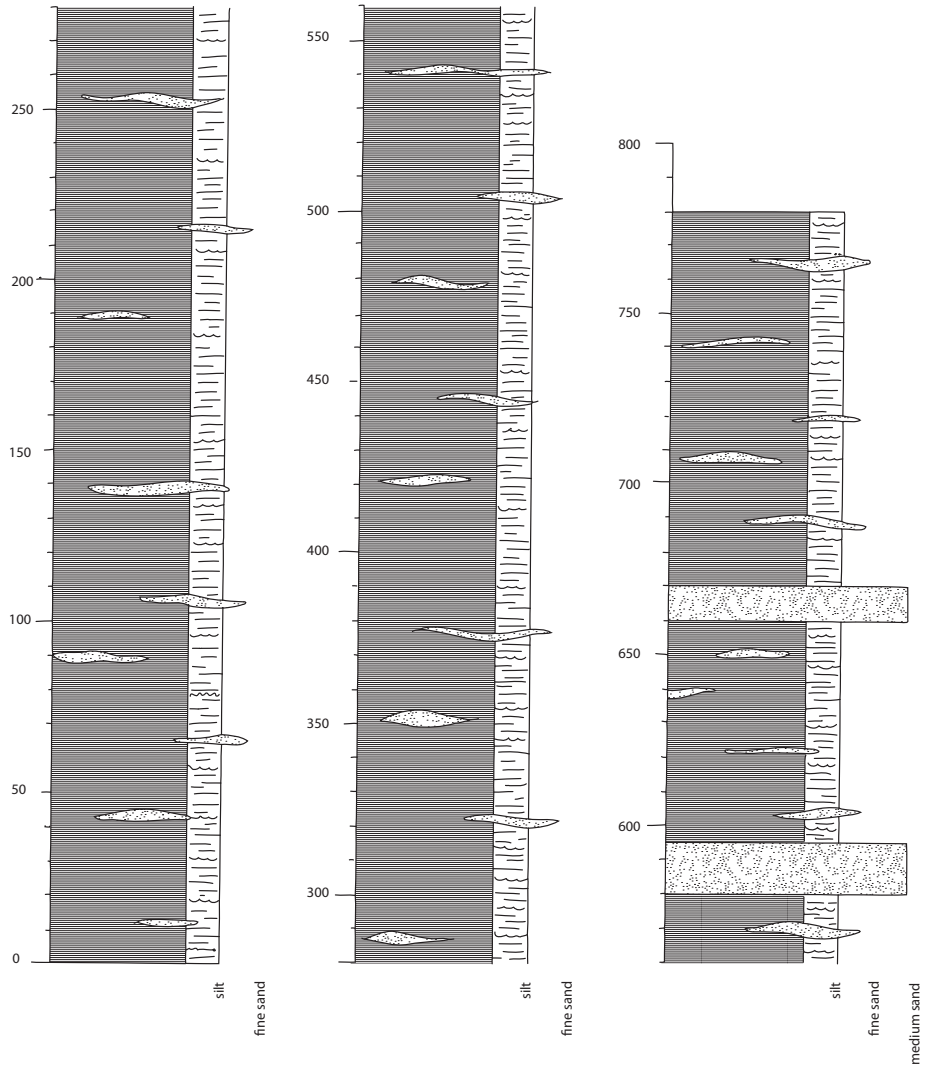


Figure 2.9: Sedimentary log of Diabaig Formation at Sheildaig Bay. Height in centimetres.

At the southernmost extent of the embayment in the southern shore of Upper Loch Torridon, near the town of Shieldaig, a small cliff of red siltstone outcrops on the side of the A896. Exposing approximately 8 m thickness, the rocks here are mapped as

Diabaig Formation II *sensu* Stewart (2002).

The outcrop is fairly homogenous in habit, consisting of predominantly planar laminated red silts, with discontinuous lenses of sandstone occurring periodically. Where bedding planes are exposed, symmetrical wave ripples of short wavelength are seen, and wrinkle structures of putative biological origin are found in nearby float of the same lithology. These will be discussed further in Chapter 5. Chemically, the silt-sized rocks appear to be sub-arkosic arenites, and no phosphate was recovered from this section.

Symmetrical wave ripples indicate deposition above the fair-weather wave base, but the overall fine grained nature of these rocks and their predominant planar lamination point toward a more quiescent distal setting, where sediment input is generically low, except for rare incursions by sandy channels. A distal delta-fringe environment is thus inferred.

Badachro Location: N 57° 41' 35.50", W -5° 43' 7.94" (Figure 2.1, locality 2, Figure 2.10)

On the southern shore of Loch Gairloch, a low cliff exposure of horizontally bedded grey shales and sands outcrops along the road leading to Badachro, just after it crosses the river Eas Bad a' Chrotha. Representing approximately 6.5 m of stratigraphic thickness, the rocks are mapped as Diabaig Formation II *sensu* Stewart (2002).

The exposure here comprises a homogenous sequence of fine sands and silts, dark grey in colour and containing unvarying planar laminations. No ripple marks or desiccation cracks are observed, but wrinkle structures of putative biological origin occur toward the top of the section. These are discussed further in Chapter 5. Chemically, the rock comprises mostly silt-sized quartz in a clay matrix, but in places bands and nodules of dark black phosphate, weathering white, are apparent.

The uniform small grain size of these rocks and the lack of any sedimentary structures indicating water motion or exposure suggest a very quiescent depositional setting. The chemical maturity of the sediments is also testament to a low-energy regime, such as may be found in deep water below the wave base and at a considerable distance from sediment sources.



Figure 2.10: Sedimentary log of Diabaig Formation at Badachro. Height in centimetres.

Fladday Location: N 57° 28' 46.82", W -6° 1' 17.86" (Figure 2.1, locality 4, Figure 2.11)

At the northern end of the island of Raasay, accessed by a narrow land bridge exposed at low tide, the small island of Fladday contains rocks of Diabaig Formation II *sensu* Stewart (2002) and the Applecross Formation. An outcrop of the former forms a large cliff section on the eastern margin of Fladday, exposing at least 2.5 m of horizontally bedded grey siltstones and sandstones.

The exposure here comprises mainly homogenous, planar laminated siltstones of dark grey colour, but in its lower portion small laterally discontinuous sandy lenses and flasers occur, along with a few decimetre-scale sand beds containing prominent cross-lamination. No ripples, desiccation cracks or wrinkle structures are present within this succession. Clay minerals and silt-sized quartz form the bulk of the rock, but in places thin bands and thick nodules of phosphate occur, displacing the laminae above and below.

Homogenous fine grained laminae lacking in sedimentary structures are here suggestive of a quiescent environment like that seen at Badachro, below the wave base and distal to clastic sediment input. It is apparent however, that currents did episodically affect these rocks, resulting in the deposition of the rare sandy units and flasers, but quiescent low-energy deposition was rapidly resumed. Such a phenomenon may be caused by storm disruption of a nearby deltaic system, or by the migration of occasional rogue distributaries.

Brochel Castle Location: N 57° 26' 31.34", W -6° 1' 34.99" to N 57° 26' 22.92", W -6° 1' 38.05" (Figure 2.1, locality 5, Figure 2.12)

To the northeast of the island of Raasay, near the homestead and ruined castle of Brochel, a large but broken exposure of sedimentary rocks occur, mapped as Diabaig Formation II *sensu* Stewart (2002). Across a stretch of shore around 400 m long, a stratigraphic thickness of approximately 44 m outcrops, dipping shallowly but variably towards the southwest.

At the lowermost extent of this outcrop, coarse red sandstone with boulder sized lithic clasts directly overlies Lewisian Gneiss. There follow at least three broad fining-upwards packages, in which massive units of coarse to medium-grained red sandstone with large-scale cross- and channel-bedding pass upwards into finer units of silt-sized

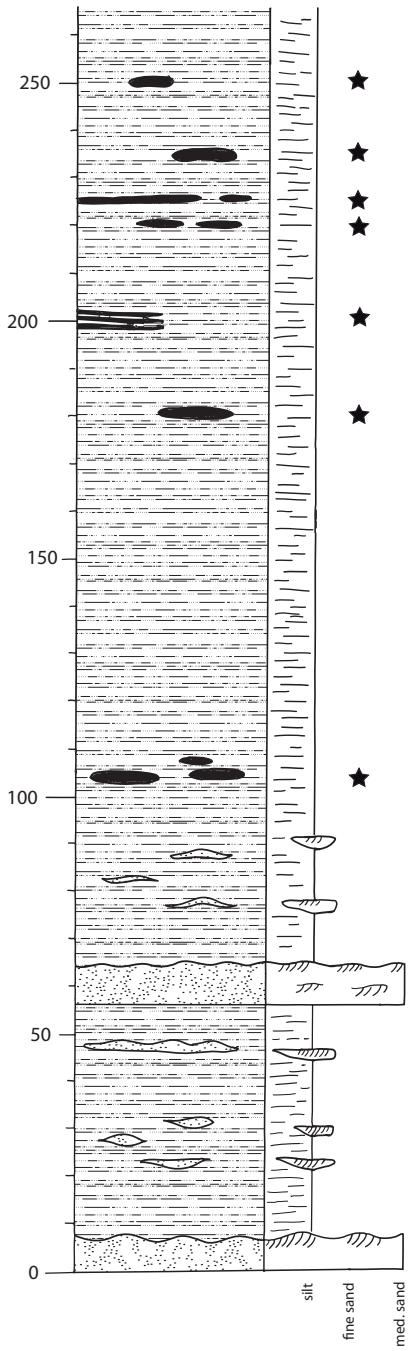


Figure 2.11: Sedimentary log of Diabaig Formation at Fladday

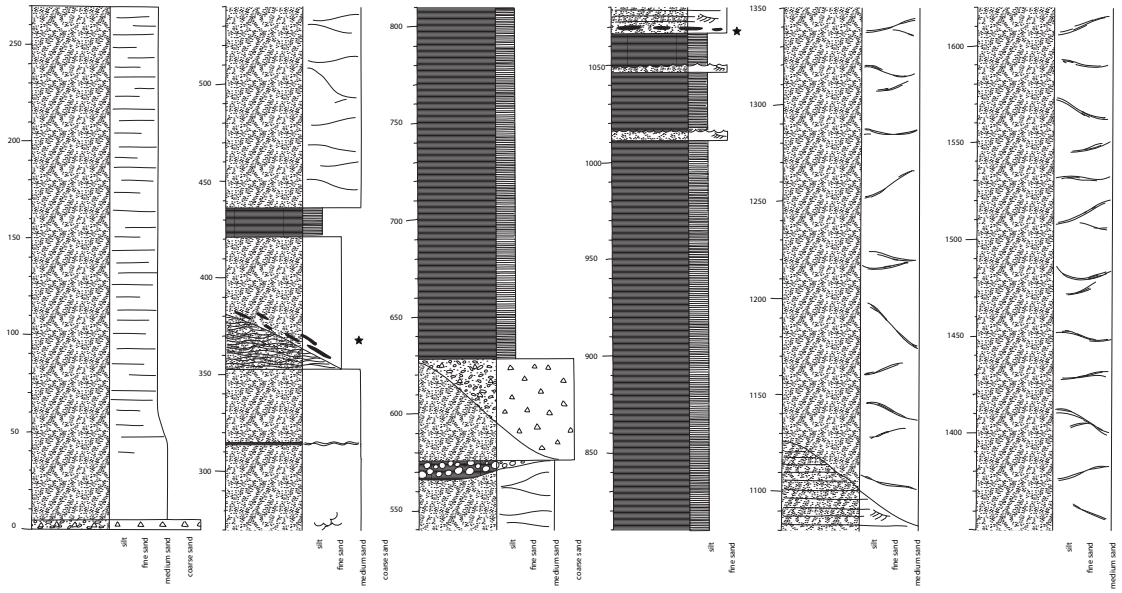


Figure 2.12: Sedimentary log of part of the exposure of Diabaig Formation at Brochel. Height in centimetres.

material, which is grey in colour and is dominated by planar laminations. These general trends are in places interrupted by smaller-scale interbeds of silt or sand, the latter often containing prominent cross beds or ripple marks. Where exposed on the surface, ripple marks are predominantly symmetrical and of small wavelength, up to only 4 cm. In some of the finer sandy units, wrinkle marks occur, whose putative biological origin is further discussed in Chapter 5. Chemically, the bulk of the rock comprises an arkosic arenite, although the finer successions contain higher proportions of clay minerals, and the lowermost part of the exposure has numerous lithic fragments. Phosphatic material also occurs ripped up in tabular clasts at the base of some sandy units, and as undulating laminae within a fine sandy horizon.

The broad fining upward cycles seen at this locality record an overall trend of decreasing current energy, and thus of increasing water depth. The base of each cycle is deposited under relatively high, directional current energies, with complex cross-cutting channel structures, and is characteristic of a delta top receiving high sediment fluxes. Upwards in the section, channel structures are lessened, and oscillating wave action becomes dominant. Such a regime is likely to be found at slightly greater depths and at greater distance from the sediment source at a delta front. At the top of each cycle, fine grained sediment is deposited under a low-energy regime, largely

undisturbed by wave or current motion. Such a regime is to be found beneath the wave base, some considerable distance from sediment sources, on a delta fringe. Repetition of these cycles indicates several episodes of deepening in the basin, followed by rapid shallowing with little accompanying erosion.

Smaller-scale variations in the overall deepening cycles represented here are testament to the temporal and lateral variation commonly present in a dynamic system. The type and habit of deposited sediment may be affected by high-energy storm events, by the migration of sediment-carrying channels, or by the short term—perhaps seasonal—changes in water depth.

Brochel Sheilings Location: N 57° 25' 59.91", W -6° 1' 53.92" (Figure 2.1, locality 5, Figure 2.12)

On the northeastern shore of Raasay, around 700 m to the south of the southernmost extent of the outcrop at Brochel castle, a small cliff outcrop of red-grey sandstones dips at approximately 5° to the southwest. Mapped as Diabaig Formation II *sensu* Stewart (2002), it presumably lies conformably above the deepening-upwards cycles exposed at Brochel castle. The outcrop is accessed by a wide forestry track descending from the road near Raasay Forest, to a shingle beach; the outcrop is to the south of the beach.

Over 4 m of rock are exposed here, and resemble the finer sandy horizons of the Brochel Castle outcrop, comprising massive units of fine to medium-grained sand, with undulating laminae reminiscent of poorly defined wave-ripples. These units are interbedded with laterally discontinuous lenses of coarser sand. Towards the top of the section, the unit becomes coarser and cross-cut by large channel structures, apparently marking the beginning of a further fining upward cycle. On one horizon within the finer sands, a peculiar macrostructure occurs, consisting of centimetre-sized pits exposed on a micaceous bedding surface. The fine scale structure of this feature, as well as possible modes of its formation, is discussed in Chapter 5. Chemically, the rock is a subarkosic arenite with relatively high proportions of muscovite. No phosphate minerals were found.

On the basis of the relatively scarce sedimentological data available from this outcrop, and when considered alongside the broad trends of the nearby Brochel Castle exposure, the depositional setting for these sedimentary rocks is proposed as a delta

front. Alternations between wave-dominated and current-dominated water motion may result in the undulating bedding, and moderate energy levels are necessary to transport the medium- to fine-grained sand.

2.4.1.2 Cailleach Head Formation

Cailleach Head Location: N 57° 55' 32.34" W -5° 24' 9.13" to N 57° 55' 34.16" W -5° 24' 13.22" (Figure 2.1, locality 1, Figure 2.13)

The Cailleach Head Formation, stratigraphically at the top of the non-marine Torridon Group, outcrops at only one locality in the northwest of Scotland, at the western tip of Cailleach Head itself, almost directly west of Ullapool, and accessed by boat or cross-country along the length of the peninsula. It is faulted into place here by the Coigach fault, so its contact with the underlying Aultbea Formation is not visible. The rocks of Cailleach Head Formation dip steeply at an angle of 50° to the south-southeast, and are exposed for around 1 km along the shore of the peninsula. The succession has been logged in some detail by Stewart (2002), recording up to 15 coarsening-upwards cyclothem packages; the uppermost of which have been mapped in finer detail in this study.

Packages begin with an undulating erosional base, followed by metre-scale beds of planar laminated mudstone or siltstone, interbedded with thin units of fine sand. Upwards, these fine sand units become thicker and more frequent, until they are dominant and the silt and mud disappear. In these fine sandy units bedding is still predominantly laminar or sometimes undulating, and sometimes slumped into complex folds and lodes. On the top surfaces of these horizons, symmetrical wave ripples of wavelength 3 cm often occur. Within these sandy units, and in those interbedded with the lower siltstones, phosphate occurs infrequently, draping the troughs of wave ripples, forming wispy undulating laminae, or as rip up clasts at the base of sand beds.

Further upsection, the sandy units become thicker and more massive, and planar lamination is lost, or is replaced by larger scale cross-bedding. Phosphate minerals and wave ripples are no longer apparent at these levels.

The changes in depositional regime recorded by these small scale sedimentological observations are concurrent with the general inference of periodic delta progradation and subsequent deepening made from the entire sequence (Stewart 2002). The finest-grained sediments are deposited under deep quiescent settings, distal to the sediment

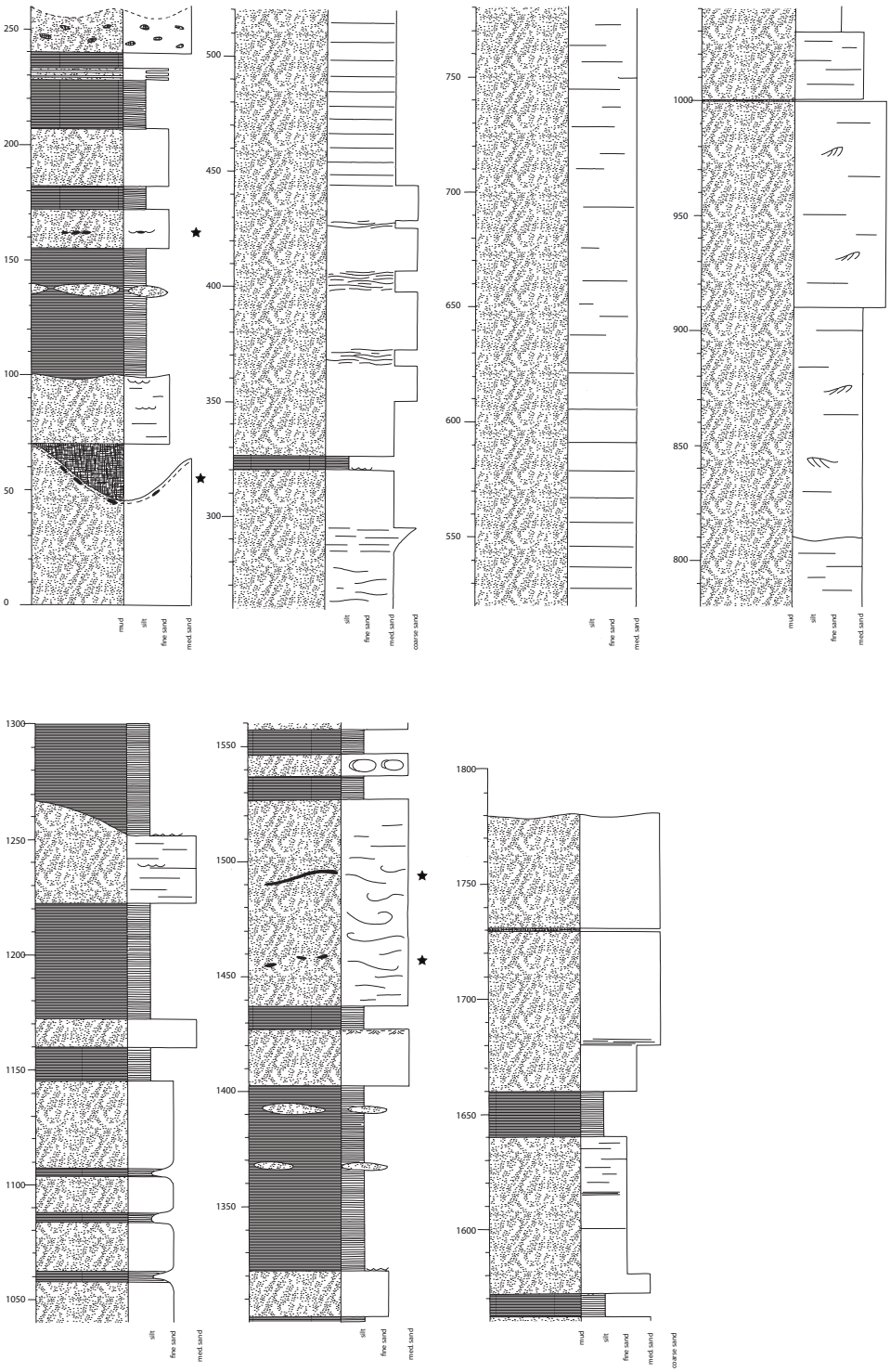


Figure 2.13: Sedimentary log of part of the exposure of Cailleach Head Formation at Cailleach Head. Height in centimetres

source. Then, as deltas prograde into the basin these muds and silts are overlain first by sheet sands that are affected mainly by oscillating wave currents, and then subsequently by coarser delta-top sediments, whose sedimentary structures are governed by current action. Deepening of the lake waters results in some erosion of these uppermost sandstones, before low energy deposition of texturally mature sediments resumes.

2.4.1.3 Sleat Group

Kinloch, Sleat Peninsula East Location: N 57° 10' 22.71", W -5° 47' 41.70" (Figure 2.1, locality 9)

At the north eastern edge of the Sleat Peninsula on Skye, on the shore to the south of the Kinloch Lodge hotel and among the forestry tracks 100 m above the shore, are scattered outcrops of grey-black sandstones and siltstones, which are mapped as Kinloch Formation, Sleat Group. The outcrops here form no continuous loggable succession, and dip varies considerably from around 15° to the east at the shore, to vertical, striking southwest-northeast at higher relief.

On the shore, large boulders weather smooth and medium grey, and are composed of interbedded sandstones and siltstones, the latter containing abundant undulating laminae weathering black. Transitions between units are sharp and often erosional, with tabular rip-up clasts deposited in the lower portions of coarser units. Sandstone beds contain faint cross-bedding and slumped laminae, but sedimentary features are masked to some extent by notable shearing and deformational strain of the rock.

Small scattered outcrops along the forestry tracks above the shore expose coarser sedimentary rocks: grey grits and decimetre-bedded sandstones of primarily quartzose composition. Centimetre-scale horizons amongst these sandstones are occasionally dark in colour and weather white, containing small quantities of dispersed phosphate.

From the scattered outcrops and scarce and deformed sedimentary features, a depositional setting can only be tentatively interpreted for these rocks. Fine grained layers are laid down under low-energy regimes, which are periodically disturbed by higher-energy incursions which erode and rework underlying layers, depositing rip-up clasts and coarse gritty layers. Such alternations may be brought about by changing water depth and/or position of delta systems, but without a continuous succession of rock it is not possible to trace the history of these changes.

Sleat Peninsula West Location: N 57° 7' 56.96", W -5° 58' 24.54" (Figure 2.1, locality 8, Figure 2.14)

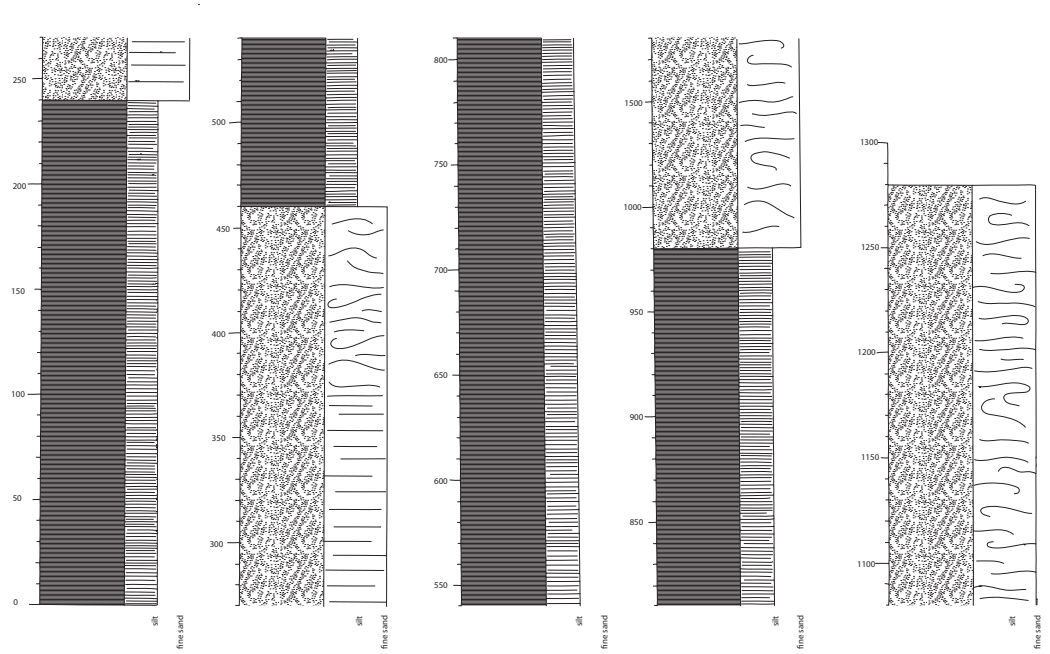


Figure 2.14: Sedimentary log of Kinloch Formation, Sleat Group at Sleat Peninsula West. Height in centimetres.

On the western side of the Sleat peninsula, just to the south of the hamlet of Tokavig, a succession of grey sandstones and siltstones is exposed on the shore, dipping steeply at 60° to the east. These are mapped as Kinloch Formation, Sleat Group (British Geological Survey 1976), and approximately 13 m of stratigraphic thickness is exposed.

The rocks here comprise alternations between pale grey fine-grained sandstone with decimeter-scale planar laminations, which are often distorted in large synsedimentary slumps, and medium grey siltstone with uniform millimetre-scale planar lamination. Boundaries between these packages are sharp, but not obviously erosional. No ripple structures, desiccation cracks or other sedimentary structures are readily apparent. It is clear that the rocks here have undergone deformational stresses, as evidenced by a faint cleavage parallel to lamination within the siltstones, so this must be considered a factor in masking sedimentological data.

Sparse data permit only a tentative interpretation of depositional environment, based only on variations in grain size and lamination. On this basis, the rocks seem to record alternations between a low-energy regime, beneath the wave base, and a higher energy setting with rapid deposition of sands on potentially unstable substrates, allowing their slumping. Such settings may be allied with a prograding deltaic model as before, accounting for periodic deposition of sheet sands at the delta front.

Kyle of Lochalsh Location: N 57° 16' 50.88", W -5° 42' 20.14" (Figure 2.1, locality 10, Figure 2.15)

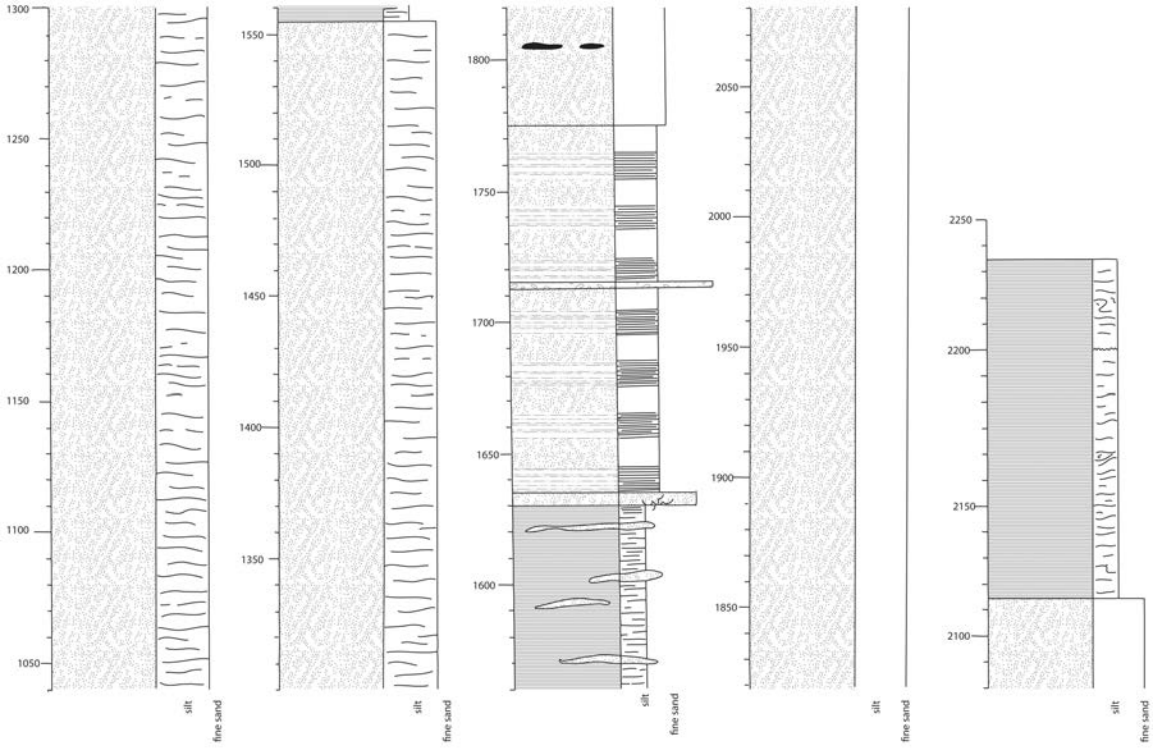


Figure 2.15: Sedimentary log of Kinloch Formation, Sleat Group at Kyle of Lochalsh. Height in centimetres.

Less than 1 km to the east of the town of Kyle of Lochalsh, a large cliff exposure of Kinloch Formation, Sleat Group, occurs along the northern side of the A87. A stratigraphic thickness of at least 22 m of dark coloured sandstones and siltstones dip vertically, striking north-south.

The rocks here have been heavily influenced by deformational stresses, and a cleavage runs more or less parallel to bedding, potentially obscuring small-scale sedimen-

tological details. Primarily, the exposure consists of medium- to fine-grained sandstones in broad upward-fining cycles. Massive, unbedded medium sandstones form the base, grading into fine sandstones with decimeter- to centimeter-scale undulating bedding and occasional symmetrical wave ripples. Further upsection, a sharp but non-erosional boundary marks a change to fine sand-silt alternations with millimeter-scale planar laminations. Initiation of a new cycle is marked by an erosional boundary and thin gravely layers at the base. Overall, the rock may be chemically described as an arkosic arenite, with large proportions of feldspar and micas—although subsequent greenschist facies deformation has resulted in the growth of chlorites amongst the polymictic sandstones. Some sandy-phosphatic material occurs in bands and lenses at the bases of coarser sandy beds.

Despite the low-grade metamorphism of this unit and the scarcity of good sedimentological structures, the general pattern of deposition here may be compared with that seen at Brochel Castle on Raasay. Upward-fining cycles record successive drops in energy, and thus an increase in water depth as depositional setting varies from current-dominated delta top, through wave-dominated delta front, to quiescent distal fringe environments. Rapid shallowing and increases in energy are marked by erosion and deposition of coarse sediments at the base of each new cycle.

2.5 Reassessing a classic stratigraphy

2.5.1 The Diabaig basin

The sedimentary features described above from the finely mapped units of the Torridon and Sleat groups show considerable variation from locality to locality. Within the Diabaig Formation in particular, there is significant variability in the depositional environments inferred from sedimentology. Given that previous reconstructions of the stratigraphic thickness of the Diabaig Formation reach a maximum of ∼300 m (Stewart 2002), such variations in environment cannot be accommodated solely by trangressional and regressional changes over time. Instead, the depositional environments may be used to argue for the preservation of a laterally variable lake basin, containing spatially separated regions of high and low clastic input, and differing water depths and current energies. An idealised reconstruction of such a lake basin is shown in Figure 2.16, with environments ranging from a desiccating, sediment-starved shoreline of Lower Diabaig, to the deep quiescent environment at Badachro, and the

high water energies and depositional rate of the delta-top at North Shieldaig.

Reconstruction of such a variable lake basin is important for the understanding of the Torridon palaeoenvironment, as well as its constituent biota, as differing conditions may be expected to favour different kinds of organisms, and different preservational conditions. This will be investigated further in Chapter 4. In addition, the recognition of such fine scale detail in an ancient lake basin is the first of its kind, and shows the resolution possible with optimal conditions of deposition, metamorphosis, and sampling. It is possible that elsewhere within the Proterozoic or Phanerozoic record such basins are also preserved, and should be sought to further enrich our knowledge of palaeo-lacustrine environments.

2.5.2 Relationships of the Sleat Group

The generally accepted and mapped stratigraphy splits the Torridonian Supergroup into the unconformably related Torridon, Stoer and Sleat Groups. The Torridon Group, described above, consists of a weakly metamorphosed sequence of fluvio-lacustrine rocks (Stewart 2002). The Stoer Group, lying unconformably beneath the Torridon, comprises a variety of sedimentary rocks of nearshore marine or lagoonal origin (Stewart 2002). The Sleat Group is found around the Isle of Skye, and appears to be fault bound, thus its relationship with the Torridon and Stoer Groups is unresolved. It is, however, metamorphosed and sheared to a greater degree than seen elsewhere, leading some to interpret it as a localized metamorphosis of either the Torridon or Sleat Groups.

Following the detailed sedimentological analyses carried out through the Torridon and Sleat Groups, it is here suggested that the metamorphosed Sleat Group is primarily derived from the Torridon Group, on the basis of the similarity in mineralogy and texture between the constituent Kinloch and Diabaig Formations. Despite the obvious shearing and growth of chlorite concurrent with greenschist metamorphism, the mapped units of Kinloch Formation at the type locality of Kinloch show striking similarity to the planar laminated fine sandstones and siltstones of the Diabaig Formation at Lower Diabaig. Variability to the sandstone units on the western shore of the Sleat Peninsula, and the coarse sandstones at Kyle of Lochalsh, is further concurrent with the lateral variability in depositional regime of the Diabaig Formation described above.

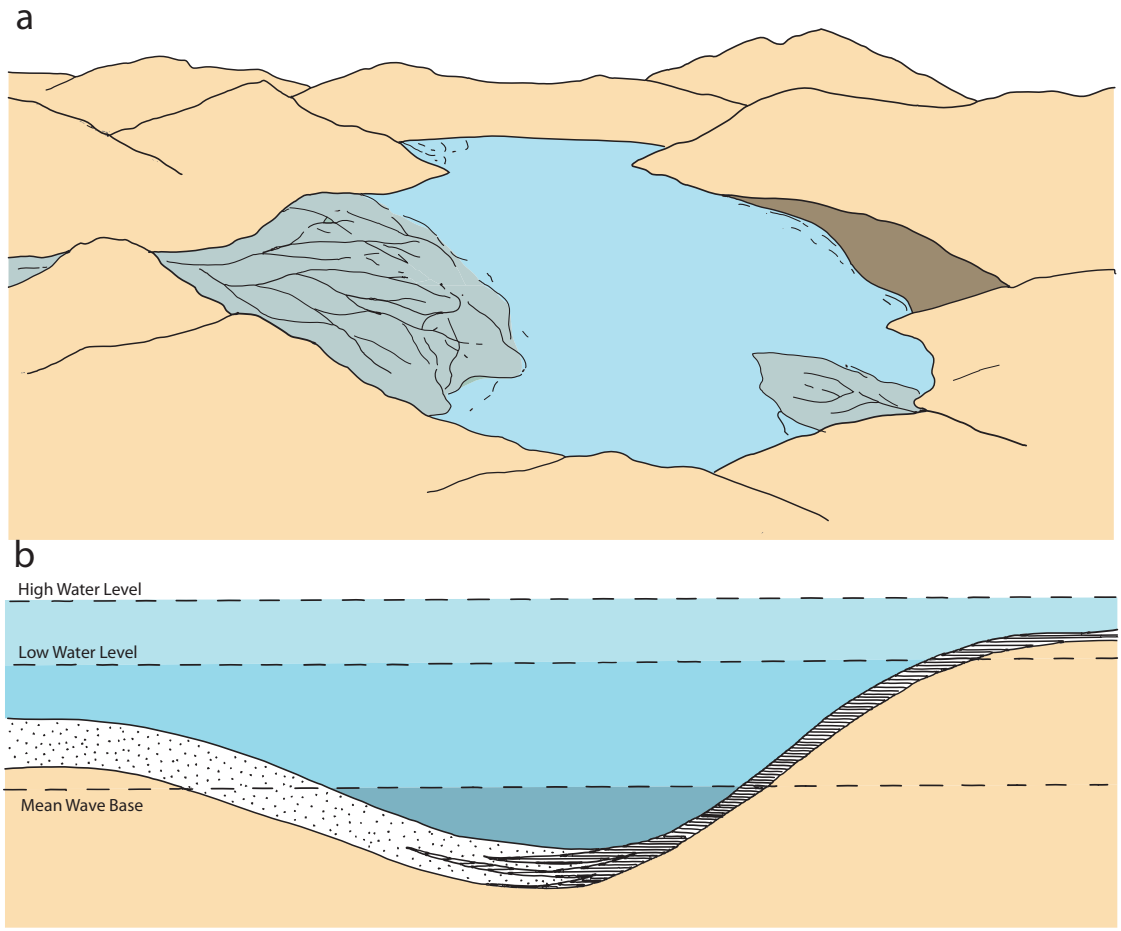


Figure 2.16: Schematic reconstruction of the Diabaig basin from sedimentological data of differing lithofacies. a) Illustration of idealised of intermontane lake basin with prograding siliciclastic deltas, and distal desiccating shorelines; b) Idealised transect through lake basin, with clastic-fed and muddy regions occurring above and below the mean fair weather wave base.

Sedimentological characterization of the Kinloch Formation has shown that it represents a sheared and slightly metamorphosed (to greenschist facies) variant of the Diabaig Formation, Torridon Group. Taking post-depositional deformation into account, these mapped units can therefore be of further use to understanding the deposition and later tectonic disruption of the Torridon lake system.

Chapter 3

Taxonomy of Torridon microfossils

3.1 Overview and previous reports

Microfossils were first reported from the Torridonian Group in phosphatic lenses (Geikie 1900), and were rudimentarily figured in the seminal work on the Scottish Highlands by Peach and Horne (Teall 1907). Since that time, with rare exceptions (Peat & Diver 1982), study of the microfossils preserved within phosphate has been neglected. Organic remains and microscopic carbonaceous compressions have been extensively reported from the grey shales of the Stoer, Aultbea and the Applecross formations (Cloud & Germs 1971, Downie 1962, 1984, Naumova & Pavlovsky 1961, Zhang 1982). These shale-hosted organic microfossils are flattened to a considerable degree, and lack secondary mineralisation. They can be imaged only after extraction by acid maceration, which exerts further damage on the delicate and partially degraded structures. Only one formal taxonomic treatment has been attempted on these shale-hosted fossils to date (Zhang 1982), and their study only as compressed residues with historical imaging and analysis tools has precluded any useful evolutionary interpretation.

The phosphate-hosted microfossils consist of carbonaceous structures suspended within a matrix of amorphous sedimentary phosphate, in a manner that loosely resembles that seen in many Proterozoic chert microfossil assemblages, as in the Bitter Springs chert (Schopf 1968) and the Gunflint chert (Barghoorn & Tyler 1965). They differ from more familiar 'phosphatised' cellular deposits, such as those containing early Cambrian soft tissues (Brasier 1990) or Doushantuo-type assemblages of Ediacaran age (Xiao et al. 1998) in that the original organic matter of the Torridon cells remains well preserved within an apatite matrix, rather than being pseudomorphed by apatite. They also differ from 'Doushantuo-type' preservation (*sensu* Brasier et al.

2010) in that they are not extractable from a host carbonate by acid maceration, since no such carbonate matrix is present.

3.2 Justifying biogenicity

As with any discovery of ancient microfossils, verification of their antiquity and biogenicity is necessary before acceptance and further analysis. Given the extreme age of the Precambrian deposits, and the diminishingly small preservation potential of these forms, the null hypothesis, which must be accepted unless sufficient evidence proves otherwise, is that any organic or mineralized structures are formed by abiogenic, rather than biogenic processes.

In striving to disprove this null hypothesis, multiple lines of evidence, from differing fields of observation and analysis, are necessary to add cumulative weight to a non-null conclusion. While the nature of the null hypothesis means that it may never be fully disproved, sufficient evidence to the contrary increases the probability of a biogenic mode of formation for any described structures.

In this particular case, accepting the organic structures found within the Torridon phosphate as billion-year-old microfossils requires a threefold verification process. Firstly, it must be demonstrated that the structures are autochthonous to the rock. Secondly, that they are not formed by abiogenic processes, and do in fact represent the fossils of ancient organisms. And thirdly, that the structures' morphologies are representative of the original morphology of the organism, or that the taphonomic and degradational sequence can be recognized. As is discussed below, these three stages of verification are dependent on one another, and the evidence in support of them becomes more tenuous with increasing inference.

3.2.1 Organic structures are autochthonous to the rock

This stage in the verification process is intended to demonstrate that the structures are not contaminants, whether introduced recently or at some point in the rock's geological history. Samples of sedimentary phosphate and shale have been prepared and analysed in several different ways: preparation by petrographic and biological thin section, acid maceration, slicing by focused ion beam; and analysis by optical microscopy, BSE imaging with EDX analysis, secondary electron imaging, TEM imaging, and Raman spectroscopy. In all of these preparations and analyses, organic

structures are recognizably of a consistent size and morphology, indicating that the structures are not contaminants introduced by a particular preparation method, or artefacts of a particular type of analysis.

When thin sections are observed under the optical light microscope, the structures are all found occluded by and completely surrounded by the cryptocrystalline phosphate matrix. They are distributed evenly and randomly throughout phosphate, and to some extent shale, not being confined to cracks or particular horizons. Thus, there is no mechanism by which the organic structures could have been introduced at a later date; they must have been trapped within at the time of formation. As it is possible to directly date the authigenic phosphate (Turnbull et al. 1996), it is possible by extension to precisely date the organic structures within it.

If the organic structures were trapped within the rock at the time of its formation, it is expected that the organic material will have undergone the same diagenetic and metamorphic changes as the rocks themselves. The thermal and diagenetic history of the organic structures can be measured semi-quantitatively through observation of the colour of macerated acritarchs and comparison with the Thermal Alteration Index of Pearson (1984). The structures macerated from the shales and phosphate have a light to dark brown colour, which indicates low to moderate burial-related alteration (Staplin 1982). Further information on the post-diagenetic history of the organic structures can be revealed from Raman spectroscopy of the structures in situ. As figured in Figure 3.10, and discussed further in this chapter, the Raman maps of the Torridon structures show a pronounced G band, consistent with a pervasive graphitization of organic material, caused by burial heating. It is worthy of note that these methods can also be used to address the possibility that the structures are in fact more ancient than the Torridon sediments, having been reworked from older sediments or sedimentary rocks. If the thermal maturation or characteristic Raman spectra are not consistent with the host rock in which they are now found—specifically if the structures show more extreme alteration—then it is possible that they have a more ancient history. In this particular case, however, the diagenetic alteration of the structures most accurately matches the thermal burial history of the Torridon rocks themselves.

Additional evidence to support syn-depositional autochthony, as opposed to reworking of previously deposited fossil material from the underlying Stoer Group or

elsewhere, comes in the form of the taphonomy and diversity of the assemblage itself. As will be discussed in subsequent sections and chapters, the Torridon assemblage has suffered a significant, but not extreme amount of taphonomic damage. The fact that some fossil specimens are preserved pristine qne three-dimensional is evidence against multiple phases of reworking and transport. In addition, while the fossil assemblage contains many taxonomic components seen in contemporary marine deposits, there are notable deficiencies, particularly in so-called 'marker' taxa (Sergeev 2009). Thus, the Torridon fossils represent a subsample of the global Proterozoic diversity, which would not be expected from wholesale reworking of marine deposits.

The observations made above are strong evidence to support the conclusion that the structures are autochthonous to the lacustrine rocks, sharing in their antiquity and slight diagenetic and burial alteration. Having established their age and provenance, it is next necessary to demonstrate their biogenicity.

3.2.2 Organic structures are formed by biogenic processes

This stage of the verification process is necessary to demonstrate that the organic structures observed inside the Torridon phosphates and shales are not byproducts of abiogenic processes, that they were created by controlled biological growth or excretion, and that they represent true microfossils.

Preparation by thin section allows viewing of the organic structures by optical microscope, and in these images the organic material appears as continuous membrane which is capable of competent deformation and even fracturing. High resolution imaging by FIB-TEM resolves these membrane structures as homogenous or layered carbon-rich coherent laminae. When these rocks are prepared by acid maceration (see process in Appendix A), the organic structures remain as coherent membranes that retain their overall shape but are flexible, forming new folds and wrinkles as they are prepared for imaging (e.g. Figure 3.16c). The existence of these structures as competent and flexible membranes that retain their structure after dissolution of the rock matrix rules out the possibility that the vesicle-like morphologies are formed coincidentally by the agglomeration of dispersed carbon particles. No abiogenic process is known to create competent membranes such as those observed in the Torridon preparations.

In comparable deposits of questionable biogenicity, putatively biogenic structures have been shown to be created by the concentration of organic material at the margins of relatively large quartz crystals (Brasier et al. 2002, 2006), being swept along by a crystallization front. High resolution imaging of the Torridon examples by FIB-TEM shows the relationship between the extremely tiny crystals of the matrix and the organic membranes (Figure 3.12). Crystals occur on the inside and the outside of the organic structures and do not cross-cut them, however the gross morphology of the vesicle structure is too large to be affected by these randomly oriented crystals. Texturally, it appears that the orientation and growth of the matrix is governed by the preexisting organic structure, rather than the structure being created by the crystals. This known abiogenic mode of formation can therefore be discounted.

Other novel analysis methods may also be employed to verify the biogenic nature of the organic structures. Laser Raman spectroscopy can be used in two dimensions to create maps of bonding structures within the rock. As seen in Figure 3.10 and 3.11, and expanded on by Schweizer (2008), these data can be combined to reveal information about the construction of the biological material. In this instance, the ratio of the carbon D band (disordered kerogen) to the carbon G band (graphitised carbon) is indicative of partially ordered carbon, deliberately constructed in biological processes (Schweizer 2008). Carbon D/G maps (Figure 3.10 and 3.11) mirror the morphology of the organic structures precisely, providing good evidence that their formation was a biogenic one.

Overall, the morphologies of the organic structures, ranging from tubular structures to sheathed clusters of spheroidal vesicles, together occupy a level of complexity of structure known to be occupied by biology in the living world today (Brasier et al. 2006). These forms lie in a discrete morphological domain between the complete random disorder of high entropy physical systems, and the strict symmetry of efficient ordered structures like crystals. The moderate irregularities in morphology of the organic structures are also characteristically biological, rather than purely physical in origin. Morphological differences may be conferred by variations in ontogeny or taphonomy, and would not be expected from uniform abiogenic processes.

In addition, fine-scale detail of the morphology, ornamentation, and ultrastructure of these organic membranes is visible at all scales of magnification, but is especially revealed by high resolution SEM and TEM imaging. These details, such as striations,

granular texture, or multilamellated membranes, are features that are not known to be readily produced by abiogenic processes, but are common in biological cell wall construction. Thus for these features, a biogenic origin is most likely.

The lines of evidence presented above make a strong case for the organic structures found in the Torridon phosphate and shale being formed biogenically, being true microfossils. Further analyses that could support this conclusion, but which have not been carried out as part of this study include measurement of stable isotopic values of the organic carbon itself, as well as of the associated minerals. Extremely light fractionations of carbon in the structures in themselves, or large sulphur fractionations in accompanying sulphides in particular are signatures of biological action.

Sedimentary phosphates of the Torridon rocks would also be good candidates for searching for accompanying molecular fossils, in the form of algal or bacterial biomarkers. Certain molecular components of microbial cells are particularly resistant to decay, leaving behind characteristic hydrocarbon skeletons that would not only add weight to a conclusion of biogenicity, but may also hint at the types of organisms represented. The phosphatic nodules provide an ideal medium for preservation of these molecular fossils, as rapid occlusion of the organic structures presumably also involved trapping and isolation of their chemical compounds, with little opportunity for later loss or contamination.

3.2.3 Microfossils preserve original morphology

While relatively simple to objectively demonstrate that the organic structures within the Torridon phosphates and shales are true ancient microfossils, the question of how representative the fossil morphology is of the original organism is a little more difficult to address, requiring more inference and subjectivity. The nature of microbial fossil preservation is such that some alteration is inevitable. Understanding this alteration is ongoing however—continuous comparison of microfossil structures with other representatives of Precambrian age, as well as with modern and Phanerozoic forms, can add to the database of original and taphonomically modified fossil features.

The key to complete understanding of post-death changes to microfossils lies in a comprehension of the taphonomic processes acting upon microbial structures. Recent experimental and observational studies have begun to document processes of decay

and preservation in a wide range of organisms both macroscopic (e.g. Briggs & Wilby 1996, Gostling et al. 2009, Sansom et al. 2010), and microscopic (Gostling et al. 2008, Raff et al. 2008, 2006). Comparing the results of these studies to features of ancient preserved microfossils currently gives some quantitative evaluation of fossil modification, allowing by extension the reconstruction of an unaltered ancient organism.

In these studies, analysis of an entire population or even consortia of microfossils, as opposed to a single form, is invaluable. Features unanimously possessed by a population are more likely to represent original detail of the fossil morphology, although it is still possible that features could be produced across a population by a particular type of preservation, such as compression. To differentiate between these two possibilities, modern experimental degradation studies like those carried out by Raff and others (2008, 2006) can give some indication of the range of alteration features. In addition, comparison between different populations within a diverse community can be used to shed light: if different morphotypes in a community have the same characteristic feature, then it is likely to be preservational in origin, but if only one population possesses it then it may be considered original. It is important to note in these comparisons that preservational processes do not exert a symmetrical bias on presence versus absence of fossil features, and caution should be taken when interpreting the absence of a feature as a notable character (Knoll et al. 2007).

Interpretation and reconstruction of preserved microfossils remains problematic, and for this reason a more in depth study of taphonomic effects on organic-walled microstructures has been carried out, creating semi-quantitative indices of alteration to allow objective assessment and comparison between microfossil assemblages. This 'taphospace' approach is outlined and implemented with the Torridon microfossil consortia in Chapter 4.

3.3 A preliminary form taxonomy

The following discussion on Torridon form taxonomy is published in Battison & Brasier (2012), for which the entire analysis and writing was completed by the present author.

A formal taxonomic treatment of the Torridonian phosphate-hosted microfossils has yet to be carried out. Many of the taxa may be comparable with material referred

to as *Torridoniphycus lepidus* Zhang, macerated from the grey shales of the Aultbea Formation (Zhang 1982). However, a much greater diversity of forms is revealed within the phosphate. Below, we provide an informal classification that distinguishes morphotypes on the basis of broad appearance, and whose relative and absolute abundances can be estimated to give an impression of the overall diversity.

All the microfossils described herein consist of at least a single, more-or less continuous membrane composed of organic carbon (Figure 3.1). The numbers and opacity of these membranes vary between fossils, and it is here assumed that this represents an original compositional variation of the wall structure. At a first approximation, these wall structures can be distinguished on their translucency. Some have opaque walls that appear dark brown, while others have lighter brown translucent walls, through which underlying structures may be seen. This is inferred to be an original feature, since any thermal maturation of the organic matter would affect all the structures equally. Generally, the more opaque walls appear to be rigid, and the more translucent walls appear to be flexible and easily folded.

Morphologically, we find that the Torridonian cellular microfossils can be accommodated within four principal architectural types: isolated coccoids, clusters of coccoids, non-septate filaments, and septate-filaments.

'Isolated coccoids' range in shape from spherical to ellipsoidal, with a maximum elongation ratio of 1:3.5. Maximum dimensions of single coccoids reach 450 μm in diameter, with a mean of 16.1 μm and a large standard deviation of 18.5 μm.

'Clusters of coccoids' include spherical and ellipsoidal coccoidal cells, which may or may not be surrounded by a single external membrane. Maximum dimensions of clusters are 130 μm along long axis, with a mean of 38.5 μm and a standard deviation of 27 μm.

'Non-septate' filaments include empty tubular sheaths with no internal divisions or constrictions. Occurring most often as short broken fragments, these can reach a length of more than 100 μm. Diameters are notably bimodal. The smaller forms have a mean diameter of 3.4 μm diameter, with a standard deviation of 1.6 μm, while the larger forms have a mean diameter of 14.3 μm, with a standard deviation of 6.1 μm.

'Septate filaments' are much rarer. Cell walls of these forms comprise oblong cells, approximately twice as long as wide, separated by straight partitions. A bimodal size distribution is seen, with modal diameters of either 1.5 μm or 12.5 μm.

Morphological differences between microfossils plus notable differences in wall opacity can be used to define eight morphotypes, into which the majority of the phosphate-hosted Torridon Group assemblage can be informally be assigned: ICD, ICL, CCL, CCD, NFL, NFD, SFL, and SFD (Table 3.1). Further morphological features of use to delineate form taxa include: the presence and location of dark internal bodies within the microfossils; the presence and number of extra external membranes; and the nature of any splits or breaks in the membrane surface. While more than 150 form taxa could be defined in this way, many are likely to be little more than taphomorphs. We therefore, focus here upon the eight main morphotypes outlined in Table 3.1, and whose typical members are shown in Figure 3.1.

Morphotype	**Cellular Architecture**	**Wall Opacity**
ICD	Isolated Coccoid	Dark
ICL	Isolated Coccoid	Light
CCD	Cluster of Coccoids	Dark
CCL	Cluster of Coccoids	Light
NFD	Non-septate Filaments	Dark
NFL	Non-septate Filaments	Light
SFD	Septate Filaments	Dark
SFL	Septate Filaments	Light

Table 3.1: Salient characteristics of the informal morphotypes

A detailed survey of morphological diversity and disparity was carried out using 15 polished thin sections of richly fossiliferous phosphate from both the Diabaig and Cailleach Head formations. Within the sedimentary phosphate, the organic structures can occur at high densities, with up to 35 discrete fossils per 1 mm of transect (200 μm wide). In total, 1235 microfossils have so far been recorded and assigned to the above described form taxa.

As shown in Figure 3.2, the most abundant forms comprise isolated coccoids (77%), both light-walled and dark-walled varieties, although the dark walled structures appear to be twice as common. Assuming no taphonomic bias, this is taken to reflect an original predominance of such simple forms. Analyses of the sizes of these

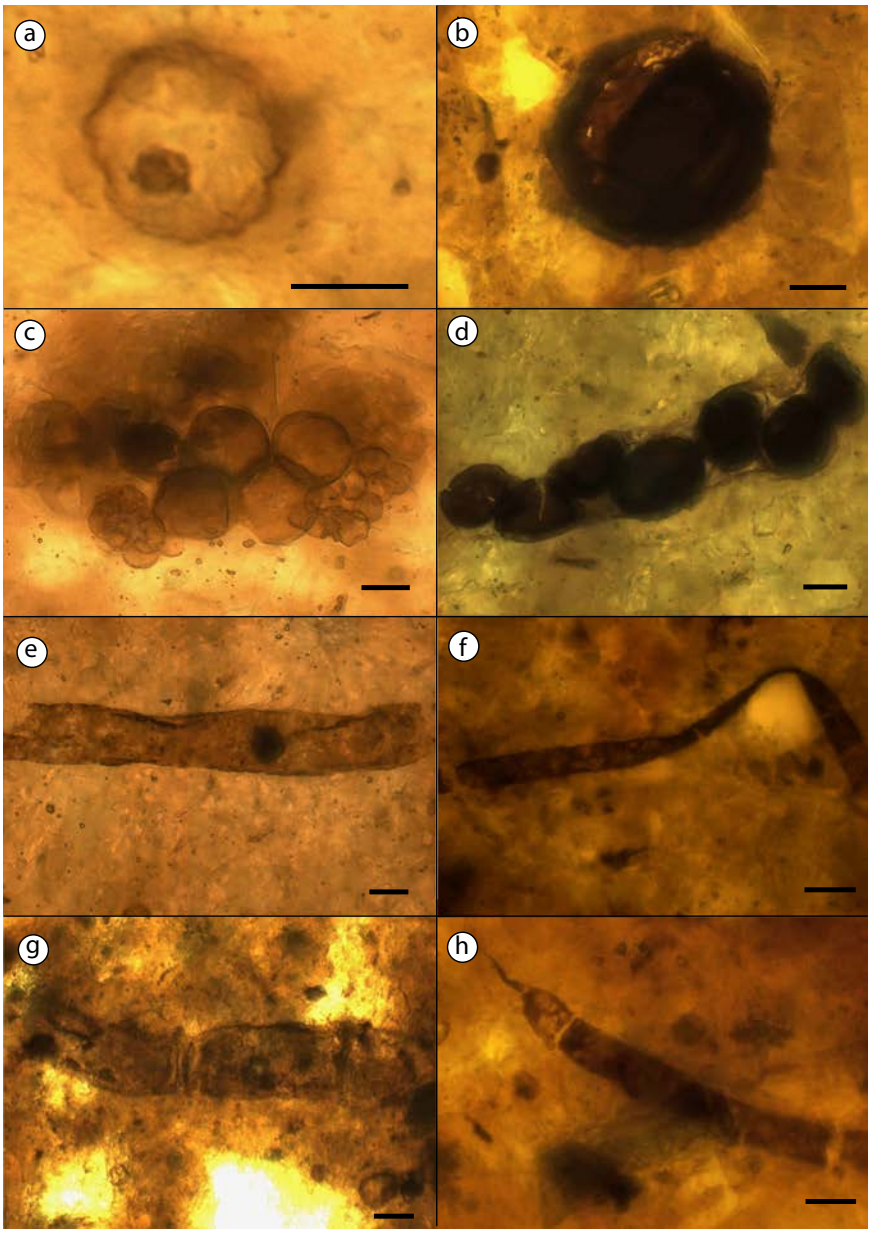


Figure 3.1: Photomicrographs to illustrate the eight informal morphotypes established herein. a) Microfossil grouped as ICL, from phosphate in the Cailleach Head Formation. Sample CAI-2d from Cailleach Head; b) Microfossil grouped as ICD, from phosphate in the Diabaig Formation. Sample DIA-13d from lower Diabaig; c) Microfossil grouped as CCL, from phosphate in the Cailleach Head Formation. Sample CAI-2d from Cailleach Head; d) Microfossil grouped as CCD, from phosphate in the Cailleach Head Formation. Sample CAI-7b from Cailleach Head; e) Microfossil grouped as NFL, from phosphate in the Cailleach Head Formation. Sample CAI-2d from Cailleach Head; f) Microfossil grouped as NFD, from phosphate in the Diabaig Formation. Sample DIA-13a from lower Diabaig; g) Microfossil grouped as SFL, from phosphate in the Cailleach Head Formation. Sample CAI-2f from Cailleach Head; h) Microfossil grouped as SFD, from phosphate in the Diabaig Formation. Sample DIA-13a from lower Diabaig. All scale bars 10 μm.

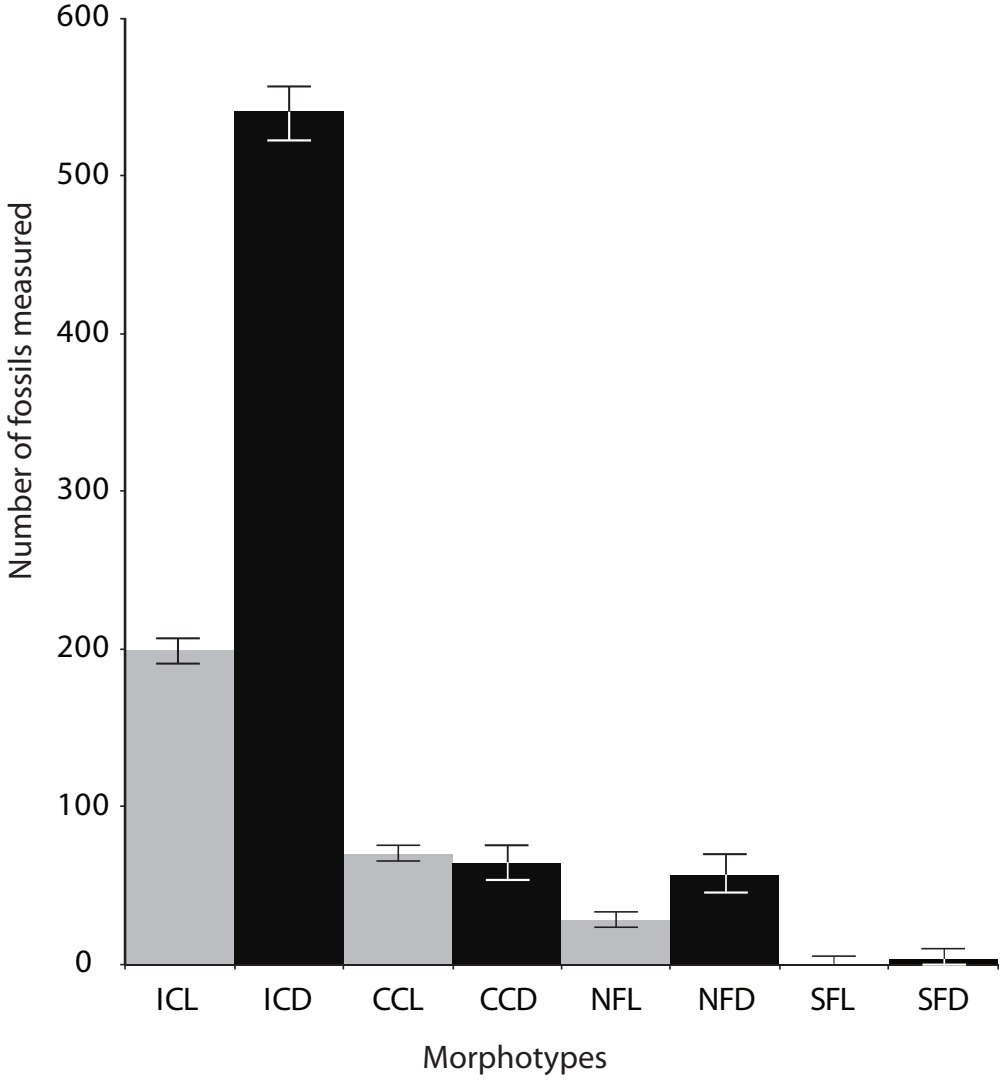


Figure 3.2: Chart illustrating absolute total abundance of each informal morphotype from microfossil survey. N = 963. ICL = 199, ICD = 541, CCL = 70, CCD = 64, NFL = 28, NFD = 57, SFL = 1, SFD = 3. Error bars show standard error of measurement.

coccoids, normalised to spherical equivalents (to account for both ellipsoidal and spheroidal coccoids) show a bimodal distribution (Figure 3.3), one centred around a mode of normalised spherical diameter of 11 μm and a second mode normalised spherical diameter of 16 μm.

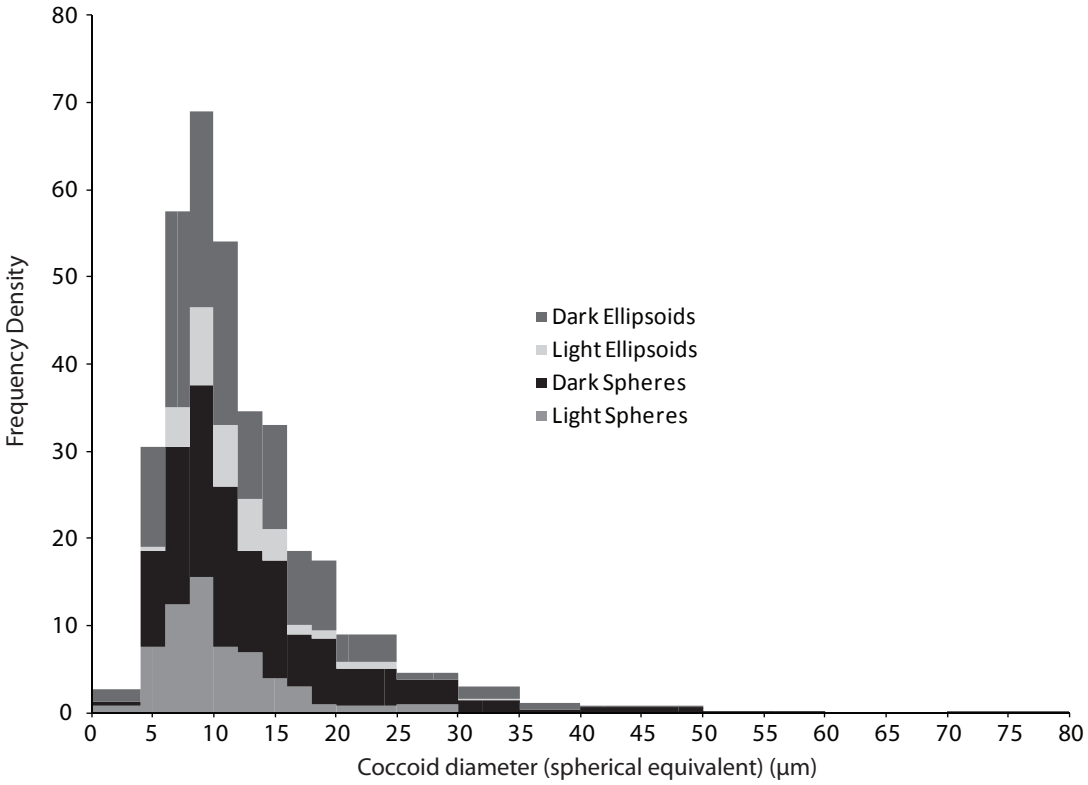


Figure 3.3: Histogram illustrating the distribution of coccoid diameters from microfossil survey. N = 740. Data encompass morphotypes from form taxa ICL and ICD, and from spherical and ellipsoidal cells.

Clusters of coccoids are the second most abundant morphotype (14%),with light-walled and dark-walled forms occurring in similar abundance. In general, the cluster volume increases with individual cell volume, and with the number of cells. Figure 3.4 illustrates that, in general, the larger clusters contain a greater number of cells, and that the clusters can be between 2.5 and 100 times the size of the constituent cells. Such a large range suggests that variation in size is caused primarily by coccoid number, rather than by coccoid size. Clusters may be either tightly compressed or more loosely associated. When the coccoids are densely packed into the cluster, they demonstrate mutual compression of the walls, and may also show evidence of compression by an external sheath surrounding the entire cluster. Where the cells are less

tightly packed, no such compression occurs, although the boundary of the cluster is usually well defined.

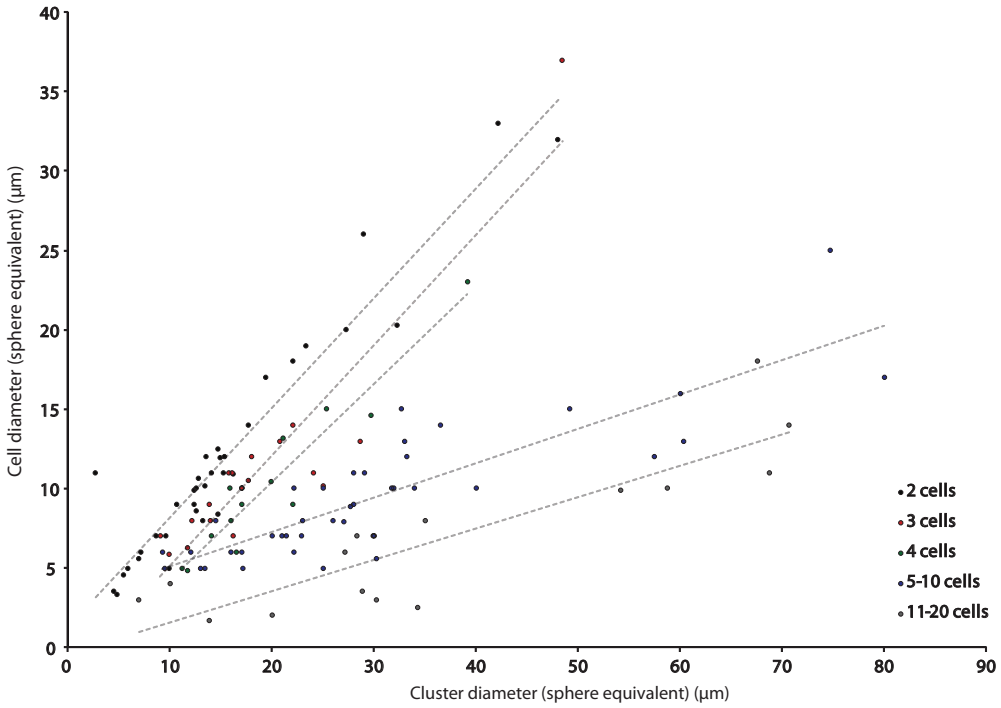


Figure 3.4: Scatter chart showing the relationship between cluster size and constituent cell size, with reference to the number of cells in cluster. Data from microfossil survey includes morphotypes from form taxa CCL and CCD. N = 124. Lines of best fit illustrate strong positive correlation, with decreasing dependence on cell size with increasing cell number in a cluster. For 2 cells, $R^2 = 0.9463$; for 3 cells, $R^2 = 0.8487$; for 4 cells, $R^2 = 0.9119$; for 5-10 cells, $R^2 = 0.7297$, for 11-20 cells, $R^2 = 0.7703$.

Non-septate filaments are less abundant (8%) than coccoid clusters. In these, there is a notable predominance of darker walled forms. Statistical distribution of the filament diameter (Figure 3.5) suggests a range of sizes consistent with the presence of more than one species of filamentous form. The most abundant group has a modal diameter of 2 μm, with examples commonly ranging up to around 5 μm. A second group has a modal diameter of around 10 μm, although these filaments have been observed up to 23 μm in diameter.

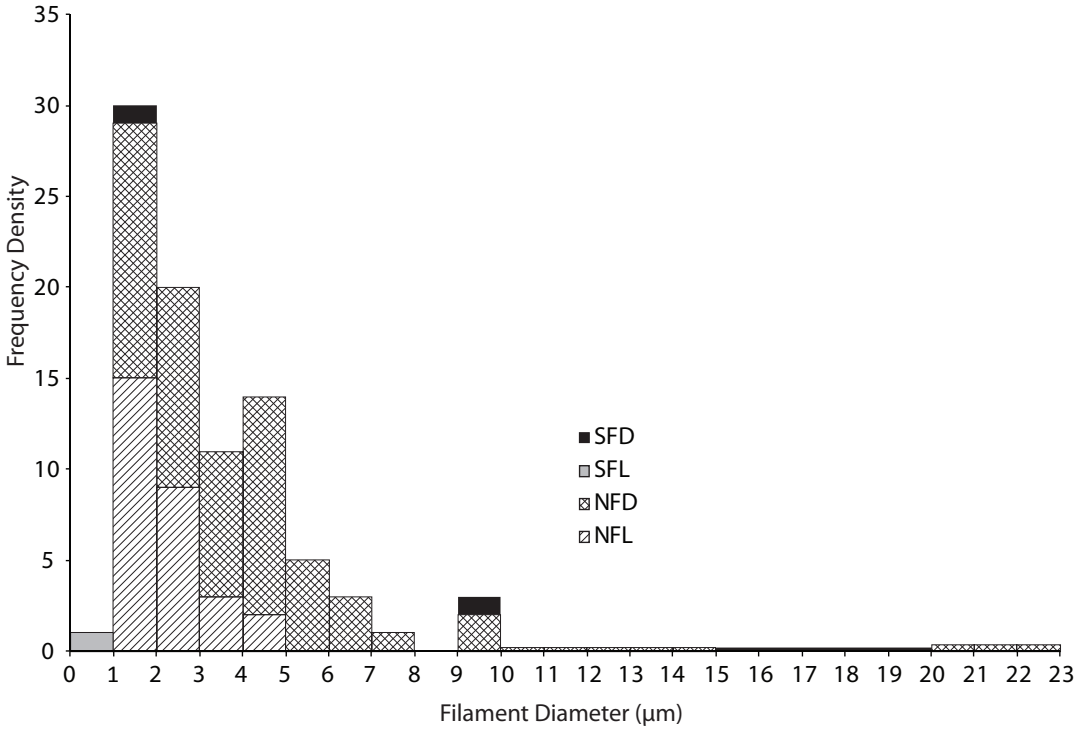


Figure 3.5: Histogram illustrating the distribution of filament diameters from microfossil survey. N = 89. Data encompass morphotypes from form taxa NFL, NFD, SFL and SFD.

Septate filaments are rare in the measured assemblages, with only four specimens being noted in the survey. Of these, two specimens had a sheath diameter of 1 and 2 μm respectively, while the other two specimens attained diameters of 10 and 15 μm. These size differences may reflect two distinct populations.

While this form taxonomy provides a useful way to characterize the majority of microfossils, some forms show more distinctive morphotypes that deserve a brief mention here. One such example is shown in Figure 8a, which illustrates an ellipsoidal coccoid which is approximately 24 μm along its longer axis. It is classified as morphotype ICD (dark walled, isolated coccoid) under the above discussed informal scheme. However, tubular or globular surficial features on the outer wall make the microfossil worthy of note, and it has been previously illustrated by Strother et al. (2011).

A further group of specimens likewise classified as dark walled isolated coccoids (ICD) are remarkable because of their great size (Figure 3.6b and c). Reaching diameters of up to 450 μm, they are preserved in varying degrees of degradation and fragmentation. The intact specimen shown in Figure 3.6b displays an approximately radial striated pattern on its outer wall (shown in inset)—broadly comparable to structures seen in *Valeria elongata* of the Mesoproterozoic of the Siberian platform (Nagovitsin 2009), as well as containing at least four spherical coccoid bodies within, each around 40 μm across. Comparative specimens have an outer wall with a finely verrucated structure (Figure 3.6c). As Javaux et al. (2003, 2001, 2004) and Knoll et al. (2006) have noted, a large size as well as complex wall ornamentation is highly suggestive of a eukaryotic affinity for such microfossils.

Some microfossils have morphologies that do not directly fit into the above scheme of informal taxonomy. Of particular note are the enigmatic structures shown in Figure 3.6d and e. These forms show a globular base approximately 25 μm in diameter, attached to a broad tubular structure around 8 μm wide, ranging from 20 μm to around 100 μm long. The longer tube is smoothly curved into a U-shape. Both forms have a single-layered wall which is very dark and nearly opaque. This wall is pitted and broken in many places, likely owing to a reasonably advanced stage of degradation. It seems unlikely, however, that this morphology could have been formed by purely taphonomic means. Morphologically, it calls to mind certain simple forms of chitinozoan (for instance *Agnochitina hansonica* (Soufiane & Achab 2000)), although

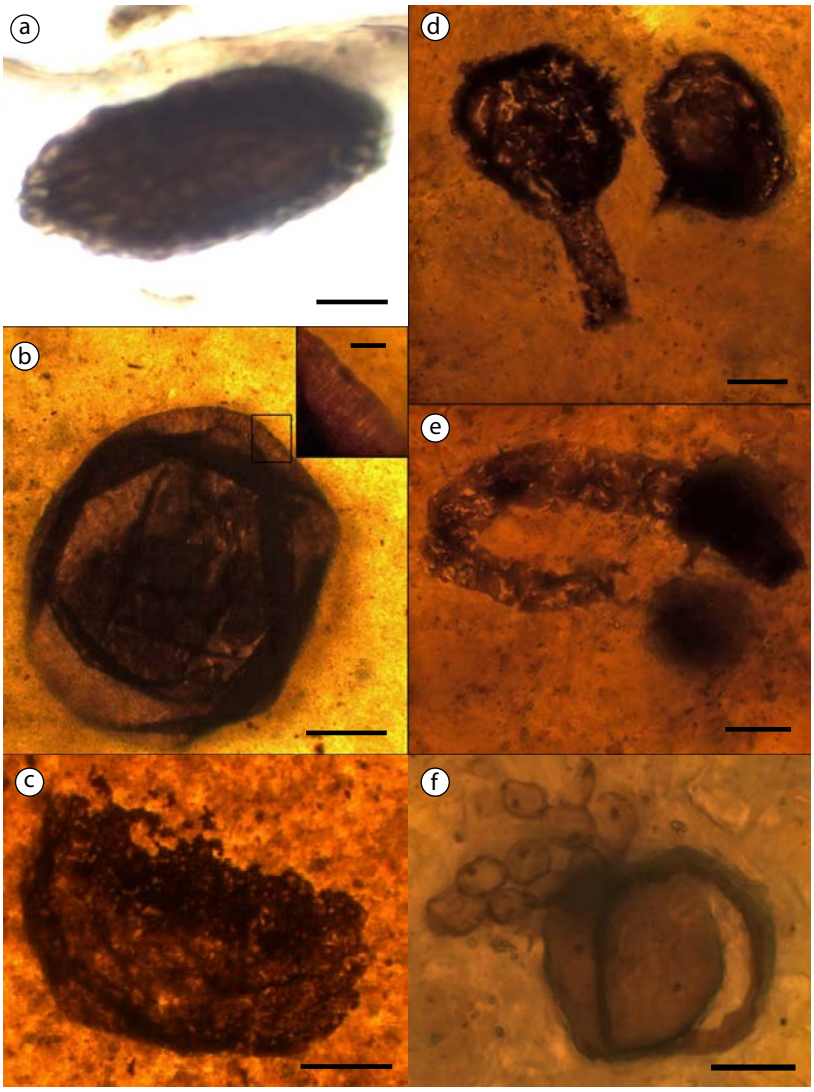


Figure 3.6: Photomicrographs illustrating microfossils of note discussed in text. a) Isolated dark walled ellispsoidal coccoid showing a regular cellular or tubular reticulation on the surface. From phosphate in the Diabaig Formation. Sample FFA1-1.45a from Shelidaig Bay; b) Isolated dark walled megaspheric coccoid with a subradial striation on outer wall (shown in inset), and containing at least four smaller cellular bodies within. From phosphate within the Diabaig Formation. Sample FLA-3a from Fladday; c) Fragmented isolated dark walled megaspheric coccoid showing a finely verruacted wall structure. From phosphate within the Diabaig Formation. Sample FLA-3a from Fladday; d) Dark walled coccoid microfossils with broad tubular neck-like structure attached (apparently torn away in right-hand specimen). From phosphate in the Cailleach Head Formation. Sample CAI-28 from Cailleach Head; e) Dark walled coccoid with long curved tubular structure attached. From phosphate in the Cailleach Head Formation. Sample CAI-2e from Cailleach Head; f) Complex microfossil showing the emergence of an adjoined cluster of at least ten light walled ellipsoidal coccoids from a single point on a larger, dark walled spherical coccoid. From phosphate in the Cailleach Head Formation. Sample S20-x from Cailleach Head. a, b inset, d-f scale bars 10 μm; b, c, scale bars 100 μm.

neither a spiny surface nor a chitinous wall can be confirmed.

Another enigmatic form (Figure 3.6f) consists of a dark walled coccoid approximately 20 μm in diameter, from which seemingly emerges a cluster of conjoined, light walled ellipsoidal coccoids, around 6 μm along their long axis. Microscopy confirms that this is unlikely to be an accidental juxtaposition, suggesting that the smaller cells are excysting from within a larger, more resistant walled cyst. Such an observation matches with other occurrences, in which clusters of small coccoids are entirely contained within dark walled coccoids (such as in the megaspheric form in Figure 3.6b) or occur as loosely associated clusters with no external wall. Attempts have been made by Zhang (1982) to relate these apparently excysting forms to a cellular lifecycle of *Torridoniphycus*. We believe that such an interpretation is somewhat oversimplified however, as the morphotypes preserved in the Torridon rocks likely represent both taxonomic and ontogenetic variants, which cannot be directly compared.

The Torridonian microfossils preserve a range of wall architectures. Most common are resistant opaque walls of the kind commonly found in acid resistant acritarchs of this age and younger (Downie 1984). Also found are delicate translucent walls with a thickness of less than 0.5 μm and a characteristic crinkled fold pattern (Figure 3.1a). It is likely that low grade metamorphism subsequent to the entombment of the fossils will have altered the structure of the organic material making up the wall somewhat, as suggested by a pronounced G-band displayed in Raman spectra of these fossils (see below). However, the co-occurrence of these wall structures within a single fossil suggests that these differences are not purely taphonomic and likely reflect original differences in wall chemistry and architecture. Although the chemical composition of the wall structures has yet to be demonstrated, preliminary analysis by TEM lends support to this view (see below). Meaningful taxonomic distinction can arguably be made between the lighter walled vegetative cells, and the darker walled cyst-like structures, which may represent resting stages or protective adaptations to a frequently desiccating habitat.

Following death, occlusion by a preserving medium, such as sedimentary phosphate, will help to exclude bacterial scavengers. Even so, this need not halt the process of autolysis occurring within the cell. Plasmolysis of the internal contents of the cells involves shrinking and dramatic volumetric reduction of the cytoplasmic material, and the detachment of the delicate cell membrane from the cell wall. The

fossilised product of this process typically leads to formation of an opaque organic 'spot' located centrally or eccentrically inside a fossil cell, representing the condensed contents of the original cell (Francis et al. 1978). The cell wall retains its shape owing to rigidity conferred by cellulose in eukaryotes or mucus in prokaryotes, although the relatively rapid loss of turgidity will result in small folds and crinkles appearing on the surface (e.g., Figure 3.1a).

The phosphatic matrix preserves not only the cells living at the time of formation but also a taphonomic spectrum of deceased and partially decayed microflora in the region of the sediment-water interface. Such death assemblages are able to preserve organic structures at various stages of degradation, and display characteristics such as advanced plasmolysis and shrinking, abrasion and damage by detrital and chemical material, and, ultimately, disintegration of the organic material (Figure 3.7). In addition to the purely physiochemical degradation of the organic microfossils, there is considerable evidence for a biological role in decay and recycling of the organic matter. Smooth edged holes in the organic cuticle that makes up the resistant darker-walled cysts differ considerably from irregular tears caused by abrasion by siliciclastic grains (Figure 3.7e). We here suggest that these could have been caused by heterotrophic bacterial degradation of the organic wall. Possible evidence for a relatively abundant heterotrophic bacterial population exists in the form of dispersed or concentrated baccilate forms in the phosphatic matrix. These features are generally ellipsoidal in shape, of length around 1 μm and width around 0.5 μm. They contain no identifiable carbonaceous wall, but are instead identified as lighter coloured inclusions. They are distributed randomly and consistently throughout the phosphatic matrix, but their interpretation as heterotrophic bacteria is supported by their occasional pseudomorphing of spherical or ellipsoidal structures of the same scale as the organic-walled coccoids (Figure 3.7f). Heterotrophic and other bacterial populations have been reported to be preserved in rapidly forming substrates, in particular dental calculus or tartar. Here, the resident baccilate microorganisms form a biofilm of plaque, which over a period of several days hardens to plaque as a result of biological mediation of calcium accumulation. The bacteria are themselves engulfed in the rapidly hardening tartar, and are preserved as baccilate inclusions (e.g., Jordan & Keyes 1964). Studies have been made of such forms in hominid fossils, allowing even the interpretation of bacterial taxonomy (Linossier et al. 1996). We therefore predict that, it the sedimentary phosphate were precipitating sufficiently rapidly in the Torridon lakes, the labile

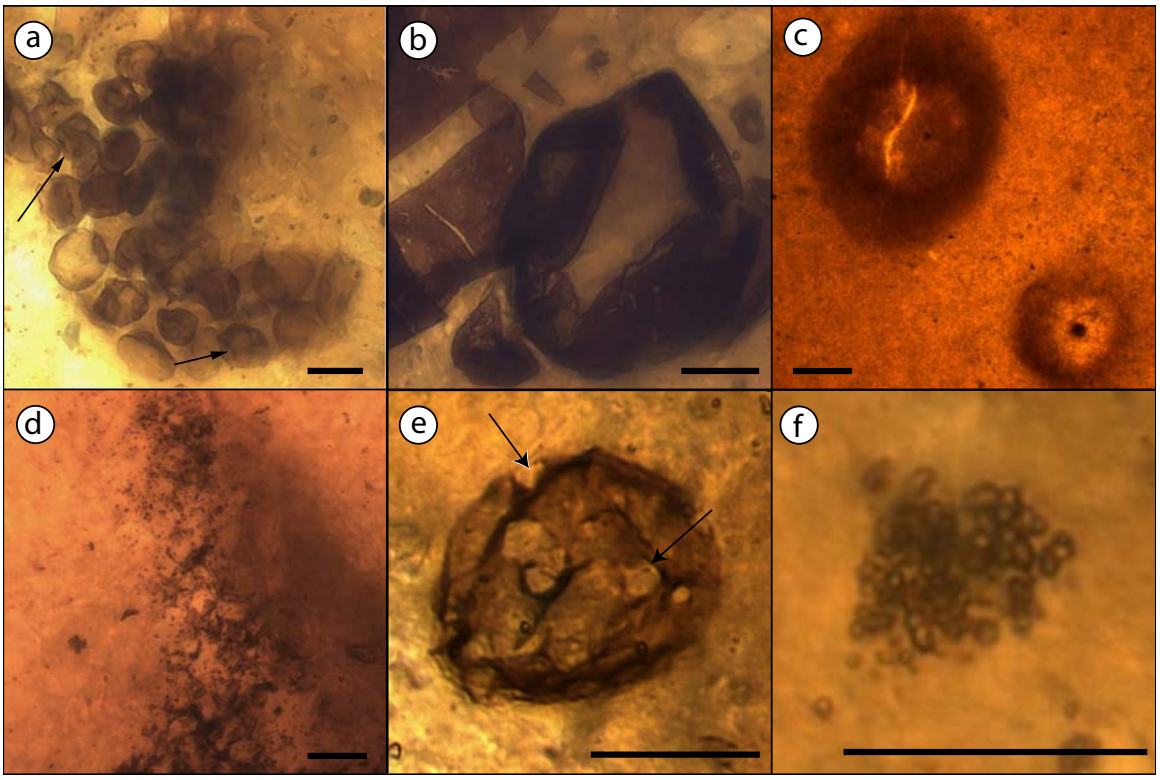


Figure 3.7: Various modes of degradation and decay of microfossils from the Torridonian phosphate. a) Advanced shrinking of coccoids (arrowed), driven by rapid loss of turgidity. From phosphate in the Cailleach Head Formation. Sample CAI-2a from Cailleach Head; b) abrasion and physical damage of cellular wall structures. From phosphate in the Cailleach Head Formation. Sample CAI-2b from Cailleach Head; c) Degraded and dispersed carbon in two spheroidal structures. Walls become and indistinct 'ghost' of carbon, but darker inclusions and tears are still visible. From phosphate in the Diabaig Formation. Sample FLA-3a from Fladday; d) disintegration and dispersal of the carbon making up a cellular sheath. From phosphate in the Diabaig Formation. Sample DB1-4.95ppa from lower Diabaig; e) Cellular wall structures, putatively damaged by heterotrophic bacteria, leaving rounded holes (arrowed). From phosphate in the Cailleach Head Formation. Sample CAI-2a from Cailleach Head; f) Pale coloured baccilate inclusions in the phosphatic matrix, inferred to represent heterotrophic bacterial sheaths pseudomorphic a decayed cellular structure. From phosphate in the Cailleach Head Formation. Sample CAI-2d from Cailleach Head. a-c, e scale bars 10 μm. d, scale bar 100 μm.

bacterial component could be preserved in the same way.

The occurrence of pristine organic-walled microfossils alongside a taphonomic spectrum of partially to completely decayed organic structures is strongly suggestive of a plastic preserving medium that captures a large consortia of living and dead organisms. The taphonomic information contained within the phosphatic matrix therefore provides a rich resource for understanding the nature of physical and biological degradation of the lake floor communities at this time.

3.4 A new assemblage through new methods

The above discussion has focused on analysis of the Torridon microbiota through optical microscopy. Increasingly, however, new techniques are being pioneered in the field of palaeontology to resolve fossil material in unprecedented detail with a view to decoding taxonomy, evolutionary histories, and taphonomy of enigmatic fossils in deep time. In collaboration with researchers worldwide, a selection of these tried-and-tested methodologies, as well as experimentation with new techniques, are here attempted with the Torridon assemblage, with results that fundamentally affect the interpretation of the fossil forms.

3.4.1 Secondary electron SEM

The study of organic-walled microfossils has rarely made use of secondary electron SEM imaging, presumably because the typical shale-hosted compressional mode of preservation of these fossils results in little relief that can be of use in such an analysis. Even fossils three-dimensionally preserved in occluding media such as chert or carbonate are limited in their suitability for the technique, as in order for the fossils to be imaged they must be dissolved from the host rock, thus removing their support and their infilling material; they deflate to give a two-dimensional appearance.

It is still of some use, however, to use the enhanced resolution possible with secondary electron SEM imaging to resolve fine-scale details of enigmatic ornamentation or structure within fossils, and has therefore been attempted within the Torridon assemblage.

In this study, fossil material was removed by acid maceration of phosphates from the Diabaig Formation at the type locality of Lower Diabaig. Thin sections of the

same material were prepared for comparison. Details of the preparation and imaging of the material are outlined in Appendix A, and preparation of material was carried out in collaboration with Charles Wellman at the Department of Animal and Plant Sciences, University of Sheffield.

As may be expected, the range of morphologies visible in SE-SEM analysis is broadly comparable to those observed within thin sections of the phosphate. There were, however a number of unique forms observed in these analyses that have not yet been encountered in occluded phosphate samples. This is likely due to the mass-processing of material during preparation by acid maceration, as well as the unique resolution afforded by the SE-SEM imaging process. Of note are two morphotypes, the first (Figure 3.8c) comprising a vesicle around 50 μm in diameter, ornamented with regular pits around 10 μm across, with each pit possessing a raised 'collar' approximately 2 μm wide and 2 μm high. This form bears some resemblance to *Cheilofilum hysteriopsis* Butterfield, in its possession of flanged openings, but its rarity and identification only in macerated material viewed by SE-SEM precludes further interpretation. The second form (Figure 3.8d) is a spherical hollow vesicle around 20 μm in diameter, with a spongy textured wall, and irregularly distributed with rounded or subcircular holes around 3 μm across. The morphotype is particularly notable for its retention of three-dimensional structure following maceration, indicating the unique rigidity of the wall. While bearing superficial resemblance to cenospheres, an abiogenic structure produced as a result of incomplete combustion, a biogenic interpretation is here maintained owing to the similarity in carbonaceous microstructure of this wall to other fossils in the assemblage.

In addition to these newly observed forms, many simple vesicles and tubular morphotypes encountered within the phosphate are seen, with the SE-SEM imaging affording enhanced resolution of their shape and wall structure. In particular, differences in the physical responses of structures to compression hint at differences in cell wall architecture. Two principal wall responses are observed. First, notably thin-walled vesicles (wall <0.5 μm) accommodate compression with fine wrinkles irregularly distributed across the surface, and are apparently more prone to small tears (Figure 3.8b). In contrast, thicker walled (wall at least 1 μm thick) specimens accommodate flattening with broad rounded velvet-like folds, or large creases (Figure 3.8a). The thinness of these walls and their flattening during preparation does not permit resolution of any ultrastructural lamination, but synthesis of taphonomic response

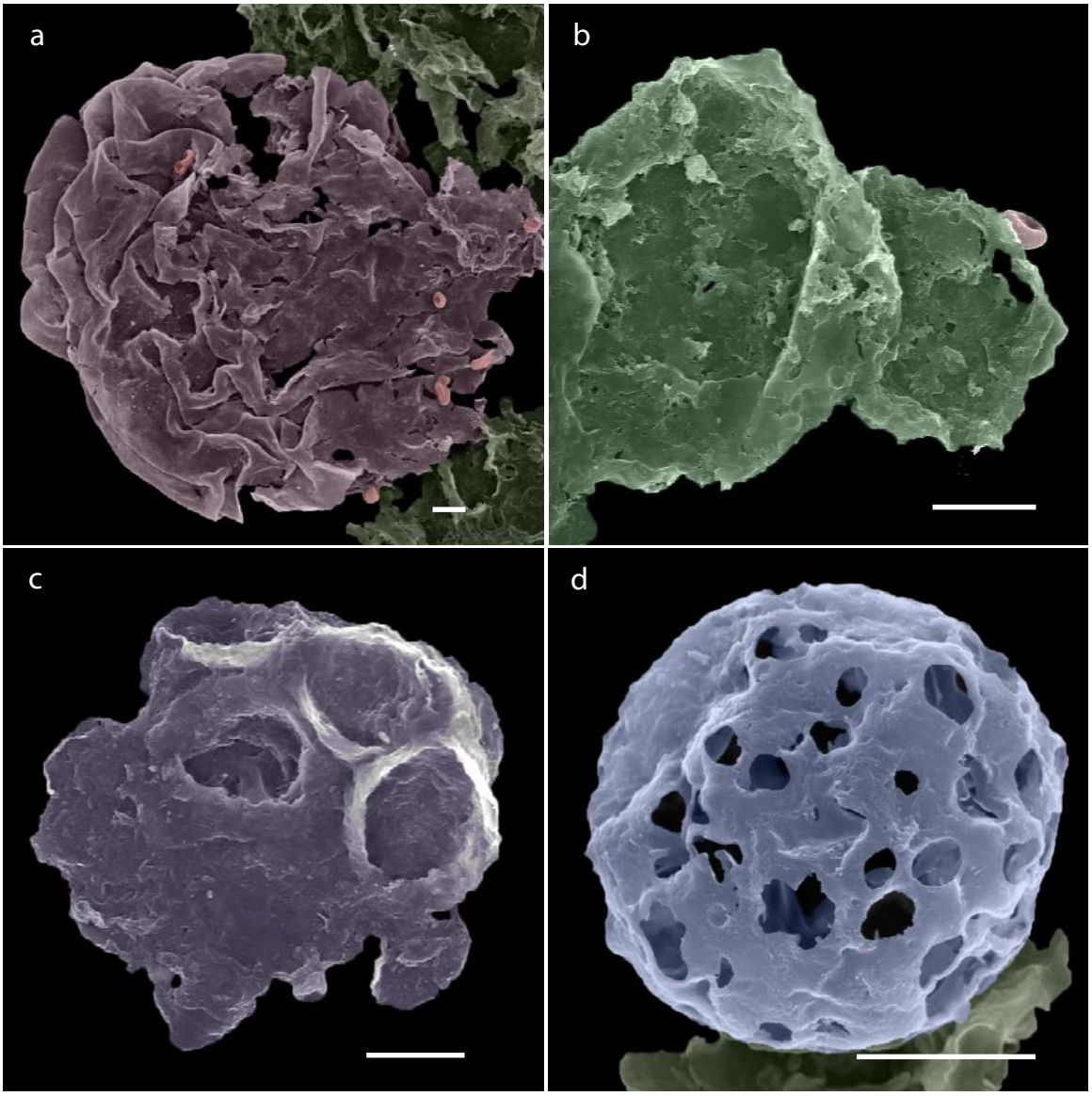


Figure 3.8: Microfossils imaged and analysed by secondary electron SEM, coloured for easier interpretation. a) Large, thick-walled vesicle, showing 'velvet-like' folds; b) Smaller, thin-walled vesicles with a crinkled surface and finely irregular outline; c) Vesicle with large hemispherical pits bounded by raised rims or 'collars'; d) Subspherical rigid vesicle retaining it 3D structure, and bearing many irregular rounded holes. Sample CAI-7, macerated from phosphate from Cailleach Head. All scale bars 10 μm.

and wall thickness may be used to enhance interpretation of fossils studied by optical microscopy.

Distributed abundantly amongst the structurally distinguishable vesicles and sheaths is non-vesicular membranous organic matter, with an irregularly pustulate and pitted texture and an amorphous architecture. The size and nature of this material is likened to the amorphous extra-polymeric substances (EPS) secreted by mat-forming organisms in modern microbial ecosystems. This material is occasionally seen contained within phosphate as light-walled membrane, but its texture and extent is revealed in high resolution by this SE-SEM analysis.

Of particular note, amongst the vesicles, sheaths and EPS imaged by this method are small coccoid or baccilate forms seen to be colonising some of the larger fossil structures to a greater or lesser degree, associated with pits within those structures and apparently embedded within a membrane that links them to the host fossil (Figure 3.9). These forms are herein interpreted as fossils of heterotrophic bacteria preserved feeding on the larger Torridon microbial flora. Justification for their autochthony and antiquity are detailed below.

They must be coherent organic-walled structures in order to have survived the acid maceration process involved in sample preparation, and they were not observed in a control preparation where deionised water was evaporated under the same conditions and imaged in the same batch. Their distribution is limited to only some larger structures, and not others, where it may be expected that passive contaminants would be evenly distributed. Their occurrence on both the upper and lower surfaces of select vesicles, as well as being nestled within folds, is also indication that they were attached prior to the evaporative preparation. Close association with pitting of a similar size and shape in the larger fossil form, and occasional occurrence within their own pits is evidence against coincidental juxtaposition, and they must be relatively well adhered to the fossil structures to have survived the maceration process intact, although some are found isolated and pits are found unoccupied. They are commonly found partially embedded within the apparently continuous membrane of the larger fossil structure, or are adhered via a membrane that is indistinguishable from the larger vesicle wall, suggesting their coeval formation and preservation. All of the baccilate structures, while retaining a degree of three-dimensionality similar to

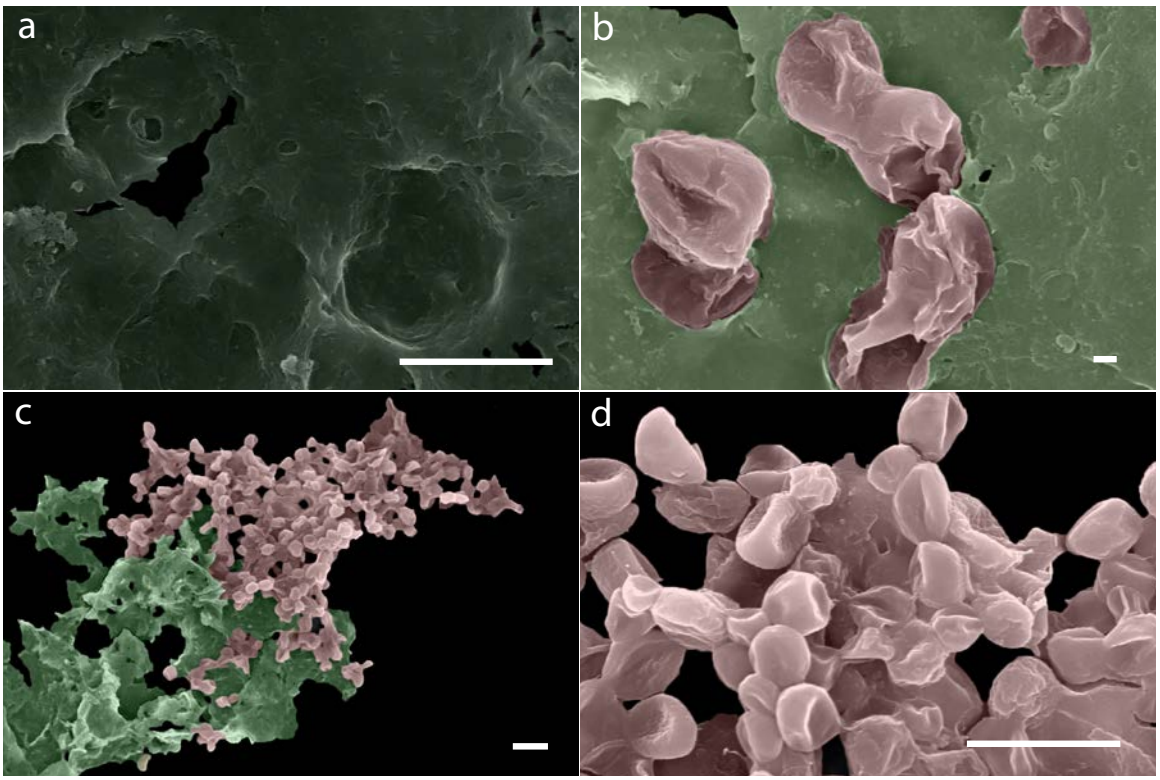


Figure 3.9: Evidence of bacterial heterotrophy in secondary electron SEM images. a) Rounded pits and occasional holes, irregularly distributed on the surface of larger vesicles' walls; b) Collapsed coccoid or baccilate vesicles ∼5 μm across (red), occupying pits in the walls of larger vesicles, occasionally with a thin raised lip; c) Densely packed colony of coccoid and baccilate vesicles (red) continuous with amorphous degraded vesicular material (green); d) Higher magnification of colony in (c), showing collapsed coccoid and baccilate structures arranged randomly with supporting and sheathing membrane. Sample CAI-7, macerated from phosphate from Cailleach Head. a, c-d, scale bars 10 μm; b, scale bar 1 μm.

the thickly folded walls of some larger vesicles, have suffered some degree of taphonomic deflation, which would not be expected from living contaminant bacteria. In addition, the surfaces of the structures are granular and in places show taphonomic degradation similar to the larger structures, although perhaps a differing chemistry means that they are not as susceptible to tearing or disintegration. Finally, they are similar in size, shape and distribution, even to the extent of fully pseudomorphing larger vesicles, to the bacteriomorphs described above and published in Battison & Brasier (2012), from within the occluding phosphate matrix, and are therefore interpreted as the same heterotrophic bacteria.

Having been observed in different preparations of the Torridon material, it may be assumed relatively confidently that these structures are autochthonous to the rock and dating to around one billion years ago. Combined with the added evidence of pitting and embedding, their heterotrophic nature may also be assumed, making this the earliest example of heterotrophy in the fossil record. Such a claim would, however, require further substantiation in the form of Raman spectroscopy or isotopic analysis, which could help to verify their autochthony and chemical composition to be compared with modern heterotrophic bacteria.

3.4.2 Raman spectroscopy

Raman spectroscopy is an imaging and analysis technique, which produces data on the constituent atoms, functional groups, and bonding of a sample, on the basis of characteristic spectra. These spectra are produced by Raman scattering after inelastic collisions of monochromatic laser radiation with a given sample. The inelastic collisions result from vibrational transitions of chemical bonds which, when normalised to excitation wavelength, produce sets of Raman peaks that can be used to identify unknown compounds. Although some compounds are not 'Raman active' owing to their structure, there is a vast library of organic compound spectra that are used in identification of living or freshly fixed material.

Raman spectroscopy is increasingly used in palaeontological applications, being informative on the maturity of organic material, and offering the opportunity to resolve chemical differences which may not be visible thorough traditional microscopy techniques (Allwood et al. 2006, Brody et al. 2001). It has been used to substantiate the antiquity, and justify the biogenicity or otherwise of organic material in the ∼3.5

Ga old Apex Chert (Brasier et al. 2002, Marshall et al. 2007, Schopf et al. 2002), and to infer metamorphic grade and palaeoenvironment of fossil materials (Allwood et al. 2006). Additionally, its utility in decoding the mineralogical histories of permineralised microfossils, such as those of the Doushantuo formation, has been examined (Schweizer 2008).

In the study of ancient carbonaceous or kerogenous material, two particular wavelength bands are identified, and their relative intensities compared to give information on moleculo-chemical structure and thermal maturity: referred to as the 'G band' and the 'D band' (Tan et al. 2004).

The carbon 'G band' is represented by a peak at around 1580 cm^{-1}, and results from scattering from graphitic domains (Lespade et al. 1982). Such domains consist of planar carbon rings which in kerogen produce spectra similar to those of isolated graphite microcrystals. The peak shape and position is affected by the sizes of graphitic crystallites, and the degree of atomic order within them (Pasteris & Wopenka 2003). Even highly disordered macromolecular carbonaceous material and fresh organic matter have been shown to produce a 'G band' (e.g. Bény-Bassez & Rouzaud 1985).

The carbon 'D band' consists of a peak at around 1350 cm^{-1} and is attributed to disordered carbon material that may be produced by the coalescence of molecular carbon. All but the most ordered carbon material, such as diamond, possess a 'D-band' (Tan et al. 2004).

Macromolecular carbon structure is sensitive to metamorphic grade, and this is reflected in a change of shape of the spectra (Jehlicka et al. 2003). An increase in metamorphic grade results in a sharpening of all peaks and a decrease in relative D-band intensity as the size of graphitic domains increases (Kudryavtsev et al. 2001). Thus, both the original composition of carbonaceous material, and its subsequent metamorphic history affect the shape and relative intensities of D and G bands.

Within a single microfossil assemblage, metamorphic alteration may be assumed to be constant, and therefore any variation in D or G band intensity can be attributed to original chemical heterogeneities in the organic structures. Such spatial variations

may be revealed by two- or even three-dimensional mapping of G and D band intensities, and particularly highlighted by mapping of G/D band ratios.

The Torridon assemblages offer an ideal subject for study by Raman spectroscopy, consisting of carbonaceous fossils of apparently different taxa, three-dimensionally preserved within a cryptocrystalline phosphate matrix. Raman spectroscopy was therefore applied for the first time to organic-walled, phosphate-hosted microfossils in this preliminary study. Four different fossil specimens were selected for analysis at the Centre for Geobiology, Department of Earth Science, University of Bergen, in collaboration with Nicola McLoughlin and David Wacey. Raman maps for two of these specimens are presented here, owing to instrumental difficulties. Methodology for preparation and analysis by Raman spectroscopy can be found in Appendix A. Despite movement of the stage during creation of the Raman maps, no loss of resolution occurred, as confirmed by no widening or loss of peaks in individual Raman spectra. Instrumental difficulties with this preliminary analysis also means that no individual spectra could be figured, but have been confirmed in comparison with the maps.

Figure 3.10 illustrates Raman maps for apatite, carbon D band, G band, and the G/D ratio for a 'dark-walled' Torridon taxon; and Figure 3.11 illustrates the same maps for a 'light-walled' variety. As per thediscussion of biogenicity earlier in this chapter, it is thought that the the colour differences of the wall represent differences in the original wall chemistry or structure rather than thermal alteration. Such differences may be a result of differing taxonomy, life stage, or preservation.

In all of these maps, the spatial distribution of both carbon bands is more or less concordant with the distribution of brownish material visible in optical micrographs, indicating that these structures are indeed carbonaceous. Apatite is restricted from areas with strong carbon signals, suggesting a distinct separation in mineralogy between the fossil walls and the surrounding matrix. In some cases, however, such as in Figure 3.10, disordered D band carbon is seen distributed patchily throughout the apatitic matrix, which is likely the signal of fine non-fossiliferous particulate carbon disseminated throughout. The presence of this particulate organic material is informative to the processes of formation of the phosphate itself, as will be discussed in Chapter 6. Its characteristic disordered bonding is substantially different to that of

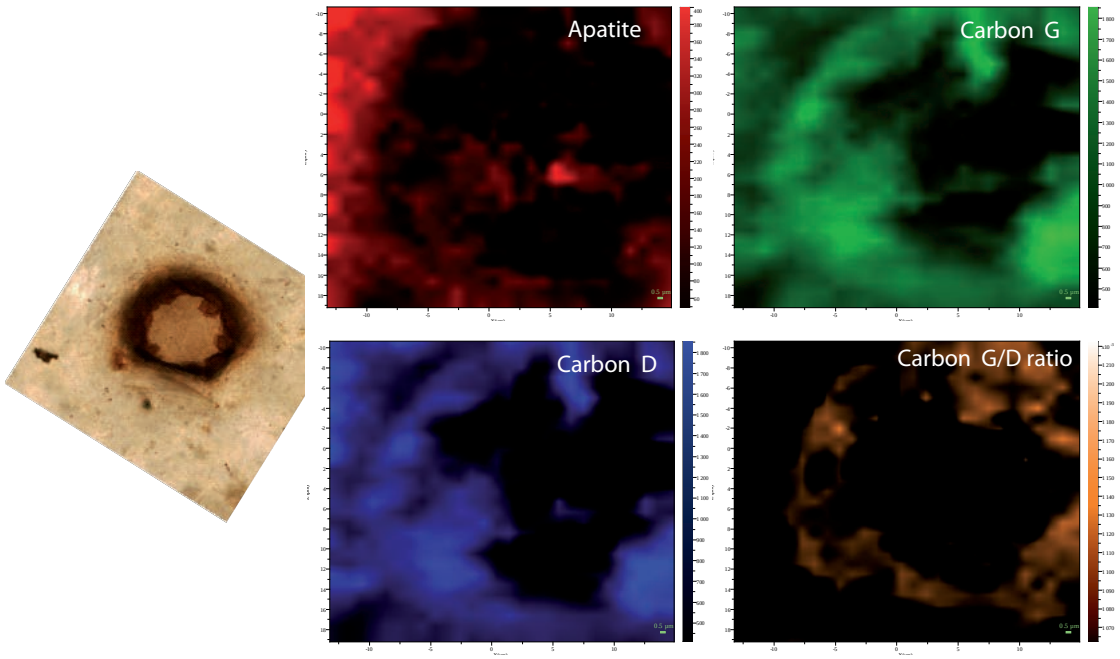


Figure 3.10: Laser raman maps of a large, dark walled fossil. Optical micrograph of the fossil shows distinct dark outer wall with break at surface where it intersects the surface of the section. Apatite map shows it to be absent from the fossil wall, and, to some extent, the fossil lumen. Carbon G-band and D-band maps both have strong signals in the region of the fossil wall, but there are also high concentrations in the matrix. Carbon G/D ratio map more precisely picks out the structure of the fossil providing a good chemical match for morphology. Fossil approximately 30 μm in diameter. Sample CAI-7b from Cailleach Head.

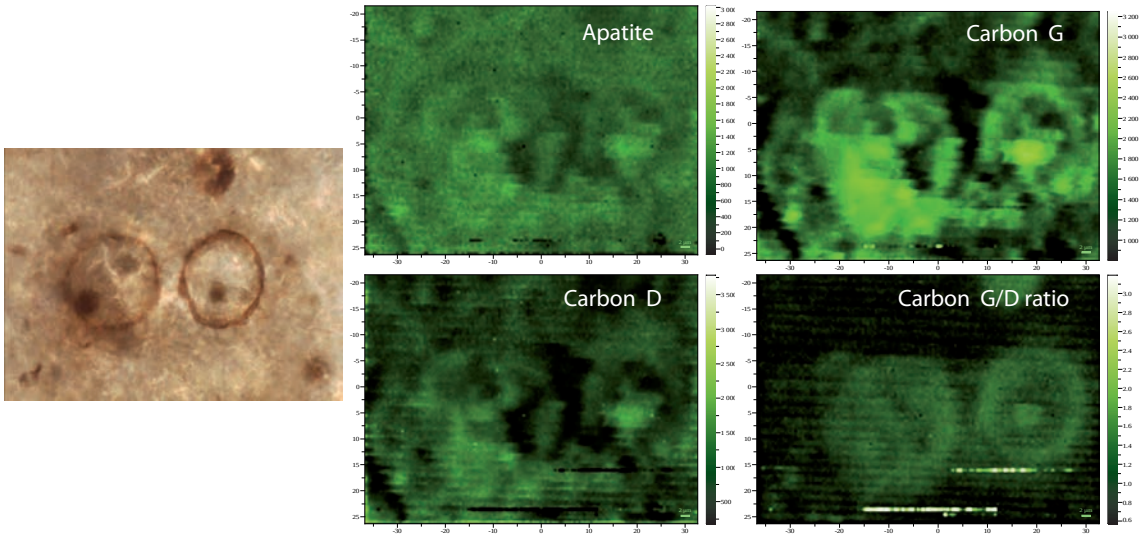


Figure 3.11: Laser raman maps of two small, light-walled microfossils. Optical micirograph shows two subcircular vesicles, each bearing a small amorphous dark spot eccentrically. Apatite is distributed irregularly throughout the matrix and in the region of the fossils. Carbon G-band and D-Band maps also show irregular distribution, but with elevated concentrations of both in an indistinct structure. Carbon G/D ratio maps resolves this structure into the two vesicle structures with their internal spots, providing a good chemical match for morphology and demonstrating these internal objects are carbonaceous. Wall structure is not distinct, instead inwardly and outwardly diffuse. Horizontal banding due to stage movement between scans. Fossils approximately 12 μm in diameter each. Sample CAI-7b from Cailleach Head.

the fossil material, further indicating its non-structural character.

The G/D band ratio maps bear a striking resemblance to the optical photomicrographs of the fossil in most cases, providing a relatively precise chemical match for morphology otherwise represented by colour and physical structure of organic material. In both the light-walled and dark-walled taxa, the wall structures seem to be continuous and solid, unlike similar permineralised cells of the Rhynie Chert (Schweizer 2008).

While there does not appear to be any notable chemical heterogeneity in the walls, there is an identifiable difference in structure between dark-walled and light-walled forms. G/D ratio maps of dark-walled cellular fossils (Figure 3.10) show a relatively rapid shift from low, zero-line ratios, to high ratios in the wall, to low again in the cell lumen. There is very little dispersion of carbon either inside or outside the wall, marking a crisp chemical boundary. In contrast, the light-walled forms show a much higher degree of scatter across the wall transition, even when optical micrographs appear to show a narrow contiguous wall structure. In Figure 3.11 this is reflected by a gradual increase from the outer matrix to the wall zone, followed by a gradual decrease inside the cell lumen. The differences between this and the crisp chemical gradient of the dark-walled forms presumably reflects differences in the preservation of fossil walls, contingent on variations in the original chemical structure of each. Dark-walled forms retain their structural and chemical wall during fossilisation, whereas the material that makes up the wall of the light-walled fossils is more readily dispersed under the same fossilisation conditions. This provides further evidence to support the interpretation of these fossil structures representing resistant and labile walls respectively.

Within the lumen of some light-walled forms, single dark spots are seen located centrally or eccentrically. Raman spectroscopy has also assisted in the characterisation in the composition of these spots. Figure 3.11 shows two light-walled forms which each contain a small amorphous brown spot. The Raman maps show high intensities of both carbon D band and G bands in the region of the spots, and the G/D band ratio maps highlights them with defined edges separate to the dispersed material of the fossil wall. These results indicate that they are formed primarily of carbon, and that their preservation potential is somewhat different to that of the wall. This is consistent with their interpretation as the condensed organic remnant of cytoplasmic

and sub-cellular material, rather than as later mineral growths.

Finally, the patchy and heterogeneous nature of the apatitic signature within the matrix of all fossil material, and its complete absence in the lumina of some structures (e.g. Figure 3.10), cannot be fully explained by the presence of carbon. It appears that another molecular phase is present here, but cannot be easily mapped or resolved from the peaks presented by individual spectra. It is, however, indication that apatite alone is not responsible for the preservation of the Torridon microfossils, which will be discussed further in Chapter 6.

3.4.3 FIB-TEM analysis

In addition to optical microscopy, varieties of electron microscopy are used for the study of fine-scale structures in a wide variety of biological and paleontological fields, owing to the ability of these techniques to resolve exceptionally small structures. As has been illustrated above, secondary electron images of fossil structures are only informative when some three-dimensional structure exists, and therefore limit the study of occluded microfossils that are fully surrounded by a supporting matrix. Backscattered electrons and transmission electron microscopy (TEM) enable fine scale resolution of fossils within a matrix, but these techniques require sections through the fossil and matrix material. In the application of transmission electron microscopy, ultra-thin sections are cut using a focused ion beam or diamond knife, through which electrons may pass, whereafter their energy attenuation is recorded and mapped two-dimensionally.

TEM imaging and analysis of microfossil material, in particular of acritarchs, has recently been explored as a means of characterising the ultrastructure of fossil walls (Javaux et al. 2003, 2004, 2010, Marshall et al. 2005, Moczydlowska et al. 2011, 2010, Moczydlowska & Willman 2009, Schiffbauer & Xiao 2009, Willman & Cohen 2011). Such fine scale detail permits the classification of notably different wall structures, allowing taxonomic subdivision, assessment of ontogenetic stages and progression, and even alliance with modern microbial groups (Moczydlowska et al. 2010). For example, Moczydlowska and others (2011) identified a characteristic three-layered ultrastructure, comprising a trilamellated sheath sandwiched between a lower layer of high energy attenuation, and an outer layer of low energy attenuation, as characteristic of eukaryotic Chlorococcalean algae. This may be preserved in fossil material

and is thus an indication of eukaryocity in acritarchs.

The Torridon microfossils are ideal candidates for examination by FIB-TEM, possessing contiguous walls with remnant three-dimensional structure, completely surrounded by translucent phosphate. In a preliminary study to test the application of FIB-TEM to these phosphate-hosted microfossils, a small, light-walled coccoid was chosen for study at the Centre for Microscopy, Characterisation and Analysis, University of Western Australia, in collaboration with Dave Wacey. The details of preparation and imaging of this fossil are given in Appendix A.

Figure 3.12 shows the lower wall portion of a three-dimensional coccoid, with crystalline material oriented chaotically in the cell lumen, a distinctive wall, and quartz and crystalline material at the exterior. Elemental maps of two differing areas of the wall (Figure 3.12 top and bottom) show variously the distribution of carbon, phosphorus, oxygen, calcium, aluminium and iron.

Both raw image and maps show that the wall structure of the cell, appearing as a pale broken band around 500 nm thick around the lower part of the crystalline material, is preserved more or less intact and *in-situ*. It is made entirely from carbon, and is clearly folded and broken in places, indicating both flexile and brittle deformational responses to preservational damage, which in turn is indicative of a flexible wall structure with limited strength. There is no evidence of a multi-layered ultrastructure, and thus a eukaryotic nature cannot at this stage be inferred for this fossil, although comparative data for vegetative and reproductive cells is currently lacking.

The preservation of the wall structure varies laterally, and appears to be related to the surrounding matrix mineralogy. The best preservation occurs when the phosphatic crystalline material occurs on both the inside and the outside of the wall, as in the lower portion (Figure 3.12 bottom). Where different mineral phases occur within the lumen compared with externally, in this case phosphatic crystals and quartz respectively, the wall is thinner and more readily fragmented. This may be related to the speed of crystallisation of the phosphatic material and differential pressures exerted when in contact with detrital quartz.

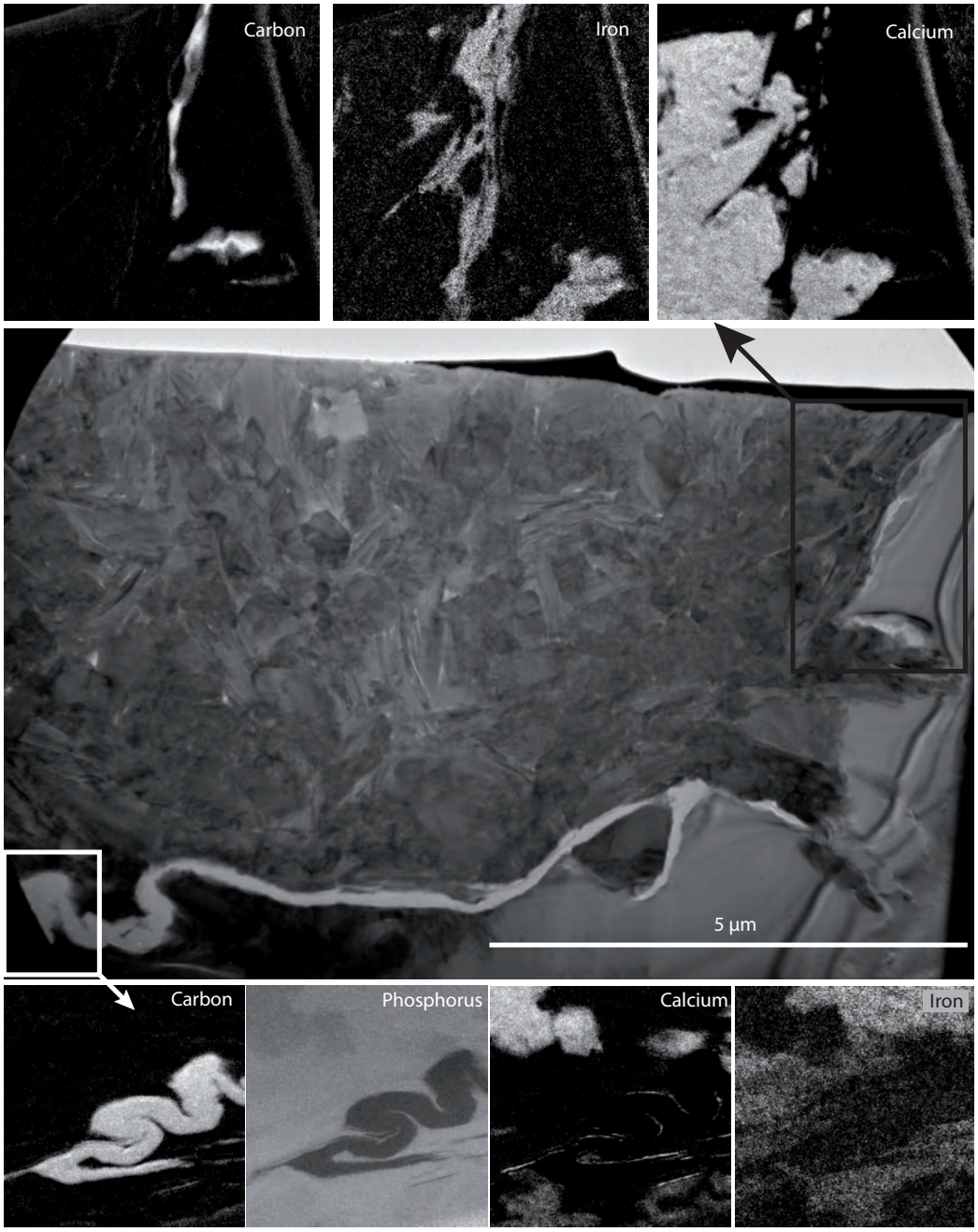


Figure 3.12: FIB-TEM image and element maps of a small, thin-walled vesicle. TEM image of FIB wafer (centre) shows brightly coloured single layered wall structure, filled by a chaotic mixture of minerals. External to the wall, large quartz material (top) and more mixed crystallite (bottom) are present. Wall is broken in places, and at the top, minerals seem to lie parallel to it. Elemental maps of two portions of the wall are shown, illustrating the amorphous carbon-rich material making it up, and the complex relationships of phosphorus, calcium and iron in the surrounding crystallite. No carbonaceous material is seen in the cell lumen, indicating that cytoplasm is not preserved.

In addition to resolving wall structure, the FIB-TEM images and maps of these uniquely three-dimensional fossils allow analysis of the preservation of the cell lumen. In this fossil, it can be seen that no carbon occurs within the cell, being confined entirely to the wall. This rules out the possibility that any cell contents are preserved in their original form, lending support to the interpretation of occasional dark spots as condensed cytoplasmic remnants, rather than nuclei within preserved cytoplasm.

Elemental mapping of the phosphorus-rich crystalline material inside the cell lumen and partially externally shows three distinct mineral phases. These are discussed fully in Chapter 6, but the intimate juxtaposition of all three phases with the carbon wall is suggestive of a rapidly and complexly precipitating matrix using the fossil wall as a template for growth, rather than affecting the morphology with differential growth.

3.4.4 FIB-SEM and FIB-SEM-EDX analysis

Further high resolution data may be derived from SEM Backscattered Electron (BSE) and Energy-Dispersive X-ray (EDX) imaging. Flat surfaces of microfossil-bearing phosphate perpendicular to the original thin section surface are successively exposed by FIB milling, and can be imaged by traditional BSE-SEM methods, and combined with elemental mapping techniques such as EDX, to further analyse the three dimensional structure and preservation of the microfossils in situ. Details of this technique, being pioneered in collaboration with Dave Wacey at the Centre for Microscopy, Characterisation and Analysis at the University of Western Australia are included in Appendix A.

To study the spatial information afforded by the three-dimensional preservation of microfossils within the Torridon phosphate, a small cluster of small, light-walled cells were identified by optical microscopy, and then a trench that transected them cut perpendicular to the section surface. The trench was progressively milled by FIB, and SEM-BSE images taken as each fresh surface was exposed at 200 nm intervals.

As Figure 3.13 shows, the SEM-BSE images reveal the morphology of the cell cluster beneath the section surface, showing the changing shape of the fossil walls (appearing as continuous dark lines in each section) both vertically and laterally. The walls themselves are preserved almost entirely intact, with only minor splitting.

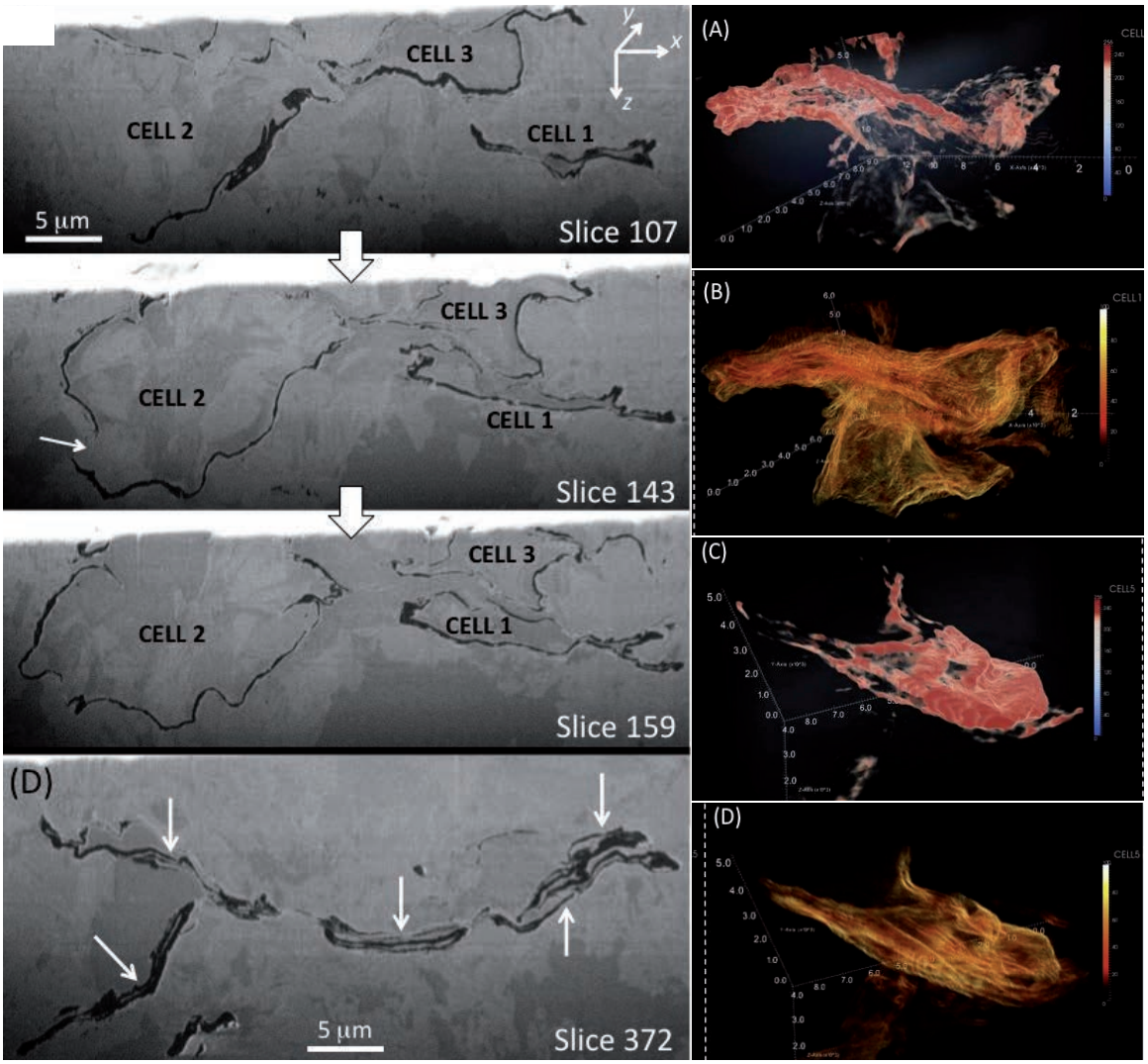


Figure 3.13: Serial FIB-SEM images through a compressed cluster of thin-walled vesicles (left hand side), and slice-based three-dimensional reconstruction of two select cells (right hand side). Serial FIB-SEM images show dark-coloured carbonaceous wall of at least three cells, in differing states of compression, with deformation changing with distance through the cluster. 3D reconstructions of cells in (A) and (C) show the fragmentary and inconsistent nature of the wall, and enhanced curvature rendering in (B) and (D) reveals fine scale folding in three-dimensions. Sample CAI-2f from Cailleach Head, images supplied by David Wacey.

The homogeneity of the fossil walls is consistent with the observations made by FIB-TEM: that the composition is entirely carbonaceous and unlaminated. The overall consistency in thickness and flexibility of the walls demonstrates the efficiency of preservation of the phosphatic minerals, when compared with other fossilizing media such as quartz or carbonate (cf. Kempe et al. 2005, Moreau & Sharp 2004).

All cells show a degree of compression and folding, concurring with optical microscopic evidence that physical deformation has occurred. Compression is not uniform, however, and cells that are completely closed, with upper and lower layers touching, are directly adjacent to cells that have received relatively little compaction. This unexpected observation suggests either that minerals precipitate at different rates within the cells, or that the fossilising fluids permeated cell structures at different rates—perhaps promoted by breaks in fossil wall—allowing some structures to retain their three-dimensionality while others are unfilled and thus compressed. The former possibility is herein considered less likely, as the crystalline material is of consistent random mixture and grain size throughout the matrix and infills, providing no textural evidence for differing rates of precipitation.

Three-dimensional reconstruction of the fossil structures from the serial slice dataset provided by the successive SEM images (Figure 3.13 right hand side) illustrates the very fine variable folding and deformation of the fossils. They also emphasise a high degree of fragmentation of the wall on a fine scale, presumably from chemical degradation, which can to some extent be retroactively reconstructed by enhanced curvature rendering of the fossil remnants. These 3D recontructions, in addiiton to the fine-scale observations of crystalline mineral texture, confirm that the carbonaceous membranes represent continuous, hollow fossil walls, rather than the draping of membrane or sheath material over minerals.

Imaging with FIB-SEM-BSE has proven valuable in decoding the compressional and degradational histories of the preserved Torridon microfossils. It allows three-dimensional reconstruction of forms that may be interpreted as simple carbonaceous laminae if encountered in petrographic thin section, and thus provides important evidence on the biogenicity of such structures.

Larger, dark-walled fossil forms could be identified and sectioned perpendicular to petrographic thin section surface in the same way, but their size limits the serial image

reconstruction. Instead, a single FIB-milled surface was used for *in-situ* elemental analysis, which revealed several significant differences between the large darker-walled structures and the smaller light-walled fossils.

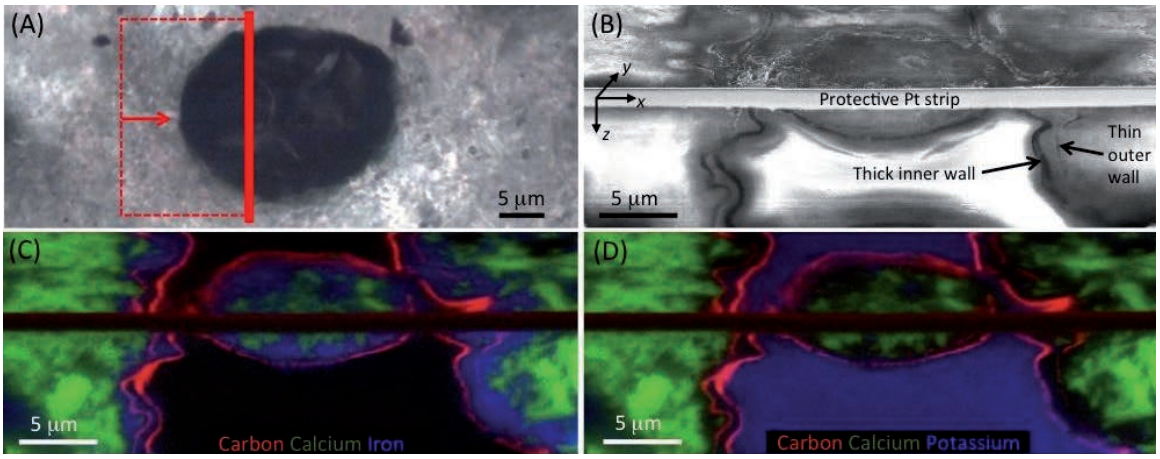


Figure 3.14: FIB-SEM-EDX imaging and elemental mapping of a large, dark-walled fossil. A) Optical micrograph illustrating direction of FIB-milled trench, and ultimate position of section, perpendicular to section surface. B) FIB-SEM image of FIB-milled perpendicular surface (below Pt strip) and polished section surface (above Pt strip), revealing double-wall fossil structure. (C) and (D) EDX element distribution maps for same field of view. Reveals potassium concentrated in cell lumen, carbonaceous inner and outer wall, zone of iron-rich mineral between the walls and directly external to them, and calcium-rich, presumably phosphatic matrix.

Of particular note, mapping of carbon, previously shown to be confined to a single cell wall, reveals a distinctive double-layered structure to the encompassing vesicle (Figure 3.14), which is consistent with interpretations of fossil eukaryotes (Javaux et al. 2003, 2001). The inner wall appears to be thicker (up to 1 μm) and more continuous than the outer wall, which is itself thin and diaphonous ($\sim$200 nm). No modern forms are known with this particular double-wall structure, but its form is suggestive of the growth of a resistant cyst within a more flexible, labile vegetative cell (Moczydlowska et al. 2010, Strother et al. 2011).

Elemental mapping also reveals a distinct zonation of elemental concentrations, presumably related to a mineralogical zonation within these large forms, not previously seen in the light-walled morphotypes. This elemental and inferred mineralogical distribution is discussed further in Chapter 6.

3.5 Formal Taxonomy

The following formal taxonomy describes specimens from the Torridon Group of northwest Scotland with reference to standard naming and descriptive protocols. Samples are compared with previously described Proterozoic taxa, including synonomys where relevant (Appendix D), and a total of 25 species are identified, of 17 genera. Eight forms are described for the first time but are unnamed pending publication of a monograph. Further discussion of this taxonomy is included in Chapter 9.

All formally described taxa were collected and identified by the author, from the full range of localities described herein (Chapter 2) and by Battison & Brasier (2012). Precise locations of named samples can be found in Appendix B. Locations of fossil individuals within slides are identified by a mark on section backing glass, made with a diamond pen. All specimens are currently deposited fin the Department of Earth Sciences, University of Oxford, but may be transferred to the Oxford Museum of Natural History following publication of monograph. Please refer to most recent publication for location of these specimens.

Group: Non-septate filamentous sheaths.
Genus *Siphonophycus* Schopf 1968

Siphonophycus inornatum Yun 1981 (Figure 3.15a)
Description: Tubular, nonseptate, unbranched filaments; commonly spherical in cross section; straight, bent or folded, sometimes twisted; smooth surface, up to 188 μm long (incomplete specimen). Filaments commonly gathered in bundles and perpendicular to the laminae of the stromatolites; 3.1-9.4 μm wide, averaging 6.2 μm (108 filaments measured); wall thickness about 0.5-1.0 μm.

Remarks: Fine filaments of *Siphonophycus inornatum* are seen as isolated sinuous or broken individuals or as interwoven mats embedded within amorphous organic mucilage, subsequently torn into fragments. They are uncompressed in the phosphate and are gently contorted in all directions. In macerated samples, short broken fragments are common.

Material: Hundreds of examples as isolated individuals or bond together in matlike fragments, from thin sections of phosphate and macerates of shale from the

Cailleach Head Formation and the Diabaig Formation.

Siphonophycus solidum Butterfield et al 1994 (Figure 3.15b)
Description: A species of *Siphonophycus* with filament diameters 16-32 μm. Unbranched, nonseptate, smooth-walled filamentous microfossils. Mean - 22.9 μm, s.d. = 5.7 μm, n = 21

Remarks: Wider nonseptate filaments are relatively scarce in the Torridon assemblage, but when present are often found in close association with finer *Siphonophycus inornatum*. They are broken into short fragments and sometimes contain small spore-like bodies.

Material: Tens of specimens broken into short fragments, from phosphates and macerated shales of the Cailleach Head and Diabaig Formations.

Genus *Volyniella* Aseeva 1974

Volyniella glomerata Jankauskas 1980 (Figure 3.15c)
Description: A few thin strands, folded together in a more or less annular coil. Diameter of the fibres 0.5-1.2 μm (holotype 1-1.2 μm), diameter of the coil as a whole 15-30 μm (holotype 30 μm). As a result of decomposition of filaments, the shape of the coil may be distorted. Differs from other species in its coiled form and the size of the filaments.

Remarks: Specimens of *Volyniella glomerata* from the Torridon Group are tightly coiled into annular spirals, or more loosely lemniscate as a result of detachment of filaments. Torridon examples are slightly larger than the described species, with filaments up to 4 μm wide, and maximum diameter of spheroidal coils up to 35 μm.

Material: Five specimens of differing preservation from acid macerates of shales and phosphates from the Cailleach Head and Diabaig Formations.

Genus *Archaeorestis* Barghoorn 1965

Archaeorestis unnamed species (Figure 3.15d)
Representative form: Individual figured in Figure 3.15d; section CAI7mac, from the

Cailleach Head Formation, Torridon Group, Cailleach Head, northwest Scotland. Housed at the Department of Earth Sciences, University of Oxford

Description: Nonseptate, tubular branched hollow filament with a coarsely reticulate surface texture. Branches arise from primary filament at approximately 90°, bear no identifiable septa or swellings, and are of comparable diameter. Diameter of filament 9-13 μm, distal ends are bluntly rounded, proximally broken or open. Maximum length of main filament 43 μm, maximum length of branches 17 μm. No reproductive structures identified.

Remarks: This form differs from previously described species of *Archaeorestis* in its diminutive size, but is otherwise similar in morphology, surface structure and terminal shape.

Material: Two specimens from macerates of the phosphate from Cailleach Head Formation.

Unnamed form A. (Figure 3.15e)
Representative form: Individual figured in Figure 3.15e; section TOR08-45 from the Cailleach Head Formation, Torridon Group, Cailleach Head, northwest Scotland. Housed at the Department of Animal and Plant Sciences, University of Sheffield.

Description: Asymmetric hollow tubular structure comprising a widened end with rounded and slightly bulging terminus, tapering gradually and terminating in a bulging spheroidal cell that communicates freely with the rest of the structure. Length of tube including terminal structures 64-130 μm, mean 109 μm. Width of widened end 19-31 μm, tapering to less than 10 μm. Bulbous terminal cell 12-15 μm in diameter. Specimens often broken at narrow end, to produce closed funnel-like form, or at both ends resulting in tapering conical tube. Wall thick and dark. No reproductive structures known.

Remarks: Careful examination of multiple specimens confirms that their morphology is not a result of superposition. The marked asymmetry of this form makes it distinct from any previously described genera. It is preserved in a variety of states of fragmentation in the Torridon rocks, and typically the wall is almost opaque. Fragmentation of the bulbous parts is common, and as a result tapering conical filaments

represent this form in the majority.

Material: Tens of specimens in varying degrees of physical and chemical degradation, from macerated phosphates and shales of the Cailleach Head and Diabaig Formations.

Group: Septate filaments

Genus *Archaeoellipsoides* Horodyski and Donaldson 1980

Archaeoellipsoides conjunctivus Zhang 1985 (Figure 3.15f)
Description: Large-sized ellipsoids connected end to end. The ends are rounded, flat or slightly caved in. Ellipsoidal envelopes are single layered with a smooth surface; 29.4-36.4 μm long, 16.8-17.0 μm wide, 1.8-2.1 times as long as wide, averaging 33.7 μm long (standard deviation = 3.1), 16.9 μm wide (standard deviation = 0.1) and 2.0 times as long as wide (four individuals measured).

Remarks: Small fragments of these uniseriate chains are preserved in the Torridon phosphates, and macerates separate them, so only elongate rectangular cells are found. Cells have two layers but no encompassing sheath.

Material: Tens of specimens, articulated in thin sections of phosphate from the Cailleach Head Formation, or disarticulated in acid macerates of phosphate and shales from the Cailleach Head and Diabaig Formations.

Genus *Veteronostocale* Schopf and Blacic 1971

Veteronostocale unnamed species (Figure 3.15h, i)
Representative form: Individual figured in figure 3.15h, section CAI-2e, from the Cailleach Head Formation, Torridon Group, from Cailleach Head, northwest Scotland. Housed in the Department of Earth Sciences, University of Oxford.

Description: Trichomes multicellular, uniseriate, unbranched, not attenuated toward apices, constricted and separated at septa, composed of equidimensional spheroidal cells, common sheath apparently absent. Trichomes solitary or in subparallel associations, straight to gently curved, composed of 9-10 cells, total length around 100 μm.

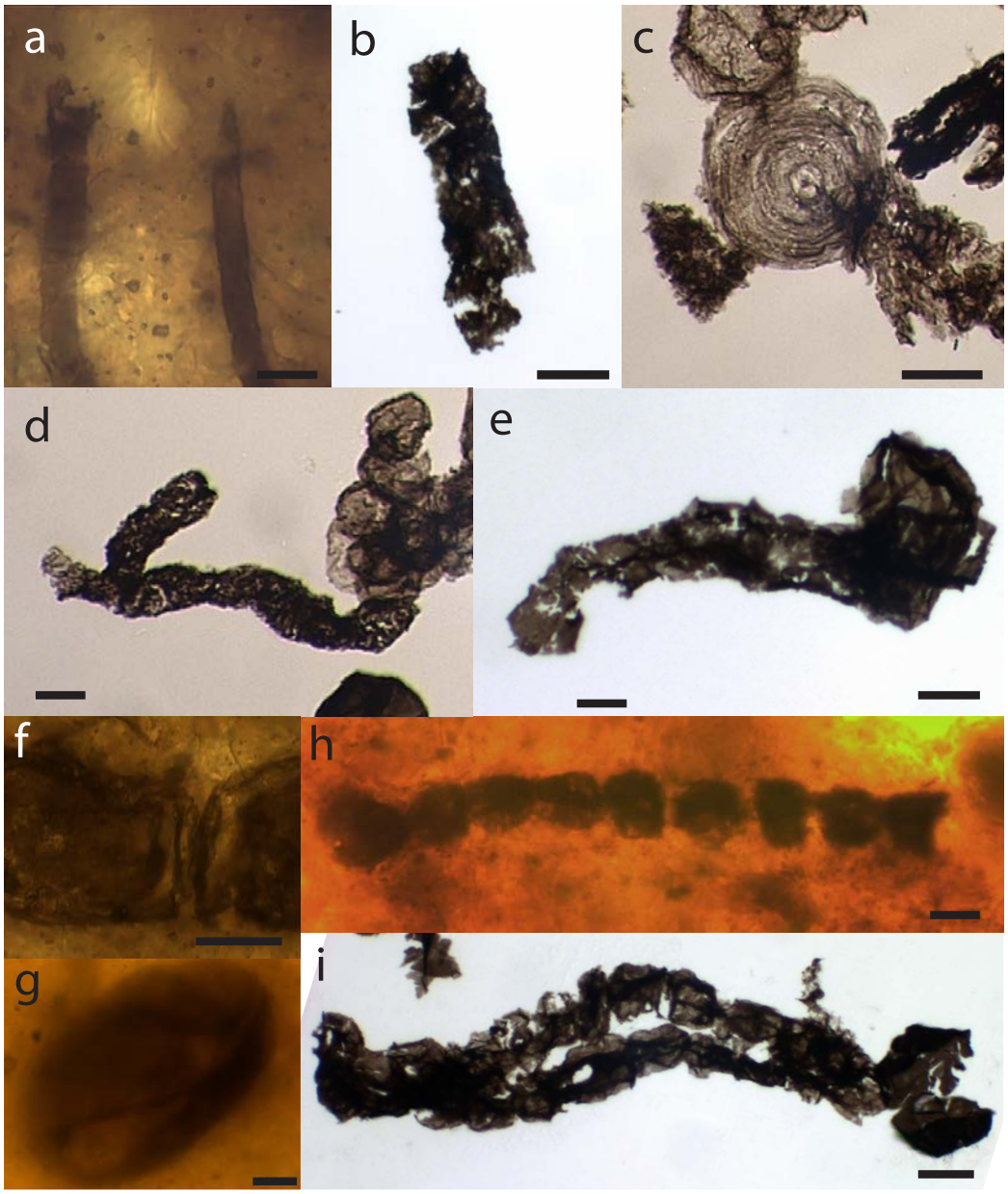


Figure 3.15: Formally described taxa from the Torridon Group. a) *Siphonophycus inornatum*. Sample CAI-2a, phosphate from Cailleach Head; b) *Siphonophycus solidum*. Sample T11-106, macerate of shale from Lower Diabaig; c) *Volyniella glomerata*. Sample CAI-7mac, macerate of phosphate from Cailleach Head; d) *Archaeorestis* unnamed species. Sample CAI-7mac, macerate of phosphate from Cailleach Head; e) Unnamed genus and species A, asymmetric tubular structure with bulbous ends. Sample TOR08-45, macerate of shale from Cailleach Head; f) *Archaeoellipsoides conjunctivus*. Sample CAI-2f, phosphate from Cailleach Head; g) *Archaeoellipsoides obseus*. Sample FLA-3a, phosphate from Fladday; h) *Veteronostocale* unnamed species. Sample CAI-2e, phosphate from Cailleach Head; i) *Veteronostocale* unnamed species. Sample TOR08-45, macerate of shale from Cailleach Head. a, scale bar 5 μm; b, scale bar 20 μm; c, scale bar 15 μm; d-i, scale bars 10 μm.

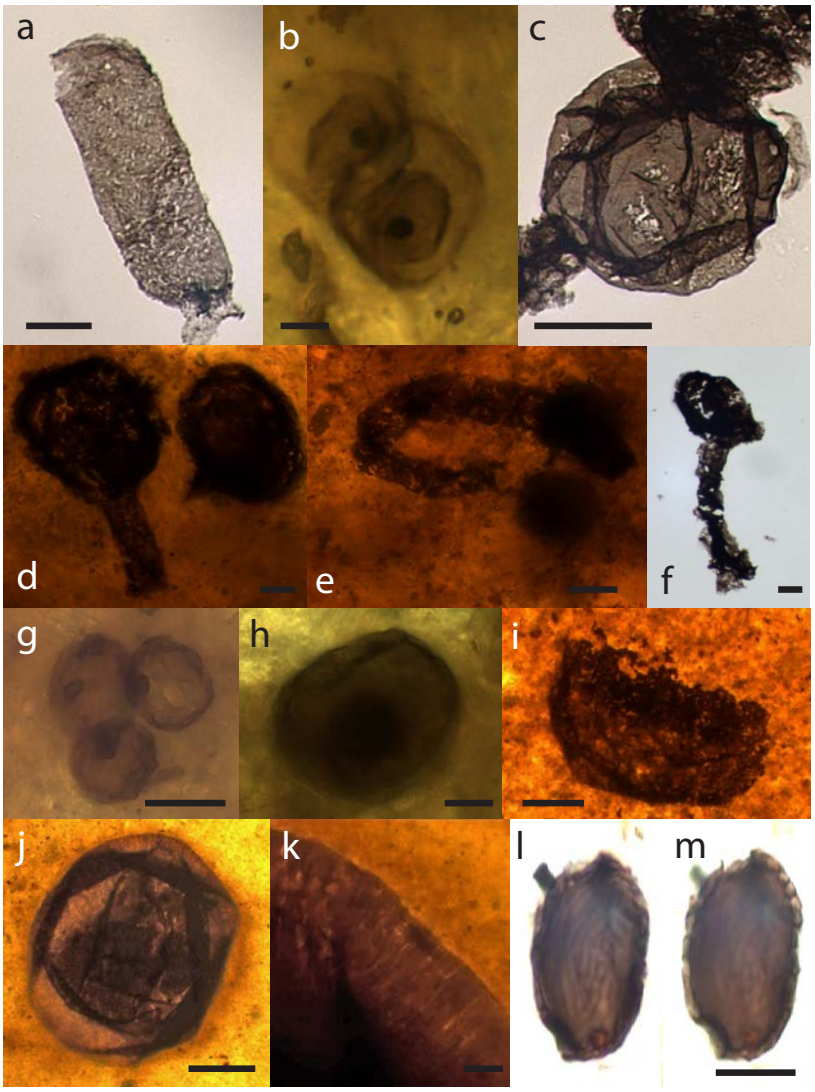


Figure 3.16: Formally described taxa from the Torridon Group. a) *Archaeoellipsodes bactrophycus*. Sample CAI-7mac, macerate of phosphate from Cailleach Head; b) *Globophycus minor*. Sample CAI-2f, phosphate from Cailleach Head; c) *Leiosphaeridia levia*. Sample CAI-7mac, macerate of phosphate from Cailleach Head; d) *Germinosphaera* unnamed species. Sample CAI-2e, phosphate from Cailleach Head; e) *Germinosphaera* unnamed species. Sample CAI-2e, phosphate from Cailleach Head; f) *Germinosphaera* unnamed species. Sample DIA-13mac, macerate of phosphate from Lower Diabaig; g) *Protosphaeridium parvulum*. Sample CAI-2b, phosphate from Cailleach Head; h) *Pterospermopsimorpha pileiformis*. Sample CAI-2f, phosphate from Cailleach Head; i) *Valeria* unnamed species. Sample FLA-3a, phosphate from Fladday; j) *Valeria lophostriata*. Sample FLA-3a, phosphate from Fladday; k) Striae on surface f *Valeria lophostriata* in (j). Sample FLA-3a, phosphate from Fladday; l-m) Unnamed genus and species B, vesicle with complex cellular wall structure. Sample FFA1-1.45a, phosphate from North Sheildaig. a, scale bar 20 μm; b, scale bar 5 μm; c, scale bar 30 μm; d-h, k-m, scale bar 10 μm; i-j, scale bar 100 μm.

Cells spherical to subspherical, diameter 7-11 μm. Reproductive structures unknown.

Remarks: This new form is most similar in appearance to *Veteronostocale amoenum*, but differs in possessing larger cells some separation between cells in the filament. One example, from macerates of shales at Cailleach Head, seems to show two trichomes running parallel and attached at either end.

Material: Two specimens known from thin section and acid macerate of phosphate from the Cailleach Head Formation.

Group: Isolated vesicles

Genus *Archaeoellipsoides* Horodyski and Donaldson 1980

Archaeoellipsoides obesus Zhang 1985 (Figure 3.15g)
Description: Large-sized ellipsoidal envelopes, rounded ends, single layered, solitary; 9.5-64.4 μm long, 2.2-22.4 μm wide, averaging 35.5 μm long (standard deviation = 14.7) and 11.2 μm wide (standard deviation = 5.8); 1.8-4.8 times as long as wide (averaging 3.4; 36 individuals measured). Envelopes empty or with 1-2 vesicle-like inclusions, which are situated in the middle part or near the ends of the envelopes. Inclusions are 2.5-7.8 μm in diameter with an average of 4.6 μm (standard deviation = 2.3; six inclusions measured). Envelopes are mostly straight, sometimes curved or slightly constricted at the middle portion.

Remarks: Short ellipsoidal cells of *Archaeoellipsoides obesus* are relatively common in the Torridon, occurring in particular abundance in the phosphates of the Diabaig Formation. They occur singly, and do not contain inclusions.

Material: Hundreds of specimens of varying preservation in thin sections of phosphate from the Cailleach Head and Diabaig Formations.

Archaeoellipsoides bactroformis Sergeev et al 1995 (Figure 3.16a)
Description: A species of *Archaeoellipsoides* differentiated by its length and high L/W. Solitary or gregarious single- and double-layered, large, rod-like, often curved, empty ellipsoids with rounded ends. Length 50->150 μm; width 5.0-14.5 μm; L/W = 3-25. Ellipsoid wall medium or coarse grained, its thickness <0.5- >1 μm. Outer

envelope (when present) fine grained and <0.5 μm thick.

Remarks: Individuals of *Archaeoellipsoides bactroformis* are seen in abundance in acid macerations of the phosphate and shales from the Cailleach Head and Diabaig Formations, and have not yet been identified in thin section. Walls are typically very thin, and the elongate vesicle may be folded or coiled. Rare examples contain dark elongate bodies centrally, which may be the remnant of an internal trichome or cytoplasmic material. Average dimensions for the Torridon material are 25 μm wide and around 100 μm long.

Material: Tens of specimens from acid macerations of the phosphate and shales of the Cailleach Head and Diabaig Formations.

Genus *Globophycus* Schopf 1968

Globophycus minor Oehler 1977 (Figure 3.16b)
Description: Cells spheroidal, solitary, with coarsely rugose surface texture and encompassed by a hyaline, unlamellated sheath. Cells about 8.2 μm in diameter (1 specimen); sheaths up to 0.7 μm thick, irregularly concentric about cell. Actinomorphic to circular organic structure present near periphery of cell.

Remarks: Few examples of *Globophycus minor* are found in the Torridon phosphates, perhaps owing to the fragility of their thin membranes. They occur singly or in loose pairings, and contain amorphous organic spots centrally or near the periphery.

Material: Seven examples of good preservation from thin sections of phosphate from the Cailleach Head Formation.

Genus *Germinosphaera* Mikhailova 1986

Germinosphaera unnamed species (Figure 3.16d-f)
Representative form: Individual figured in figure 3.16d, section CAI-2e from Cailleach Head Formation, Torridon Group, Cailleach Head, northwest Scotland. Housed at the Department of Earth Sciences, University of Oxford.

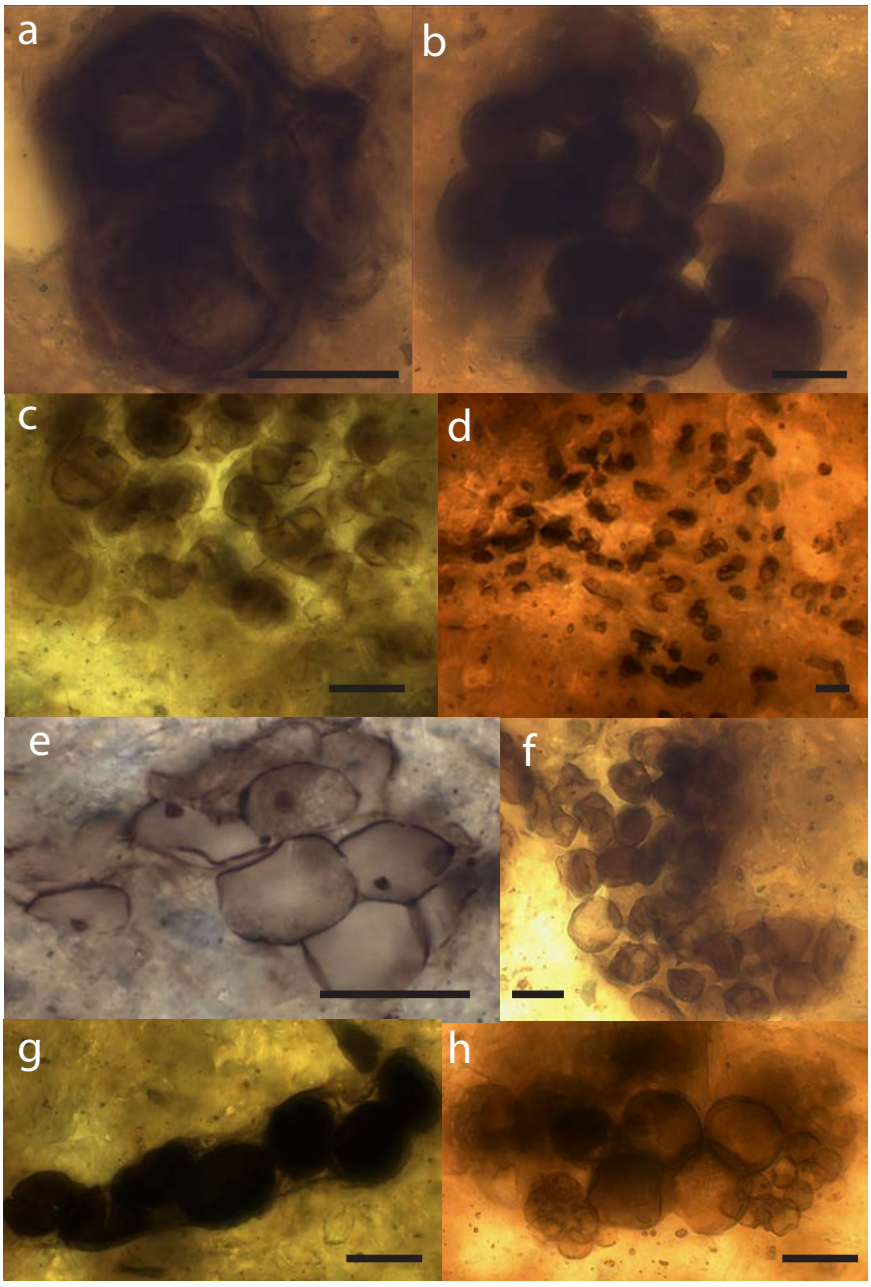


Figure 3.17: Formally described taxa from the Torridon Group. a) *Gloeodiniopsis lamellosa*. Sample CAI-2b, phosphate from Cailleach Head; b) *Maculosphaera kingstonensis*. Sample CAI-2b, phosphate from Cailleach Head; c) *Myxococcoides distola*. Sample CAI-7b, phosphate from Cailleach Head; d) *Myxococcoides kingii*. Sample CAI-2c, phosphate from Cailleach Head; e) *Myxococcoides minor*. Sample FFA1-1.45a, phosphate from North Sheildaig; f) *Myxococcoides staphylidion*. Sample CAI-2a, phosphate from Cailleach Head; g) Unnamed form C, sheathed chain of dark vesicles. Sample CAI-7b, phosphate from Cailleach Head; h) Unnamed form D, bimodally sized vesicles in cluster. Sample CAI-2d, phosphate from Cailleach Head. a, g-h, scale bars 20 μm, b, f, scale bars 10 μm; c, e, scale bars 15 μm; d, scale bar 5 μm.

Description: Spheroidal or ellipsoidal vesicle bearing one wide, unbranched, untapering hollow tubular process that communicates freely with the vesicle. Vesicle 15-50 μm in diameter; process 10-15 μm wide, 30-90% of vesicle diameter, of variable length up to 125 μm, distal end broken. Processes straight or broadly curved, untapering and not narrowed at base, with distinct change in slope between vesicle and process. Surface of vesicle and process dark, opaque and irregularly rugose. No internal structures observed. No excystment structure.

Remarks: This form differs from previously described species of *Germinosphaera* in possessing a single broad process that is a significant fraction of the vesicle diameter. Distal ends are consistently broken so terminal structure is unknown.

Material: Several examples seen in varying states of preservation in thin sections of phosphate from the Cailleach Head Formation, and macerated shales from the Diabaig and Cailleach Head Formations.

Genus *Leiosphaeridia* Eisenack 1958

Leiosphaeridia levia n. comb. Zhang and Walter 1992 (Figure 3.16c)
Description: Vesicle circular to subcircular, originally spheroidal; wall granular spongy, folded, with dense, coarse, surface texture; no excystment structure. Vesicle diameter 25-85 μm

Remarks: Large thin-walled vesicles attributable to Leiosphaeridia levia on account of their size range and wall textures, are relatively abundant, showing no excystment structure and, typically, no internal contents. Surface texture in the Torridon examples range from smooth to somewhat granular. Average diameter 63 μm.

Material: Hundreds of examples of generally good preservation in thin sections and acid macerates of phosphates and shales from the Cailleach Head and Diabaig Formations.

Genus *Protosphaeridium* Timofeev 1960

Protosphaeridium parvulum Timofeev 1966 (Figure 3.16g)
Description: Envelopes of diameter 10-35 μm, smooth, spherical, slender, single layered, provided with spreading folds. Colour light yellow. Some variability is found in the dimensions of different specimens. Similar to *P. papyraceum* from which it differs in its smaller size.

Remarks: More abundant than the larger forms, the small vesicles of *Protosphaeridium parvulum* occur throughout the phosphate and shale thin section and macerates. They are single or loosely associated with one another, and often contain a single amorphous organic spot centrally or eccentrically. No excystment structures are seen.

Material: Hundreds of relatively well preserved examples from thin sections and acid macerates of the phosphates and shales of the Cailleach Head and Diabaig Formations.

Genus *Pterospermopsimorpha* Timofeev 1966

Pterospermopsimorpha pileiformis Timofeev 1966 (Figure 3.16h)
Description: External envelope spherical, diameter 80 μm, dense, wrinkled, yellow in colour. Internal envelope spherical, diameter 60 μm, coarse, stout, brown. Differs from *P. binata* in its more spherical form, simpler structure of the internal nucleus and in its denser outer envelope.

Remarks: Examples of *Pterospermopsimorpha pileiformis* from the Torridon are somewhat smaller than for the described species, reaching a maximum diameter of 43 μm. Shape of the vesicle ranges from spheroidal to ellipsoidal. In other respects the forms are very similar, and the dense outer layer may be disrupted, leaving the inner vesicle relatively pristine.

Material: Tens of examples of varying preservation in thin sections and acid macerations of the phosphate from the Cailleach Head and Diabaig Formations.

Genus *Valeria* Jankauskas 1980

Valeria lophostriata Jankauskas 1980 (Figure 3.16j, k)
Description: Circular to sub-circular (originally spherical), single walled organic vesicles. The vesicle is of medium thickness and flexibility. This results in well-developed, clear and sharp-bounded folds. No excystment mechanism has been recorded. Most specimens are fractured, cracked or incomplete (particularly the larger ones). The vesicles displays an extremely diagnostic polarly arranged, hemispherical sculptural pattern, which consists of parallel, tightly packed striae. The striae are extremely thin, their thickness and elevation being less than 1/4 μm; thus, they are hardly resolvable individually under conventional transmission-light optics. However, the sculptural pattern of larger specimens (which consist of individual fragments) reveals that the striae consist of tightly arranged linear sequences of extremely tiny granulae. Thus, the possibility of optical resolution of this particular type of ornamentation is directly proportional to the diametric dimensions of the specimen. Dimensions 450-700 μm

Remarks: The single specimen of *Valeria lophostriata* from the Torridon is large, up to 450 μm in diameter, and thus their striae are visible, especially at the margins, approximately 2 μm wide. They appear to contain several dark internal bodies. Megaspheroidal vesicles attributable to *Valeria* sp. but preserved at different stages of decay are present within phosphatic nodules of the Diabaig Formation.

Material: One entire specimen of good preservation and several heavily decayed forms from the Diabaig Formation.

Valeria unnamed species (Figure 3.16i)
Representative form: Individual figured in Figure 3.16i, section FLA-3a from the Diabaig Formation, Torridon Group, at Fladday, northwest Scotland. Housed in the Department of Earth Sciences, University of Oxford.

Description: Circular to subcircular vesicles, often torn and fragmented, consisting of a single wall. Vesicle wall relatively thick, with richly irregular pustulate texture, producing a rough and spongy appearance. Vesicles 250-270 μm in maximum diameter, with no inclusions and no excystment structure observed.

Remarks: This form differs from previously described species of *Valeria* in the absence of a striated wall, bearing instead a pustulate texture. It is otherwise com-

parable in size and wall thickness. Megaspheroidal vesicles attributable to Valeria sp. but preserved at different stages of decay are present within phosphatic nodules of the Diabaig Formation.

Material: Three fragmented examples from thin sections of the phosphate of the Diabaig Formation.

Unnamed form B. (Figure 3.16l, m)
Representative form: Individual figured in Figure 3.16l, m, section FFA1-1.45a, from the Diabaig Formation, Torridon Group, at North Shieldaig (Fish Farm), northwest Scotland. Housed in the Department of Earth Sciences, University of Oxford.

Description: Spheroidal to ellipsoidal multilamellated vesicle with complexly structured outer wall, may or may not contain densely packed polygonomorphic cells. Outer wall is composed of many discrete sausage-shaped cellular elements, with internal domains that are equidimensional or elongated along the vesicle's long axis. Vesicle length 21-24 μm and 10-13 μm wide. Average diameter of cellular elements of wall 2-3 μm, thickness of outer wall 2-3 μm. Up to three smooth layers internal to this wall, and internal cavity may be filled with closely adpressed cells up to 5 μm in diameter, showing mutual compression that gives them a polygonal morphology.

Remarks: This form was figured by Strother et al. (2011) and Battison & Brasier (2012), and evades comparison with any known taxa. Its small size combined with a consistently complex wall make higher taxonomic affinity difficult to establish, as it is much smaller than classically considered eukaryotes (Javaux 2007, Javaux et al. 2003, 2001, Knoll et al. 2006).

Material: Convincing examples of this morphotype have only been recovered from thin sections of the phosphate from the Diabaig Formation. Eight discrete examples have been found.

Group: Clustered vesicles

Genus *Gloeodiniopsis* Schopf 1968 emend. Knoll and Golubic 1979

Gloeodiniopsis lamellosa Schopf 1968 emend. Knoll and Golubic 1979 (Figure 3.17a)
Description: Spheroids and ellipsoids with single, double to multiple outlines, solitary or in groups of 2, 3, 4, up to 8 individuals within a common envelope. External outlines mostly rounded; the internal ones rounded, constricted in the middle or polyhedral. Collapsed, shrunken or mutually adpressed spheroids form polyhedral bodies with sharp edges and folds which are often arranged in triradiate manner at the meeting points of three polygonal surfaces. Occasional single inclusions filled with homogeneous finely granular carbonaceous matter are centrally or eccentrically placed within the outlines. Average diameters of spheroids and ellipsoids, expressed as means $\pm$ standard deviation, 10 $\pm$ 2 μm for the internal outlines, 14 $\pm$ 2.8 μm for the external outlines, and 12.5 $\pm$ 3.5 μm for single outlines (n = 100,100 and 50, respectively). Groups within particular microenvironments are more uniform in size, shape and state of preservation. Occasional single inclusions (central or eccentric) are spherical, elongated or constricted in the middle, 2.5-8.0 μm (average 4.23 x 5.34 μm, n = 11).

Remarks: Multiple sheaths are found around isolated vesicles, and adpressed clusters of up to six spheroidal thin-walled individuals. Typically three outer enclosing layers are present, and the constituent cells may have a single amorphous dark spot located centrally or eccentrically in the cell. Average diameter of entire cluster around 45 μm, constituent cells 15-20 μm across. No excystment observed.

Material: Several well preserved examples from thin sections of phosphate from the Cailleach Head and Diabaig Formations.

Genus *Maculosphaera* Licari 1978

Maculosphaera kingstonensis Licari 1978 (Figure 3.17b)
Description: Cells commonly elliptical, occasionally spheroidal, seldom angular, rarely polyhedral, typically solitary or commonly in pairs loosely associated with numerous other cells. Occasionally colonial, associated in uniserial chains, or closely appressed, forming mats of hundreds of cells within laminae. Cell surface coarsely to finely reticulate. Cell diameter ranging from 6 to 25 μm. Wall about 0.5 μm thick. Sheath not present around individual cells but questionably present around colonial aggregates. Most cells possess a single, dark, subcentrally or eccentrically located spot (rarely more than one) which ranges from 0.3 to 2.2 μm and averages about 1 μm

in diameter. Reproduction is by binary fission in one or possibly two planes. Other reproduction unknown.

Remarks: Dark walled cells are spheroidal or ellipsoidal and loosely associated in clusters of around 10 individuals, with individuals rarely touching. Average diameter of vesicles is 10 μm. No dark bodies are observed internally, and excystment structures are absent.

Material: Tens of examples from thin sections of phosphate from the Cailleach Head and Diabaig Formations.

Genus *Myxococcoides* Schopf 1968

Myxococcoides distola Knoll et al 1991 (Figure 3.17c)
Description: A species of *Myxococcoides* consisting of 7-13 μm vesicles characteristically occurring in pairs. Vesicles in loose colonies of a few to many hundred individuals. Unicells and pairs uncommonly enclosed in a thin membrane

Remarks: Loose associations of tens of thin-walled, translucent vesicles that are arranged in dyads and occasionally tetrads are preserved in three dimensions within phosphate. No common sheath is present and contact between cell pairs or tetrads is rare. Vesicles typically contain a dark amorphous spot located eccentrically within the cell. Dyad or tetrads up to 12 μm in diameter, clusters up to 120 μm across.

Material: Loose clusters occur relatively rarely in thin sections of the phosphate from the Cailleach Head formation.

Myxococcoides kingii Muir 1976 (Figure 3.17d)
Description: Cells more or less spherical, shape sometimes altered by relationship with neighbouring cells; cells sometimes in pairs. Indistinct organic matrix present throughout colony, sheaths occasionally present. Cell surface smooth, sometimes slightly granular, sheath, where present, smooth. Diameter of cells ranges from 2.7-5.0 μm (average 3.9 μm, 107 specimens measured). Outline of colony indistinct, but colonies up to 55 μm in diameter have been observed.

Remarks: Loose associations of small, translucent cells are relatively common amongst the phosphatic deposits, and these clusters may or may not be embedded in a common mucilage or carbonaceous mass. Spheroidal cells 3-4 μm in diameter and rarely in contact with one another. No common envelope present and dark internal bodies are rare.

Material: Tens of examples from thin sections of phosphate from the Cailleach Head and Diabaig Formations.

Myxococcoides minor Schopf 1968 (Figure 3.17e)
Description: Cells commonly spherical to subspherical, occasionally ellipsoidal, frequently somewhat flattened by compression against adjacent cells; solitary, or clumped in a more or less ellipsoidal colony composed of a few to about 40 cells. Surface texture varies from psilate or nearly psilate to finely and regularly punctate and reticulate. Cell diameters vary between about 8.8 and 10.5 μm, with an average diameter (25 cells measured) of 9.7 μm. Cell walls robust, distinct, about 0.7 μm thick. Cells commonly embedded in a somewhat granular, non-lamellated organic matrix up to 3 μm thick at the periphery of the colony. Colonies vary in number of component cells, the cells being geometrically unordered in relation to colony shape.

Remarks: Very close associations of thin translucent cells result in compression and a polygonal shape. Pale or dark amorphous spots are commonly present within cells. External envelope, if present, is thin and diaphonous. Clusters up to 75 μm in diameter, and individual cells slightly larger than described for the species around 12-14 μm.

Material: Several well-preserved examples from thin sections of phosphate from the Diabaig Formation.

Myxococcoides staphylidion Lo 1980 (Figure 3.17f) Description: Cell-like units, spheroidal to ellipsoidal, occasionally polyhedral in crowded clusters. Surface smooth, unornamented, light-brown. Wall thin, solid or broken, rarely obscure, diffuse, thickness usually less than 0.8 μm. Individual units not encompassed by any envelope. Rarely solitary, usually 10-70 individuals clumped in three dimensional, globular or grape-like clusters or in two dimensional net-like aggregations. Halo-like common

envelope surrounding the cluster may be present or not. Clusters occasionally embedded in amorphous, dark brown, common matrix. Diameter of spheroids and long axis of ellipsoids 1.6-12.1 μm, averaging 5.5 μm (standard deviation = 2.23 μm; 286 specimens measured). Dimension of cluster from 16 μm - 100 μm across

Remarks: Irregular clusters of small spheroidal thin-walled vesicles are relatively common, although degradational shrinkage separates individuals that would have originally been in contact. No external membrane is present, and internal bodies are rare. Spheroids are typically less than 10 μm in diameter, and occur in clusters of up to 30 individuals.

Material: Tens of examples in varying degrees of preservation, in thin sections of phosphate and occasionally acid macerations of phosphate and shale from the Cailleach Head and Diabaig Formations.

Unnamed form C. (Figure 3.17g)
Representative form: Individual figured in Figure 3.17g, section CAI-7b from the Cailleach Head Formation, Torridon Group, at Cailleach Head, northwest Scotland. Housed at the Department of Earth Sciences, University of Oxford.

Description: Dark, thick-walled vesicles arranged uniserially or pseudo-biserially in a chain or elongate cluster, enclosed by a thin common sheath. Vesicles spheroidal to subsphaeroidal, up to 20 μm in diameter, and comprising a single, thick opaque wall; occasional excystment by median split. Outer sheath thin, smooth, diaphonous, single layered.

Remarks: While elongate clusters of vesicles have been described (e.g. *Glenobotrydion aenigmatis*), the forms described here differ in their thick, cyst-like wall, and uniserial arrangement within a common sheath.

Material: Two well preserved specimens from thin sections of phosphate from Cailleach Head.

Unnamed form D. (Figure 3.17h)
Representative form: Individual figured in Figure 3.17h, section CAI-2d from the Cailleach Head Formation, Torridon Group, at Cailleach Head, northwest Scotland.

Housed at the Department of Earth Sciences, University of Oxford.

Description: Irregularly shaped clusters of spheroidal vesicles of two distinct diametric modes. Larger vesicles are on average 21 μm in diameter, and smaller vesicles approximately 5 μm. Smaller vesicles occur on the outer periphery of the cluster, and are compressed into broadly spheroidal masses comprising up to 6 cells. Vesicle walls are thin, single layered, translucent and smooth, and an encompassing sheath is absent. Internal bodies occur rarely within the smaller vesicles. No excystment structures are known.

Remarks: Clusters of bimodally sized vesicles have not yet been described from the Proterozoic fossil record. The size, distribution, and close association of smaller vesicles is suggestive of their formation by multiple fission of the larger vesicles.

Material: Two well-preserved specimens are known from the phosphate of the Cailleach Head Formation.

Chapter 4

Comparison of Torridon microfossils

4.1 Taphonomy

The Torridon assemblage offers the opportunity to study more than just taxonomy. Taphonomic alteration of the range of microfossils from different lithofacies presents a method of more fully understanding represented species and their morphological alteration, as well as types of taphonomic environment, and relationships between taphonomy and represented diversity.

4.1.1 Introducing taphospace and data collection

In order to objectively assess taphonomy, it is necessary to devise a method of classifying the degree of taphonomic alteration that is applicable to deposits of organic-walled microfossils from a variety of preservational lithologies: shales, cherts and phosphates.

Previous work on taphonomy has been qualitative (Butterfield et al. 1994), or has classified modes of degradation as constructive or destructive, referring to the volumetric changes occurring within the microfossil (cf. Grey & Willman 2009). As a classification scheme, it is limited, as taphonomic processes may be a combination of both, or neither. Although quantitative indices have been proposed for alteration of acanthomorphic acritarchs (Grey & Willman 2009) and modern cyanobacterial assemblages (Bartley 1996), neither of these indices have broad applicability across microfossils assemblages in the Proterozoic and elsewhere.

The following describes a newly devised index that refers directly to ways in which any organic structure may be modified, logically dividing these into physical, chemical,

and biological effects, and subsequently using the original grades of alteration in a three-dimensional plot to represent a 'taphospace'.

4.1.1.1 Physical

Physical changes that may affect degrading organisms are shriveling, shape change, folding, tearing, and fragmentation, in addition to mineral and imprinting and holes formed by adjacent mineral grains. The latter two changes are not considered here as they are dependent on specific depositional or preservational environments. Physical damage can be caused by either intrinsic factors such as fluid loss or extrinsic abrasion and damage.

Shrivelling and shape change are most commonly the results of fluid loss following cell death and possibly as a response to osmotic differences in water potential. In these cases, rounded cell structures will become more polygonal in outline and small folds may develop. In more extreme cases, more notable volumetric reduction may be evident—this is especially apparent in colonial fossils, where individual cell elements are shrinking away from one another, and in filaments, where the body of the filament is reduced and the structure takes on a thread-like appearance.

Folds may be formed as a result of shriveling, but may also be created as a result of external influences, most commonly compression. This will be especially prevalent in shale-hosted deposits, where the laminae of the sediment directly crush three dimensional organisms during their formation. Folds can be identified in organic-walled microfossils by sharply defined changes in opacity where several segments of wall overlap one another. In spherical structures, they appear arcuate, subparallel to the cell circumference; in filamentous or irregular fossils, they can alter the overall morphology considerably.

Tearing and fragmentation of organic structures is most likely to be driven by external factors such as sedimentation-related abrasion, and transport-driven distortion. Tears may form linear and angular breaks in an otherwise coherent wall, and with progressive severity of tearing will result in missing segments and ultimate break-up of the original structure. At this stage, it may be difficult to recognise the morphology of the original form.

The degree of physical deformation that an organic-walled microfossil undergoes will be related to the severity of the physical stresses, but also partly to the original chemistry and architecture of the organism's wall. Thinner, delicate walls will be more conducive to deforming and tearing under slighter stresses than thicker, multilamellar walls, and this must be borne in mind when interpreting taphonomic grade. Post-mortem changes in the chemistry of wall structures, which itself may be difficult to detect through standard techniques, may cause them to become more rigid and prone to tearing or shattering (Schopf & Klein 1992).

4.1.1.2 Chemical

Chemical changes in the composition and/or structure of organic-walled microfossils may result in more subtle alterations of the appearance of the fossil walls, including wall darkening or lightening, flocculation of carbon in the wall, and dissemination of fine organic particles. In addition, aliphatisation (Kodner et al. 2009, Versteegh & Blokker 2004) and aromatisation (Marshall et al. 2005) of carbonaceous walls can occur, but these processes are not included here as they are not exclusively recognisable in fossil material. Chemical changes may be driven by intrinsic factors involved in cell death, or external variations in the decay microenvironment.

Wall darkening may occur as a result of thermal maturation of the rocks containing the fossils, and a basic index of maturation of palynomorphs has been used sporadically for Proterozoic shale-hosted microfossils (e.g. Oehler & Logan 1977, Samuelsson et al. 1999). Such an index cannot be applied directly to microfossils preserved in occluding media like chert and phosphate, as the opacity of the substrate may alter the appearance of the fossils. Darkening could also be result of fluid loss after death of a microorganism, rendering the colorimetric index of maturity overly simplistic. If wall darkening occurs over the entire surface of an organic structure, it can be difficult to detect, as the original colour and opacity of the wall is unknown. It may be more readily observable, however, if select parts of a wall structure are darkened adjacent to comparatively unaltered wall, producing a patchy appearance. Such discontinuous chemical alteration is more likely to be driven by changes in the local decay microenvironment than by thermal alteration or fluid loss.

Lightening of the wall of an organic microfossil, which may be caused by externally or internally driven dissolution of the organic compounds, is beset by the same detection problems as with darkening. If lightening has occurred over the entire wall,

it may be difficult to detect, or assess the severity, as the initial colour and opacity of the wall is unknown. As with darkening, however, if lightening occurs in isolated patches over the wall surface, it may be distinguished from the comparatively unaltered wall, giving an irregular patchy appearance.

More extreme chemical changes to organic walls of microfossils, resulting from more comprehensive changes in chemical structure and composition, may be detected as flocculation of carbonaceous material in the wall. This will likely be accompanied by darkening, but is most easily recognised by a clumpy and colloidal appearance of the organic matter making up the wall, which then may be partly disarticulated as structural coherence of the wall breaks down. Flocculation appears to be driven by a combination of intrinsic cell breakdown, and changing conditions of the external decay microenvironment.

Continued chemical alteration of organic walls will result in further breakdown and ultimate dissemination of organic particles. At this stage, fine particles of carbon form a 'shadow' of the original microfossil morphology, and their chemical and physical dispersal may cause edges to appear indistinct and fine scale details to be lost. Owing to this progressive loss of information, microfossils at this grade of chemical disintegration can be difficult to recognise unequivocally. In particular, shale hosted microfossils which can only be studied following acid maceration will not preserve this taphonomic grade, as the organic particles will be completely disarticulated from their original loose association. Such constraints must be borne in mind when interpreting taphonomic grade from observations.

4.1.1.3 Biological

Biological interactions within a recycling heterotrophic and saprophytic microbial ecosystem can be expected to leave traces in the taphonomic record of organic-walled microfossils, although these features may often go unremarked. The action of internal cell autolysis processes and external bacterial or protistan attack can create dark internal spots, wall dissolution and even pseudomorphing of the fossil structure by bacteria.

Upon the death of a cell, processes of autolysis are immediately initiated, which result in the breakdown of the internal contents of the cell. This, in combination with osmotic fluid loss as a result of suspension of active ionic pumping in the cell,

lead to plasmolysis of the cell contents, with the cytoplasmic material and cell membrane pulling away from the more rigid wall, and ultimately condensing into a dark, organic-rich spot contained within the cell wall. This spot, seen commonly in both shale-hosted and silicified or phosphatised microbiotas (e.g. Knoll 2003), could be misinterpreted as a preserved nucleus, but the inevitability of cell autolysis under even the most rapid preserving conditions makes such an interpretation incredibly unlikely. Thus, where the cell wall is not breached, and preservation occurs before chemical or biological consumption of the cell contents, they can be expected to be found as a dark organic-rich spot within their corresponding vesicle or filament.

Heterotrophic attack by bacteria or protists is a common process in modern microbial communities (e.g. Cota et al. 1996), and it can be expected that since their evolution, some trace of their action could be left in fossilised microorganisms. Heterotrophic organisms tend to colonise the inner or outer surfaces of target organisms, usually as a more-or-less coherent biofilm (Raff et al. 2008), and will dissolve and consume the organic matter adjacent to them, leaving pits or holes in the wall of the victim cell. These structures may be distinguished from abiogenic tears, or original surface ornamentation, by their roundedness and irregular distribution across the surface, respectively.

More extreme heterotrophic attack will result in more complete consumption of the organic wall material, associated with more extensive colonies of heterotrophs. In these cases, the heterotrophs themselves may be preserved, instead of the organic matter that they are feeding on. In occluding media such as chert or phosphate, these will appear as pale baccilate structures of consistent size and shape, attached to remnants of organic wall, or pseudomorphing the broad shape of the original structure. They are lighter in colour, owing to the small amount of organic carbon contained in their flexible membranes or mucus capsules. Pseudomorphic bacteria have also been described from phosphate-permineralised fossils of the Doushantuo (Xiao & Knoll 2000) and experimental work (Raff et al. 2008, 2006), although the pseudomorphed structures are unlikely to be recovered from shale-hosted deposits, owing to their weak spatial association with little or no binding carbon.

Physical	
P0	No physical change
P1	Folding and shape change
P2	Tearing
P3	Fragmentation
Chemical	
C0	No chemical change
C1	Wall lightening or darkening
C2	Wall flocculation
C3	Carbon dissemination
Biological	
B0	No biological changes
B1	Dark internal spot preserved
B2	Pits or holes from wall consumption
B3	Baccilate pseudomorphing

Table 4.1: Summary of taphonomic features characteristic of differing grades of alteration. Qualitative identifying features are more or less ordinal, although it is recognised that alteration features may be interlinked or occurring as a result of exclusively different processes.

4.1.2 Construction of a taphospace

Having noted these changes within the physical, chemical, and biological taphonomic domains, an index is required that can classify the morphological features for comparison between deposits, and further interpretation of diversity and preservational environment. Those features described above, despite being qualitative, are more or less ordinal in their severity, and so can be placed on a scale representing increasing taphonomic grades, in each of the domains, outlined in Table 4.1, figured in Figure 4.1, and explained below. A potential refinement of this scheme may include quantitative measures of degradation under each domain, for example, the degree of tearing. In this study, the concept of taphospace is explored for the first time, and therefore these ordinal, qualitative characters are used for preliminary analysis.

Physical alteration ranges from the slight, internally driven changes in shape as a result of autolysis, through increasing amounts of distortion and damage until an organic-walled structure loses much of its characteristic morphology. In the system detailed above, folding and shape change are grouped together, because they are often interlinked, regardless of the cause. All but the finest three-dimensionally preserved fossils will display some kind of shape change or folding (P1). Progressively more

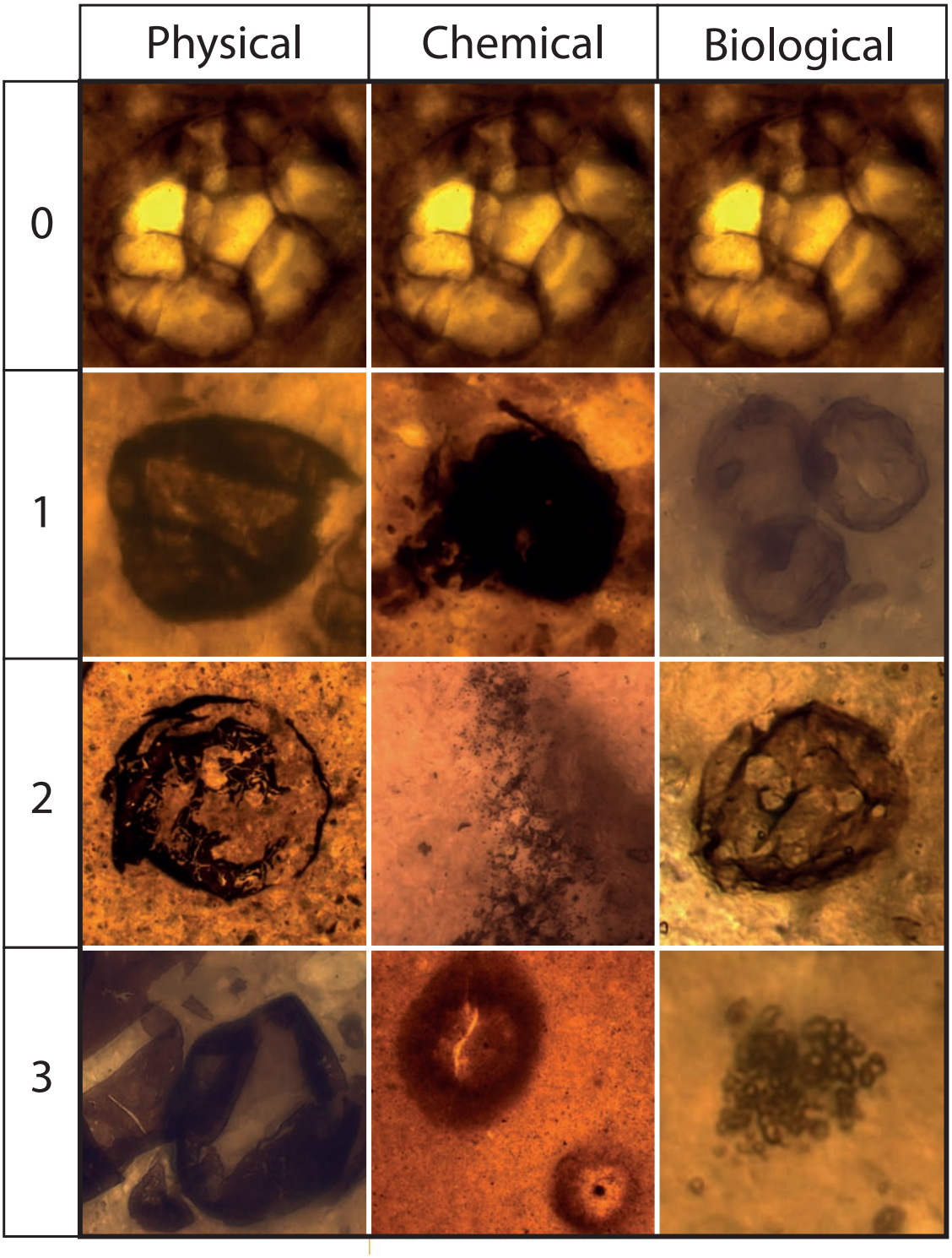


Figure 4.1: Plate illustrating examples of each taphonomic grade, in the physical, chemical, and biological domains. Figured examples all sourced from thin section samples of phosphate from the Diabaig and Cailleach Head Formations.

intense abrasion or distortion will create tears (P2), which will coalesce until the wall is fragmented (P3). Under some individual circumstances, the order of these changes may be reversed or mixed, but the above scheme is considered to be the general case.

The slightest chemical changes that an organic fossil can undergo will be represented morphologically by a change in colour of the wall (C1). Whether darkening as a result of thermally driven graphitisation, or lightening as a result of early thinning and dissolution, where recognised, this will be the first stage of chemical change and will be most easily identified where parts or patches of the wall are altered. Progressive chemical alteration of the structure and composition of the wall will lead to a flocculation of the carbon (C2), and then ultimately to the creation and dissemination of fine isolated organic particles (C3).

Biological taphonomy begins with cell death and, unless preservation occurs extremely rapidly, autolysis will occur. Cellular structures preserved at this taphonomic grade will contain a dark internal spot (B1), although this spot may be later lost through chemical alteration, physical disarticulation, or heterotrophic consumption. Biological degradation increases with the addition of external heterotrophic components, first by the creation of pits and holes by their consumption (B2), and later by the more-or-less complete loss of carbon, and maintenance of the fossil structure only by pseudomorphing by baccilate structures of those heterotrophic organisms (B3). In some cases, B1 and B2 can occur together or in reversed order, but a general case is considered here for simplicity.

With this sequence of ordinal qualitative taphonomic characters, it is possible to create a three dimensional plot upon which data collected from various fossil deposits can be represented and therefore visually and directly compared. At high taphonomic grades for each domain, and particularly when the three are combined, microfossil structures and their taxonomic and taphonomic characters become difficult to recognise, and special care must be taken not to over- or under-interpret these forms.

A sample cube plot is shown in Figure 4.2, as a wire frame, with a sample dataset. The plot is constructed from taphonomic character data collected from fossil structures, with individual unit cubes coloured if they are occupied, with tone manually adjusted to represent the abundance of taxa of that taphonomic grade, in proportion to the highest count, providing a taphonomic 'hotspot' and surrounding occupation

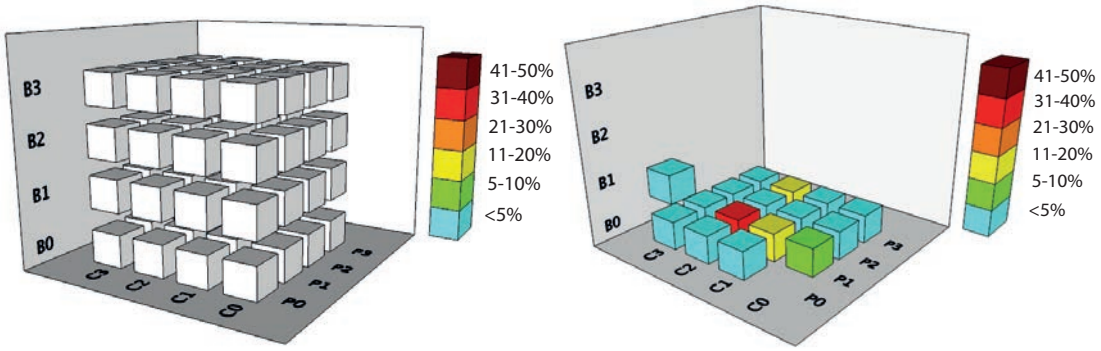


Figure 4.2: Construction of 'taphospace' plot. Empty wireframe plot (left hand side), illustrating typical positions of ordinal grouped criteria. Sample dataset (right hand side), showing how data is input. Occurrences of combination of particular taphonomic features allow the respective domain to be coloured; repeated occurrences of that feature alter the colour from cold to warm tones. Tones calculated based on proportion of highest count, to provide occupation space around 'hotspots' of taphonomic alteration.

space. It may be possible to develop a program environment that can automatically plot entered taphonomic data, but this is beyond the scope of this work. The plots figured herein were drafted manually using *Google Sketchup 7* and *Adobe Illustrator 5*.

Taphonomic character data were collected for the Torridon and Gunflint microbial assemblages, and are presented in the succeeding chapters and sections, to enable characterisation and comparison between different depositional environments, and objective assessment on the effects of taphonomy on diversity.

4.2 Variation between palaeoenvironments

Exceptional preservation of organic-walled microfossils in phosphatic nodules of the Torridon Group has allowed informal form taxonomic treatment of these fossils (Chapter 3), and the fine scale sedimentological variations between lithofacies in the phosphate-hosting formations has enabled reconstruction of a laterally variable depositional basin (Chapter 2). In modern lake basins of similar lateral and thus environment variability, such as that of Lake Balkhash, southeastern Kazakhstan, it may be expected that changes in clastic input, depth, and basin topography will bring about variations in the resident biota. Ecosystems are expected to alter in composition dependent on chemical and physical conditions, which have been shown to vary considerably in the

Torridon lakes. The exceptional preservation of microfossils conferred by preservation in phosphate throughout the lake environments offers a unique opportunity to objectively measure these ecological responses in an ancient environment. Objective form taxonomy combined with application of the taphonomic indices defined above in Chapter 3, and in reference to the depositional environments inferred in Chapter 4 for four of the principal microfossil deposits of the Diabaig Formation: Lower Diabaig (Figure 2.1, locality 3 and Figure 2.4), Badachro (Figure 2.1, locality 2 and Figure 2.10), Fladday (Figure 2.1, locality 4 and Figure 2.11), and North Shieldaig (Figure 2.1, locality 6 and Figure 2.8); and for the Cailleach Head Formation biota (Figure 2.1, locality 1 and Figure 2.13) gives a holistic view of the component biota as well as the degradational environment.

Some consideration must be made of the likelihood that differences observed in the assemblages derive not from original ecological variation, but from preservational bias. In this, the taphonomic characterisation is invaluable, providing an objective view on diversity modification by the fossilisation process, and enabling prediction of any likely losses from the assemblage. In addition, where all form taxa in a particular assemblage are recognised but vary in their relative abundances, strong evidence is provided for non-preservational effects, as fossilisation bias may be expected to bring about complete loss of members from an assemblage.

In the analyses below, the variable environments within the Diabaig Formation are first compared, followed by differences between the Diabaig Formation and the Cailleach Head Formation.

4.2.1 Variation within the Diabaig Formation

The location of the four assemblages compared below can be found in Figure 2.1, and their inferred depositional environments is discussed in more detail in Chapter 2. These localities have been chosen as they each host abundant organic-walled microfossils in clean microcrystalline phosphate.

4.2.1.1 Lower Diabaig

Figure 4.3a illustrates the abundance of each informal form taxon, recorded from a census of the component assemblage, alongside abundance data for the whole of the Diabaig Formation. Of note in this plot is the elevated number of dark-walled

coccoids and filaments observed at Lower Diabaig, combined with a reduced abundance of all light walled forms, and especially of clusters. Given a possible protective spore-like affinity of the darker coccoid forms, the abundance of these at this locality indicates increased encystment, which may be a response to the stress imparted by the frequently desiccating environment—also colonised by abundant filamentous forms—or may be related to reproduction, occurring preferentially in this environment. The lack of complex, light-walled forms further suggests that the development or deposition of pelagic, vegetative life (in comparison with the dark-walled supposed cysts) here was compromised.

The taphospace plot for Lower Diabaig (Figure 4.3b) illustrates low to moderate chemical alteration, and moderate biological and physical taphonomic effects. Physical deformation here derives from periodically alternating water depths and current energies, and the slow rate of deposition would increase the residence time of organic structures in a suitable interface environment, thus increasing the potential for biological action. Low chemical alteration may be an indication of either rapid occlusion and lithification, or a less chemically aggressive environment brought about by the periodic exposure and drying.

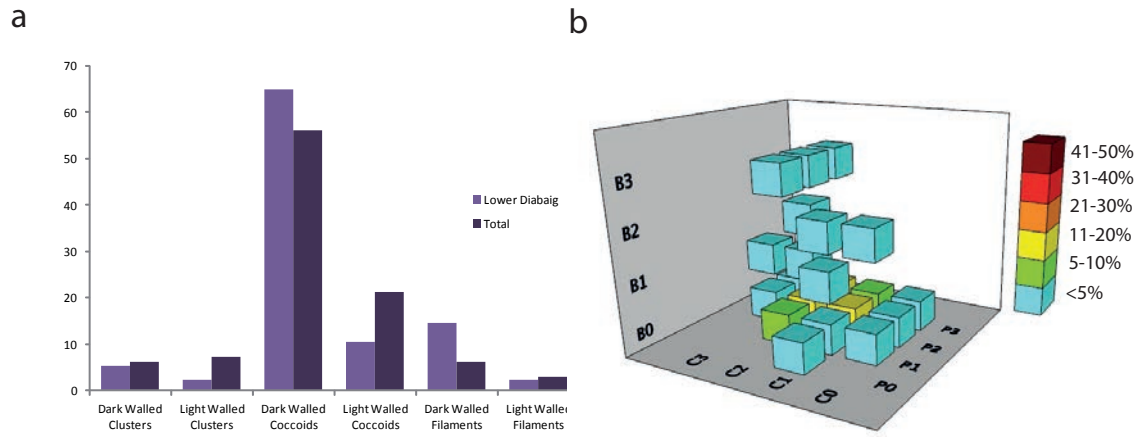


Figure 4.3: Assemblage data for Lower Diabaig. a) Comparison of morphotype abundances at Lower Diabaig, and for the entire Diabaig Formation assemblage. Vertical axis represents percentage of sampled dataset. b) Taphospace plot for Lower Diabaig. Taphonomic 'hotspots' at P1,C1,B0, and P2,C2, B0. N=100

4.2.1.2 Badachro

Figure 4.4a illustrates the abundance of each informal form taxon, recorded from a census of the component assemblage, alongside abundance data for the whole of the Diabaig Formation. Here, a comparatively high proportion of filaments is seen in combination with a generally low abundance of all light-walled structures. The deep depositional environment of this lithofacies may be the cause of the loss of delicate vegetative structures, as in the process of their deposition from upper photic waters, they are likely the first to be lost due to water-column decay, and bottom-water turbidity or stagnation may inhibit all but specialised growth. That specialised growth is represented by filamentous mat development, which may host non-oxygenic and non-phototrophic metabolisms.

The taphospace plot for the deep quiescent waters of Badachro (Figure 4.4b) indicates high grades of chemical degradation, moderate to high physical deformation, and a low biological component. Combined chemical and physical alteration of this grade may be explained by the local allochthony of the fossils. Organisms living in the water column or in more shallow current-affected environments must travel some distance, or be suspended for long periods of time, before being deposited in this distal environment. Such an interpretation is consistent with the chemical and textural maturity of the Badachro sediments. Low levels of biological alteration are likely testament to a non-conducive environment for this kind of heterotrophy.

4.2.1.3 Fladday

Figure 4.5a illustrates the abundance of each informal form taxon, recorded from a census of the component assemblage, alongside abundance data for the whole of the Diabaig Formation. In this assemblage, elevated numbers of light walled coccoids and filaments are seen, combined with a depressed number of clustered forms. The coccoids and filaments are dominant components of a vegetative benthic mat environment, and their abundance here is evidence that such a mat was thriving. Low numbers of complex clusters suggests that these pelagic components of the biota are not surviving to be deposited in these relatively deep waters, as at Badachro. The abundance of dark-walled megaspheric coccoids (Figure 4.5b) at certain horizons within this formation may indicate episodic eutrophic inputs engancing growth of larger, more complx eukaryotic forms, perhaps associated with the rare sandy in-

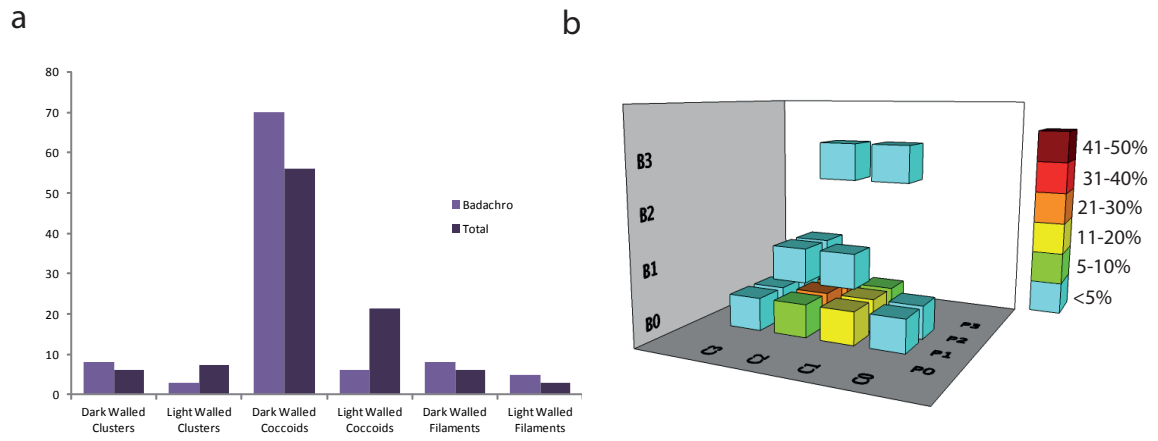


Figure 4.4: Assemblage data for Badachro. a) Comparison of morphotype abundances at Badachro, and for the entire Diabaig Formation assemblage. Vertical axis represents percentage of sampled dataset. b) Taphospace plot for Badachro. Taphonomic 'hotspots' at P2,C2,B0, and P3,C2, B0. N=100

terbeds and flasers.

The taphospace plot for this lithofacies shows moderate to high levels of both physical and chemical alteration, along with low-grade biological action. Fladday, similar to Badachro, represents a deep distal environment with chemically and texturally mature sediments, and the relatively high grades of chemical and physical alteration are again likely due to the distance travelled by locally allochthonous organic structures. The taphonomic effects are somewhat attenuated here compared with Badachro, as a thriving autochthonous biota is clearly also in evidence here, suffering little transport related degradation. The low levels of biological activity in such an environment are somewhat unexpected however, as a mat system would be expected to host heterotrophic as well as autotrophic members of the consortia. This lack of evidence of their action may be due to rapid and complete breakdown of material, or perhaps to some previously unrecognised environmental or preservational bias.

4.2.1.4 North Shieldaig (Fish Farm)

Figure 4.6a illustrates the abundance of each informal form taxon, recorded from a census of the component assemblage, alongside abundance data for the whole of the Diabaig Formation. Here, a complex assemblage is represented by a relative abun-

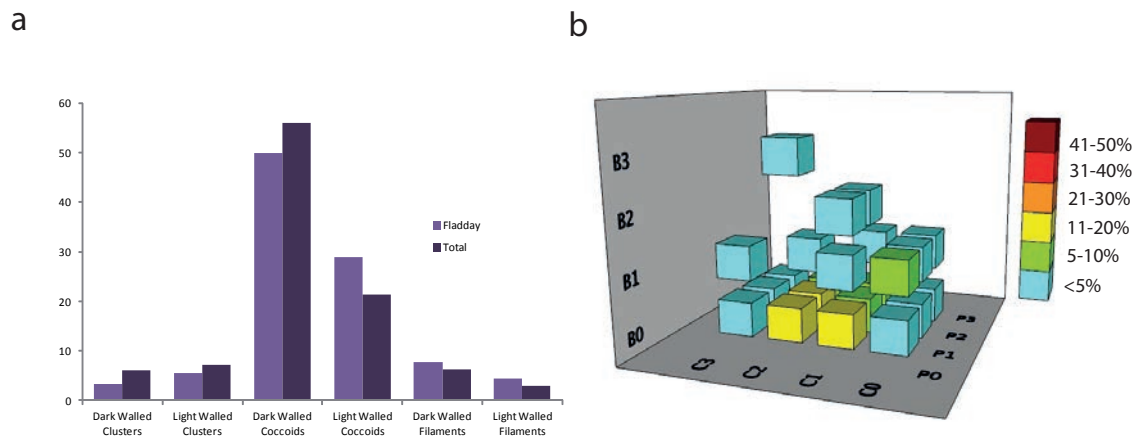


Figure 4.5: Assemblage data for Fladday. a) Comparison of morphotype abundances at Fladday, and for the entire Diabaig Formation assemblage. Vertical axis represents percentage of sampled dataset. b) Taphospace plot for Fladday. Taphonomic 'hotspot' at P1,C2,B0. N=100

dance of light-walled clustered forms, and of dark-walled coccoids. Filamentous forms are characteristically scarce. The presence of two disparate morphotypes suggests a varied source for the fossil material preserved here. Preservation of clustered forms indicates a nearby vegetative pelagic biota, which can be deposited and preserved before decay in the water column. In contrast, dark-walled coccoids imply a protective encysting response to adverse conditions. Given the likely delta-top environment of deposition for the unit, strong benthic currents may provide the necessary stresses. Alternatively, encystment may be related to reproduction in this instance. A low abundance of filamentous structures indicate poor development of mat systems, perhaps related to substrate instability or typically high depositional rates overtaking rates of biofilm or mat development.

The taphospace for North Shieldaig shows moderate levels of chemical and physical degradation, and low to moderate biological alteration (Figure 4.6b). Taphonomic processes here will be shaped by the changing depositional environment of this delta top. Nearby sources of vegetative material allow for little degradation before deposition, and typically high sedimentation rates suggest a low residence times in the decay environment. High current energies however, in combination with the proximal supply of reactive ions for chemical reactions, can bring about more intense degradation when conditions are optimal.

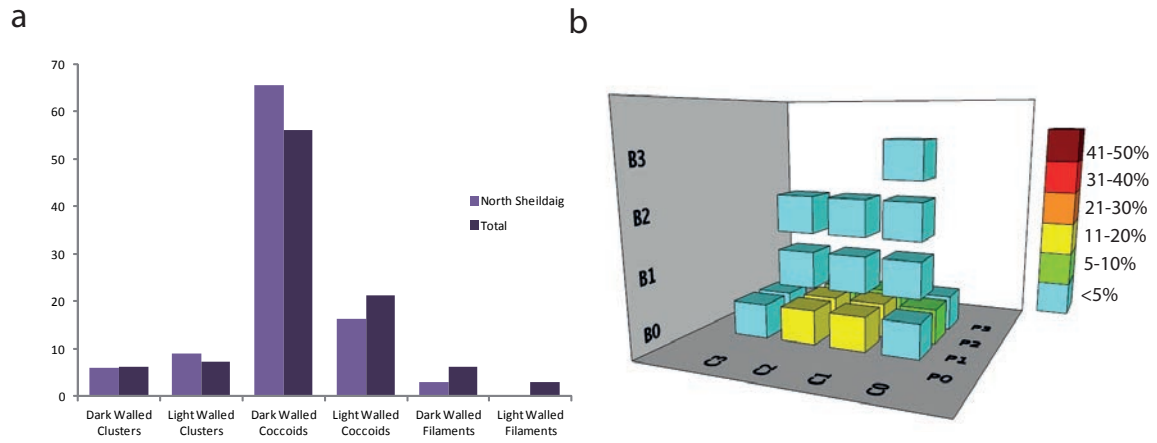


Figure 4.6: Assemblage data for North Shieldaig. a) Comparison of morphotype abundances at North Shieldaig, and for the entire Diabaig Formation assemblage. Vertical axis represents percentage of sampled dataset. b) Taphospace plot North Shieldaig. Taphonomic 'hotspots' at P2,C3,B0. N=100

In summary, phosphate-hosted assemblages in four different lithofacies and depositional environments show marked variation from one another and from the taxonomic abundances of the formation as a whole. From these data it is possible to make some general observations on the environmental conditions under which different morphotypes thrive, and how local environment shapes the component biota. Figure 4.7 illustrates the changing proportions of each morphotype through the lithofacies and environments analysed here. Filamentous forms and light-walled vegetative coccoids are benthic mat-formers, and thrive in areas of high substrate stability and low depositional rate. Dark-walled forms may be the result of encystment, most likely as a response to environmental stresses such as subaerial exposure or high current strengths. Light-walled, supposed vegetative clustered forms therefore likely represent the planktonic component of the community, and their distribution in fossil assemblages is in part controlled by water depth due to degradation during settling.

Similarly, the variation in grades of taphonomic alteration between different environments indicates the changing taphonomic processes between lithofacies, and thus point to likely non-cosmopolitan agents of change.

Biological alteration seems to be greater in shallower environments, perhaps indicating a preferential distribution of heterotrophic components of the community to these locations. Alternatively, biological action may be underrepresented in the deeper environments owing to its greater efficiency. More data from both kinds of environment, as well as non-fossil indicators of biological activity, are required to resolve this issue.

In general, physical degradation is seen to be more advanced in deeper, quiescent environments. Whilst seemingly counterintuitive, comparison with the textural and chemical maturity of the host rocks indicates that, despite a lack of local current energies, at least some of the fossil structures are likely to have been transported some distance with the distal sediments, during which they will suffer inevitable physical damage. Thus, these environments may be described as taphonomically, as well as texturally mature.

Chemical alteration observed in a fossil assemblage is the result of in-situ chemical degradation, in combination with any decay occurring before deposition of the organic material. Thus, autochthonous organisms deposited in environments non-conducive to chemical alteration have the best potential of being preserved as chemically pristine. Allochthonous organic matter will have more time to be exposed to aggressive chemical decay, which itself may be more extreme in environments with renewed sources of reactive ions and radicals, such as a nearby fluvial source.

4.2.2 Variation between Diabaig and Cailleach Head Formations

Sedimentological analyses of the various lithofacies of the Diabaig Formation and of the type locality of the Cailleach Head Formation demonstrated that they represent basins of differing character: the Diabaig Formation as a laterally variable, ephemeral lake, and the Cailleach Head Formation as a more persistent basin with cyclically prograding deltas and subsidence. It is therefore hypothesised that the component biotas of these different basins may differ in response to differing conditions, as with the varied lithofacies of the Diabaig Formation.

A comparison of overall abundance of morphotypes between the Diabaig Formation as a whole, and the Cailleach Head Formation (Figure 4.8a), illustrates a number of notable differences. Firstly, the Cailleach Head assemblage contains considerably

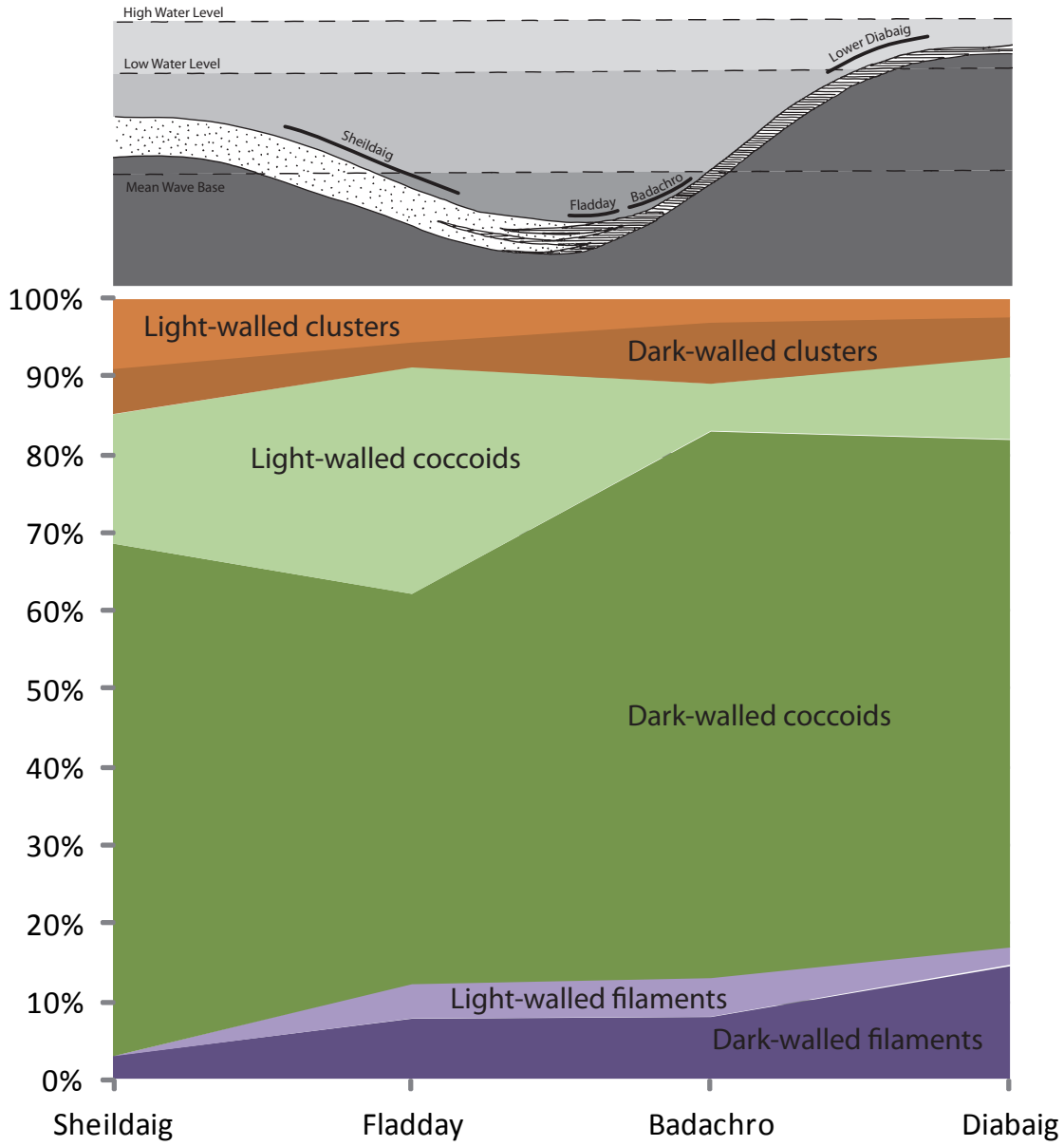


Figure 4.7: Comparison of ecosystem dominance between palaeoenvironments. Upper transect illustrates generalised depositional environments for the four lithofacies studied. Chart below uses abundance data from sampled datasets to display differing dominance of forms between lithofacies. Shieldaig N=100, Fladday N=100, Badachro N=100, Diabaig N=100

fewer filamentous forms than seen in Diabaig, and this is taken to indicate the less extensive development of binding microbial mats at Cailleach Head, as may be expected in a deltaic environment with high depositional rates. The benthic biota is instead dominated by light-walled vegetative coccoids more characteristic of early-stage biofilms (Noffke 2010). Dark-walled coccoids are also underrepresented in the Cailleach Head assemblage, and this is likely due to the absence of particular stresses. There is no evidence for subaerial exposure, and the sediments are predominantly deposited under conditions of low current action. Finally, the pelagic clustered forms are better represented at Cailleach Head than in the Diabaig Formation, highlighting the differences in nutrient regime between these two environments. The waters of the Cailleach Head biota receive continuous riverine flux of nutrients from the prograding delta systems, promoting planktonic blooms that are directly supplied to the shallow sediments.

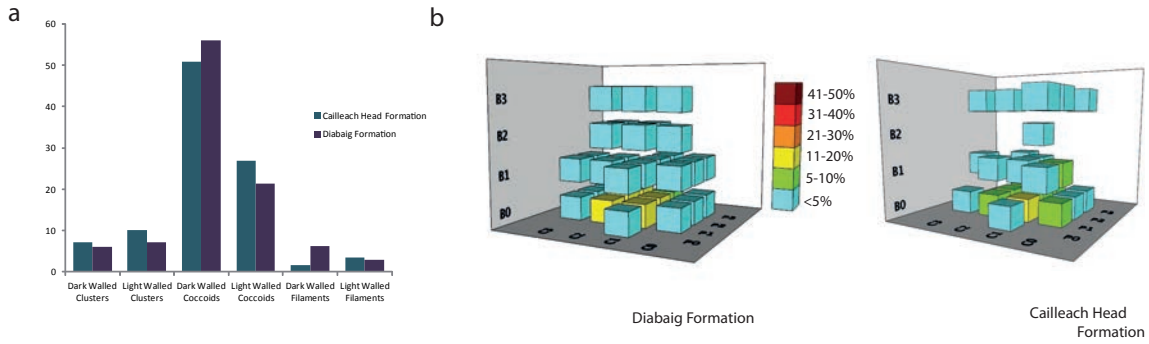


Figure 4.8: Comparison of the assemblages of the Diabaig Formation and the Cailleach Head formation. a) Comparison of morphotype abundances in the Diabaig Formation and Cailleach Head Formation. Vertical axis represents percentage of sampled dataset. b) Taphospace plots for the Diabaig Formation and the Cailleach Head formation. Taphonomic 'hotspots' at P1,C1,B0 and P2, C2, B0 in Diabaig Formation, and P1, C1, B0 in Cailleach Head Formation. Diabaig Formation N=500, Cailleach Head Formation N=100

The comparative taphospace plots of the Cailleach Head and Diabaig Formations (Figure 4.8b) show slight differences between the taphonomic profiles of these two basins. The overall profile for the Diabaig Formation, which is a combination of those variable lithofacies that make it up, and therefore should be analysed with caution, consists of moderate grades of chemical, physical, and biological alteration. In contrast, the Cailleach Head biota is preserved with low to moderate chemical degradation, moderate to high physical deformation, and moderate biological alteration.

A characteristically lower grade of chemical decay is probably the result of a direct supply of rich planktonic microbial blooms, and relatively rapid sedimentation rates quickly removing fossil material from the reactive seston layer. Physical degradation is the result of consistent water energies acting throughout the basin, transporting and locally resuspending sestonic material. Comparable levels of biological alteration between the Diabaig and Cailleach Head Formations are to be expected from the action of similar populations of heterotrophic organisms in broadly similar water chemistries and depths.

In summary, the assemblage diversity and taphonomic profile of the Cailleach Head biota, differing from that of the Diabaig basin, is characteristic of the physically active and dynamic basin suggested by the sedimentological data. Thriving planktonic communities, combined with low residence times in the reactive seston layer, combine to make this assemblage differently and subtly better preserved and informative to further taxonomic study.

4.3 Comparing the phosphate-hosted and shale-hosted biotas

Analyses of the Torridon microbiota in this study have focused on those forms preserved within sedimentary phosphate, because of their striking fidelity of preservation and three-dimensional structure. Qualitative and quantitative studies of the diversity and taphonomy of these deposits has added weight to these observations. But previous studies of Torridon microfossils have been made, not from the phosphate but from the shales and sandstones throughout the Torridon Group (Cloud & Germs 1971, Downie 1962, 1984, Peat & Diver 1982, Zhang 1982).

Precambrian microfossils are often sought and studied through acid maceration of siliciclastic rocks (e.g. Grey 2005, Vorob'eva et al. 2009), which removes all but the carbonaceous constituents of a sample. Maceration of fossil-bearing samples, compared with analysis by thin section, has both advantages and disadvantages.

Positively, maceration allows large quantities of material to be processes and analysed with ease, capitalising on the generally high abundance but significant scattering of microfossils in siliciclastic rocks. Imaging organic structures that have beem separated from their containing medium can also overcome some of the problems in study-

ing thin section preparations. It allows visualisation of compressed structures, which are typically flattened parallel to bedding, as well as large and three-dimensionally extensive formations, which may be cross cut by 30 μm thick thin sections. Additionally, the surrounding matrix of a host rock inhibits analysis of the details of fossil material, by attenuating the passage of light in optical microscopy. Dissolution of this rock matrix permits higher resolution imaging, and also facilitates alternative analysis methods, such as imaging by secondary electron SEM (Chapter 3).

The disadvantages of preparation by acid maceration are largely concerned with the loss of information. By removing the fossils from their host rock, any spatial information preserved at the time of their deposition, which may be important in interpreting life assemblages or consortia, will be lost, and all recovered structures will be scattered equally and randomly in any preparation. Similarly, certain occluding preservational media, such as well reported cherts, or the cryptocrystalline phosphates examined here, will typically preserve the three-dimensionality of fossil structures. Dissolving this occluding medium from the matrix and interior of the fossils will result in the loss of three-dimensionality, and the introduction of compression features not previously present. The preparation process itself is likely to impart some damage on the fossil material, although improvements have been made in methodology to mitigate this effect (Grey 1999), and sieving for informative size fractions may result in the loss of small-scale features.

The juxtaposition of shale-hosted and phosphate-hosted biotas in the same physical environment offers a rare opportunity to examine how assemblage diversity and taphonomy differs between the two preservational modes. Is the exceptional fidelity of preservation limited to phosphate-hosted structures? Is a different consortia of organisms represented in the phosphate than in the shale? Acid maceration was carried out on both the shale-hosted and phosphate-hosted material. In the following analyses, the effect of the preparation process is first assessed by directly comparing macerate residues and thin sections of the same, phosphate-hosted fossil material. After taking these results into account, the differences in diversity and preservation between shale-hosted and phosphate-hosted deposits are addressed, through the analysis of macerate residues from both preservational modes.

4.3.1 The effect of maceration on diversity and taphonomy

Figure 4.9 illustrates a comparison between the total abundances of morphotypes from a census of macerate preparations of phosphate and thin section preparations of the same phosphate, from Cailleach Head and Diabaig.

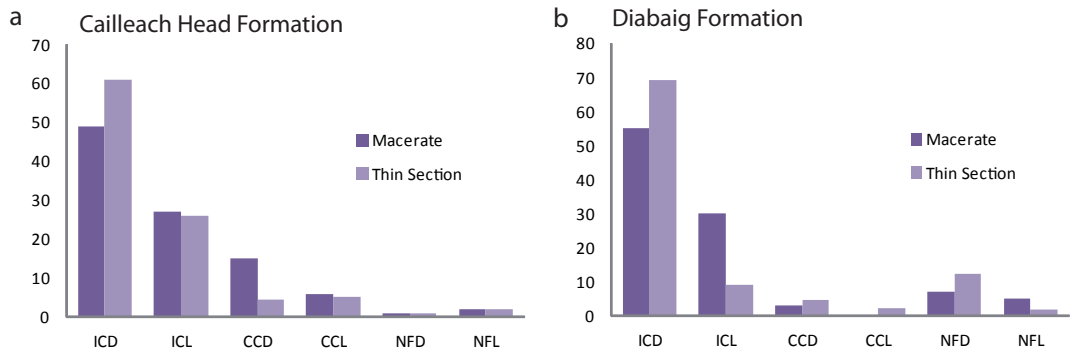


Figure 4.9: Comparison of morphotype abundances in phosphates prepared by thin section and by acid maceration in a) Cailleach Head Formation, macerates N=100, thin section N=100; and b) Diabaig Formation, macerates N=100, thin secion N=100. Vertical axis represents percentage of sampled dataset.

Both of these plots show that the material prepared by acid maceration has a greater abundance of light-walled vesicles, clusters and filaments, and correspondingly fewer dark-walled forms, than identical material prepared by thin section. This relationship seems initially counter-intuitive, as it may be expected that abrasion and chemical corrosion would occur during treatment with strong acid and sieving, thereby destroying delicate thin-walled structures. Acid maceration techniques have been developed, however, that aim to minimise damage to microfossils (Grey 1999), and these techniques were employed in preparation of the Torridon material. The overabundance of light-walled forms and clusters is therefore likely due to the sampling and processing of larger amounts of material than can be encountered in a thin section. As a result, large clustered features that may not be intersected by the thin section surface, as well as light, thin-walled structures that may be obscured by the colouration or contamination of the matrix phosphate, can be more easily visualized after extraction from the rock.

Comparison of the taphonomic profiles of macerated and thin sectioned phosphate from both the Cailleach Head Formation and Diabaig Formation are illustrated in Fig-

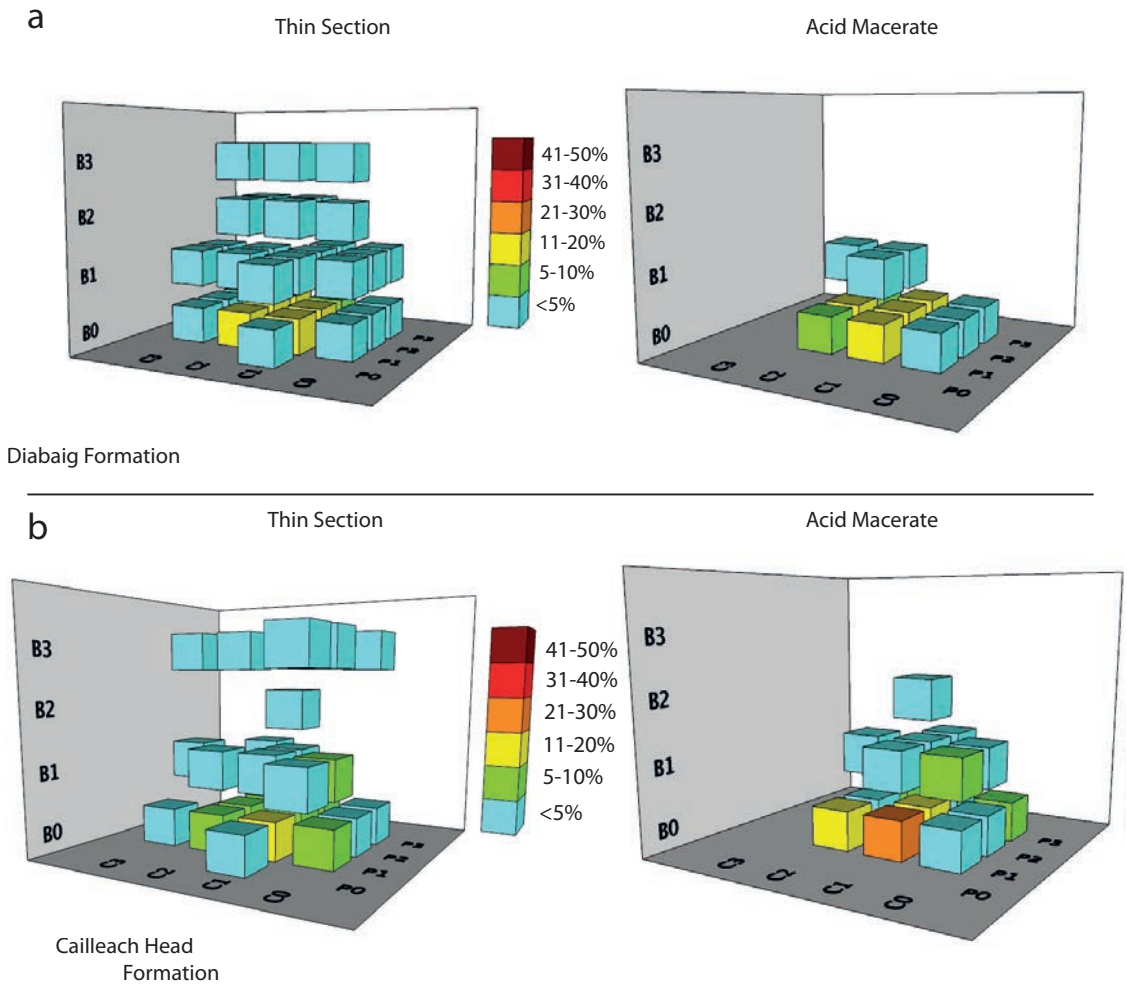


Figure 4.10: Comparison between the taphospace plots for phosphate-hosted microfossils prepared by thin section and acid maceration in a) Diabaig Formation and b) Cailleach Head Formation. Taphonomic 'hotspots' at P1,C1,B0 and P2,C2,B0 for Diabaig thin sections (N=100), and P2,C1,B0 and P2,C2,B0 for Diabaig acid macerates (N=100). Taphonomic 'hotspots' at P1,C1,B0 for Cailleach Head thin sections (N=100), and P1,C1,B0 for Cailleach Head acid macerates (N=100). Principal difference between thin sections and acid macerates appears to be the loss of biological features in macerated samples.

ure 4.10. The samples from both formations show broadly comparable amounts of chemical alteration in both the macerates and the phosphate, suggesting that this taphonomic phenomenon is unaltered by the maceration process, which is to be expected as this kind of degradation is a result of long term processes in ambient waters, unrelated to the action of acids. Somewhat predictably, there are more physically unaltered forms visible in the thin sections than in macerate residues. Loss of three-dimensional structure, and damage imparted by manual processing of fossil material will create physical damage even if the original material was pristine. In addition, there is more evidence of biological action preserved in the thin section preparations than in the macerates. This is most likely due to the fact that disruption of spatial relationships in maceration would destroy loose pseudomorphing associations of heterotrophic bacteria, thereby rendering the highest grade of biological taphonomy unobservable in macerate residues.

Comparisons of the diversity and taphonomy of material studied by thin section and by acid maceration show some minor differences that result in part from the loss of spatial information but corresponding concentration of material that occurs during preparation by acid maceration.

4.3.2 Differences between macerated phosphate and shale

Taking into account the minor changes imparted by the use of acid maceration to study the Torridon fossils, it is possible to directly compare the macerates of the shale-hosted assemblage with those of the phosphate-hosted biota, while being relatively confident that the material is fully representative of both.

Figure 4.11 illustrates the differences in absolute abundances of different morphotypes from the shales and phosphates of the Cailleach Head and Diabaig Formations.

Comparison of assemblages in shale and phosphate in the Cailleach Head Formation shows elevated numbers of dark-walled forms, and a corresponding depression in light-walled vesicles and clusters, in the phosphatic portions. In contrast, the Diabaig Formation assemblages show the opposite pattern, with the phosphate-hosted microfossils dominated by light-walled clusters and filaments, with fewer dark-walled forms, when compared to the shale-hosted biota. These differences may partly reflect the slight differences in preservational environment (see below), but might also represent different microbial consortia living and preserved in the different palaeoenvironmental

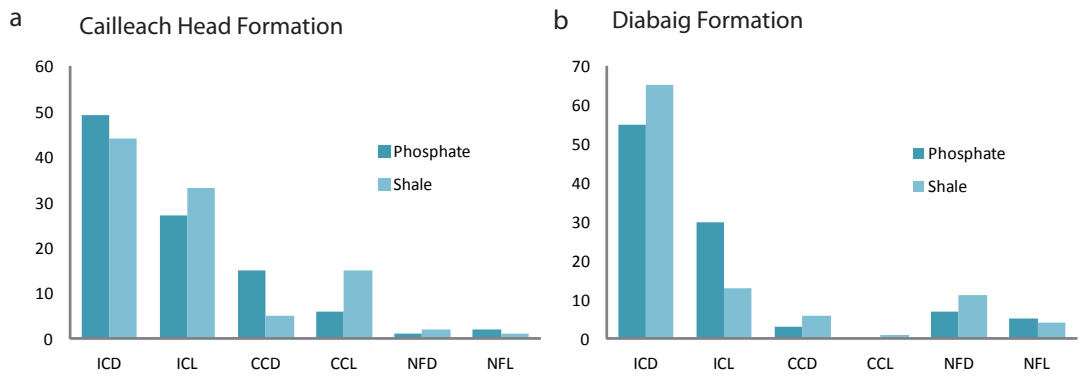


Figure 4.11: Comparison of morphotype abundances in macerated phosphates and shales from a) Cailleach Head Formation, phosphates N=100, shales N=100); and b) Diabaig Formation, phosphates N=100, shales N=100. Vertical axis represents percentage of sampled dataset.

conditions represented by the Cailleach Head and Diabaig Formations. This suggests that in the energetic waters of Cailleach Head, darker-walled resting cysts were present in the phosphogenic zone, and lighter-walled fossils were concentrated and better preserved elsewhere, possibly indicating the degradational consumption of more delicate organic structures in the phosphate-concentrating process. In the desiccating environment of the Diabaig Formation at Lower Diabaig, light-walled clusters and filaments preferentially colonise the zone of phosphogenesis, with encysting forms concentrated elsewhere, perhaps reflecting the development of phosphate-concentrating benthic mats in this lithofacies.

Plots of the taphonomic profiles of fossil assemblages from phosphates and shales of both Cailleach Head and Diabaig Formations (Figure 4.12) show some intriguing differences. At Cailleach Head, the two profiles are very similar, but the shale-hosted assemblage displays slightly lower chemical alteration, and slightly greater physical alteration. This may be explained on both sides by considering the processes that brought about their preservation. In the shales, the burial of organic structures by clastic material enables their preservation, but these clastic particles and the inevitable compression between sedimentary layers will unavoidably impart physical damage to the microfossils. The sedimentary phosphate is an authigenic mineral that clearly required certain specific conditions in which to form. As is discussed further in Chapter 6, the ionic constituents of the authigenic phosphate are likely derived directly or indirectly from breakdown of organic matter. Thus, decay of fossil material is necessary for the formation of the phosphate. A delicate balance between rate

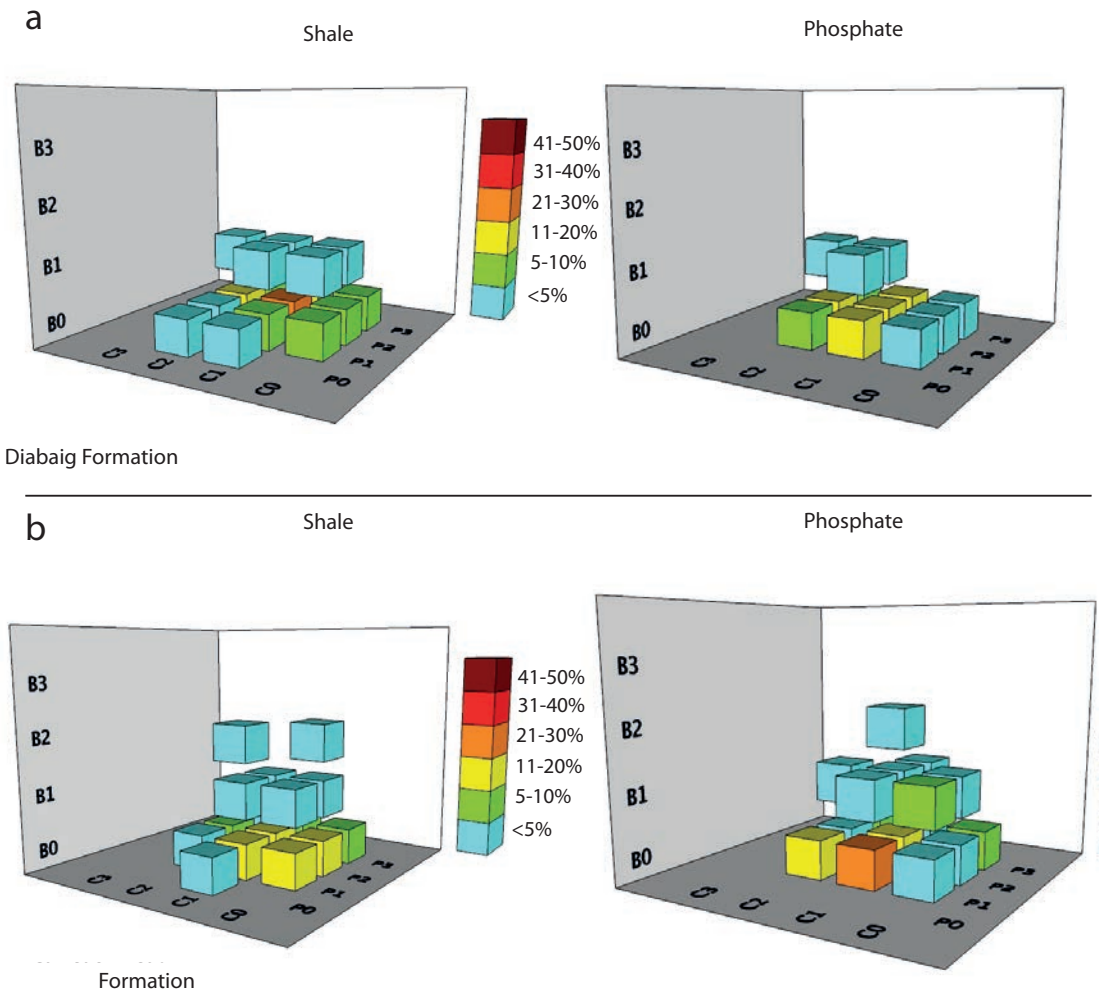


Figure 4.12: Comparison between the taphospace plots of microfossils macerated from the shales and the phosphates from a) Diabaig Formation, and b) Cailleach Head Formation. Taphonomic 'hotspots' at P2,C1,B0 for Diabaig shale (N=100), and P2,C1,B0 and P2,C2,B0 for Diabaig phosphates (N=100). Taphonomic 'hotspots' at P2,C1,B0 for Cailleach Head shale (N=100), and P1,C1,B0 for Cailleach Head acid macerates (N=100). Principal difference between thin sections and acid macerates appears to be the loss of biological features in macerated samples.

of decay and rate of precipitation and occlusion enabled some fossil structures to be preserved relatively unaltered, but the hallmark of this phosphate origin is preserved in the elevated chemical alteration seen within the assemblage.

In the Diabaig assemblage, the profiles are once again broadly similar, but in contrast to Cailleach Head, the shale-hosted biota shows slightly lower physical alteration than the phosphate. While not fitting with the explanation above of enhanced clastic damage, a consideration of the precise environment of deposition may shed some light. The sample studied here is from the type section at Lower Diabaig, which was deposited on a desiccating mud flat, where sediment is predominantly fine sand and silt. Such sediments settle gently, imparting only compressional deformation as laminae are formed. At this locality, phosphates are found at several horizons in association with reworking fabrics, so in this specific environment the constituent fossil material is more likely to be damaged by rare energetic events.

It is clear from the above analyses that the diversity and taphonomic profiles of fossil deposits can vary considerably, even within sub-centimetric sedimentological distances, as the fossilisation process is governed on a fine scale by local fluctuating microenvironments.

One further important observation from these analyses is that, despite the difference in three-dimensionality, the shale-hosted and phosphate-hosted biotas are strikingly similar, with delicate thin-walled vegetative material, and complex reproductive clusters being preserved in both. This has implications for understanding the fine-scale preservation of these forms. Clearly, simple occlusion by authigenic phosphate is not the sole cause of this exceptional preservation. Further investigation of the preservation of the Torridon biota requires the application of high-resolution techniques.

In summary, it has been demonstrated that the qualitative characters defining physical, chemical, and biological degradation of organic-walled microfossils are of some use in visualising taphonomic decay, for comparison between different environments, preservational modes, and preparation techniques. Yet, further refinements of this taphospace scheme are possible to enhance its usefulness across the field of Proterozoic palaeontology and palynology. Firstly, the scheme as it stands may be

used to compare a wider variety of fossil subgroups, allowing comparson of the taphonomic profiles of individual taxa, or specific size ranges. Such comparisons may help to identify the dependence of tf taphonomy on intrisnsic fossil factors, as well as the environment. Further, the application of multivariate statistical methods to the datasets would be invaluable in understanding the interrelationships between the different modes and characters of decay. Finally, refinement of the scheme might aim to address the issue of qualitative data, using in addition qualitative measures such as the degree of tearing or the amoung of carbon dispersal. These measures, which need not be limited to a three dimensional plot, and in combination with powerful statistical tools, may be able to provide an objective numerical index of taphonomy that is widely applicable to organic-walled microfossils.

Chapter 5

Torridon macrostructures

5.1 Introduction

Macrostructures in the Torridon were analysed by Richard Callow for a DPhil thesis. A preliminary report of these structures was published (Callow et al. 2011), for which this author's contributions in collection and interpretation were acknowledged.

In the following chapter, all material collected by Dr Callow and considerably more collected by the author are reanalysed. All interpretations are the author's own, and independent from earlier studies.

Within the Proterozoic, the preservation of organic walled microfossils may be accompanied by the production of macroscopic microbially induced structures within the sediment. In the absence of fossil assemblages, these structures may be used alone to infer the presence of life in those palaeoenvironments (Noffke & Paterson 2008).

The most widely studied macroscopic microbial structures are stromatolites, which are today very limited in their distribution (e.g. at Shark Bay, Western Australia), but were very extensive in shoreline marine deposits throughout the Proterozoic (Walter 1972). The presence of a modern analogue has much helped in the interpretation of stromatolite growth and morphology, and a wide variety of stromatolite morphotypes have been identified and even utilised in biozonation of Proterozoic strata (Walter 1972, Grey 1982). They are formed in intertidal to upper subtidal areas, from successive growths of cyanobacterial mat and carbonate or silica cementation, creating a laminated structure that is often domed or digitate as colonies strive upwards for light (Andres and Reid 2006). Planar forms are often more difficult to recognise and verify as biogenic, but are indicated by micro-scale carbonaceous layering, even when

distinct fossils are absent. Original carbonate mineralogies may be subsequently silicified, losing their microcrystalline texture, but not the overall structure (Sommers et al. 2000).

The distinctive mineralisation of stromatolite structures means that they are easily recognisable within Proterozoic records, but are clearly limited to regions of high authigenic mineral growth that favour formation of the constituent minerals. Thus, their formation occurs only under specific biochemical conditions, without which no trace of microbial life may be left. In particular, siliciclastic depositional regimes with little authigenic mineral growth offer little opportunity for stromatolite growth, and so in these settings alternative macroscopic indicators of life must be sought.

As colonies of microbes grow, they secrete extra-polymeric substances (EPS) that bind the sheaths and vesicles together into a biofilm and later a stratified microbial mat. These mats interact with the sediment beneath them or around them, conferring pliancy, or actively constructing resistant layers which may be recognised in the sediment by their peculiar architecture, even long after the carbonaceous material that formed them has decayed away. There has been a recent surge of interest in these microbial traces in siliciclastic rocks, and renewed efforts have been made to identify and classify them throughout the Proterozoic, in comparison with Phanerozoic and living examples (Noffke 2009, 2010, Noffke et al. 2006, 2001, 2003). Noffke (2010) produced an extensive account of various structures that may be produced by the action of binding and growing microbes in siliciclastic sediments, which she collectively named 'Microbially Induced Sedimentary Structures' (MISS). The application of MISS criteria and classifications allow structures observed throughout the rock record to be allied with analogous biological processes involved in biofilm or microbial mat colonisation.

Features that are classified as 'wrinkle structures' by Noffke (2010), apparently formed by a combination of mat growth, binding, biostabilisation and baffling, have been described from the Torridon Group, and therein interpreted as MISS (Prave 2002, Upfold 1984). Identification of these structures adds further evidence to support the biogenicity and habit of the organic-walled microstructures preserved in phosphate and shale here (Chapters 3 and 4), but until now they have received little critical evaluation.

The following analysis of the diverse microbial structures in the Torridon Group has been partially published by the author in collaboration with Richard Callow of Memorial University, Newfoundland (Callow et al. 2011).

5.2 Justifying Biogenicity

Consideration of these surficial wrinkle structures first requires verification that they are biological in origin. The great variability in their morphology, detailed below, makes this task a difficult one, but certain general features may be used to argue for microbial involvement rather than purely physical processes.

Firstly, the morphological ordering of the structures lies within specific bounds that are typically occupied by biology (Brasier et al. 2006). They are neither perfectly ordered nor fully disordered, indicating a decreasing complexity of organization that is characteristically biological. In addition, the minor inconsistencies in measurements within and between particular structures indicate a limitation to the permitted variation of the structures, such as would not be typically found in purely physical constructions.

Sedimentary structures have been studied from rocks of all ages and modern sediments for over a hundred years, resulting in an extensive and almost exhaustive database of recorded structures with known physical causes, and chronological constraints. By comparing the wrinkle structures to these well known sedimentary features, physical causes may be excluded and alternative mechanisms of formation must be invoked—in this case biology.

Living microbial mats are of use, in that studies of their morphology, interactions and preservation may be directly compared with structures found in the fossil record. Observations can be made of the changes in sediment pliancy, mat construction and degradation under different experimental conditions (Noffke et al. 2001). While not fully replicating the fossilisation process, these studies should provide insight into the preservation potential of such structures.

Although the wrinkle structures are recognized on the basis of their morphology on and within the sediment, there may be some degree of carbonaceous preservation

in association with microbial architectures, which would not be expected if the structures were purely physical. In an ideal situation, pristine organic walled microfossils would be preserved as a binding mat in situ, but the preservation potential for such fossils in siliciclastic environments is generally low, but disseminated organic matter may be concentrated in nearby layers.

A combination of the above-described features may be taken as strong evidence that the observed microstructures are of biological origin, and this is seen to be the case in the Torridon wrinkle structures described and classified below.

5.3 Classifying structures

A wide variety of wrinkle MISS morphologies are found in the Diabaig Formation in northwest Scotland. They are herein classified into three broad categories: modification of sedimentary features, ordered surficial structures and disordered surficial structures. Within these general groups, a number of specific morphotypes occur, but in many cases they appear to represent end members of a gradual transition of morphology, presumably dependent on preservation.

5.3.1 Modification of Sedimentary Features

These types of MISS are not recognized as 'wrinkle structures' on the bedding or lamination surfaces of the rocks, but instead are variations on 'normal' sedimentary structures that cannot be explained by purely physical mechanisms.

5.3.1.1 Sharpening of ripple crests and multi-crested ripples

Oscillating wave action is known to produce symmetrical ripples in affected sandstones, and in the rock record these are easily recognized as sinusoidal ridges and troughs that may anastamose laterally. In the Torridon sandstones these symmetrical wave ripples occur in abundance, but occasionally they show a morphology not easily explained by physical processes alone. The crests of ripples become sharpened, and the sinusoidal profile lost (Figure 5.1b). The phenomenon is apparent on both top and bottom surfaces of rippled beds, and appears as a thin groove in negative hyporelief. Such sharpenings are laterally extensive across a rippled bed, and will frequently affect many adjacent ripples.

Occasionally, not only one sharpened crest ridge will be visible, but several. The ridges lie sub-parallel to one another across what becomes a flat-topped ripple crest. When multiple ridges are present, they may not persist for great lateral distances but instead may anastamose over the flat ripple top.

The proposed mode of formation of this structure, is of ripple formation and growth with the moderating influence of thin epibenthic or shallow endobenthic microbial mats. The growth of mats in or on ripples confer a pliancy in the sediment, which then resists further distortion by oscillating currents, resulting in the formation of one or many interacting 'creases' in the ripple crests.

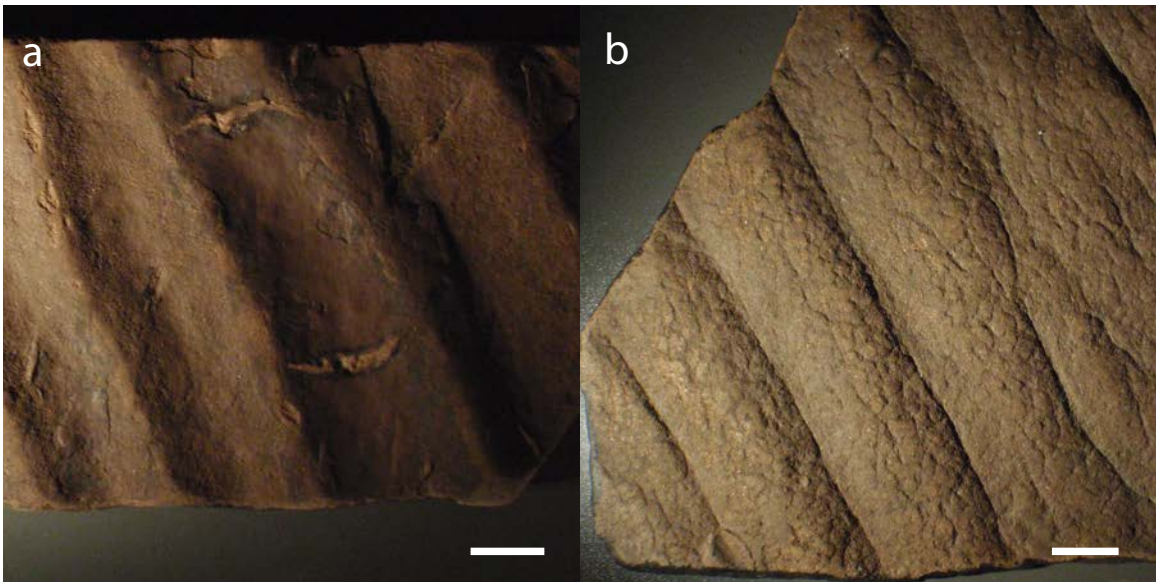


Figure 5.1: Microbial modification of sedimentary features. a) Synaeresis cracks in sandstones. Sample SHM14 from Sheildaig Peninsula. Scale bar 2 cm. b) Sharpened tops to ripples, seen here in hyporelief with associated networks. Sample SHM08 from Sheildaig peninsula. Scale bar 2 cm.

5.3.1.2 Synaeresis cracks

Synaeresis cracks differ from desiccation cracks in their limited lateral extent, and in possessing an elongated diamond-shaped cross section, as opposed to a V-shaped one. They are reasonably well reported from the geological record (e.g. Plummer & Gostin 1981), being attributed to shrinkage just below the sediment-water interface caused by variations in salinity, sediment compaction or even temperature (Plummer & Gostin 1981). Regardless of the cause of such cracks, their preservation within

sedimentary successions seemingly requires a coherence or pliancy of the surrounding sediment, to maintain the shape of the crack within the sediment body. The best explanation for such coherence at a shallow depth within the sediment is the presence of a binding endobenthic microbial mat (Schieber 2007). Early diagenetic growth of authigenic materials could also give sediments pliancy, but no mineralogical evidence is present to support this interpretation. Thus, the presence of synaeresis crack in some horizons of the Diabaig Formation can be taken as a proxy for otherwise unpreserved endobenthic mats (Figure 5.1a).

5.3.2 Ordered Surficial Structures

Occurring on the top and bottom surfaces of certain horizons, these structures are very noticeable due to their unexpectedly ordered texture. They are all classified under the MISS group: 'wrinkle structures' (c.f. Noffke 2010), but individually have very different morphologies.

5.3.2.1 'Arumberia'

Parallel series of ridges and grooves between 1 and 12 mm wide, that may anastamose slightly but are relatively continuous laterally (Figure 5.2e). Ridges and grooves may be straight, curved, or sweeping across a bedding plane. Structures such as these may be allied with the ichnotaxon 'Arumberia', abundant in the Ediacaran (McIlroy & Walter 1997).

'Arumberia' occurs in a range of lithologies, from medium sandy units to glossy micaceous siltstones.

5.3.2.2 Networks

Polygonal reticulate networks of ridges rarely more than 4 mm thick (Figure 5.2a). Ridges range from 0.2 to 2 mm high, and enclose equant polygonal domains with typically 6 sides, ranging in average diameter from around 4 to 25 mm. Variants on this morphology may identified as 'tight networks', where the polygonal domains are around 5 mm in diameter, and 'loose networks' with ∼25 mm diameter domains, although there is a more or less constant gradation between these forms. Often, the connecting nodes are raised above the ridges a further ∼1 mm. Networks occur in

positive epirelief, or in negative hyporelief where they may be allied with previously described 'elephant skin' textures (Gehling 1999, Runnegar & Fedonkin 1992).

Networks occur in a range of lithologies, from fine silty grey mudstones to red rippled sandstones, but are often associated with a fine glossy mud layer or micaceous layer, revealed in thin section to be a fine carbon-rich veneer over coarser sediments.

5.3.2.3 Ladders

As above, reticulate networks are defined by raised ridges between 0.3 and 1 mm wide and 0.2-1.5 mm high. The domains they enclose are not equant, however, being instead elongated to an aspect ratio of 7:5 to 4:1 (Figure 5.2b). Domains are on average 5 mm wide. Often, the elongate ridges are more strongly defined and higher than the transverse 'rungs', having an average height of 1.2 mm. Connecting nodes are not raised above the rest of the network. Structures are seen in positive epirelief but only rarely occur on the soles of beds.

Elongate ladder networks are typically confined to fine grey siltstones, which may or may not be rippled. Where ripples do occur, the elongations run perpendicular to the strike of the ripple crests. Owing to the generally fine-grained nature of the host rocks, a fine veneer is rarely seen, but micas may be concentrated on the wrinkled laminae.

It seems that Ladders and Networks form two end members, between which there is a gradation, from equant polygonal domains of the networks, to the elongate domains of the ladders. Thus, ladders are here characterized by a domain elongation of at least 7:5.

5.3.2.4 Nodes

A regular arrangement of rounded protrusions in positive epirelief. Nodes are rounded to subrounded, with diameter between 2 and 6 mm, and a height of 0.5-1.5 mm (Figure 5.2c). Variants on their morphology exist: in some cases the nodes have thin radiating ridges extending up to 10 mm, giving them a stellate appearance (Figure 5.2d). These 'stellate nodes' are gradually continuous with simple nodes. Spacing between

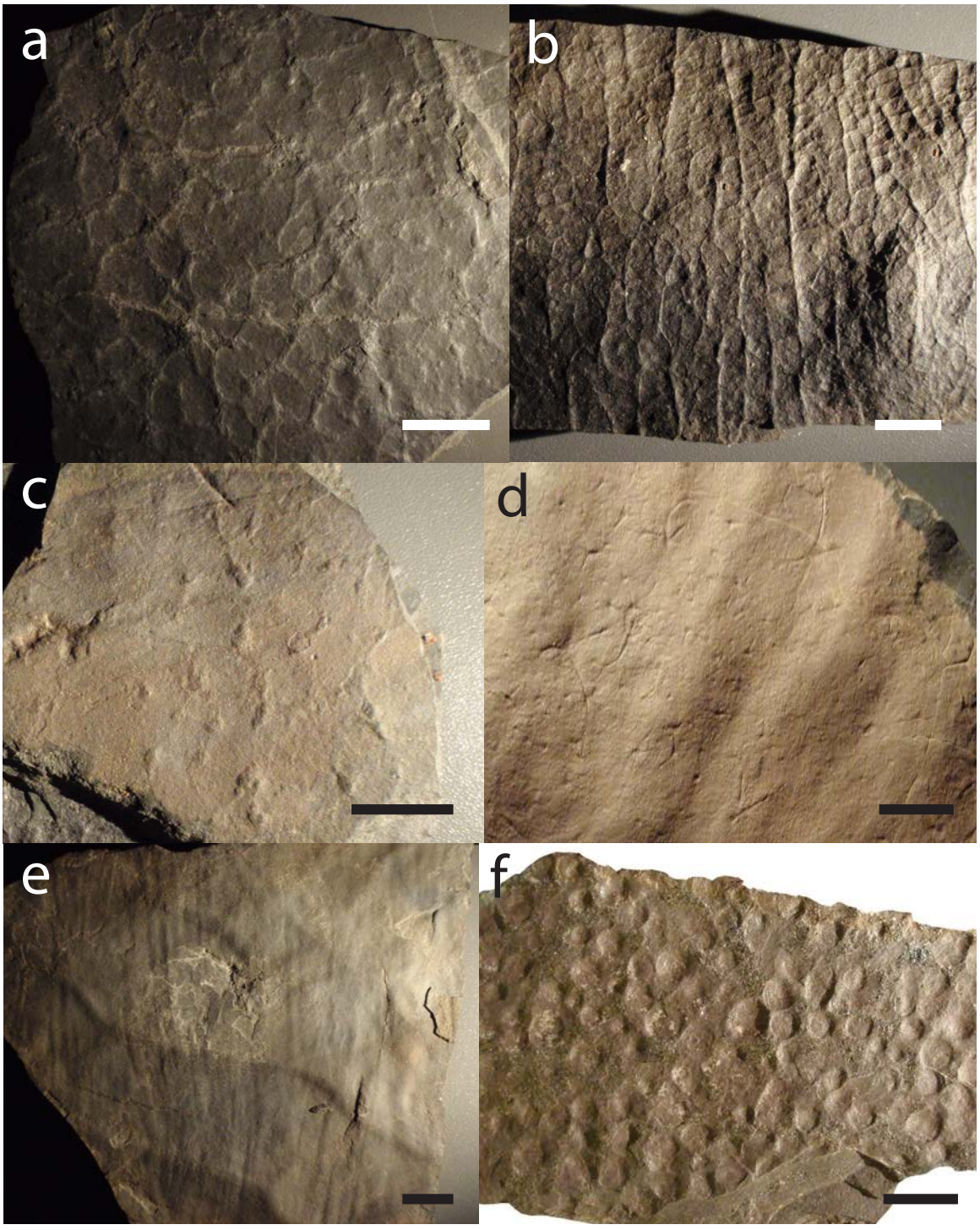


Figure 5.2: Ordered microbial macrostructures. a) Equant network with polygonal domains. Sample DBM08 from Lower Diabaig. Scale bar 2 cm. b) Elongate ladder with raised elongate ridges. Sample BRM45 from Brochel Castle. Scale bar 1 cm. c) Simple nodes. Sample DBM06 from Lower Diabaig. Scale bar 1 cm. d) Stellar nodes. Sample SHM01 from Sheildaig Peninsula. Scale bar 1 cm. e) 'Arumberia' parallel ridges and grooves. Sample DBM10 from Lower Diabaig. Scale bar 1 cm. f) Flat bottomed pits densely crowding surface. Sample BRM37 from Brochel Sheilings. Scale bar 1 cm.

nodes is similar to that seen in networks, between 5 and 20 mm.

Nodes are found on the surfaces of a range of lithologies, but are most dominant in micaceous grey siltstones. They are found in positive epirelief, but thus far have not been observed on the soles of beds.

It is possible that the nodes observed here represent an end member of a gradation to equant networks with raised interconnections. Networks may lose definition of the connecting ridges, creating the appearance of stellate nodes, and further ridge loss results in simple rounded nodes. Such differences may be related to differences in the original morphology, or preservational variants.

5.3.2.5 Flat bottomed pits and protrusions

Not regularly arranged like the above-described nodes, these pits are nevertheless uniformly rounded and have a limited range in diameter of 4-9 mm. They are densely crowded on the bedding surface, spaced 5 to 15 mm between centre points, but never overlapping (Figure 5.2f). Where two pits are closely associated, limited mutual compression is seen that distorts the rounded form. Vertical transects of the pits show them to be broadly flat bottomed, with the flattened region taking up at least 60% of the overall diameter. Occasionally small protrusions are present in the centre. No ridge or positive feature is observed around the rims of the pits. They occur in negative epirelief and are strongly associated with their counterparts in positive hyporelief. Rare occurrences of positive epirelief occur in isolated examples.

These pits were observed in abundance at only one locality, colonizing a small bedding plane of red fine-grained sandstone. The bedding surface bears abundant large flakes of muscovite, but no fine veneer is visible.

5.3.3 Disordered Surficial Structures

Some features are observed on the tops and soles of beds that do not show the characteristic organization of the above-described structures, but are nevertheless irregular features that cannot be explained by uniformitarian physical processes. Without notable organization, interpretation of these structures as biological in origin is

somewhat compromised, but comparison with the sedimentary record and modern microbial phenomena are here used to argue for their biogenicity.

5.3.3.1 Microreticulate network

In positive epirelief, these structures appear as very finely spaced pointed nodes with up to 3 mm relief (Figure 5.3a). Sharp ridges connect pointed nodes, but their close spacing means ridges are rarely well developed. Nodes are typically less than 4 mm apart, and the shape of enclosed domains is not well developed. Overall, these structures give a bedding surface a rough texture, which is typically not observed in hyporelief.

Microreticulate networks occur in a range of lithologies, from fine grey siltstones to red to orange sandy units, but they are particularly abundant in the latter. They are generally not associated with a fine veneer, but may be the locus of mica concentrations.

The node and ridge construction of these textures allows comparison to be drawn with the ordered network described above, but their extremely close spacing and this lack of symmetry precludes classification within that group. The two textures may represent end members of a gradually increasing tightness of network, but a distinction is made between microreticulate networks losing apparent order.

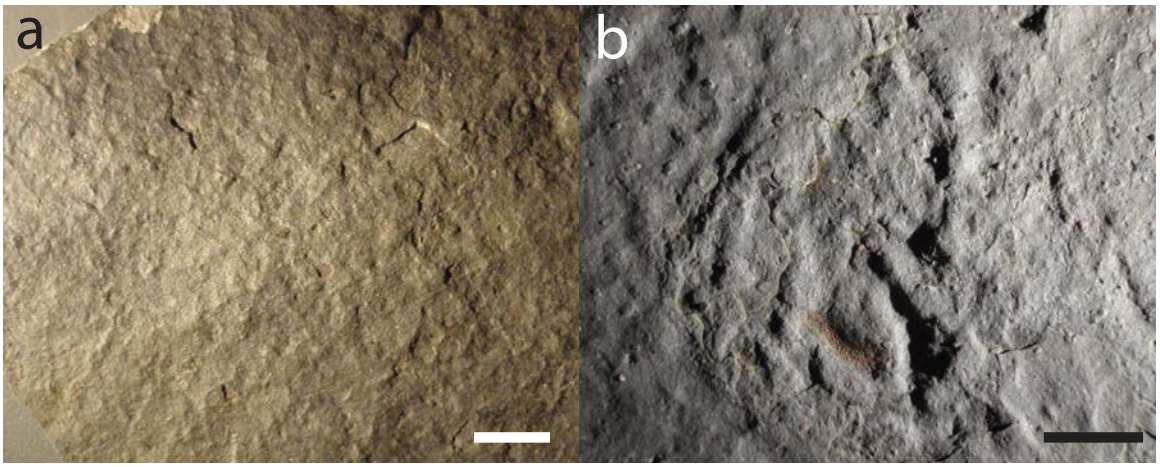


Figure 5.3: Disordered microbial macrostructures. a) Microreticulate network with low relief. Sample DBM04 from Lower Diabaig. Scale bar 1 cm. b) Irregular pits and pustulae. Sample FFM01 from North Sheildaig. Scale bar 1 cm.

5.3.3.2 Pustulae and pitting

Often occurring in irregularly shaped isolated patches, a mixture of positive and negative relief pustulation and pitting creates a blistered appearance on bedding surfaces (Figure 5.3b). Patches are up to 20 cm across, and consist of positive pustulae or negative pits between 2 and 20 mm in diameter, and 0.5-3 mm in height/depth. Dimensions of the pits and pustulae are very variable within blistered patches and between them, and there is no apparent symmetry or organization to the texture. The structures are visible in both positive and negative relief of the tops and bottom surfaces of beds.

This texture occurs primarily in grey to orange siltstones and fine sandstones, being particularly concentrated in grey-coloured laminar beds. They are occasionally associated with thin glossy veneers, which drape the structure without breaks.

5.4 Possible mode of formation

The various bedding plane macrostructures and modification of sedimentary features described above are demonstrably biogenic in origin. In combination with the associated phosphate and shale-hosted microbiota in the Diabaig Formation (Chapters 3 and 4), it may be assumed that the macrostructures are caused by the colonization of the sediment surface and pore spaces by actively growing, binding and sealing microbial mats. The interaction between mats of different character and varying physical conditions act together to produce the range of macrostructures observed here. The following hypotheses for formation are derived from studies of modern mat forming processes (e.g. Noffke et al. 2001).

5.4.1 Growth of mats

Both coccoid and filamentous microbes are known to form benthic biofilms and mats, by a combination of intertwining growth and secretion of extra-polymeric substances (EPS). Primitive biofilms form first, through the loose association of microbial individuals and clastic grains, adhered with EPS. Over time, these biofilms are built up and filamentous sheaths begin to intertwine and knit together, forming a more solid, cohesive mat structure that incorporates clastic grains. These bound mats can either form endobenthically, below the sediment-water interface, or epibenthically, on the

surface of the sediment (Figure 5.4).

Typically, endobenthic mats do not produce any form of structure through growth alone, being more involved in the modification of sedimentary features. They may be observable in thin section however, as carbonaceous layers with high concentrations of fine or micaceous material. Epibenthic mats may develop a macroscopic texture that has the potential of being preserved. Photosynthetic mats on the surfaces of sediment are known to form tufts—areas of higher relief as microbes orient upwards to maximize exposure to sunlight (Walter 1972). Such tufts may be broadly comparable with the raised interconnecting nodes of equant networks. Maturity of the mat as well as depth and water turbidity may control the growth of tufts, and therefore of the dimensions of the reticulate network, varying from dense microreticulate to loose polygonal networks.

Microbial growth does not always result in formation of laterally extensive and cohesive mats. Some bacteria and algae, for example *Nostoc* balls, are known to grow in locally confined colonies, which may or may not be surrounded by a mucilaginous sheath. Such algal colonies may be spread abundantly over the surface of the sediment, but remain locally confined and may compete for space with their neighbours. Where these colonies are not preserved directly, the depressions they leave in the underlying sediment may be retained: this is suspected to be the origin of the rare flat-bottomed pits.

5.4.2 Modification of mats and sediment

Once a microbial mat is present within or upon the sediment, it is subject to the same physical modifications as the sediment itself (Figure 5.4). In a lacustrine environment, the most dominant of these are oscillating and unidirectional currents, and changes in water composition. Oscillating currents have an effect on mats that have formed over symmetrical ripples. The mats are less easily shifted or moulded than the underlying sediment, so bidirectional motions act to crease the tops into sharpened crests, or to move the underlying sediment leading to multi-crested ripples.

Unidirectional currents have a more profound effect on the original morphology of an epibenthic mat. A constant sweeping current can elongate the filaments that make

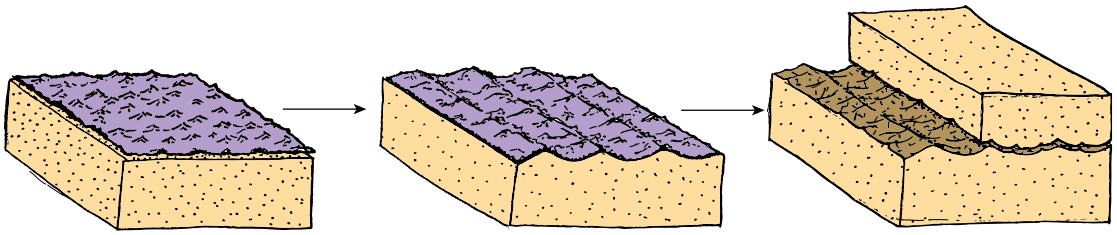


Figure 5.4: Schematic mode of formation of microbially induced wrinkle structures. Sediment surfaces are colonised by filamentous and coccoid microorganisms which bind together with extra-polymeric substances to form a mat layers. Individuals grow upwards in response to light or competition, producing a more or less ordered pattern of tufts. Subsequent physical processes alter the sediment beneath and the mat structure, creating elongations and other associated features in the mat and the underlying sediment. As the mat is buried, the organic material will be degraded, but under suitable rapidly lithifying conditions, its impression will be preserved in the underlying and overlying sediments.

up the mat, including those growing vertically in tufts. As a result, some interconnected ridges between tuft nodes become elongated parallel to the current direction, and those ridges that are perpendicular become attenuated. The result is a ladder-like network, whose elongation is dependent on the strength of modifying current. Support for this hypothesis lies in the fact that, when draping ripples, the ladders are always perpendicular to the strike of the crests, indicating the elongation being caused by oscillating currents too.

Where epibenthic mats do not develop tufts, unidirectional currents may influence them in another way, by wrinkling them into small-scale ridges and grooves perpendicular to the direction of flow creating textures recognized as 'Arumberia'. Such textures may be only formed by unidirectional currents, rather than oscillating ones, and their absence from rippled beds supports the hypothesis.

Finally, alterations in the composition of the water above a microbially bound sedimentary layer may result in the formation of synaeresis cracks, which are preserved due the pliancy conferred by endobenthic mats.

5.4.3 Preservation of mats

Following growth and modification of microbial mats in and on the sediment, subsequent sedimentation will bury them, removing them from a lit environment and

ultimately killing them. If the structures formed by the microbial mats in life are to be preserved after burial and death, the sediments must remain undisturbed and be lithified before any appreciable compression or distortion. In the Proterozoic sediments this is readily achieved, owing to a lack of bioturbation, and the common early diagenesis of sediments (Berner 1980). There will inevitably be some changes conferred by degradation and lithification, and these can act to produce variations on the original morphologies (Figure 5.4).

Firstly, the deposition of sediment onto the surface of a tufted epibenthic mat will act to attenuate some of the original relief. The tufted nodes may become flatter and wider, as will the interconnected ridges. For features that have little original relief, this flattening may result in their loss. It is hypothesized that this is the process of formation of the ordered simple and stellate nodes. Depending on the relief and resistance of the original mat structure, sediment deposition will flatten the lower-relief interconnecting ridges, to first leave nodes with remnant radiating ridges, and later to leave only the simple nodes.

Also, following burial and degradation of the organic matter of the mat, the original mat surface may become well sealed, and sampling of the rock for study may not directly intersect the original mat layer. Instead, the rock may part at laminae that overlaid the sculpted mat structure, giving approximately the same morphology, but with less definition. In these cases, nodes and ridges may have lower relief and be broader, and characteristic veneers or concentrations of micaceous material may be absent.

Finally, the process of degradation of an organic mat is likely to be a fermentative one, incorporating anoxygenic and potentially methanogenic heterotrophic processes. These processes are likely to produce gases within the sediment, which may rise but be sealed by thick clay layers or younger mats. Gas bubbles could cause irregular bulging of the sediment, and following gas escape would leave hollowed pits. This may explain the irregular occurrence of pustulae and pits in fine-grained sediments. The patchy distribution perhaps derives from an original patchy distribution of fermenting organic matter.

Thus, it can be seen that the variety of macrostructures observed within the siltstones and sandstones of the Diabaig Formation derive from the intimate association

of growing and binding microbial mats with sediment and physical processes that modify them during life and after death.

5.5 Variation between environments

Although a wide variety of macrostructure morphologies have been observed and accounted for by microbe-sediment interactions, their distribution is not ubiquitous across all lithofacies of the Diabaig Formation. Certain structures are dominant at certain localities, and can therefore be related to the specific palaeoenvironments of those localities. Macrostructures were recorded at: Shieldaig Bay and Peninsula; North Shieldaig (Fish Farm); Balgy River and Shore; Upper Diabaig; Lower Diabaig; Badachro; Brochel Castle; and Brochel Sheilings. A description of the environmental variation, and discussion of the modes of formation for each locality are given below.

5.5.1 Shieldaig Bay and Peninsula

The lithofacies here represents a relatively energetic mid-delta environment, with high depositional rates and both oscillating and unidirectional currents. The rocks comprise red sandstones and siltstones that are commonly rippled.

A range of different microstructures are seen at this locality, including networks and their accompanying 'elephant skin' negative counterparts, stellate nodes, curved 'Arumberia' ridges, and rare flat topped protrusions (Figure 5.5). The networks are broadly equant and enclose domains of diameter 4 to 7 mm, with sharp ridges less than 0.7 mm wide and up to 1.2 mm high. The nodes are predominantly simple, although some are faintly stellate and measure 1-2.3 mm in diameter. They are spaced on average 17 mm from one another. The flat topped protrusions occur rarely as isolated individuals, measuring approximately 12 mm in diameter and 1.5 mm high.

The presence of networks is indication of thriving tufted mats in this environment, and thus of good light penetration and limited water turbidity. Their equant dimensions suggest they were unaffected by directional currents. Some layers were affected by currents however, as evidenced by the 'Arumberia' texture, concurring with the sedimentological evidence that water energies were variable in this environment. The high depositional rates have an adverse effect on the preservation of the networks,

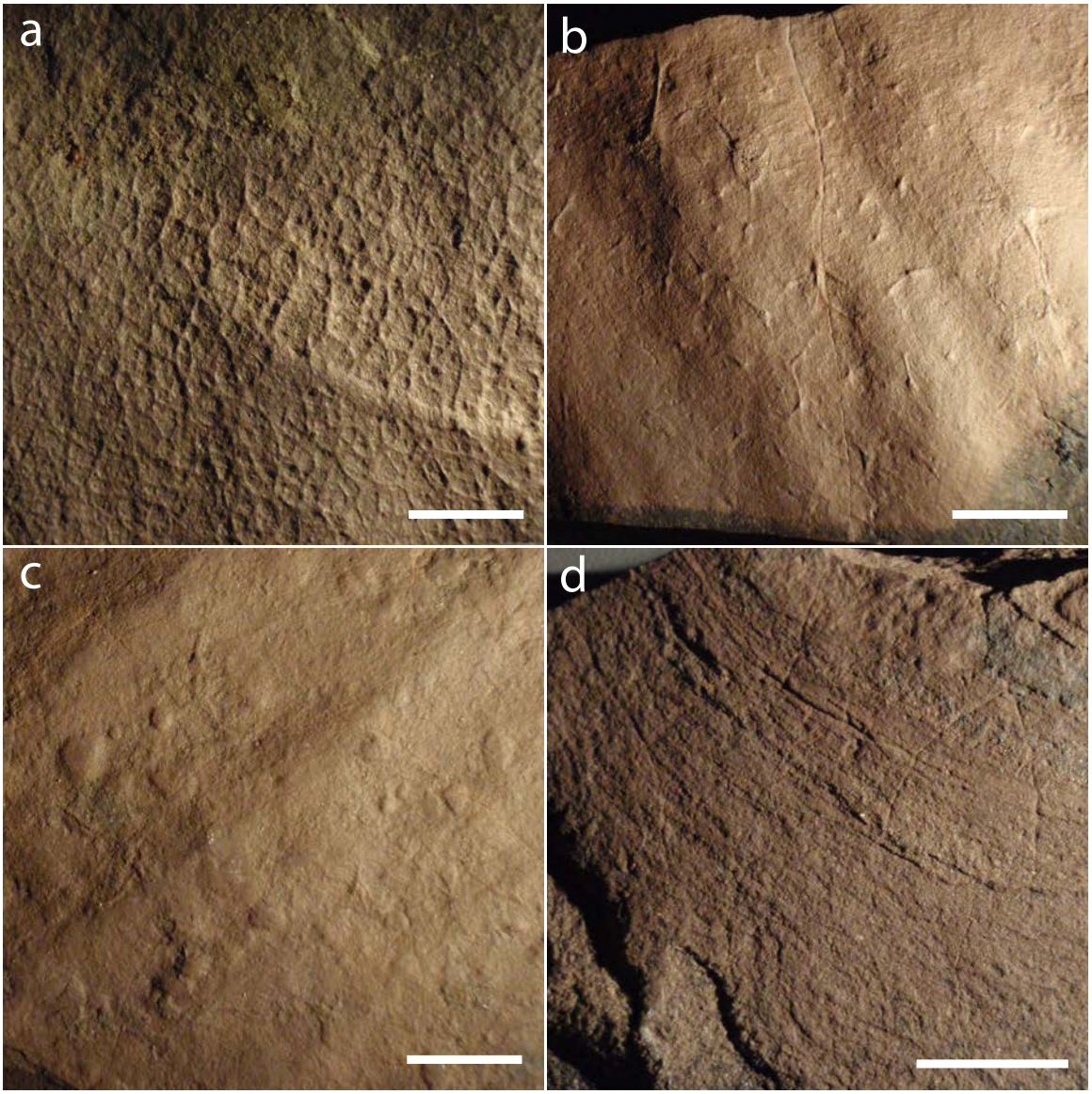


Figure 5.5: Microbially induced macrostructures from Sheildaig Bay and Peninsula. a) Equant microreticulate networks. Sample SHB03 from Sheildaig Bay. Scale bar 2 cm. b) Stellar nodes. Sample SHM02 from Sheildaig Peninsula. Scale bar 2 cm. c) Irregularly distributed flat-topped protrusions. Sample SHM22 from Sheildaig Peninsula. Scale bar 2 cm. d) curving ridges and grooves of 'Arumberia'. Sample SHM23 from Shieldaig Peninsula. Scale bar 2 cm.

resulting in the formation of organized nodes. The flat-topped protrusions, presumably representing isolated microbial colonies cast by a sealing mat in the manner of an Ediacaran 'death mask' (Gehling 1999), may be autochthonous or have been secondarily washed into the sediments. Further findings and observational data are necessary before these possibilities can be distinguished.

5.5.2 North Shieldaig (Fish Farm)

Sedimentology reveals this lithofacies to be deposited in an energetic current-dominated environment such as a delta top. Macrostructures were recovered from grey siltstones within the sequence.

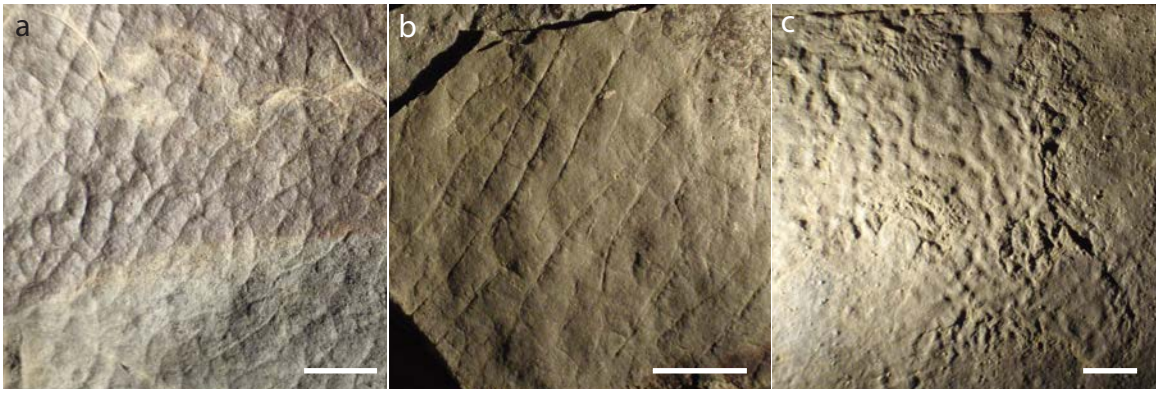


Figure 5.6: Microbially induced macrostructures from North Sheildaig. a) Equant network. Sample FFM05. Scale bar 1 cm. b) Elongate ladders with indistinct cross ridges. Sample FFM09. Scale bar 1 cm. c) Irregular pits and pustulae. Sample FFM01. Scale bar 2 cm.

At this locality, ordered macrostructures were found, comprising equant networks in positive epirelief and counterpart 'elephant-skin' structures in negative hyporelief (Figure 5.6). Networks are tight, with domains varying from 3 to 9 mm in diameter, and interconnected ridges 0.7 mm wide and 0.5 mm high. Elongated ladder networks were also found in positive epirelief and negative hyporelief on flat, unrippled surfaces, with domains approximately 5 mm wide and 7-20 mm long. Bounding side ridges are sharp but faint, measuring around 0.3 mm wide and 0.6 mm high, and transverse ridges are indistinct. Relatively large patches of pustulae and pitting are found scattered on several bedding surfaces.

The occurrence of tufted networks is indication of a lit sediment surface with limited water turbidity, allowing common colonization of these photosynthetic mats.

Concurrent with the sedimentological evidence, current strengths are fairly variable, resulting in the co-occurrence of equant networks and elongated ladders. Ladders are formed by laminar flow in unidirectional currents, as evidenced by their appearance on flat, unrippled sediment surfaces. At times, networks appear indistinct, indicating preservational alteration of the macrostructures' definition. The patchy distribution of irregular pits and pustulae are perhaps evidence for localized development of sealing and degrading endobenthic mats, which produce a bubbled, blistered texture in response to anoxygenic decay within the fine silty sediments.

5.5.3 Balgay River and Shore

The discontinuous transect through the Diabaig Formation outcropping at the Balgay river section, and along the shore to the east represents an energetic sandy delta, with high depositional rates and changing current energies as the depositional regime grades from distal prodelta, through mid-delta sheet sands, to heavily wave rippled and current swept channeled delta top. The rocks here are heavily rippled red sandstones and siltstones, and macrostructures are often found at on micaceous layers between changes in grain size.

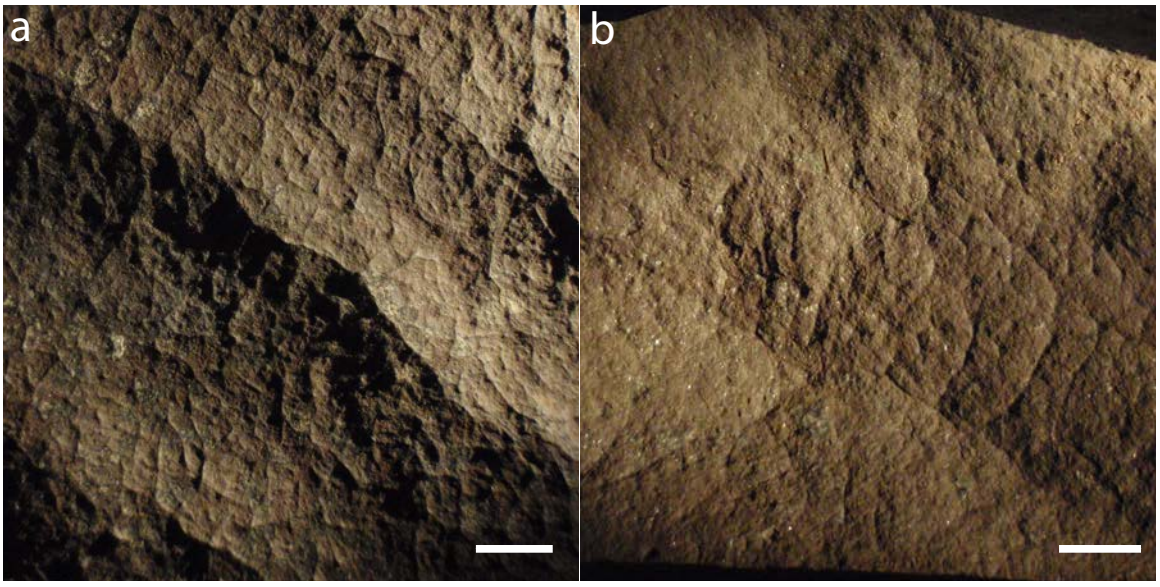


Figure 5.7: Microbially induced macrostructures from Balgay River and Shore. a) Equant networks on ripples with sharp-ridged crests. Sample BALR03 from Balgay River. Scale bar 1 cm. b) Networks with elongate ridges running perpendicular to ripple strike. Sample BALR03 from Balgay River. Scale bar 1 cm.

In the more distal prodelta parts of the section, more or less equant networks are found colonizing rippled fine sand surfaces, and are found in situ with their counterpart 'elephant skin' negative structure on the soles of adjacent beds (Figure 5.7). Networks are relatively tight, enclosing domains approximately 7 mm across with ridges 0.5 mm wide and 0.5 mm high. They occur only on surfaces with symmetrical ripples, and are associated with sharpening of the crests of these ripples. Some ridges of the network appear to run parallel to the crests, enhancing the appearance of sharpening, and there is a slight elongation of polygonal network domains and bounding ridges down the ripple slope perpendicular to crest strike.

The presence of networks in this environment, and especially between beds of differing grain size, indicate periods of low water turbidity and good light penetration, perhaps during hiatuses in deposition. The epibenthic mats clearly interact closely with the rippled surface, creasing at the crests to produce sharpening, and being somewhat elongated by the wave-derived oscillating currents. Preservation of the wrinkle structures is good, suggesting little compaction by loose sandy overlying sediment.

5.5.4 Upper Diabaig

Red sandstones and siltstones are planar laminated and occasionally rippled in this lithofacies, which represents a relatively distal prodelta depositional environment. Depositional rates and current strength varies with progressive incursions of sandy material, and the whole sequences are affected by oscillating wave currents. Microstructures are typically found near to changes in grain size.

Equant networks dominate the microstructures here, occurring in positive epirelief on the surfaces of fine sandy rippled beds (Figure 5.8). The networks are relatively tight, enclosing polygonal domains around 5 mm across, with ridges up to 1 mm high and 1 mm wide. Where they cover rippled surfaces, ridges are slightly elongated perpendicular to the strike of crests, and those ridges are somewhat better defined. The ripples themselves occasionally show multiple crests, draped by the networks.

As with the above-described rippled sandstones of Balgy River and Shore, the presence of networks at the tops of sandy beds are indication of well-lit waters perhaps during depositional hiatuses. The multi-crested ripples are testament to the draping

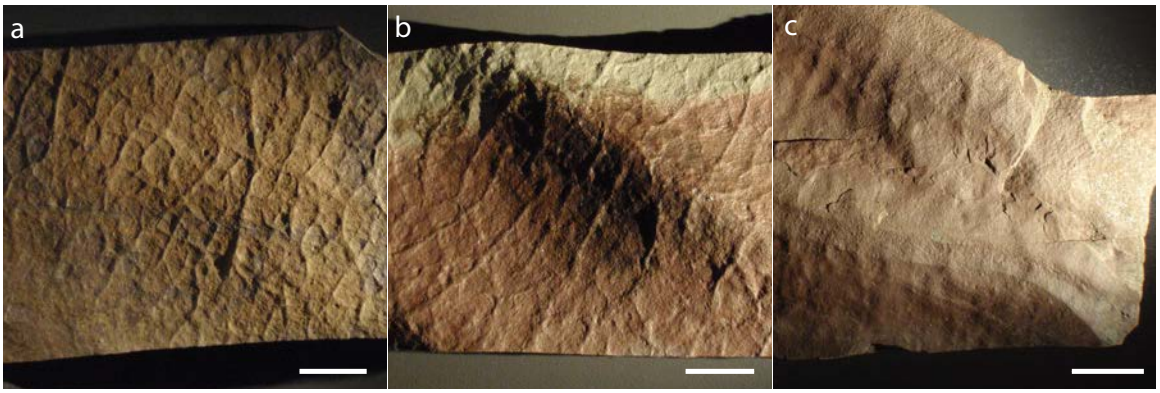


Figure 5.8: Microbially induced macrostructures from Upper Diabaig. a) Equant network. Sample UDI04. Scale bar 1 cm. b) Elongate ladder with ridges running perpendicular to ripple strike. Sample DRM09. Scale bar 1 cm. c) Multi-crested ripples with indistinct network structure. Sample DRM13. Scale bar 1 cm.

epibenthic mats interacting with the shifting sands beneath. Overall definition of wrinkle structures is good, indicating good preservation in this sandy environment.

5.5.5 Lower Diabaig

At the type section of the Diabaig Formation, heavily desiccated and rippled grey siltstones and fine sandstones are formed in a subaerially exposed shoreline at some distance from clastic input. A wide range of macrostructures is observed on the top surfaces of beds throughout the section.

Loose networks occur, with ridges ∼0.5 mm high and 0.5-2 mm wide enclosing large polygonal domains between 7 and 20 mm in diameter (Figure 5.9a). Nodes of these networks are large and irregularly textured, often reaching a diameter of 4-5 mm. More rare are tight networks, with equant domains around 4 mm in diameter and sharper ridges 0.3 mm wide by 0.5 mm high, and microreticulate networks with a maximum relief of 0.4 mm (Figure 5.9c). Simple nodes occur in close association with the loose networks, consisting of protrusions in positive epirelief around 4 mm in diameter and 1 mm high, with up to 3 radiating ridges between 3 and 10 mm long (Figure 5.9b). Straight ridges and grooves of 'Arumberia' occur on unrippled surfaces, apparently associated with pustulate textures in fine-grained silts (Figure 5.9d). Ripples are typically modified with sharpened crests, even in the absence of any other macrostructure.

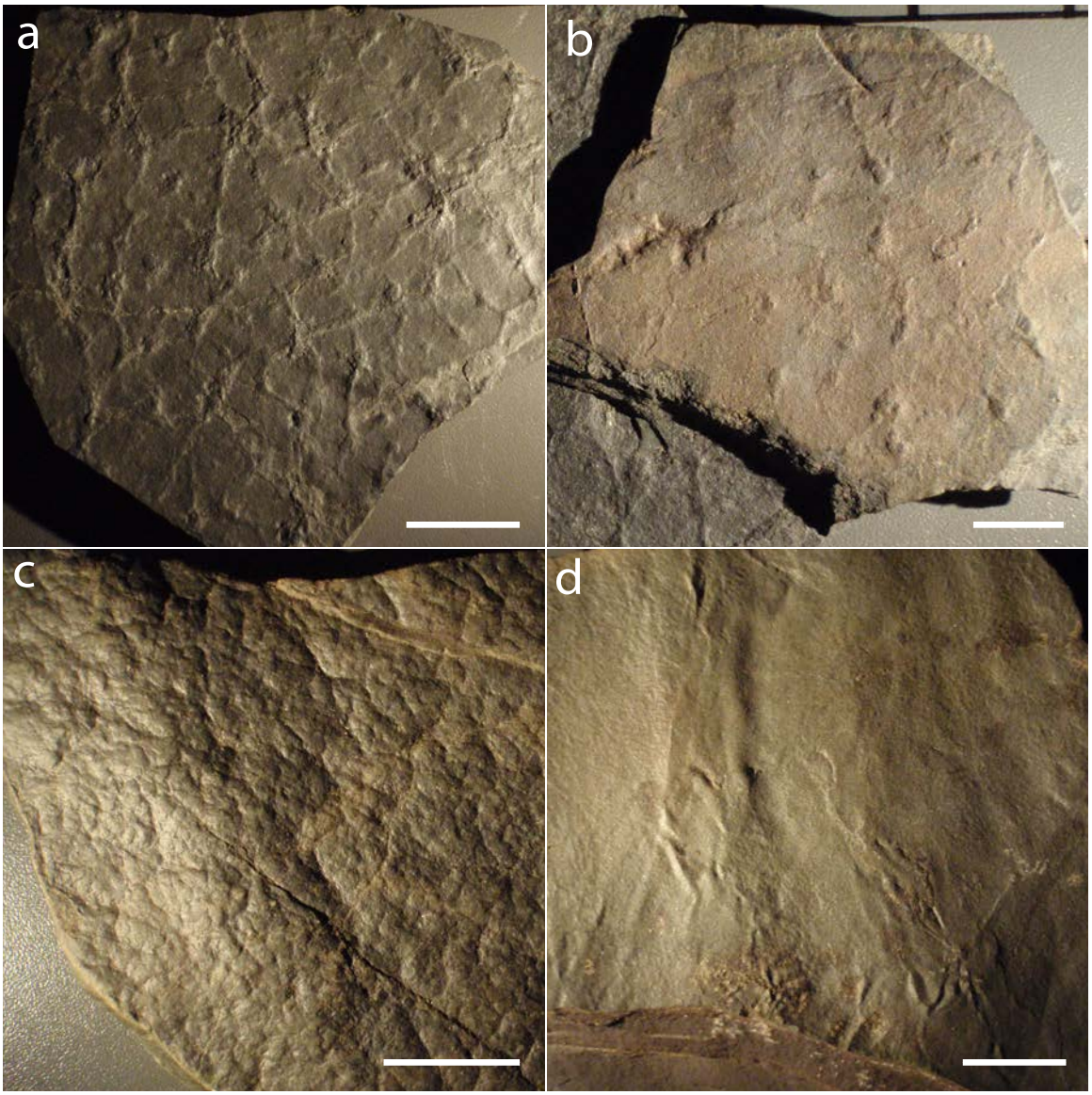


Figure 5.9: Microbially induced macrostructures from Lower Diabaig. a) Loose network with broad ridges. Sample DBM08. Scale bar 2cm. b) Simple nodes. Sample DBM06. Scale bar 1 cm. c) Fine tight elephant skin network in negative hyporelief. Sample DBM23. Scale bar 2 cm. d) Pustulate texture associated with 'Arumberia'. Sample DBM21. Scale bar 2 cm.

The presence of equant networks of tufted mats in these fine grained mud flat sediments demonstrates that water turbidity was limited to allow sufficient light for photosynthetic organisms to thrive. Networks tend to be limited to only weakly rippled horizons, and this is reflected in the persistently equant nature of the polygonal domains. The loose arrangement of the networks may be testament to growth in a more stressful desiccating environment, and thus dominance of a few established tufts rather than dense crowding of weaker ones. Low relief microreticulate networks are present, indicating the maximum development of sculpted epibenthic mats without such dominance. The notable irregularities in the morphology of these loose networks, specifically the broad nodes and expanded ridges, as well as the presence of stellate nodes amongst the assemblage, are probably results of preservational alteration of the original microbial structures. Dense smothering siltstones that are the common constituent of this rock have a greater compressional effect on the underlying mat structure, resulting in flattening and broadening, and ultimately the loss of some interconnecting ridges, creating stellar nodes. In addition, the desiccating depositional environment may mean that mats are periodically exposed and thus subjecting them to extra degradational pressures, resulting in some loss of pristine morphology even before burial.

Where microbial mats do not form an identifiable sculpture, they are preserved in the rock as 'Arumberia' textures, which are oriented sub-parallel to ripple crests and so were probably formed by mat wrinkling in response to bidirectional oscillating currents . The same sealing mats are responsible for the formation of sharpened ripple crests as the fine sandstones beneath them are shifted, as well as the irregularly distributed patches of pustulation and pitting, that indicates sealing of gas bubbles produced by degradation of buried organic matter.

5.5.6 Badachro

The lithofacies at Badachro comprises dark grey siltstones and fine sandstones that were deposited in a deep water, distal environment with little clastic input and no appreciable wave or current action.

No ordered networks were found in this lithofacies, and microstructures instead consist of microreticulate textures, 'Arumberia', and irregularly distributed pustulae and pitting (Figure 5.10). Microreticulation has a maximum relief of 0.5 mm, and

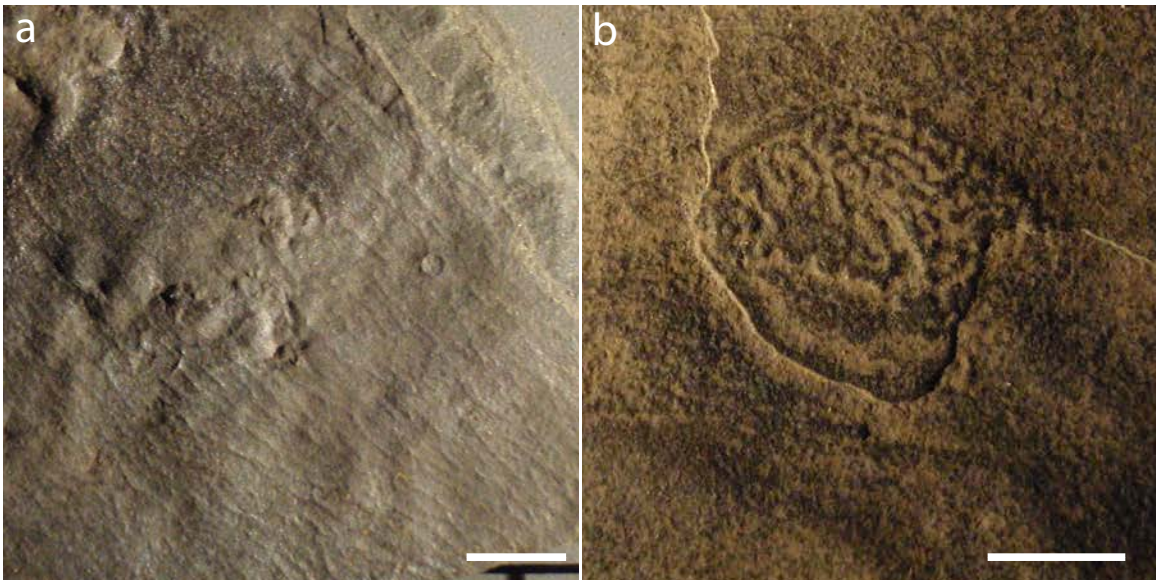


Figure 5.10: Microbially induced macrostructures from Badachro. a) Fine elongate ridges of 'Arumberia'. Sample BDM22. Scale bar 1 cm. b) Isolated patches of pustulae. Sample BDM25. Scale bar 1 cm.

does not show any symmetry. Ridges and grooves of 'Arumberia' are closely spaced (wavelength of around 1 mm) and anastamosing, but laterally straight. Pustulate textures are extensive across entire bedding planes but vary locally in the size of pustulae and pits, up to a maximum diameter of ∼20 mm.

Overall, the assemblage of macrostructures at this locality is fundamentally different to those seen elsewhere, and this is likely testament to the substantially different depositional conditions. The absence of tufted mat networks reflects non-optimal conditions of growth for these photosynthetic mats: most likely due to the sediment surface being beyond the reach of the photic zone. Alternatively, anoxygenic conditions may prevail that limit the growth of microbes using oxygen for their metabolisms. Some mats are present, however, as evidenced by the 'Arumberia' textures, whose wrinkled profile also suggests some weak current action that is not otherwise recorded in the sediment.

5.5.7 Brochel Castle

A long section to the south of Brochel castle exposes coarsening upward packets of siltstones and sandstones, reflecting successive progradations of delta systems into the Diabaig lakes. Macrostructures were recovered from the finer grey silty portions of

these packets, deposited under more distal conditions, but still affected by oscillating and unidirectional currents.

Microstructures at this locality range from small, tight networks to elongate ladders, 'Arumberia' textures and occasional crest sharpenings and synaeresis cracks (Figure 5.11). Networks expose domains 3-8 mm across, with relatively sharp ridges 1.5 mm high and 0.7 mm wide, and are common on rippled surfaces where they enhance crest sharpening. There is typically an unclear distinction and gradation between these and more elongate ladder networks, occurring even on the same bedding plane. Elongate ladders occur on flat, unrippled surfaces, containing multiple polygonal domains between raised, elongate ridges, and are often not straight but curving over a bedding plane. 'Arumberia' textures are abundant on flat and rippled surfaces, running parallel to ripple crests in the latter.

The presence of tufted mat networks indicates well lit bottom waters for at least part of this succession, but the predominance of non-sculptured 'Arumberia' suggests more prolonged conditions of water turbidity and poor light penetration. Where networks do occur, their irregular elongation is testament to locally variable strengths and directions of currents, as may be expected in these shallow prodelta to delta to environments. Oscillating currents of wave action are typically not associated with ladder formation, and instead cause crest sharpening beneath sculpted equant networks. Synaeresis cracks in association with 'Arumberia' textures indicate well developed endobenthic mats in this region.

5.5.8 Brochel Sheilings

At the southernmost extent of the outcrop of Diabaig Formation at Brochel, within a thick package of red medium grained sandstones from a mid deltaic palaeoenvironment, an isolated bedding plane exposes densely crowded flat-bottomed pits (Figure 5.11d).

Pits occur as described above, and are found intimately associated with part and counterpart in situ in very mica-rich laminae. The occurrence of these structures here, and their interpretation as crowded rounded benthic colonies of algae or bacteria indicate optimum conditions for their growth and preservation, that is not seen or preserved elsewhere. Conditions may be favourable due to shallow waters, a hiatus in deposition and fluvial input of high concentrations of nutrients. With just one isolated

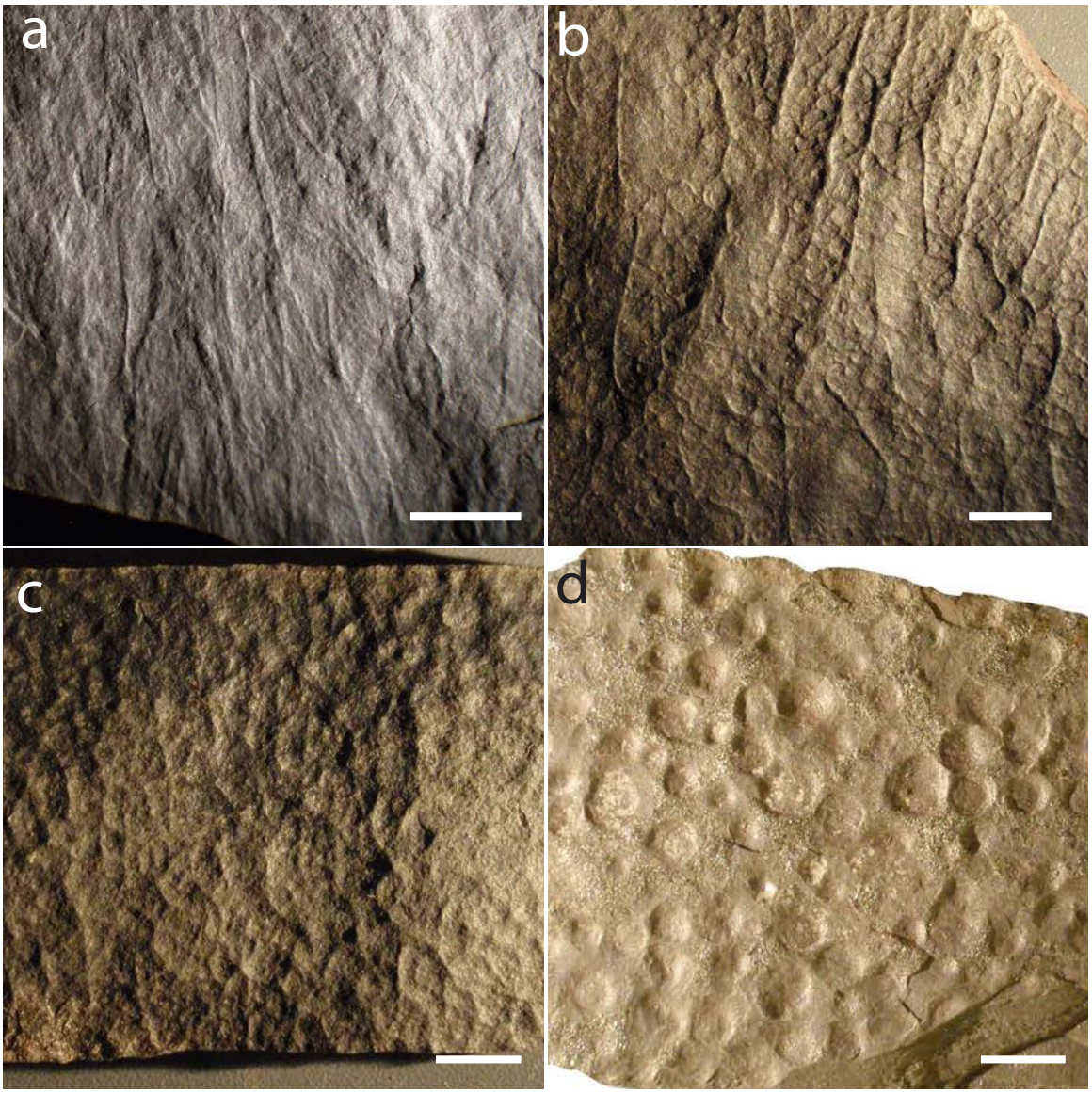


Figure 5.11: Microbially induced macrostructures from Brochel Castle and Sheilings. a) Intertwining ridges of 'Arumberia'. Sample BRM44 from Brochel Castle. Scale bar 1 cm. b) Elongate ladders with multiple domains between elongate ridges. Sample BRM48 from Brochel Castle. Scale bar 1 cm. c) Tight equant networks. Sample BRM56 from Brochel Castle. Scale bar 1 cm. d) Densely crowded flat-bottomed pits. Sample BRM37 from Brochel Sheilings. Scale bar 1 cm.

	Sheildaig Bay and Peninsula	North Sheildaig	Balgay River and Shore	Upper Diabaig	Lower Diabaig	Badachro	Brochel Castle	Brochel Sheilings
Sedimentary Modification								
Sharpened or multiple ripple crests			x	x	x		x	
Synaeresis cracks							x	
Ordered Structures								
'Arumberia'	x				x	x	x	
Networks	x	x	x	x	x		x	
Ladders		x		x			x	
Stellate nodes	x			x	x	x	x	
Simple nodes					x			
Flat bottomed pits and protrusions	x							x
Disordered Structures								
Microreticulate network	x			x	x	x	x	
Pustulae and pitting	x	x		x	x	x		

Table 5.1: Summary of wrinkle structures and their distribution amongst the lithofacies of the Torridon Group

occurrence, however, it is difficult to infer more about these structures' origin, and so more examples and supporting sedimentological data should be sought.

5.6 Summary

Macrostructures are here analysed in detail from the Diabaig Formation of northwest Scotland, following preliminary reports (Callow et al. 2011, Prave 2002, Upfold 1984). A wide range of macrostructures are attributed to the interactions of microbial mats with physical sedimentary processes. By comparing described macrostructures between lithologically characterized facies, it is possible to relate particular macrostructure morphologies to certain prevailing conditions. For example, equant networks formed by tufted epibenthic mats form where the sediment surface is well lit, and where no strong currents act to elongate tufts and ridges (Table 5.1, Figure 5.12).

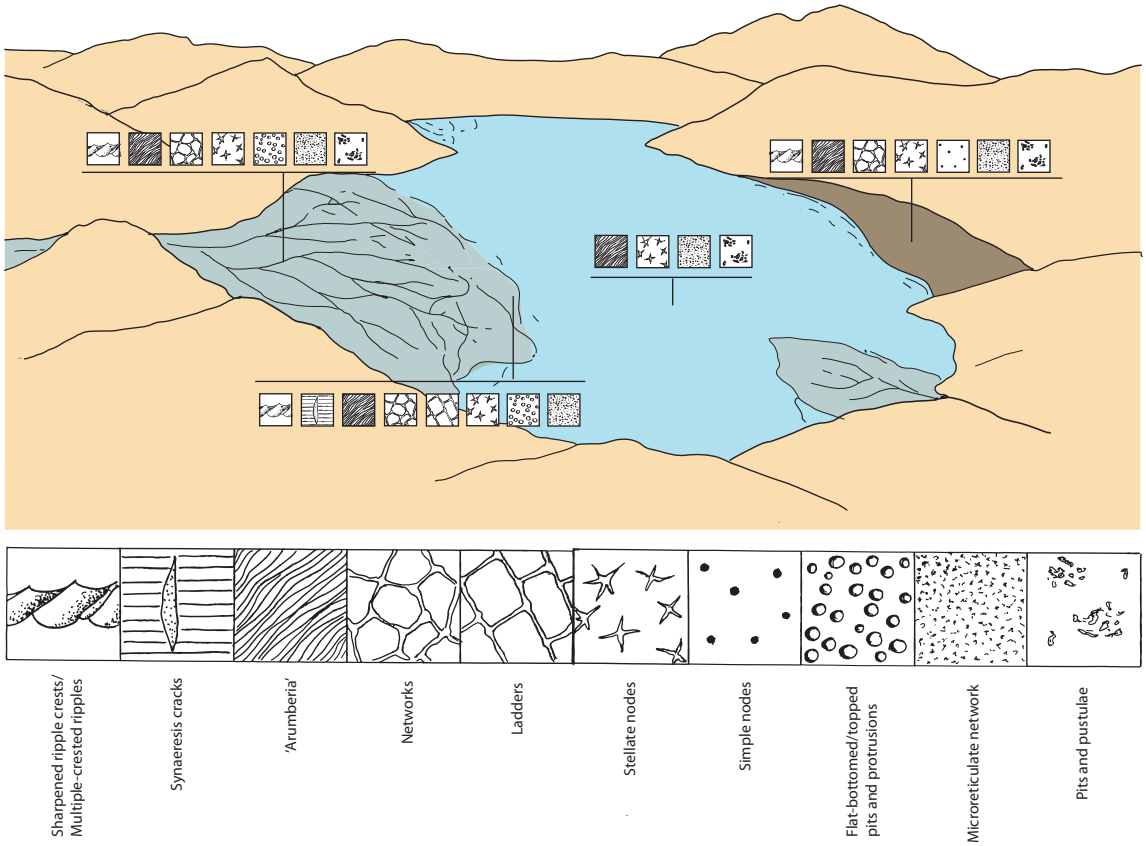


Figure 5.12: Location of wrinkle structures within the idealised Diabaig Basin. Data from all wrinkle-bearing Diabaig localities.

The correlations are not fully predictive, however, as the dataset is not yet sufficiently extensive and the formation of these wrinkle structures is not fully understood in modern analogues. It is possible that, given assimilation of data from wrinkle structures elsewhere in the sedimentary record, such as the 'elephant-skin' structures of the Ediacaran (Gehling 1999), the occurrence of macrostructures may be used as palaeoenvironmental indicators.

Chapter 6

Torridon phosphates

6.1 Previously reported phosphate in Torridon

Nodules of phosphate were first noted from the sedimentary rocks of the Torridon Group by Jethro Teall in Peach and Horne's seminal work on the geology of Scotland (Peach et al. 1907). They described and figured microfossils from the phosphate, but did not enter into detail as to the sedimentological context. Similarly, the Torridon Group was included in a census of Precambrian-Cambrian phosphate deposits (Cook & Shergold 1986), but as they are not volumetrically significant or economic, they have received little subsequent attention. A later more detailed description was carried out by Rodd & Stewart (1992), and the phosphates were included in a thorough review of the Torridon Group by Stewart (2002), from grey shales of the Diabaig Formation at Lower Diabaig, but little more than stratigraphic positions were noted. In the sedimentological analyses carried out as part of this study, phosphate was recovered from six different localities in the Diabaig Formation, and from the Cailleach Head Formation at Cailleach Head, considerably expanding the known dataset.

Most phosphate deposits are thought to form in marine environments (Föllmi 1996), and the presence of phosphate has even been used as a proxy to infer a marine depositional setting for the Torridon Group (Stewart 1969). The overwhelming sedimentological evidence for a lacustrine environment (Chapter 2) however contradicts this conclusion, and thus a new hypothesis must be formed and tested that can explain the occurrence of this phosphate in a non-marine setting. In the below analyses, successive levels of magnification are used to image and characterize the Torridon phosphate, and then occurrences are compared between environments before an idealized mode of formation is proposed.

6.2 Description of phosphate and associated minerals

In order to obtain the maximum amount of sedimentological and petrological information from the phosphatic nodules of the Torridon Group, data were collected on a variety of scales, from structural field evidence, through to high resolution FIB-TEM imaging.

6.2.1 Large scale sedimentology

Black and waxy sedimentary phosphate occurs within the Diabaig Formation at the base of the Torridon Group, and in the Cailleach Head Formation at the top of the group (Stewart 2002). Variously, it occurs as: laterally extensive bands up to 2 cm thick; millimetric and sub-millimetric veneers on argillaceous bedding surfaces; discontinuous nodules up to 2 cm thick, oriented parallel and subparallel to the bedding surface; and elongated rip-up clasts often less than 1 cm thick and 3 cm long, reaching a maximum of 45° inclination from the bedding surface, often concentrated near the bases of massive sandy horizons. The habit of the phosphate varies between formations, and also between locations within the Diabaig Formation. Overall, its appearance is not regular or cyclic, but neither is it confined to restricted spatial or temporal horizons. Within the Diabaig Formation, laterally discontinuous bands can be found within fine sandy portions of the section at the type locality of lower Diabaig (Figure 2.1, locality 3), and thick lenses with restricted width are seen in Fladday, off the island of Raasay (Figure 2.1, locality 4). At Cailleach Head (Figure 2.1, locality 1), no continuous bands were observed, but many sandy beds contain rip-up clasts of variable size and orientation. Some laminated shales, for example those of the Diabaig Formation at Badachro (Figure 2.1, locality 2), also contain a considerable amount of disseminated phosphate and carbonaceous material, giving them an overall dark waxy lustre. In general, the *in-situ* bands and nodules of phosphate form upon laminar surfaces of the grey shales, but occasionally are found draping the troughs of wave ripples in more sandy horizons and can be seen at the edges of desiccation cracks.

6.2.2 Optical microscopy

In thin section, the sedimentary phosphate appears amorphous and cryptocrystalline and broad transitions are seen between zones of particular crystal sizes. Organic material or fossil structures are not limited to a particular crystal size domain, being equally distributed throughout entire bands or nodules. There appear to be two interfingering phases of phosphate in equal abundance in the lenses and bands. Occasionally, layering can also be picked out within the phosphatic matrix, derived variously from differing quantities of organic or clastic material, or between phosphatic crystal size, or composition. The boundaries within the phosphatic layers are sharp, but mostly not erosional, and the clastic grains suspended within the phosphatic matrix fine upward smoothly and conformably. The edges of rip-up clasts illustrate their plastic nature at time of formation, with rounded edges, and smooth deformation around larger clastic grains. The microfossil structures are preserved within all these phosphatic occurrences, and no variation in preservation has been found to correspond to crystal size, composition or sedimentary texture at this scale.

6.2.3 SEM BSE and EDX analyses

Imaging phosphate with SEM backscattered electrons (BSE) is a useful technique for visually differentiating between different textures of phosphate observed through optical microscopy, as well as resolving fine scale details within phosphatic material. BSE images reveal differing mineralogies as variable shades of grey, dependant on the elemental scattering of electrons within the instrument. Methodologies and equipment for preparation and analysis are detailed in Appendix A.

In particular, the apparently 'pure' gelatinous phosphatic material at some localities can be compared with more 'granular' textures, to deduce the mineralogical origin of the difference.

Figure 6.1 illustrates comparative images of 'pure' phosphate texture and a 'granular' texture that appears darker and more heterogeneous in optical images. It can be seen in these images that the differences is conferred by the amount of material contained within a phosphatic matrix. In the granular texture, a polymictic mixture of grains is visible, oriented randomly within an apparently homogenous phosphatic cement (Figure 6.1b,d,f). Without elemental analysis, it is not possible to discern the mineralogy of these clasts, but their rounded nature indicates a detrital, rather

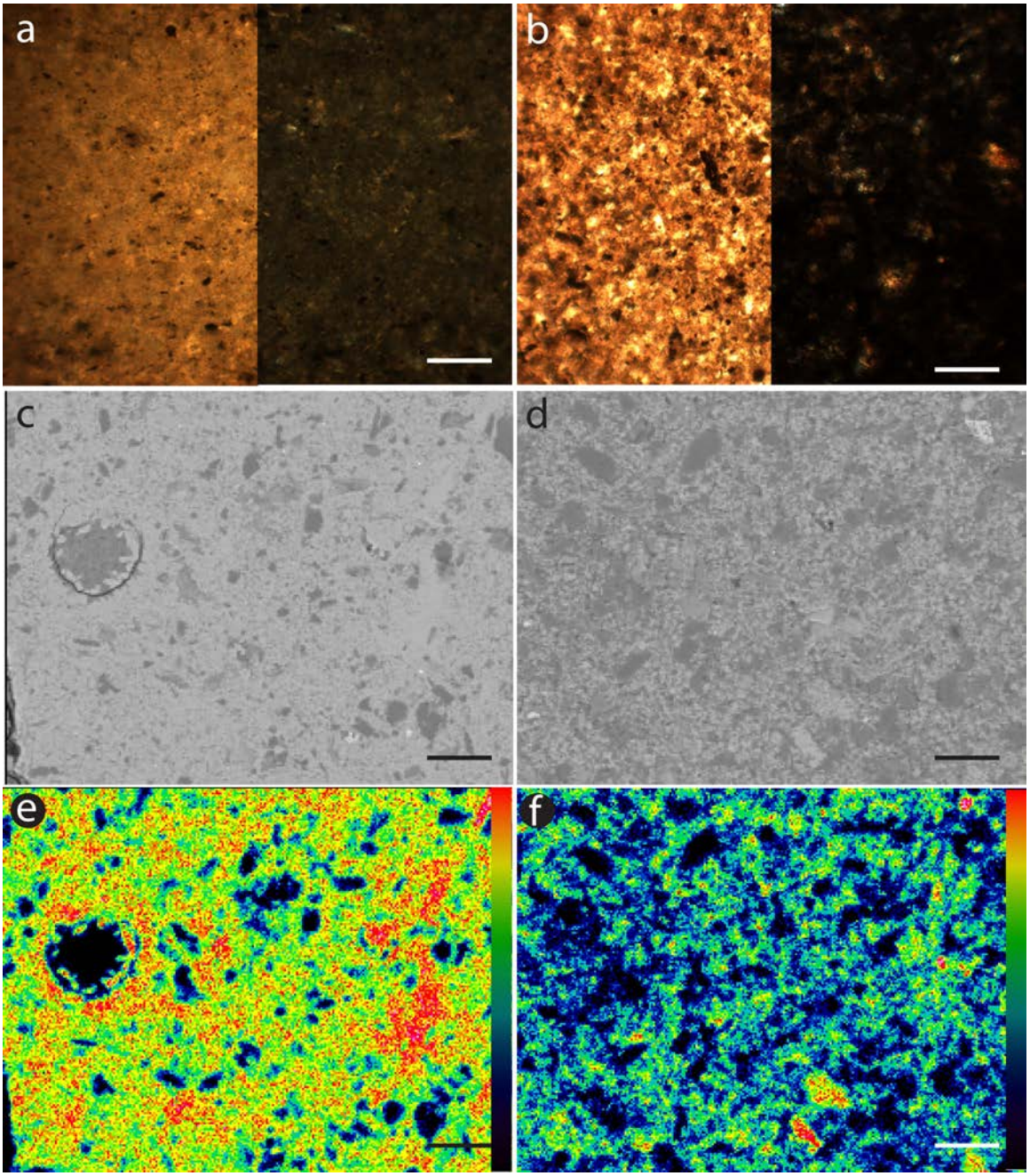


Figure 6.1: Textural and chemical differences between 'pure' phosphate and 'granular' phosphate from the Torridon Group. a) Optical photomicrograph illustrating pure phosphate texture. Plane polars left hand side, cross polars right hand side. Scale bar 200 μm. b) Optical photomicrograph illustrating granular phosphate texture. Plane polars left hand side, cross polars right hand side. Scale bar 200 μm. c) SEM-BSE image of pure phosphate texture. Scale bar 10 μm. d) SEM-BSE image of granular phosphate texture. Scale bar 10 μm. e) SEM-EDX phosphorus map of pure phosphate texture Scale bar 10 μm. f) SEM-EDX phosphorus map of granular phosphate texture. Scale bar 10 μm.

than crystalline origin. The two illustrated textures represent end members, between which there is a gradual transition of increasing detrital material to a more granular fabric.

Despite being able to resolve detrital grains contained within the phosphatic matrix, that matrix appears a more or less homogenous grey in BSE images, with no apparent distinction between different crystals (Figure 6.1c,d). Thus, it may be concluded that the phosphate crystals are too small to be easily resolved by SEM imaging alone.

Combining BSE images with *in-situ* energy dispersive x-ray spectroscopy (EDX) provides additional information on elemental abundances and distribution on a micron to sub-micron scale within a scanned section. Through the production of point spectra and two-dimensional maps, it is used to infer mineralogy observed in a BSE image (Figure 6.1e,f).

A number of salient observations were made using this technique. Firstly, that the extremely finely crystalline material interpreted as phosphate throughout is in fact composed of calcium and phosphorus, in broadly equal quantities, consistent with a apatitic mineralogy. It also allows characterization of the polymictic material present in granular textures, showing variously high concentrations of silicon and oxygen, suggesting quartz, and of potassium and aluminium enriched siliceous grains, suggesting feldspar. Throughout the phosphatic and shale material, fine tabular minerals are observed sporadically, that are enriched in iron, aluminium, silicon and oxygen with minor potassium, here interpreted as glauconitic clay group phyllosilicates. EDX maps are also useful in detecting spatially limited minerals such as pyrites, where they occur, as well as the common interfingering relationships between authigenic phosphates and glauconitic clays.

Despite the high concentrations of organic matter, both disseminated and as structured organic-walled microfossils, within the phosphate, detection of carbon is compromised in BSE and EDX imaging. The reasons for this are twofold. Firstly that the material must intersect the section surface to be detected by the SEM techniques, and much of the organic matter observed in optical microscopy is occluded within translucent phosphate. Secondly, during preparation for SEM imaging the sections are carbon-coated to prevent ionization, and this surficial carbon floods the signal,

meaning detection of small laterally inconsistent carbon blebs is unlikely.

Although unable to image the fossil material contained within the phosphate, combined BSE and EDX imaging of the phosphate and its associated minerals is a valuable semi-quantitative tool for mapping out variations in texture and mineralogy within phosphate occurrences, and between differing sedimentary environments.

6.2.4 Raman

Raman analysis was employed primarily for the imaging of carbonaceous fossil material (Chapter 3), but the identification of specific peaks within a spectrum can permit characterisation of particular bonding energies and thus of different mineral phases. Thus, in the matrix surrounding the images fossil structures, it was possible to identify the strong apatite peak at around 960 cm^{-1}. Mapping the intensity of this peak illustrates high concentrations of apatite in the matrix, but not in the fossil wall (Figure 6.2a). The resolution of this technique is limited, however, and although spatial maps of apatite intensity appear blotchy and heterogeneous, the changes are not sufficiently well defined to pick out other mineralogies.

Raman spectroscopy does have an advantage over EDX characterisation, in that carbon may be resolved alongside other Raman-active minerals. In this case, and as far as the resolution will permit, apatite can be seen fully surrounding carbonaceous structures, confirming the intimate association of surrounding matrix and preserved fossil.

6.2.5 FIB-TEM

In addition to elucidating the fine scale structure and preservation of fossil walls (Chapter 3) this high resolution imaging technique also permits the fine scale crystalline structure of the phosphate to be imaged.

In the thin-walled fossil coccoid that was sectioned and analysed, phosphate-rich crystalline material was encountered on both the inside and outside of the wall. It appears to comprise fine randomly oriented crystals of three different mineralogies, as indicated by varying amounts of electron attenuation. By combing the TEM images with EFTEM and EELS techniques for elemental detection, the three minerals were

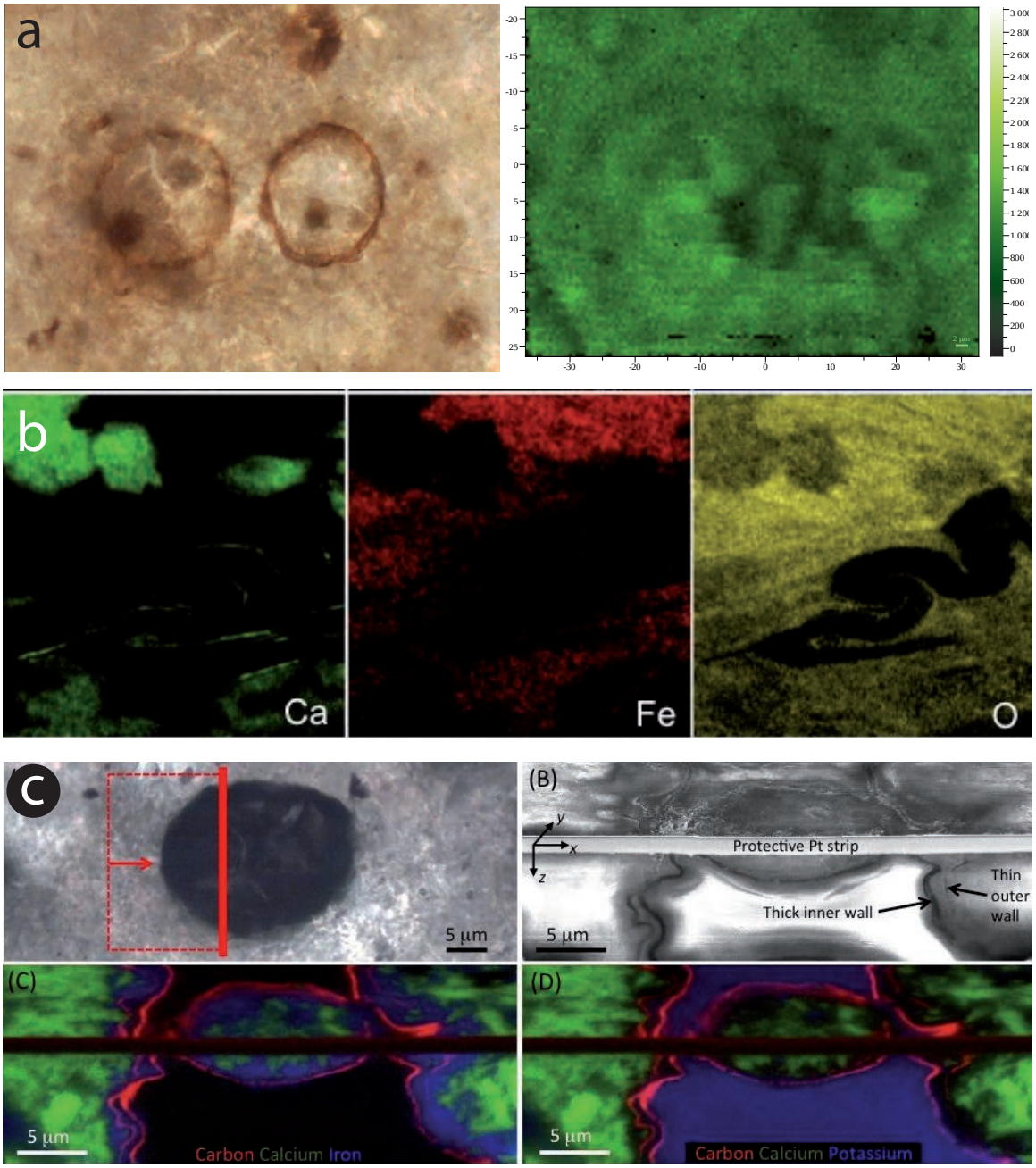


Figure 6.2: Application of high resolution techniques to studying phosphate in the Torridon Group. a) Laser Raman map of apatite peak intensity (right) for the phosphate surrounding thin-walled vesicles shown in the optical micrograph. Field of view approximately 45 μm. b) Elemental distribution maps from FIB-TEM imaging of a thin-walled vesicle. Shows alternations between calcium and iron-bearing minerals in the matrix. Field of view approximately 500 nm. c) FIB-SEM-EDX mapping, as illustrated previously in Chapter 3. Shows zonation of elemental concentrations around a large carbonaceous vesicle, with iron-bearing minerals closest to the wall, and potassic clays filling the lumen.

characterised as follows (Figure 6.2b).

The first, a blocky prismatic mineral that makes up around 60% of the crystallite, is rich in calcium, phosphorus and oxygen. It is interpreted as an apatite. Secondly, making up around 10% of the crystalline mass is a fibrous mineral composed of iron, phosphorus and oxygen, and interpreted as an iron phosphate such as heterosite. The remaining 30% of the crystallite is made up of more complex, heteromorphic crystals that are rich in iron, aluminium, silicon and oxygen, and thus are interpreted as an iron-rich glauconitic clay. The presence of apatite and glauconitic clay are consistent with the observations made by SEM-EDX, and the absence of iron phosphate in the SEM analyses may reflect the iron phosphate's limited distribution or low concentrations.

In the FIB-TEM images, all three mineral phases can be seen abutting the carbonaceous fossil wall, largely are random orientations but in some portions (e.g. top right of Figure 3.12) appear to be slightly layered sub-parallel to the wall structure. In general though, the complex intermeshed mineralogy suggests the fine crystalline texture within and outside the fossil cells is primary and not induced by secondary recrystallisation. Therefore, the composition of this crystallite should give some indication of the composition of the original, precipitating fluid.

6.2.6 FIB-SEM-EDX

During milling of a large fossil for examination of its wall structure by section-perpendicular SEM, it was also possible to combine elemental mapping techniques to provide high resolution *in-situ* analysis of the phosphate mineralogy surrounding the structure.

In the single case examined, the maps parallel and perpendicular to the section surface revealed a distinct zonation in elemental abundances in the matrix within and surrounding the fossil structure (Figure 6.2). The cell lumens contains a single potassium-rich phase, potentially a potassium-rich clay like illite. External to the cell wall, and also between the double walls of this fossil structure, is an iron-rich mineral, which irregularly grades to apatite, indicated in Figure 6.2 by a concentration of calcium. This apatite is heterogeneous, and is intergrown with the iron-rich mineral,

inferred here to be iron-rich glauconitic clay.

This distinct zonation around a large, double-walled fossil is considerably different to that observed by FIB-TEM to surround smaller, thin-walled spheroids. This may indicate a difference in fossilisation process between the larger and smaller microfossils, with the larger double walled spheroids consistently developing this zonation, perhaps in response to differing taphonomic processes. Alternatively, either the zoned preserving mineralogy, or the mixed crystallites seen in FIB-TEM analysis are typical of Torridon preservation, and the alternative preserving mode is a rare example not representative of the whole.

The application of these techniques in studying microfossil preservation is a relatively new undertaking, carried out in collaboration, and as yet the results are limited to these preliminary analyses. As such, it is not yet possible to readily distinguish between the alternative interpretations above, as more established imaging methods do not possess the resolution to make the distinction. This is therefore a topic for active future investigation with high-resolution techniques.

6.3 Variation of phosphate between environments

Phosphate occurs at several different localities within the Torridon Group, each representing a distinct lithofacies and palaeoenvironment. As these phosphates have been shown to contain different assemblages of microorganisms (Chapter 4), it may be expected that the palaeoenvironmental variation may also result in differences in the habit of phosphate and its associated minerals.

SEM-EDX analysis has been shown to be a quick and relatively informative tool for imaging and semi-quantitatively analyzing mineralogy in thin section. Therefore, it is used here in combination with optical microscopy and sedimentological observations, to deduce petrological differences between those phosphate-bearing lithofacies of the Torridon Group.

6.3.1 Lower Diabaig

Phosphate at the type locality of the Diabaig Formation occurs in abundance in certain parts of the exposure of this desiccating shoreline lithofacies, forming laterally extensive dark waxy lenses and bands up to around 1 cm thick (Figure 6.3a). They are interbedded with the grey planar laminated shales and fine sandstones with little disruption, and occasionally found overlying beds containing tabular mud-rip up clasts, indicating phosphate formation directly following a period of flooding. One isolated example was found as float, where black waxy lenses of phosphate form levees 1 cm wide and around 5 mm thick, either side of a large sand-filled desiccation crack.

All examples of phosphate in this lithofacies were found as primary textures that have not been reworked. It is possible, therefore, to visualize the nature of the transition from non-phosphatic siltstones to richly phosphatic bands, within the space of a thin section (Figure 6.3b). This transition, clearly seen repeated at the base of a phosphate band, as well as within the bands themselves, comprises a dark carbon-rich band at the top, with pure gelatinous phosphate, often containing microfossils beneath, passing gradually into granular phosphate which becomes more clastic-rich downsection (Figure 6.3c,e,f). The laminar repetition of these textures is easily recognized in transverse section, but in sections taken parallel or sub-parallel to bedding, undulations in the laminae result in a patchy distribution of the 'pure' and 'granular' phosphate textures.

In addition to the general repetition of phosphatic mineralogies seen in transverse section, a rarely occurring spherulitic texture was also observed, at the transition between carbon-rich and carbon-poor parts of a nodule (Figure 6.3d,g,h). These spherules are typically around 300 μm across, and comprise radiating blade-shaped crystals of a mineral rich in iron, aluminium, silicon and oxygen, interpreted as iron-rich glauconitic clay. When observed though transmitted light, they seem to be surrounded by a thin halo up to 50 μm thick of diffuse carbon. It is possible that these spherules precipitated inside degrading megaspheric fossils, such as those described as *Valeria* sp. Alternatively, the halo of carbonaceous material may be a product of crystallization exclusion, as these minerals precipitated from a central point source.

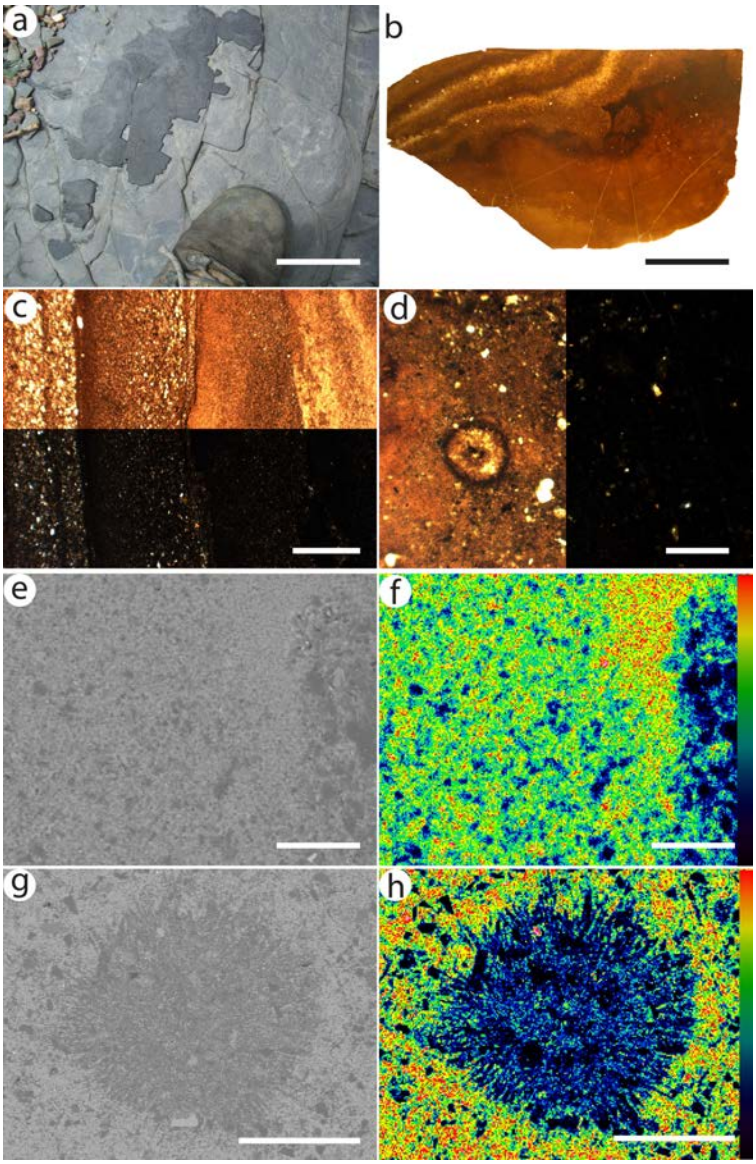


Figure 6.3: Phosphate sedimentology, petrology and mineralogy at Lower Diabaig. a) Sedimentological setting for phosphate. Phosphatic lenses and bands occur for some distance along bedding planes. Scale bar 10 cm. b) Thin section texture, illustrating lateral alternations between different phosphate textures and sand content. Scale bar 5 mm. c) Optical photomicrograph of *in-situ* alternations of phosphate textures grading downwards form a carbonaceous layer, through pure to granular phosphate. Plane polars top, cross polars bottom. Scale bar 1 mm. d) Optical photomicrograph of spherulitic texture at boundary between pure and granular phosphate. Plane polars left hand side, cross polars right hand side. Scale bar 500 μm. e) SEM-BSE image of homogenous pure phosphate texture. Scale bar 10 μm. f) SEM-EDX phosphorus map of field of view in (e). Scale bar 10 μm. g) SEM-BSE image of blade-like crystals in spherulitic structure. Scale bar 100 μm. h) SEM-EDX phosphorus map of field of view in (g). Scale bar 100 μm. Sample DIA-13d from Lower Diabaig, Diabaig Formation.

6.3.2 North Shieldaig (Fish Farm)

At the northern edge of Shieldaig bay, the lithofacies comprises coarse and medium grained sands and silts that were deposited in an energetic delta top setting. The phosphates occur in discontinuous uneven layers and lenses typically less than 1 cm thick (Figure 6.4a). They have a sandy texture, and are found within undulose-bedded fine sands of somewhat lower water energies (Figure 6.4b).

Microscopically the phosphates here are relatively pure and gelatinous, with only scattered microfossils and wispy laminae picked out by sparse biotites (Figure 6.4c,e). Within the surrounding sandy sediments, dark carbonaceous laminae are relatively thick and embedded with coarse sand clasts larger than the surrounding matrix, sometimes associated with thin bands of iron-rich glauconitic clay that are themselves rich in carbon (Figure 6.4d,f). It is likely that these carbon-rich bands represent the condensed remnants of EPS-bound microbial mats, in which large grains could episodically become embedded.

6.3.3 Shieldaig Peninsula

Small amounts of phosphate were found among this red sandy lithofacies, which represents deposition in a mid-delta setting. Sparse, laterally discontinuous lenses appear dark and sandy, and are found interbedded with medium-grained sandstones, apparently not reworked.

Sufficient phosphate was extracted for only one thin section from this locality, and optical microscopy revealed it to be dark and carbon rich, with a granular texture rich in siliceous grains of varying sizes (Figure 6.5a,b). No structured microfossils were identifiable. SEM-EDX mapping revealed a broad mottling within the granular texture, consisting of a general apatitic mineralogy with rounded to subrounded patches of potassium rich clay around 1 μm across, with gradual outer margins (Figure 6.5c,d). These patches may represent episodic sections through an underlying undulating clay lamina, but their consistent size across the section surface indicated that they are perhaps a primary feature broadly comparable to the spherulitic texture seen at Lower Diabaig, but lacking the blade-like crystallinity. The high degree of carbon dissemination within the matrix suggests that any organic membrane that originally surrounded the clay-rich zone will have decayed away, and given that the

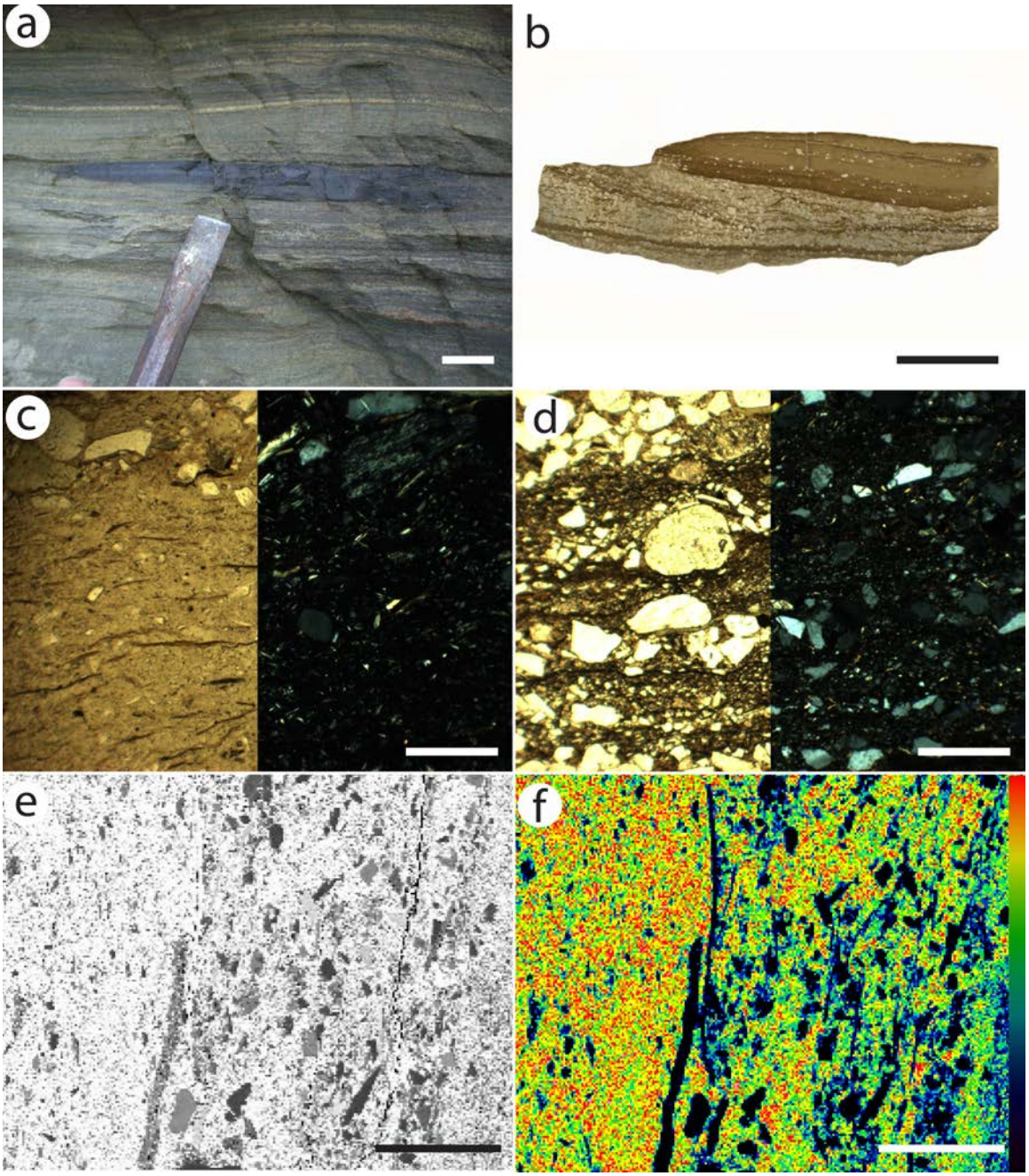


Figure 6.4: Phosphate sedimentology, petrology and mineralogy at North Sheildaig. a) Sedimentological setting for phosphate. Phosphate occurs as thick irregular sandy bands. Scale bar 2 cm. b) Thin section texture, illustrating laminar fabric within phosphate, and a sharp boundary with sandstone. Scale bar 5 mm. c) Optical photomicrograph of gelatinous phosphate rich in mica. Plane polars left hand side, cross polars right hand side. Scale bar 100 μm. d) Optical photomicrograph of carbonaceous layers in the matrix with larger grains embedded. Plane polars left hand side, cross polars right hand side. Scale bar 100 μm. e) SEM-BSE image of pure phosphate texture. Scale bar 10 μm. f) SEM-EDX phosphorus map of field of view in (e). Scale bar 10 μm. Sample FFA1-0.45a from North Sheildaig.

margins are gradual, this may have occurred prior to completion of the precipitation process.

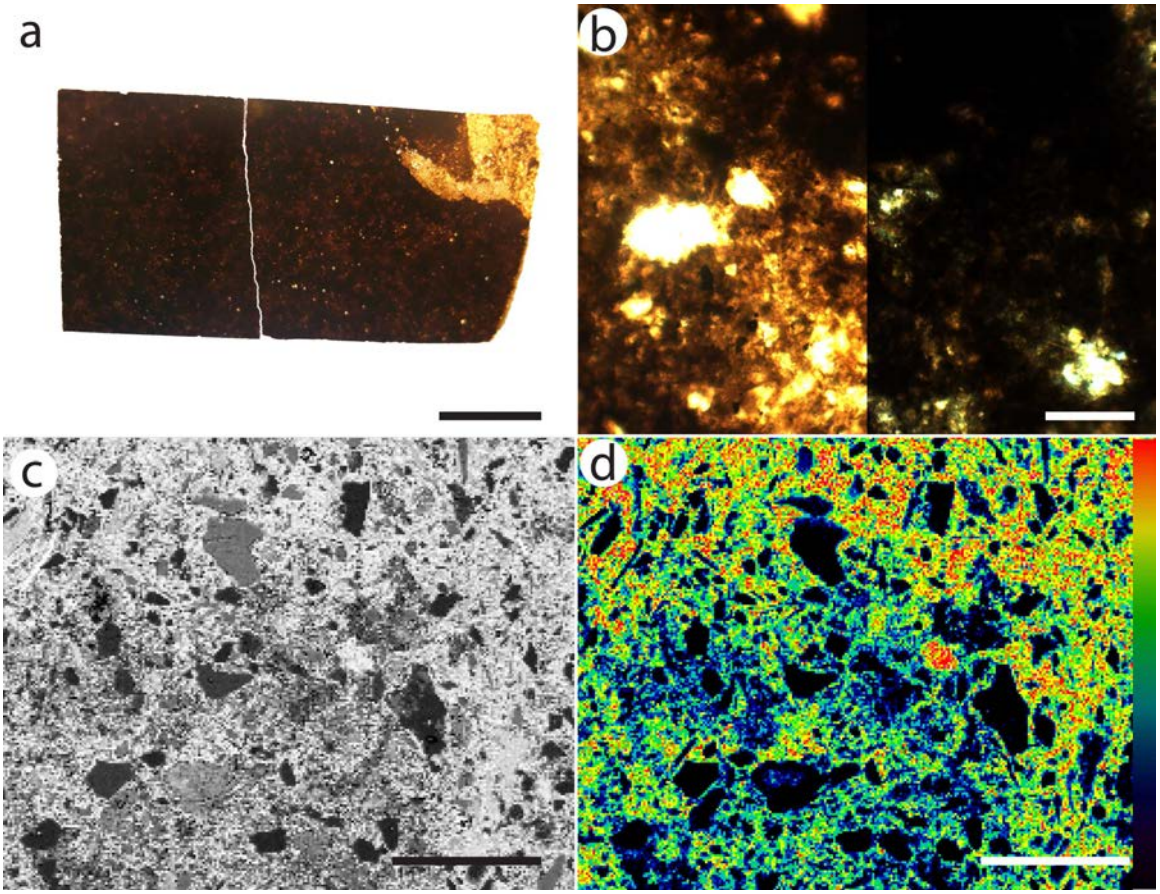


Figure 6.5: Phosphate sedimentology, petrology and mineralogy at Sheildaig Peninsula. a) Thin section texture, illustrating dark sandy material with localised blotches. Scale bar 5 mm. b) Optical photomicrograph of very carbon-rich granular phosphate that makes up the bulk of the material. Plane polars left hand side, cross polars right hand side. Scale bar 1 mm. c) SEM-BSE image of homogenous granular and clastic-rich phosphate texture. Scale bar 10 μm. d) SEM-EDX phosphorus map of field of view in (c). Scale bar 10 μm.

6.3.4 Fladday

Phosphate is relatively abundant in the grey shaly portions of this lithofacies, which was deposited in a quiescent prodelta setting. It appears dark and waxy, and is seen in section as laterally continuous bands less than 5 mm thick, and more constricted lenses that attain a greater thickness of up to 15 mm. In places, lenses and bands

protrude from the surrounding planar laminated shales, having a somewhat metallic lustre, and occasionally bands are bounded by fine-scale pinch and swell structures of seemingly different mineralogy (Figure 6.6a).

Optical microscopy reveals a variety of phosphatic textures, ranging from very clastic-rich granular forms, to purer and more gelatinous textures that are typically mottled with a greenish mineral, and closely associated with darker carbonaceous or iron-rich material (Figure 6.6b,c). Higher resolution SEM analyses show that the granular fabric is made up of abundant but individual rounded crystallites of phosphate around 2.4 μm across distributed evenly throughout a siltstone matrix (Figure 6.6e,f). The apparently purer portions comprise more massive phosphate textures interfingered with irregular zones of iron-rich glauconitic clay with locally concentrated iron oxides. Thus, the major locus of phosphate precipitation and authigenic mineral growth seems to be associated with these iron- and carbon-rich zones, with characteristically dispersed phosphates elsewhere.

One exception to this rule at this locality is within the bands bounded by fine pinch and swell textures (Figure 6.6d). Microscopically, these show a curious symmetry, consisting of a thin central quartzose band around 5 μm thick, bounded either side by phosphates of a granular texture which then grades outwards, showing an increase in aluminosilicates, micas and calcium, followed by a relatively rapid increase in silicon and glauconitic clay, to the boundary of the pinching and swelling nodular structures (Figure 6.6g,h). These nodular features comprise an outer zone of banded silica and iron-rich glauconitic clay, enclosing an inner massive zone of interfingered iron-rich clay and silica, containing increasing concentrations of calcium inwards, and occasionally large euhedral crystals of pyrite. This mineralogy and texture is unique to the phosphate bands seen at Fladday, and its precise mode of formation is unknown. It is typical, however, that such nodular formations in sedimentary rocks are often formed in local microenvironments where some trigger causes elevated ionic concentrations (e.g. Prager & Ginsburg 1989). Such local conditions may be brought about by the metabolic actions of specific microorganisms that may be found in a layered microbial mat, with pyrite being formed by the action of iron-reducing or sulphur-reducing bacteria, for example. A microbial interpretation for this unique mineralogy is consistent with the findings of microfossils within the phosphate, and with the overall mode of formation assumed for phosphates across the Torridon Group (see below).

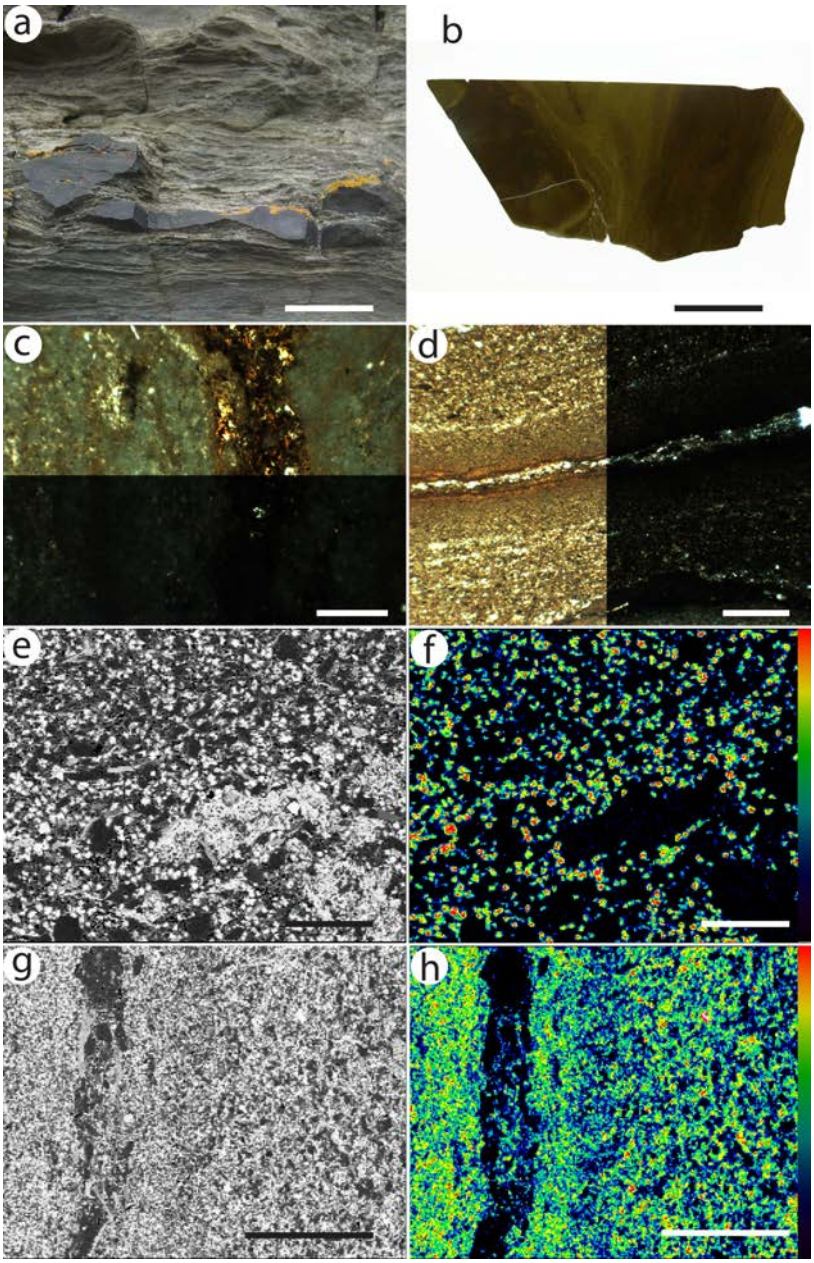


Figure 6.6: Phosphate sedimentology, petrology and mineralogy at Fladday. a) Sedimentological setting for phosphate. Phosphatic lenses and bands occur for some distance parallel to bedding planes. Scale bar 2 cm. b) Thin section texture, illustrating lateral alternations between different textures and mineralogies. Scale bar 5 mm. c) Optical photomicrograph of phosphatic material heavily intergrown with green clay mineral in the vicinity of pyritic layers. Plane polars top, cross polars bottom. Scale bar 50 μm. d) Optical photomicrograph of symmetrically zoned phosphate within nodule-bounded lens. Plane polars left hand side, cross polars right hand side. Scale bar 200 μm. e) SEM-BSE image of small phosphatic crystallites spread evenly throughout the martix. Scale bar 20 μm. f) SEM-EDX phosphorus map of field of view in (e). Scale bar 20 μm. g) SEM-BSE image of dense granular phosphate in zoned region. Scale bar 20 μm. h) SEM-EDX phosphorus map of field of view in (g). Scale bar 20 μm.

6.3.5 Brochel Castle

The lithofacies at this locality comprises several coarsening upward packages of siltstones and sandstones, representing variable water energy conditions as the depositional setting passes from distal prodelta through to energetic delta top. Phosphates here are found within fine sandstones of the mid-delta, supplied with symmetrical wave ripples and occasional unidirectional currents. They occur as fine undulating laminae within decimetre-scale sandy beds, and as large rip-up clasts, up to 15 mm thick, concentrated at the bases of more massive unlaminated sandy beds (Figure 6.7a,b). These occurrences suggest formation of phosphate during hiatuses and quiescent times, occasionally with subsequent energetic reworking. Phosphate is also occasionally found draping the sinusoidal surfaces of waver ripples.

Microscopic texture of the phosphate is broadly bimodal: carbon-rich granular phosphate makes up the laminated material within sandy beds and on the surfaces of ripples, as well as some rip-up clasts; purer, carbon-poor gelatinous phosphate is found within rip up clasts, commonly with a thin, carbon-rich edge to the rounded clasts (Figure 6.7c). It would appear, therefore, that relatively immature phosphate deposits, which develop thin layers that are subsequently covered by sandy sediment, are rich in carbon and heavily diluted by clastic material. The rip-up clasts appear to come from thicker bands, presumably from deposits that had developed over a longer period of time, and these have a different texture, containing much less carbon and siliciclastic material (Figure 6.7d-f). A hint of the close association of carbonaceous layers with the purer phosphate, seen *in-situ* at Lower Diabaig, is seen in the thin layers of carbon occasionally seen at the edges of the rounded rip-up clasts. In one exceptional case, tangled fossil sheahs can be seen colonising the darker upper boundary of the purer phosphatic material (Figure 6.7d), providing strong evidence fot the microbial mat origin of these upper carbonaceous layers.

6.3.6 Badachro

Within the planar laminated grey shales of this distal quiescent setting, phosphate is found in bands up to 20 mm thick, appearing darker than the surrounding shale, or weathering white (Figure 6.8a), and forming resistant bands that protrude from the surrounding shale. Faint laminations are evident within the phosphates, continuous with the shaly lamination, which is suggestive of similar rates of phosphate formation

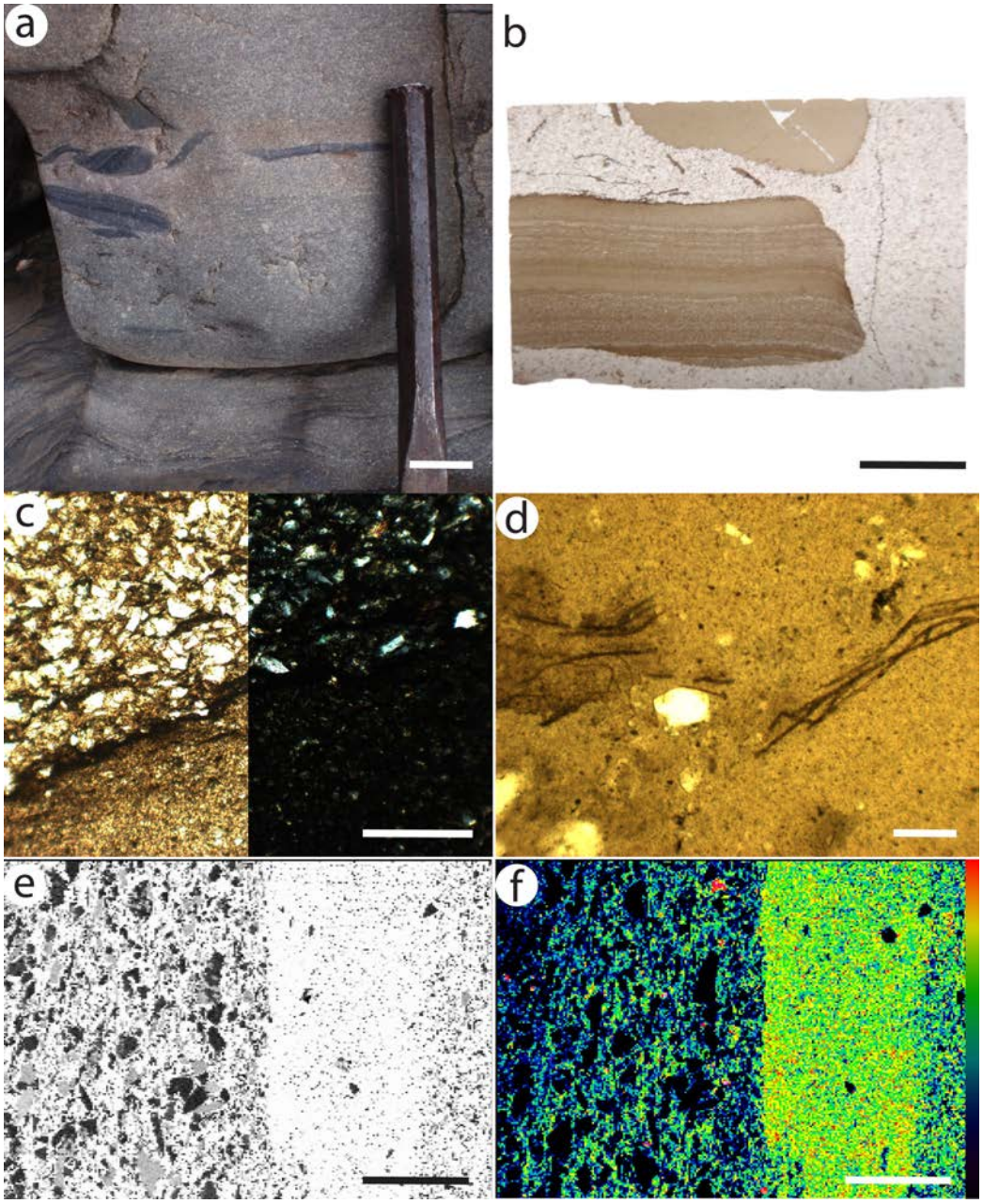


Figure 6.7: Phosphate sedimentology, petrology and mineralogy Brochel Castle. a) Sedimentological setting for phosphate. Layered phosphatic rip-up clasts occur with phosphate-carbonaceous layers near the bases of massive sandstone beds. Scale bar 2 cm. b) Thin section texture, illustrating lateral alternations between different textures and mineralogies. Scale bar 5 mm. c) Optical photomicrograph of dark carbonaceous material at edges of clasts. Plane polars left, cross polars right. Scale bar 500 μm. d) Optical photomicrograph of interwoven filamentous microfossils forming a carbonaceous band. Scale bar 50 μm. e) SEM-BSE image of alternation between phosphate textures within a clast. Scale bar 20 μm. f) SEM-EDX phosphorus map of field of view in (e). Scale bar 20 μm.

and sediment deposition at this locality (Figure 6.8b).

Microscopically, the phosphates here comprise a uniform granular texture rich in siliciclastic material and also rich in disseminated carbon as well as structural microfossils (Figure 6.8c-f). Fine laminations are picked out by variations in the amount and size of clastic material, and some carbon-rich layers also occur, appearing dark and opaque. In contrast to the granular texture seen at Fladday, here the matrix phosphate is fine and massive, forming a continuous interstitial texture. Some iron-rich glauconitic clay is concentrated in clastic bands where phosphate concentrations are low, suggesting a cyclic alternation between phosphate and glauconitic clay formation, continually diluted by fine-grained sediment rain.

6.3.7 Cailleach Head

Within the repetitive cyclothems of the Cailleach Head Formation at Cailleach Head, which represents periodic basin infills by prograding deltas, phosphate occurs in various habits. It is seen as black waxy layers of variable thickness forming undulating laminae on the surfaces of thin centimetre- to decimetre-bedded fine sandstone beds, and weathering bluish-white as drapes in the troughs of weathered wave ripples (Figure 6.9a,b). It is also found abundantly at the bases of larger, more massive sandy beds as rounded rip-up clasts of varying dimensions, reaching a maximum thickness of around 10 mm (Figure 6.9c). The surrounding mineralogy is predominantly sandy and quartzose, but is broadly associated with iron-rich patches and well-formed cockscombs of marcasite.

Rip-up clasts, which are densely packed at the base of phosphate beds and therefore can be easily sampled by thin section, show a full range of phosphate textures and associated mineralogies (Figure 6.9). Some clasts are formed of pure, gelatinous phosphate with varying amounts of quartzose clastic material within (Figure 6.9d,f,g). Clasts that appear granular typically have higher concentrations of clastic and carbonaceous material, but the phosphate is also associated with high concentrations of potassium-rich clay. Further clasts that appear dark and spongy through transmitted light are composed almost entirely of clay minerals and carbonaceous material, with almost no phosphate within them. As these varied mineralogies and textures are found solely as rip-up clasts, it is not possible to decode their original sedimentological ordering. It is clear, however, that both the phosphatic and clay-rich mineralogies formed contiguous plastic cements on or within the sediment that allowed them to

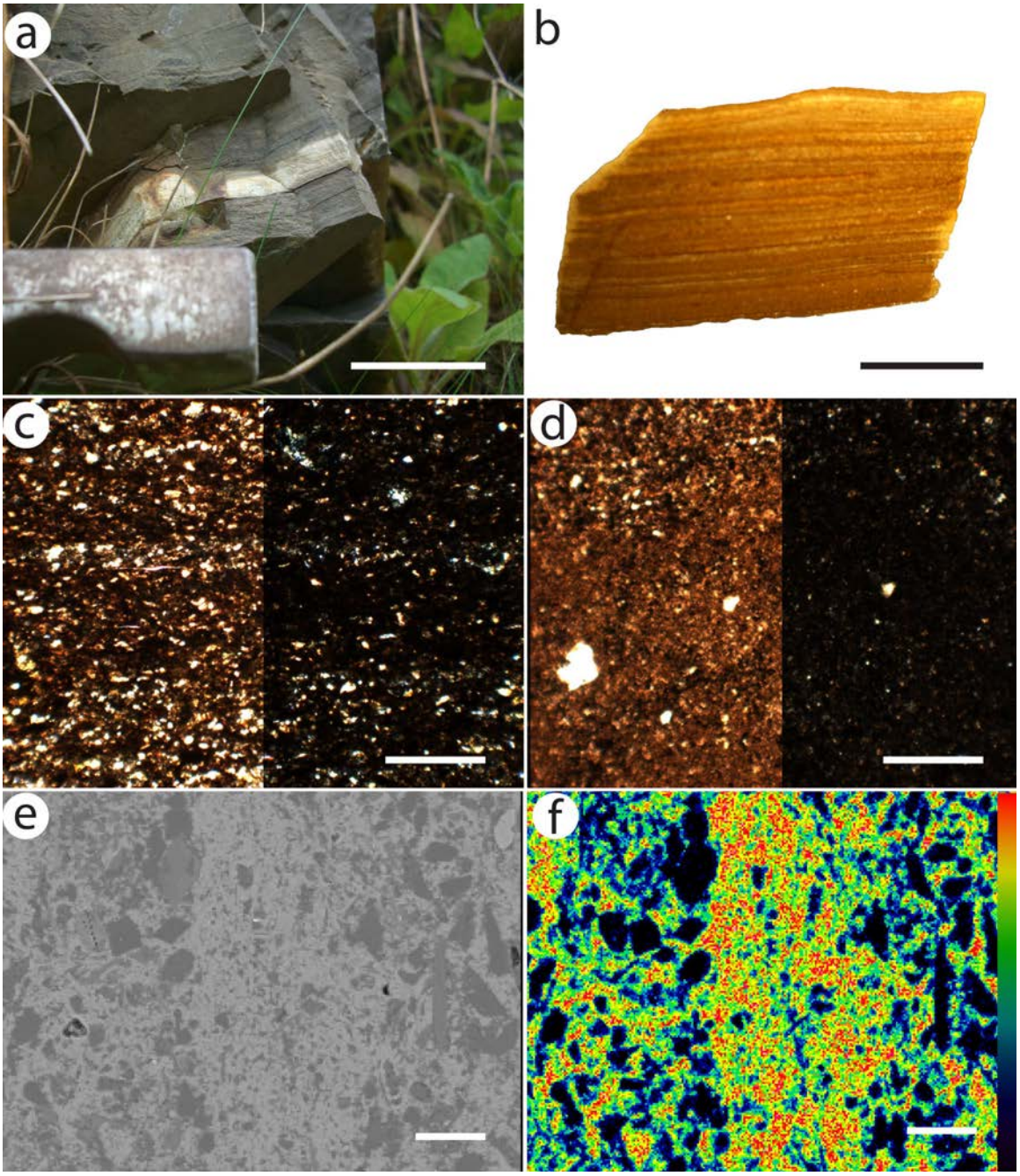


Figure 6.8: Phosphate sedimentology, petrology and mineralogy at Badachro. a) Sedimentological setting for phosphate. White-weathering phosphate is interbedded with shaly layers. Scale bar 2 cm. b) Thin section texture, illustrating fine scale laminar alternations between phosphate textures. Scale bar 5 mm. c) Optical photomicrograph of dark carbonaceous laminar granular phosphate. Plane polars left, cross polars right. Scale bar 500 μm. d) Optical photomicrograph of dark carbonaceous granular phosphate parallel to bedding. Plane polars left, cross polars right. Scale bar 50 μm. e) SEM-BSE image of layers in phosphate concentration. Scale bar 10 μm. f) SEM-EDX phosphorus map of field of view in (e). Scale bar 10 μm.

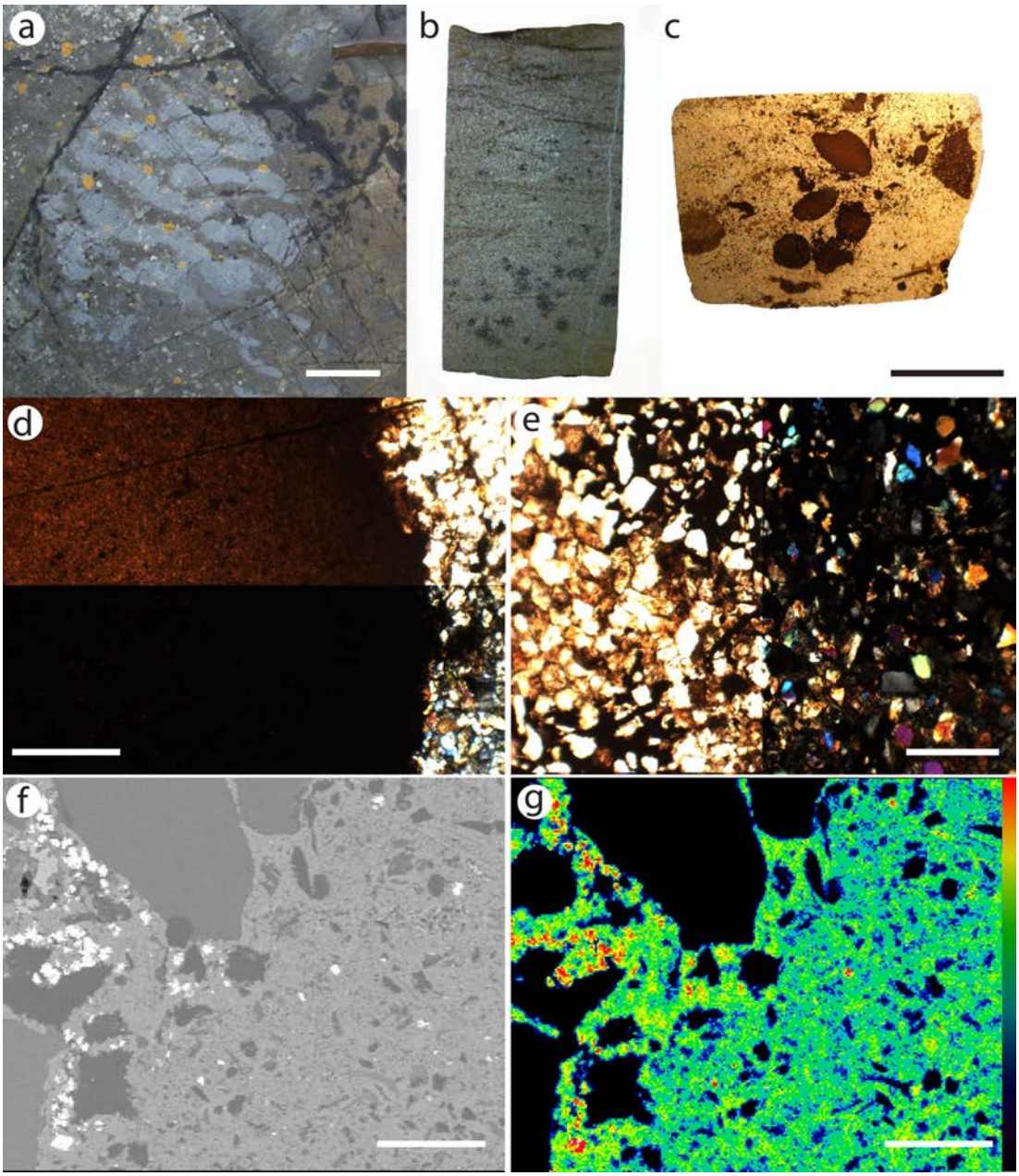


Figure 6.9: Phosphate sedimentology, petrology and mineralogy at Cailleach Head. a) Sedimentological setting for phosphate. White-weathering phosphate is found in the troughs of symmetrical wave ripples. b) Thin section texture, illustrating laminar and 'leopard-spot' textures beneath surficial thin phosphate layer. Scale bar 5 mm. c) Thin section texture, illustrating small, densely distributed rip-up clasts. Scale bar 5 mm. d) Optical photomicrograph of dark zonation towards the edge of phosphate clasts. Plane polars top, cross polars bottom. Scale bar 500 μm. e) Optical photomicrograph of interstitial iron oxide making up 'leopard-spot' texture. Plane polars left, cross polars right. Scale bar 500 μm. f) SEM-BSE image of invaginated edge of phosphate grain. Scale bar 10 μm. g) SEM-EDX phosphorus map of field of view in (f). Scale bar 10 μm.

be subsequently reworked into the rounded clasts seen here.

Fossils are only found preserved in the purer phosphatic textures, and although SEM-EDX analysis does not permit resolution of carbonaceous structures, some fossil-like morphologies are apparent, picked out by potassium-rich clays. These clays form sharp-bounded circular structures that show size, morphology and fragmentation consistent with some large dark-walled organic microfossils from this assemblage. Such an observation is consistent with observations made by FIB-SEM-EDX, that large microfossils are associated with a zonation of clay mineralogies, but the scarcity of these structures precludes further interpretation.

Sections taken through the *in-situ* phosphate bands in the troughs of wave ripples illustrates the gradual transition from clastic material to granular, carbon-rich phosphate, within around 2 mm of sediment (Figure 6.9b). The phosphate penetrates into interstitial spaces of the sandstone and, following a relatively sharp termination of clastic grains, becomes a faintly laminated continuous phosphate band. This phosphate is intimately associated with widely distributed patches of interstitial iron oxide material, which confer a 'leopard-spot' appearance to the sandstone beneath the phosphate layer (Figure 6.9e). These iron oxides may be derived from marcasitic material, and their presence alongside the *in-situ* phosphate is important for interpreting modes of formation (see below).

The above description of phosphate occurrences and microstructure from various lithofacies of the Diabaig and Cailleach Head Formations has highlighted general similarities and localized differences between phosphate mineralogy. The microtexture of pure and granular phosphatic material is relatively constant, and palaeoenvironment seems to control the dominance of either habit. Broadly, it seems rapid development of immature phosphates results in a granular form rich in clastic particles, carbonaceous material, and, commonly, clays. Thicker, more mature deposits comprise purer phosphate with little disseminated organic matter, or associated clay, and are often overlain by a well-defined carbonaceous band of likely microbial mat origin.

6.4 Potential sources, sinks, and modes of formation

Most models for large-scale formation of sedimentary phosphate in modern settings involve the concentration of PO_4^{2-} in upwelling areas by the mass appearance and subsequent death of metazoans (e.g. Föllmi 1996). In the absence of metazoans in the Precambrian, this mechanism cannot operate, and thus largely non-uniformitarian abiogenic or microbially assisted mechanisms must be invoked to explain the presence of phosphate (Föllmi 1996). Within a lake system, understanding is further complicated, as processes of phosphatisation are understood to operate largely in marine settings (Föllmi 1996, Glenn et al. 1994, Krajewski et al. 1994). Thus, the presence of phosphate deposits throughout the sedimentary rocks of the Torridon Group is enigmatic and requires special consideration of sedimentological and mineralogical associations in order to decode its source and mode of formation.

Large-scale Proterozoic phosphate deposits have been reported worldwide, many dating to the Precambrian-Cambrian boundary (Cook & Shergold 1986), although recently Papineau (2010) has identified two major Proterozoic phosphogenic events around 2 Ga and 1 Ga ago. Although the timing of the Torridon deposition is broadly correlated with the 1 Ga phosphogenic event, its lacustrinality and limited size suggests that the phosphate here may derive from non-cosmopolitan processes, only tangentially related to the marine event at this time. Thus, the Torridon is here considered an isolated case, with modes of concentration and precipitation derived directly from local sedimentological and mineralogical data.

6.4.1 Sources

Similar to the supply to marine basins, the primary flux of phosphate to non-marine waters on long timescales is through continental weathering, which delivers dissolved and particulate phosphate via riverine fluxes (Föllmi 1996). Within the Torridon, the direct proximity to the ancient Lewisian landmass and its strong underlying landscape unconformity suggest that this was the primary source of phosphate to the lake basin. The observed textural and chemical immaturity of the basal rocks of the Torridon however, in combination with the limited development of weathering profiles within the Lewisian, suggest that chemical weathering of this nearby continent was not extensive. This may go some way to explaining the overall low concentrations of

phosphate within these basins.

Short-term fluxes may be ultimately responsible for the episodic occurrences of phosphate throughout the Torridon basin, and are likely to derive from liberation of organic and inorganic dissolved and particulate phosphate from shallow unlithified sediments. This phenomenon has been documented in some Phanerozoic sedimentary columns, driven by either mechanical reworking of sedimentary layers, or by redox-driven desorption of phosphate from iron oxides, known as the 'iron pump and shuttle' (Shaffer 1986). In Phanerozoic sediments, the iron pump and shuttle plays a small part in phosphate concentration, owing to the general immobility of the redox boundary within sediments because of higher oxygenation of water columns and bioturbated pore waters. In the Proterozoic, however, waters are more susceptible to anoxia, as ambient oxygen levels are lower. In lacustrine environments in particular, seasonal stagnation and microbial action can easily result in anoxia or euxinia of bottom waters, causing the redox boundary to move up through the sediment, if not into the water column itself. Iron pump and shuttle is therefore considered a viable mechanism of liberating phosphate to the sediment and water on a regular basis, and the abundance of iron oxides and iron-bearing minerals in the Torridon rocks are an indication that it may play a major role.

6.4.2 Sinks

Within the Proterozoic, the only permanent sink for phosphate of any volumetric significance is within authigenic precipitates, and this is similarly the case within the Torridon. It is possible that some small amount of phosphate is retained in organic fossils, which sequestered it for structural and metabolic molecules during life. These molecules are very labile, however, and the overall high degree of carbon dissemination seen within shales and phosphate nodules suggests intense degradation and recycling of available nutrients.

The occurrence of phosphatic deposits in the Torridon rocks does not appear to be cyclic, nor is confined to one particular lithofacies. Within a single deposit, lenses and bands are often not laterally extensive. These observations suggest that phosphogenesis in these rocks is driven more by varying local microenvironmental conditions than by regional changes in fluxes of phosphatic material.

6.4.3 Mode of Formation

The following proposed synthesis of phosphogenesis within the Torridon lakes is derived from observations of phosphatic microtexture and associated minerals described above.

Phosphate is delivered in dissolved ionic and particulate form via rivers to the lake basins. It is supposed that riverine particulate flux is low, as little detrital phosphate is found among the siliciclastics of the Diabaig or Cailleach Head Formations. The dissolved ionic phosphate will then be taken up by the resident microbiota for utilization in structural components and metabolic processes, where it will remain sequestered as organic phosphate until death of the organism. These microorganisms are both planktonic and benthic, the latter forming microbial mats which may sequester more phosphate within EPS. Some dissolved organic phosphate will become adsorbed onto the surfaces of iron oxides and hydroxides also delivered to the lakes by riverine flux.

In time, the planktonic organic phosphate-bearing biomass will die, settle and be deposited, joining a life and death assemblage of benthic organisms in a flocculent seston layer at the sediment surface, where it will begin to decay. Degradation of the labile organic matter will release phosphate into this seston layer, where it is available for uptake by other organisms, but is temporarily concentrated at the decay site. Aerobic degradation of the organic matter will also use up locally available oxygen and may bring about anoxia of these bottom waters, which are already susceptible because of low atmospheric and aquatic oxygenation. Seasonal stagnation of lake waters may also contribute to this bottom water anoxia.

Anoxia at the sediment water interface and in the water column will cause the redox boundary to move upwards through the sediment, promoting the desorption of dissolved phosphate from the iron oxides, and its liberation into pore waters beneath the sediment-water interface and within the seston layer. The combination of dissolved phosphate contributed by degradation of organic material, the concentration within benthic EPS, and from the redox-driven iron pump causes local supersaturation with respect to phosphate. In the absence of carbonate anions in this freshwater environment, calcium is free to combine with phosphate ions and initiate the slow precipitation of cryptocrystalline apatite within the seston layer. Small-scale concentrations of other ions, such as iron or potassium, may occur as a result of specific

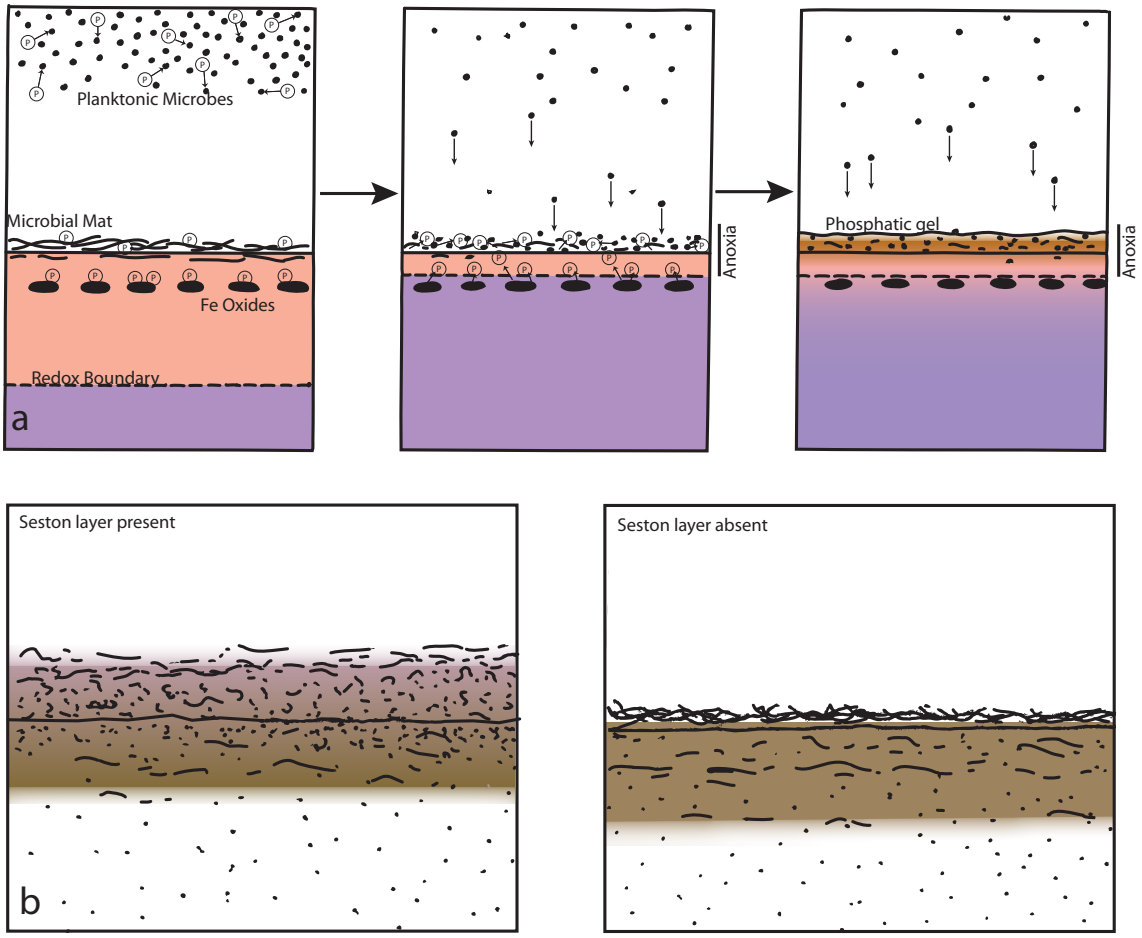


Figure 6.10: Proposed mode of formation of phosphate in the Torridon Group. a) Mechanism of concentration and precipitation of phosphate. Phosphate ions from riverine or reworking flux are taken up by biomass in the water column and on the sediment surface, causing microbial blooms. Phosphate is also adsorbed on the surfaces of iron oxides in oxidising conditions (left panel). Upon death of the microbial bloom, organisms sink to the sediment surface where they are decayed oxygenically, ultimately causing anoxia in these bottom waters. Degradation releases phosphate from the organic matter, and reducing conditions bring about desorption of phosphate from iron oxides (centre planel). The phosphate is thus concentrated in a thin layer above and below the sediment-water interface, where supersaturation will lead to precipitation of cryptocrystalline apatite, containing the organic and clastic matter present in this zone (right panel). b) Differences in sediment-water interface environment, resulting in differing phosphate textures. When a seston layer is present, a larger area above the sediment surface is supersaturated with respect to phosphate, resulting in 'pure' textures that grade downwards into more granular, clastic rich phosphate. Without a seston layer, phosphate forms primarily beneath the sediment surface, resulting in granular textures rich in disseminated carbon.

microbial metabolisms occurring in a structured microbial mat, and can result in co-eval growth of authigenic minerals such as iron-rich glauconite or potassic clays. These specific microenvironments occur particularly around organic microfossils because of their complex biochemistry, and may contribute to their exceptional preservation.

The combination of organic and redox-iron derived phosphate provides an opportunity for relatively rapid precipitation of authigenic apatite under supersaturation conditions. This permits the rapid occlusion of organic matter from the flocculent seston layer, allowing preservation of a consortia of microorganisms, both living and dead, in a range of degradational states. Supply of phosphate from the iron pump means that decay of phosphate-bearing organic matter need not be complete to allow precipitation, thereby allowing preservation of many pristine, undecayed forms.

The *in-situ* arrangement of phosphatic microtextures seen at Lower Diabaig and, less well-preserved, elsewhere, supports this hypothesis for phosphogenesis. The coherent carbonaceous layer containing interwoven sheaths represents a diaphanous, EPS-bound microbial mat draping the surface of the seston layer. Beneath, carbon-poor, gelatinous cryptocrystalline phosphate with minor authigenic clays preserve a full taphonomic spectrum within organic-walled microfossils, which contains the ancient sediment-water interfaces as a gradational increase in fine clastic particles. Phosphate concentrations remain high even below the interface, as interstitial spaces are filled with authigenic apatite and clays, but are more carbon-rich as they incorporate more degraded, buried organic matter from previous generations. Alternations of this typical package occur with subsequent sedimentation, microbial colonization and authigenic growth over previous semi-lithified units.

The above-described transect illustrates phosphate formation in a zone with a well-developed seston layer, therefore allowing development of adjacent gelatinous and granular phosphate textures. In less maturely developed systems however, perhaps where benthic communities dominate or currents sweep the sediment floor free from a seston layer, the same phosphate liberation occurs but takes place below the benthic mat layer and therefore slightly below the sediment water interface. As a result, in these localities granular phosphate dominates, representing interstitial pore growth of apatite, trapping siliciclastic particles and decayed organic matter within the phosphatic matrix.

The abundance of phosphatic rip-up clasts indicates that reworking played a major part in the phosphogenic process. Rip-up clasts are typically well rounded, of locally mixed microtexture and mineralogy, and are found in massive sand beds not associated with original phosphatic layering. These observations indicate that the occluding phosphates and clays remained plastic for some time to allow them to remain coherent but deformable when reworked, even over great distances with appreciable current energies. It is possible that full lithification did not take place until burial dewatering along with the surrounding sediments, which is supported by the fact that shaly laminae are rarely deformed around phosphatic lenses.

The holistic mode of formation of phosphate in the Torridon rocks presented above synthesizes known phenomena of limnic dynamics, phosphorus cycling, biological ecosystems and sediment-mineral interactions. Through close observation of sediment and phosphate textures and minerals this model for local phosphogenesis explains the occurrence and distribution of phosphate across the Torridon basins. It is consistent with the variable textures seen in differing lithofacies and palaeoenvironments, and goes some way to explaining why preservation within the Torridon is exceptional.

Chapter 7

Deeper in the Proterozoic: the Gunflint Formation

7.1 Global Proterozoic Context

Deeper in Proterozoic time, it can be expected that the rocks will preserve increasingly non-uniformitarian processes, with respect to biology, and by extension, sedimentology and chemistry. As biological communities are expected to be less diverse and less abundant deeper in time, this should be detectable in the fossil record they leave. Correspondingly, biogeochemical cycling can be expected to fundamentally differ deeper in time, and the sedimentological records from these periods must take this into account.

One great problem for understanding biological evolution in the early Proterozoic is that it is probably a time of major biological revolution, and yet the antiquity of the rocks means that their preservation is compromised. It is likely that the eukaryotic cell evolved over a long time, under the stable conditions of the so-called 'boring billion', between 2 Ga and 1 Ga (Holland 2006), so rocks of this age would be ideal to target for transitional forms. Yet well-preserved sedimentary rocks from this time period are scare, with many having been strongly affected by orogenies and intracratonic deformation. To properly understand biotic evolution at this time, the best preserved deposits must be targeted, and interpreted alongside sedimentological and chemical information that may hold clues to their taphonomy and taxonomic interpretation.

The existence of large-scale phosphorites in the Proterozoic is a paradox for biogeochemical cycling and mineral deposition (Föllmi 1996). Most mechanisms for

deposition of phosphorites focus on the Phanerozoic concentration of phosphorus in sediments by mass death and accumulation of metazoan material. However, before the appearance of metazoans, the occurrence of large scale deposits of phosphorite, seen around 2 Ga (e.g. Jatuli-type formations of Finland (Äikäs 1980, Laajoki & Saikkonen 1977) and the Jhamarkotra Formation, Aravalli Supergroup, India (Banerjee 1971, Chauhan 1979)) and at the Proterozoic-Phanerozoic transition (e.g. Meishucun Formation, China (Yueyan 1986) and the Lady Annie deposits of Queensland, Australia (Rogers & Keevers 1976)), is more difficult to explain. What is the source of the phosphorus, and how is it concentrated? Could abiogenic mechanisms alone explain the large scale deposits, or do microbes have a role to play?

One of the problems in understanding the formation of the Precambrian phosphorites is the sheer size of the reported deposits. For obvious reasons, many reports focus on deposits which are economically viable, and somewhat counter-intuitively, a vast concentration of phosphate will serve to mask important sedimentological and structural information that may point to the mechanism of its formation. A relative scarcity of sedimentologically described phosphate deposits from the Precambrian compounds this problem.

In a review of the timing and environments of Precambrian phosphorites, Papineau (2010) identifies repeated occurrences of massive phosphate deposition during marine transgression across Archaean basement rocks. Many of these occurrences cluster around 2.1-1.8 Ga in age, representing a global 'phosphogenic event'. In this same work, he highlights the important roles of certain lineages of bacteria in concentrating phosphate in these environments, although the precise mechanism of precipitation still remains unclear. As a conclusion, Papineau suggests that predictions from his transgressional model should stimulate the search for more phosphorites in the Palaeoproterozoic, which should, by extension, assist in understanding how and why phosphate forms in the Precambrian.

Following this prediction, and the expectations of biology outlined above, a search was initiated for phosphate in the Gunflint Formation of Ontario, Canada, which falls within the time span of the Palaeoproterozoic 'phosphogenic event' highlighted by Papineau (2010). Its cherty iron-rich rocks have preserved a large and varied suite of carbonaceous and iron-mineralised microfossils (Awramik & Barghoorn 1977, Barghoorn & Tyler 1965, Knoll et al. 1978, Schelble et al. 2004), and have the potential

not only to elucidate processes of chemical sediment formation, but also serve as a comparison with the microfossiliferous Torridon phosphates described previously.

7.2 Geology

7.2.1 Background

The Gunflint Iron Formation belongs to the Palaeoproterozoic Animikie series, and outcrops in a broad band across the south western margin of Ontario, Canada (Figure 7.1). Constrained to a minimum age of 1878.3±1.3 Ma by U-Pb dating of zircons in its upper portions (Fralick et al. 2002), it forms part of the classic 'banded iron formations' of this time period, and contains a now-famous assemblage of enigmatic microfossil structures (Awramik & Barghoorn 1977, Barghoorn & Tyler 1965, Knoll et al. 1978).

Stratigraphic studies have differed in fine scale detail, but generally divide the 120 m-thick formation into four members (Fralick & Barrett 1995, Goodwin 1956): a localised basal conglomerate overlying a peneplained Archaean surface, followed upward by the 'Lower Gunflint Member', consisting of algal and oolitic cherts interstratified with thickly bedded chert carbonates and minor volcaniclastic shales. Upwards, the 'Upper Gunflint Member' comprises basal algal cherts and interbedded chert-carbonates and thinning-upwards grainstone units. In places, extensive tuffaceous shales with accretionary lapilli occur. The formation is capped by a limestone member, before passing conformably into black shales of the Rove Formation (Fralick & Barrett 1995).

The depositional setting for the whole formation was originally described as a nearshore transgressive sea migrating towards the northeast (Goodwin 1956), and various subsequent studies have suggested a supratidal to subtidal setting (Lougheed 1983), and a subtidal or lower intertidal setting as a requirement for the development of the grainstone units (Simonson 1985). Bidirectional currents visible in certain sections are suggestive of tidal activity (Ojakangas 1983), while the presence of hummocky cross stratification bears testament to the effect of storms on the shoreline setting (Fralick 1988). The alternating packages of planar bedded chert-carbonates and grainstones are interpreted as representing fluctuating sea level (Morey 1983), possibly caused by nearby volcanic and intrusive igneous activity. Hough (1958) suggested a freshwater setting for the Gunflint rocks, with material being derived from

an adjacent landmass, and cyclic deposition controlled by fluctuation in lake level. The complex structural relationships between the units of the formation and their lack of lateral continuity, while lending support to the idea of isolated lake basins, also makes this interpretation difficult to confirm. Various mineralogical observations suggest episodic exposure to, and isolation from, marine waters in a lagoonal setting (e.g. Goodwin 1956). Planavsky et al. (2009) measured iron isotopes from the Gunflint rocks, an used them in combination with studies of stromatolites and microfossils to conclude a marine setting for the formation and a potential hyrothermal source of iron.

It is clear that conflicting evidence within the rocks of the Gunflint Formation is unable to fully verify a marine or lacustrine depositional setting, thus sedimentology is here analysed on a small scale without recourse to a global setting.

The development of cherty packages, both as stromatolitic bodies and as layered chert-carbonates, is dependent on water depth, current strength, resident biota, and the stability of the underlying substrate. In general, the cherts are thought to have formed in shallower shelf regions characterised by a more intense current or wave activity. Such activity will break up the newly formed cherts, initiating the formation of grainstones (Ojakangas 1983). Cherts require a substrate with long-term stability in order to develop, so true cherty stromatolites are likely to only form along the shoreline, away from easily destabilised granular substrates (Morey et al. 1991). In contrast, the chemical carbonates will form in a deeper, more quiescent environment that is not regularly swept by strong currents (Ojakangas 1983). The silica in the cherts is postulated to be sourced directly from warm, silica-rich seawater (Simonson 1985), and the ferrous iron in the iron formation may be delivered to the waters from weathering of a nearby landmass, or by volcanic input—either through hot hydrothermal fluids, or by reaction of water with extruded lavas (Isley 1995). A volcanic source of the iron is considered most likely, as there is a notable absence of maturely weathered basement in the vicinity of the Gunflint rocks.

7.2.2 Sedimentological study

Owing to the fragmented nature of outcrop of the Gunflint Formation in Ontario, and the disagreements between small-scale regional stratigraphic reconstructions (Fralick & Barrett 1995, Goodwin 1956, see above), much stands to be gained from detailed sedimentological observations of those outcrops. With these, it should be possible to

directly assess palaeoenvironments which may be laterally discontinuous, and to then fit them into a laterally and temporally variable basin model, as with the Torridon lakes (Chapter 2).

Localities were chosen by extent and quality of outcrop. Very little is available for study due to heavy forestation, and rock exposure is limited to where roads and rivers cut through the landscape. A map of the localities described, ordered from east to west, is shown in Figure 7.1.

Mink Mountain, to the western extent of Gunflint extent in Ontario, one of the classic localities, from which several fossil bearing strata have previously been described (Schelble et al. 2004), was revisited, but outcrop here was covered by new agricultural landscaping and migration of gravel bars within river exposures. No fossils or sedimentological data could be recovered from these locations.

7.2.2.1 Schreiber Channel

Location: N48°47'51.0" W087°20'48.0" (Figure 7.1, locality h)

This classic microfossiliferous Gunflint locality consists of an outcrop along the north shore of Lake Superior, approximately 7.4 km west of Schreiber beach. It is accessible by footpath from the beach, or by boat. In bad weather, waves cover the shoreline outcrop.

In a bedding surface outcrop measuring approximately 10 by 40 m and sloping at an angle of around 10° to the south, a thin veneer of chert no more than 50 cm in thickness covers a polymictic conglomerate with complex interacting stromatolitic domes.

The conglomerate, usually allied to the sporadically occurring Kakabeka conglomerate (Fralick & Barrett 1995), comprises large rounded boulders of predominantly dark green-grey fine to medium crystalline basaltic rock, presumably derived from the Archaean-age pillow lavas that outcrop at Schreiber beach (Polat & Kerrich 1999). Other, less abundant rock types are of buff-coloured carbonate and coarse white quartzite and vein quartz. The matrix is a fine-grained dark grey meta-sandstone.

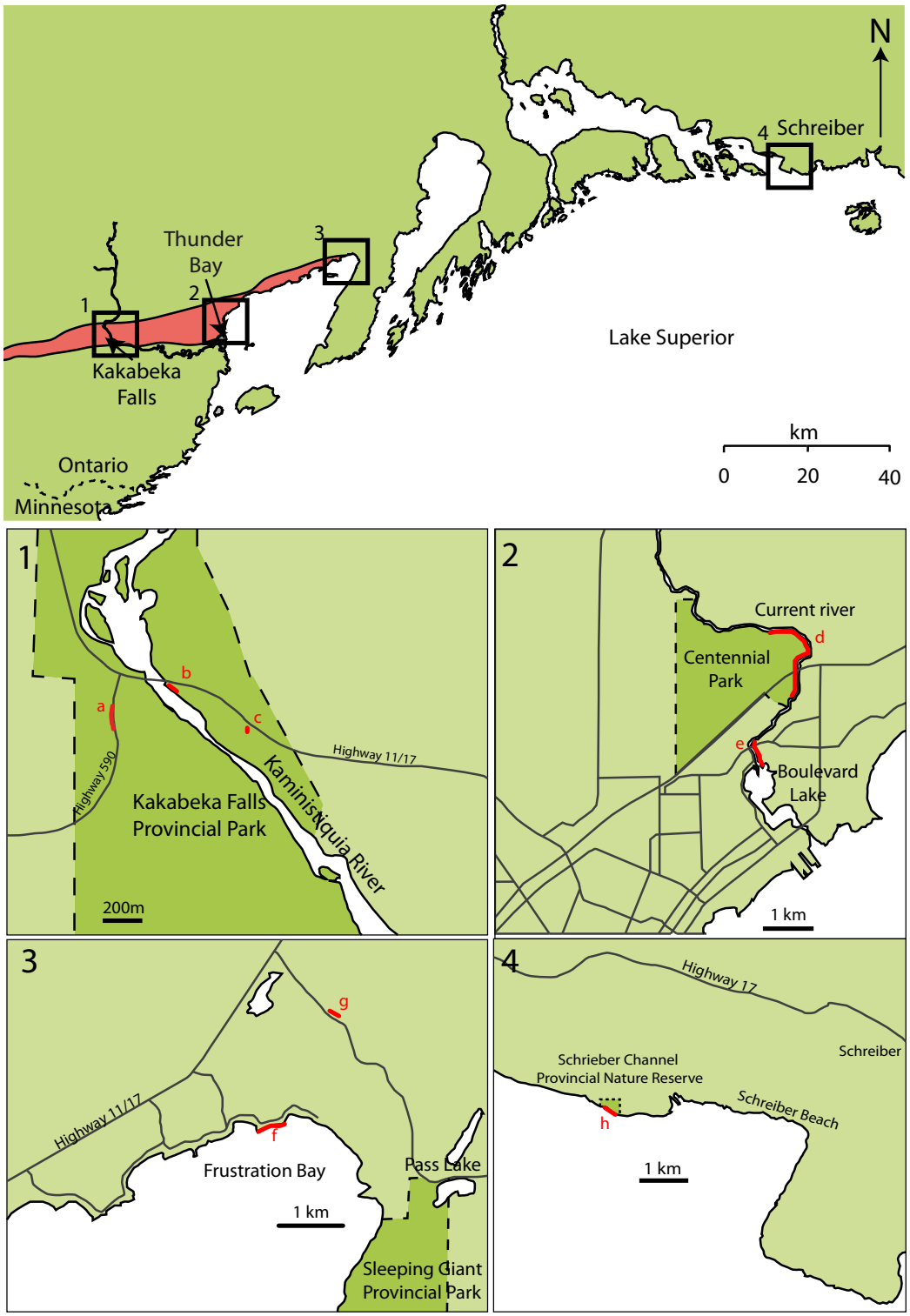


Figure 7.1: Outcrop map of the Gunflint Formation. Insets show regions of interest: 1) Kakabeka Falls region; 2) Thunder Bay township; 3) Frustration Bay; and 4) Schreiber region. Lithofacies and outcrops included in this study, shown in red: a, Kakabeka road cut; b, Kaministiquia river shore; c, Kakabeka car park; d, Centennial Park; e, Boulevard Lake; f, Frustration Bay; g, Pass Lake; h, Schreiber Channel

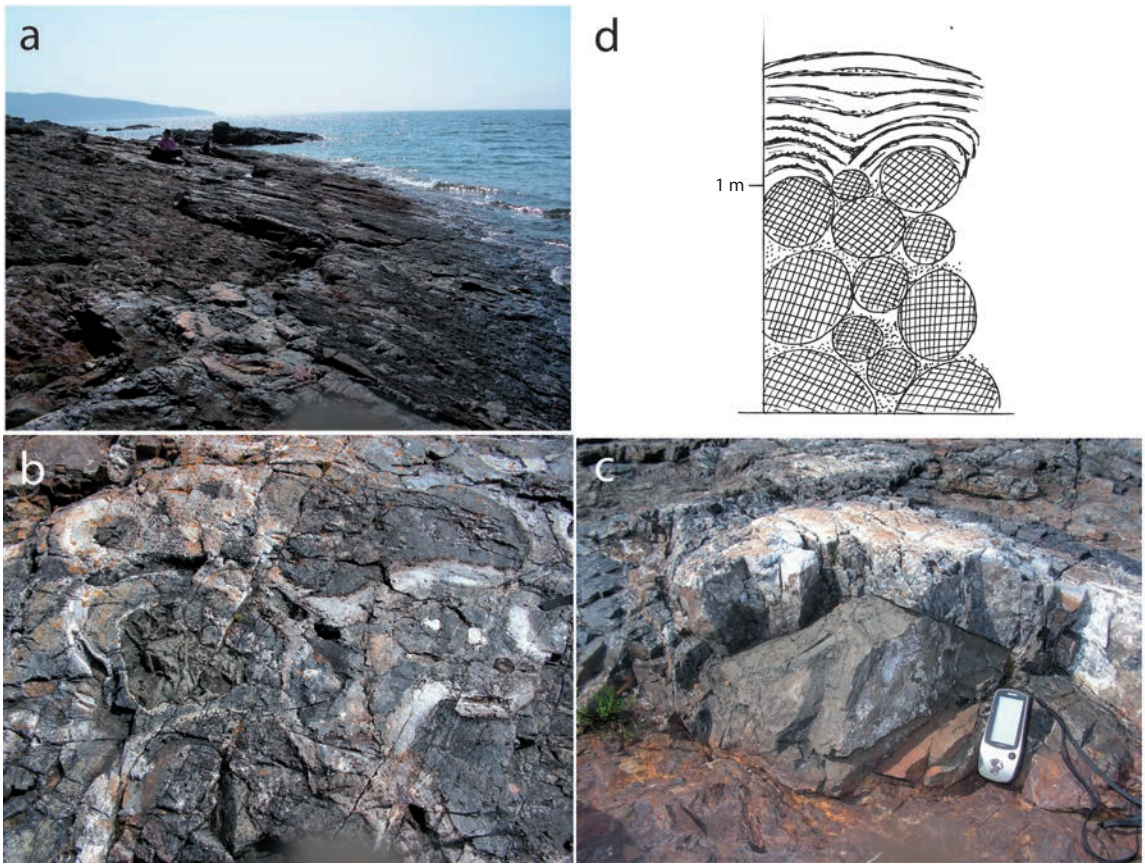


Figure 7.2: Summary of sedimentological structures at Schreiber Channel. a, View looking east along outcrop, showing cherty veneer with rings of weathered stromatolitic domes, tilted and overlying dark boulder-conglomerate. Field of view approx. 4 m. b, Surface view of concentric rings of weathered stromatolites with white outer edges and dark central regions. Range in sized of rings. Top right shows three interacting domes. Field of view 2.3 m. c, Section through chert dome overlying and curving around large basalt boulder beneath, showing low curvature of domes. d, Generalised sketch section of this lithofacies: domal cherts of varying texture and composition directly overlie basalt-boulder-conglomerate with minor sandstone matrix.

The cherty veneer, belonging to the lowermost Lower Gunflint Member of Goodwin (1956), begins on approximately the same plane, and consists of domal structures of low curvature, ranging from 20 cm to 120 cm in diameter, that nucleate on the larger of the volcanic boulders. Subsequent erosion now exposes the interior of the domes, revealing them as concentric rings of chert differing in colour and texture (Figure 7.2). At least four different types of chert were identified in the field: black, with a hackly fracture and unfilled vugs; buff-coloured, with a spheroidal texture; grey and glassy, in places translucent, with microdigitate columns; and white and amorphous. The thicknesses and orders of these characteristic chert types varied between individual domes. The innermost layer tends to formed of black, hackly chert which then passes into a lighter variety, but subsequent alternations of the different types may follow any order. Boundaries between layers appear sharp but not erosional.

Viewed from above, the domes are approximately circular in profile, although where two or more structures have formed adjacent to one another, they show mutual compression before layers form that cover the multiple domes as a whole (Figure 7.2b, top right of image). Buff-coloured medium grained carbonate fills the interdomal spaces, but has been eroded away in many places.

Domal structures of chert in the geological record are usually interpreted to be the result of cyanobacterial stromatolite building. This is corroborated in the Schreiber Channel cherts by the rich assemblages of filamentous and coccoidal microfossils found within the black cherts of the domes (Awramik & Barghoorn 1977, Barghoorn & Tyler 1965). Assuming a biological mode of formation for these structures, they can be compared with rare modern examples forming today on the shore of the hypersaline lagoon at Shark Bay, Australia (Papineau et al. 2005, Playford & Cockbain 1976). A lower intertidal to upper subtidal environment is likely for their formation, and they owe their cherty mineralogy (as opposed to the carbonate forming modern stromatolite domes) to the silica-rich ocean widely postulated for the Palaeoproterozoic (Siever 1992). This likely environment of formation is probably similar to that which deposited the underlying conglomerate, as an energetic shoreface would be necessary to move and smooth such large clasts. The relative scarcity of clastic grainstone also supports an energetic depositional environment with low net clastic deposition. The preferential nucleation of stromatolite domes on the larger boulders is likely due to their greater stability over time.

7.2.2.2 Frustration Bay

Location: From N48°34'19.8" W088°47'09.6" to N48°34'24.9" W088°46'52.0" (Figure 7.1, locality f)

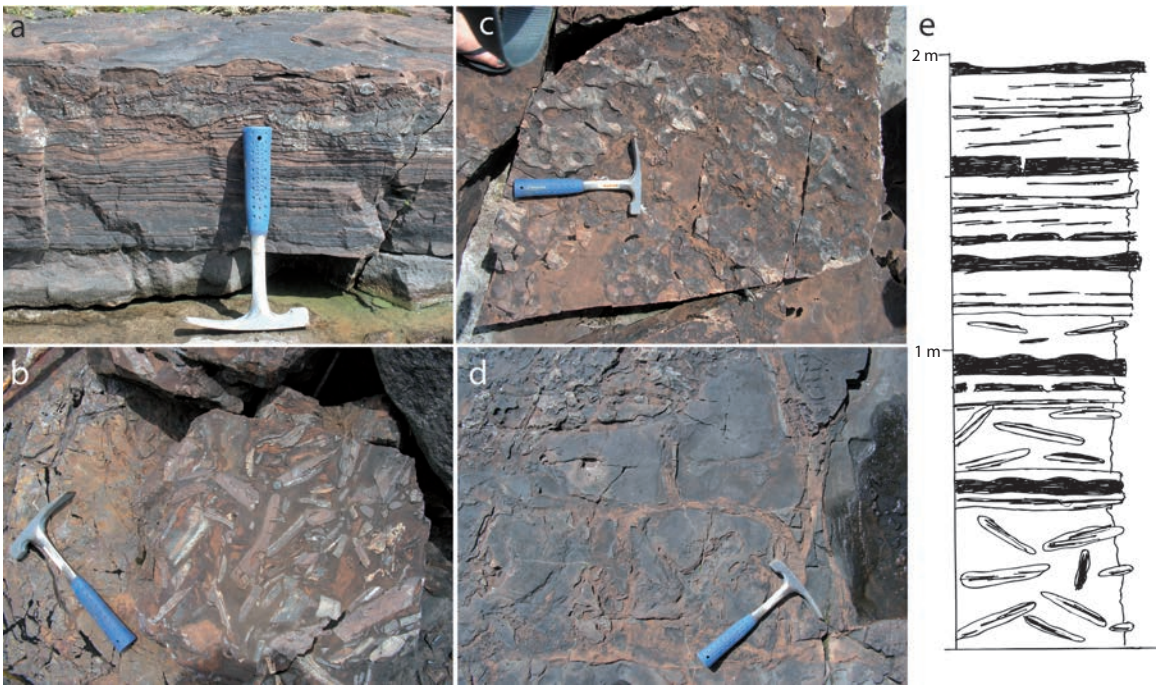


Figure 7.3: Summary of sedimentological structures at Frustration Bay. a, small cliff section showing thin beds of chert and carbonate, mostly laminar, somewhat disturbed. b, bedding-parallel section of chaotic tabular breccia of chert-carbonate bands set in carbonate grainstone matrix. c, Bedding-parallel section of unbrecciated chert layer with rippled surface, heavily weathered. d, Bedding parallel section of chert, polygonally cracked and unfilled with grainstone. e, Sketch graphic log of brecciated and laminar-bedded chert-carbonates.

Occurring along the north shore of Lake Superior, to the west of Sleeping Giant Provincial Park, this outcrop is accessed by the Eldorado Beach Road from Highway 11/17. It consists of an exposure approximately 3 m wide of erratically but shallowly dipping intraformationally brecciated chert carbonates along a 150 m long stretch of the shore. It is likely to lie within the Upper Gunflint Member of Goodwin (1956).

Stratigraphic thickness is difficult to estimate due to the chaotic and erratic bedding dip, as well as likely lateral variation in extent of brecciation. The outcrop represents at least 2 m of stratigraphic thickness, measured from the laminated and

unbrecciated portions (Figure 7.3e).

Unbrecciated, laminar rocks are apparent towards the top of the section at the eastern end of the shoreline exposure, the rock consists of centimetre- to decimetre-scale alternations between an orange-coloured carbonate and siderite chert grainstone, and tabular black to buff-coloured chert. Fine undulating laminations are apparent in both of these lithologies: in the chert, these are picked out by varying concentrations of organic matter and iron carbonate, and in the chert-carbonate grainstone, by concentrations of siderite rhomboids, iron oxides, glauconites, and chalcedonic quartz. The upper surfaces of the cherty bands often show uneven but broadly symmetrical ripples of around 15 cm wavelength. Cherty bands tend to be fractured, and the cracks are infilled by carbonate grainstone. This becomes more extreme towards the bottom of the section and the western edge of the outcrop, until planar bedding is lost altogether, to be replaced by tabular breccia of both the chert and the carbonate bands, supported by a matrix of yet more orange finely granular carbonate.

In places, the sequence of deposition, lithification and brecciation is more complex, consisting of more than one phase. The tabular clasts of chert and laminated carbonate are set in an amorphous matrix of granular carbonate, which is itself brecciated with cracks infilled by dark grey chert. In places, the grainstone is more thoroughly reworked, and the cherty intraclasts are rounded.

The chert bands hold clues to the likely depositional environment for this rock. Ripples in the top surface, although irregular, would have been formed by oscillating wave currents, and polygonal cracks infilled by sandy material have the characteristics of desiccation cracks more commonly seen in terrigenous sediments. Alternation between granular carbonate deposition and chert formation suggests periodic changes in water chemistry, perhaps affected by fluctuating water depth. The occurrence of wave ripples and desiccation cracks only at the top of the chert bands may indicate a transitional period from deeper, calmer, chert forming waters, to shallower and more agitated water where carbonate may be deposited. Thus a fluctuation between a lower subtidal to lower supratidal environment is inferred from the laminar record.

There is good evidence in the lithofacies to suggest a microbial role in the formation of the sedimentary structures. Fluid escape structures are well preserved, indicating a semi-sealing endobenthic and perhaps epibenthic mat (Noffke 2010). Fine

'crinkly' laminations are common, perhaps indicating fine epibenthic mats overgrowing the sediment surface. In some places, domal, possibly stromatolitic structures are apparent, infilled by secondary chalcedony. In these, the ghosts of former microbial laminae are picked out by spherical micro-concretions.

The extensive syndepositional brecciation of the lower parts of this outcrop is testament to an episodic, violently energetic environment at the time. Either rapid lithification of both the chert and the grainstone, or an extremely low rate of deposition will have allowed reworking of large undeformed tabular clasts into the chaotic breccia, and the multiple phases of brecciation under more energetic conditions. The presence of glauconite within the grainstone favours a low rate of deposition. In an intertidal setting, episodic storms could be responsible for sudden and violent reworking of the lithified sediments.

7.2.2.3 Pass Lake

Location: N48°35'36.9" W088°46'05.7" (Figure 7.1, locality g)

An approximately 30 m long by 3 m high outcrop on the left hand side of Highway 587 leading to Pass Lake at the north of Sleeping Giant Provincial Park exposes a folded and locally somewhat brecciated sequence of grey to black cherts interbedded with orange coloured grainstone carbonate.

The lithology is broadly comparable to those unbrecciated sequences seen at Frustration Bay, and would likely be placed in the Upper Gunflint Member of Goodwin (1956). In this outcrop however, the chert beds are somewhat more abundant than the carbonate, and they are notably more laminar without undulating top surfaces or evident desiccation cracks.

Predominance of chert bands gives the rock a competency that allows the open, 10 m wavelength, antiformal and synclinal folds to be accommodated without loss of laminar structure. To the southern extent of the outcrop, however, extensive chaotic brecciation begins, giving the outcrop an identical appearance to the lower brecciated units of Frustration Bay. This represents intraformational brecciation, rather than resulting from post-diagenetic deformation, as it consists of cherty tabular clasts set in a massive carbonate grainstone matrix. Thus, the change from competent laminar chert bands to chaotic breccia likely represents an original lateral discontinuity of

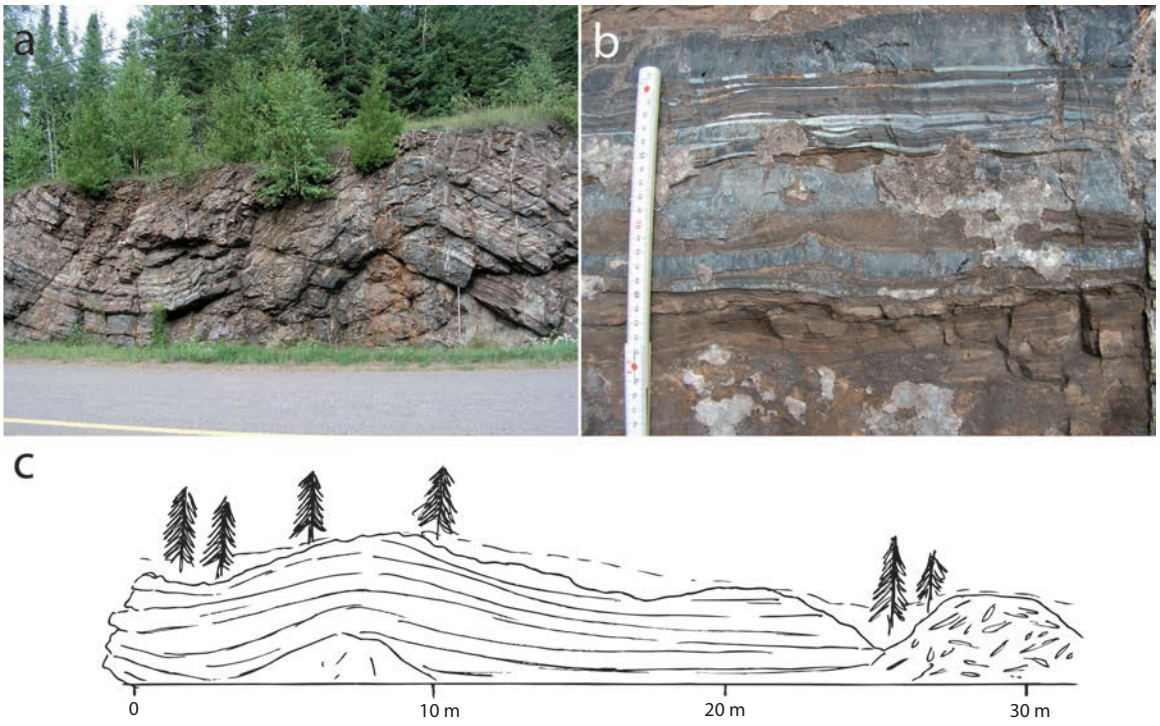


Figure 7.4: Summary of sedimentological structures at Pass Lake. a, Open synformal and antiformal folds in competant laminar chert-carbonate beds. Field of view approx. 10 m. b, Laminar, slightly undulating alternating beds of grey-black chert and dark orange carbonate. c, Sketch of outcrop at Pass Lake, looking East. Brecciation at southern end due to lateral variation in lithofacies and depositional environment.

lithofacies, and therefore of the local palaeoenvironment.

Owing to the broad similarity between the lithologies at this location and that at Frustration Bay, which is only approximately 2 km distant, a similar palaeoenvironment of deposition is inferred. The lack of ripple structures or desiccation cracks at the Pass Lake exposure point towards a deeper, lower subtidal environment, below the mean wave base where desiccation is unlikely. Such an interpretation is further supported by the dominance of cherty layers, which are more likely to form in deeper water than the grainstone carbonate.

7.2.2.4 Centennial Park

Location: From N48°28'46.4" W089°11'16.3" to N48°29'24.5" W089° 11'29.9" (Figure 7.1, locality d)

Sporadically exposed along a 2 km stretch along the Current River in Centennial Park is a sequence of horizontally bedded clastic and chemical sediments. The rocks vary in lithology and habit, and are dipping shallowly to the south, so that moving upstream transects successively older rocks in the sequence.

Overall, the rocks of this locality most closely resemble those of the Lower Algal Chert Facies of the Lower Gunflint Member of Goodwin (1956), and consist primarily of alternations between carbonate grainstones and chert interbeds, and fine silty terrigenous material.

The lowermost units at the northernmost extent of accessible outcrop comprise a complex association of dark chert grainstone and orange-coloured carbonate grainstone. Chert occurs as series of fine undulating laminations, as small and large rip up clasts up to 30 cm across, and as thicker beds that may be cracked and tilted into teepee structures, or may bear many regularly sized circular holes filled with carbonate grainstones (Figure 7.5a). Massive carbonate sediment is interbedded with these indurated chert layers, and forms the matrix for rip-up breccia.

Beds of large rip-up clasts and teepee structures require an energetic environment for their formation, and the circular weathering structures in some chert beds may be attributed to weathering by meteoric waters during desiccation and exposure. These



Figure 7.5: Summary of sedimentological structures throughout Centennial Park outcrops. a, Complex laminated and fenestrally weathered black chert interbedded and infilled by granular orange carbonate. Lithofacies represents rapidly lithifying beach rock. b, Up section, planar laminated siliciclastic shales indicating quiescent deep water environment. c, Pinching and swelling interbeds of chert-carbonate further up section, with faint cross-beds in carbonate layers. d, Decimetre-scale shale beds between chert-carbonates, suggesting short term or small scale depth fluctuations. e, Sketch graphic log of succession of lithofacies at this locality.

are the hallmarks of an energetic intertidal setting with rapidly lithifying bottom sediments, and this exposure has been interpreted as a beach rock by Franklin (1991).

Towards the south and up section, there is a sharp change in lithology to fine, planar laminated shales with minor granular carbonate, which are exposed as tall river cliffs and flat benches dipping gently to the south. Quartz veins cross-cut the shales in all directions, but no other deformation is apparent. The shales are without cross laminations, ripples or desiccation cracks. On the bedding surface of some layers, irregular patterns of pits, protrusions and ridges up to several millimetres high are apparent (Figure 7.15d, e) and transverse sections show these to be formed by small irregular nodules of pale blue cryptocrystalline chalcedonic quartz. Adjacent laminae in the shales are bent around these nodules, suggesting they formed syndepositionally and pre-compaction.

The lack of sedimentary features characteristic of water motion or of desiccation implies a calm water environment for deposition of these rocks. The irregular distribution of chalcedonic nodules suggests a sporadically occurring nucleation source, and their overall similarity in appearance to some inferred taphomorphic macrostructures of the Ediacaran (Brasier & Antcliffe 2009, Liu et al. 2011) leads to the tentative conclusion that their formation may have been induced by decomposition of organic matter. These structures will be revisited further in this chapter. A lower subtidal or deeper palaeoenvironment is inferred from the sedimentary structures.

Further up section the lithofacies changes once again. Thick beds of planar laminated shale are still present, but they are interbedded with sequences of decimetre scale chert-carbonate beds, separated by thin shaley partings. Laminations continue through all beds, but in some chert-carbonate units, cross lamination can sporadically be seen. Chert-rich layers have a typical gradation in colour from black and hackly at the base, to a grey chert grainstone at the top.

The continuing presence of unrippled, undesiccated shales implies prevailing deep water conditions. These are periodically interrupted by phases of chert-carbonate formation, which is occasionally influenced by directional currents. It is likely that this facies represents a slightly shallower environment than the preceding one, where currents and shallow water processes can bring about the formation of chert carbon-

ates in a lower subtidal, possibly distal deltaic setting.

Towards the top of the section, the shaley units in general become scarcer, and the chert-carbonate beds more abundant and thicker, although there are exceptions to this general trend where thick shale units are found which contain black chert lenses. This continues a general trend of shallowing, perhaps into the upper subtidal zone, which allows the formation of the chert-carbonate. The general trend is overprinted by signals of shorter-term water depth fluctuations, which bring about the shale deposition, or lateral variation in basin shape that result in a diachronous signal of shallowing.

In summary, the exposure at Centennial Park records a number of different lithofacies ranging from beach rock, through deep-water shales, to shallow, current swept chert carbonates. The outcrop, though incomplete, records initial shallow water conditions, followed by a sudden increase in water depth, followed by progressive but irregular shallowing, that is consistent with a rapid transgression followed by a slow and uneven regression.

7.2.2.5 Boulevard Lake

Location: From N48°27'58.5" W089°11'56.3" to N48°28'08.6" W089°12'03.4" (Figure 7.1, locality e)

Before the Current River enters Lake Superior, it is dammed within the bounds of Thunder Bay Township, forming Boulevard Lake. Around the north eastern edge of the lake, a succession of clastic and chemical sediments outcrop, allied with the Lower Algal Chert Facies of the Lower Gunflint Member of Goodwin (1956), dipping shallowly to the south east. They are mostly exposed on their bedding surfaces, and although there are gaps, a stratigraphic thickness of at least 5 m is represented in the roughly 350 m long outcrop, with the lowermost rocks in the section occurring to the south.

The lowermost exposure at the southern tip of the inlet comprises medium grained orange carbonate, finely laminated but undulose in places, interbedded with occasional thin and discontinuous lenses of black waxy chert, weathering white. Around 2 m thickness occurs here, with chert laminations increasing in number upwards. Where exposed on bedding surfaces, the laminations appear as concentric lobate

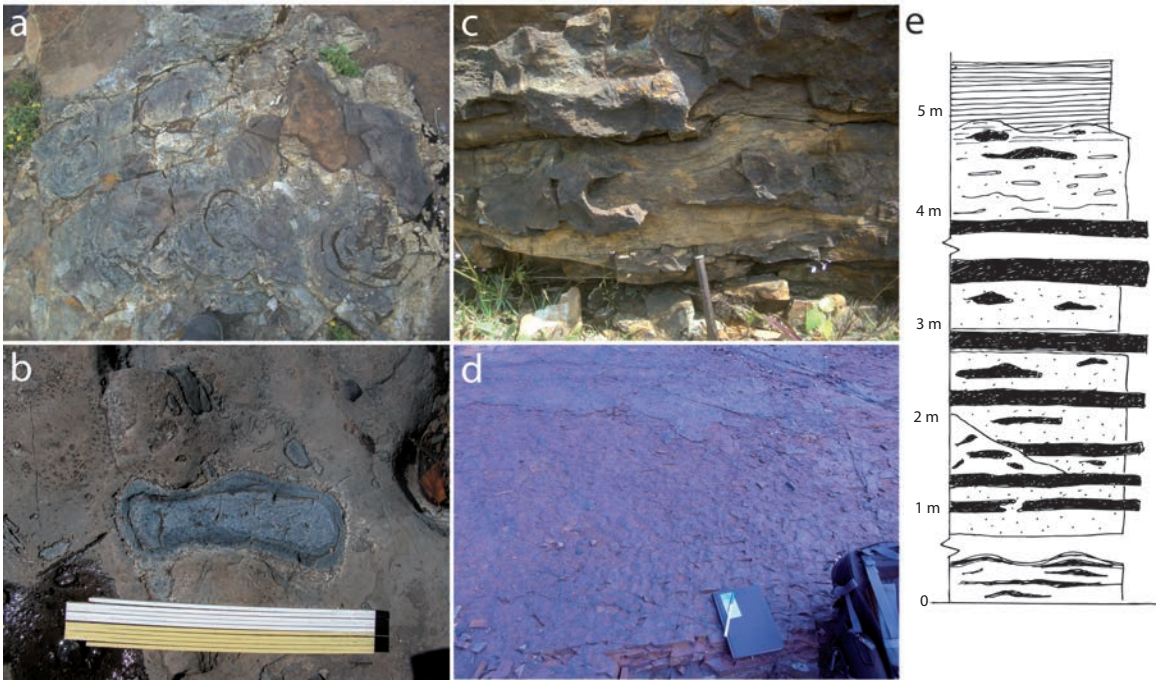


Figure 7.6: Summary of sedimentological structures at Boulevard Lake. a, Concentric circular and lobate structures in lower part of the section. Field of view approx. 2 m. b, Thicker broken bands and lenses of dark chert interbedded with grainstone carbonate, whose laminations bend around chert lenses. Field of view approx. 60 cm. c, Concentrically zones fine mud rip up clasts in carbonate grainstone matrix. d, Bedding parallel surface of pyritic shales, showing large scale wrinkled structure. e, Sketch graphic log of lithofacies at this outcrop.

rings picked out by cracks where carbonate has weathered away. In appearance and mineralogy they resemble the algal domes of Schreiber Channel, although they are not as abundant. Chert also occurs as irregular bands and thin nodules without a domal structure, and these are often polygonally cracked, with the cracks infilled by grainstone carbonate. The carbonate matrix between the chert contains small cherty grains and rip up clasts.

Such sedimentological data, in combination with the algal dome structures, together imply an energetic environment in shallow and occasionally desiccating waters. A lower supratidal to intertidal environment is therefore proposed for the formation of these sediments.

Up section, and towards the north of the outcrop, chert layers become thicker and more abundant, although they no longer possess any domal structure. The resultant planar bedded chert-carbonate is variable in habit, occasionally dominated by thick cherty packages, but most often consisting of decimetre scale beds of orange-coloured carbonate with laminations, containing thick nodules up to 15 cm thick and 50 cm long of black chert. In these cases, laminations within the carbonate beds bend around the chert nodules, indicating that they formed before compaction and lithification of the sediment.

This lithofacies makes up the bulk of the Boulevard Lake outcrop, but represents just less than 2 m stratigraphic thickness, as single bedding planes are exposed as benches for some distance. On these bedding planes, lateral variation in lithology is clearly apparent, with up to 5 m wide 'channels' of grainstone carbonate cutting across an otherwise planar bed of black chert. The boundaries of these channels are sharp, and the carbonate matrix often contains angular rip-up clasts of chert and more carbonate.

Lacking the characteristics of supratidal desiccation, this lithology necessitates a greater and more consistent water depth. The crosscutting areas of carbonate within chert bands are here interpreted as erosional infills, created by channels cutting through early-lithified sediment, or by initial irregularities in the basin floor. The channel-cut explanation is favoured to explain the rip-up clasts within the carbonate, and so pointing towards a subtidal delta top-type setting with periodic, laterally

confined reworking of the sediment.

Towards the northern edge of the exposure, the orange granular carbonate-chert bands are suddenly succeeded by a unit 150 cm thick, of fine, pale, buff carbonate with minimal chert. Instead, lenticular rounded clasts and lenses of blue-grey mud ranging in size from less than 1cm to more than 15 cm across, but less than 1 cm thick, are arranged subparallel to the undulose laminations within the carbonate. These have a concentrically zoned structure, which may have resulted from post-reworking alteration. Occasional thick mud laminations drape the carbonate and rip-up structures.

The occurrence of fine mudstones amidst the grainstone carbonates requires periods of quiescence to deposit them initially, followed by periodic energetic reworking events. Multiple reworking events are probable, as evidenced by the fine mudstone drapes throughout the thickness of the unit. An intertidal flat environment with fine mature clastic input would allow for periods of calm for mud deposition, settling, and semi-lithification, and incursions of the sea which rework those sediment flats into a more massive carbonate unit.

Overlying this carbonate-mud reworked unit, by a sharp undulating erosional boundary, are a succession of well-indurated, planar laminated, red metallic shales, of around 2.5 m stratigraphic thickness. These shales are heavily cleaved, so most sedimentary structures in transverse section are obliterated, but irregular wrinkles are visible on bedding surfaces at a number of scales. In places, the wrinkles have a relief of up to 1 cm. The shales are irregularly interbedded with coarser units of grainstone containing well rounded and occasionally annealed non-crystalline grains up to 2 mm across.

The erosional contact to the metallic shales marks a sudden change of water depth and sedimentary regime. The shales themselves, as far as can be deduced through pervasive cleavage, have no evidence for desiccation or ripples, and so they were probably deposited in a deep-water quiescent environment. The wrinkles on the bedding surfaces are similar in appearance to some more irregular microbially induced wrinkle structures, and this will be discussed further in this chapter.

In summary, the exposure at Boulevard Lake represents a fluctuation in water depth and sedimentation from shallow intertidal at the base, through subtidal deltaic

and channel-cut environments, to shallow clastic tidal flats. Erosion is followed by a sudden deepening to fine shelf or bathyal shale deposits. Broadly this fluctuation can be described by a small scale transgression and regression cycle, followed by a large erosional transgression.

7.2.2.6 Kakabeka Road Cut

Location: N48°24'17.8" W089°37'56.8" (Figure 7.1, locality a)

Near to the Kakabeka Falls Provincial Park, road cuts expose low cliffs of classic ribbon banded iron-chert-carbonate. The most informative of these is on the right hand side of Highway 590, shortly after the turning from Highway 11/17, heading south. Here, a broken outcrop almost 100 m long and on average 3 m high, exposes alternating vitreous chert-taconite and orange grainstone carbonate layers with notable nodular structures and algal laminations, likely belonging to the Lower Algal Chert Facies of the Lower Gunflint Member of Goodwin (1956).

Planar laminated grey-black vitreous chert is ribbon-banded with orange grainstone carbonate, with occasional beds containing cherty rip-up clasts set in a carbonate matrix. Undulating wispy laminations within the carbonate are an indication of potentially biological banding in this lithology. Chert occurs as laterally consistent bands, as pinching and swelling structures, or as nodules of short lateral extent. Often, it is seen draping over the undulating top surface of carbonate beds, with the appearance of a hardground, and nodules forming beneath it may represent syndepositional chert growth below the sediment-water interface. In one more massive bed of vitreous grey chert, a large, tightly curved algal bioherm with microdigitate structures, is picked out by variations in chert colour: ranging from black and vitreous to white and opaque.

Undulations in the top of carbonate beds and the draping cherty 'hardground' suggest alternating chemistries during deposition, and an environment that frequently has high current energies with which to sweep a hardground surface clear of newly formed material. Algal dome structures, as at Schreiber Channel and Boulevard Lake, are most likely to form in an intertidal environment, with the hardground structures within the lower intertidal zone. No major temporal changes in water depth are evident here, with differences observed most likely due to lateral heterogeneities in



Figure 7.7: Summary of sedimentological structures at the Kakabeka Road Cut outcrop. a, Dark grey chert of varying habit, interebedded with orange carbonate grainstone with fine undulating laminations. b, Tightly curved cherty bioherm with microdigitate laminations. Carbonate and chert layers drape the entire structure. Field of view approx. 150 cm.

sedimentation style.

7.2.2.7 Kakabeka Car Park

Location: N48°24'10.3" W089°37'56.8" (Figure 7.1, locality c)



Figure 7.8: Summary of sedimentological structures at the Kakabeka Car Park outcrop. a, Laminar, fine scale alternations between black hackly chert and fine granular carbonate. b, Soft-sediment deformation of chert-carbonate layers. Field of view approx. 40 cm across.

Within the car park of the Kakabeka Falls Provincial Park is one of the classic exposures of ribbon banded iron formation, typically placed within the Lower Algal Chert Facies of the Lower Gunflint Member of Goodwin (1956).

The outcrop is around 3 m high and just 5 m across, and shows erratic deformation of individual layers, probably caused by soft sediment slumping and intraformational brecciation. Layers are formed from three main mineralogies: black vitreous chert

with hackly to crystalline fracture; orange granular carbonate with fine laminations; and deep red iron-rich finely granular siderite. Black chert and orange carbonate together form competent layers that are gently folded or fractured into tabular clasts, and set in a matrix of the deep-red siderite. Very fine lamination within the chert bands is formed by alternations in crystal size and in concentration of ferrous material. No sedimentary structures other than lamination and diagenetic deformation are evident.

The absence of ripple or current bedding in this exposure of ribbon chert-carbonate implies a depositional setting below the mean wave base. However, as with other deposits of laminated cherts and carbonates, a relatively shallow water environment within the photic zone is still inferred. Syndepositional deformation may have been caused by instabilities in the basement substrate, such as may be found on the shoulder of a continental slope, or could be caused by episodic storm events.

7.2.2.8 Kaministiquia River Eastern Shore

Location: N48°24'17.2" W089°37'38.7" (Figure 7.1, locality b)
Within the Kakabeka Falls Provincial Park, just upstream of the main falls themselves, an exposure of shale in the river cliff on the eastern shore approximately 3 m high by 10 m wide represents rocks probably attributed to the Tuffaceous Shale Facies of the Upper Gunflint Member of Goodwin (1956).

Dark grey to buff-coloured fissile shales are horizontally bedded and crosscut by the river cliff, and are interbedded with rare bands of thin red- to black-coloured chert. Few bedding planes are exposed, but where they are, wrinkle structures are often apparent on the upper surface, as well as raised ridges that correspond to internal tube-shaped structures of pale blue chalcedony as seen at Centennial Park. These structures may have a microbial origin, and will be discussed further in this chapter. In the chert bands, dark brown indurated nodules of very high Fe concentration occur up to 1 cm thickness, coalescing into bands in places.

The persistently laminar habit of these shales, as well as their consistent fine grain size leads to an inevitable palaeoenvironmental interpretation of deep quiescent waters. Rare chert bands may indicate slight fluctuations in water level, or temporal changes in water chemistry, but a deep stable slope or bathyal setting is likely.

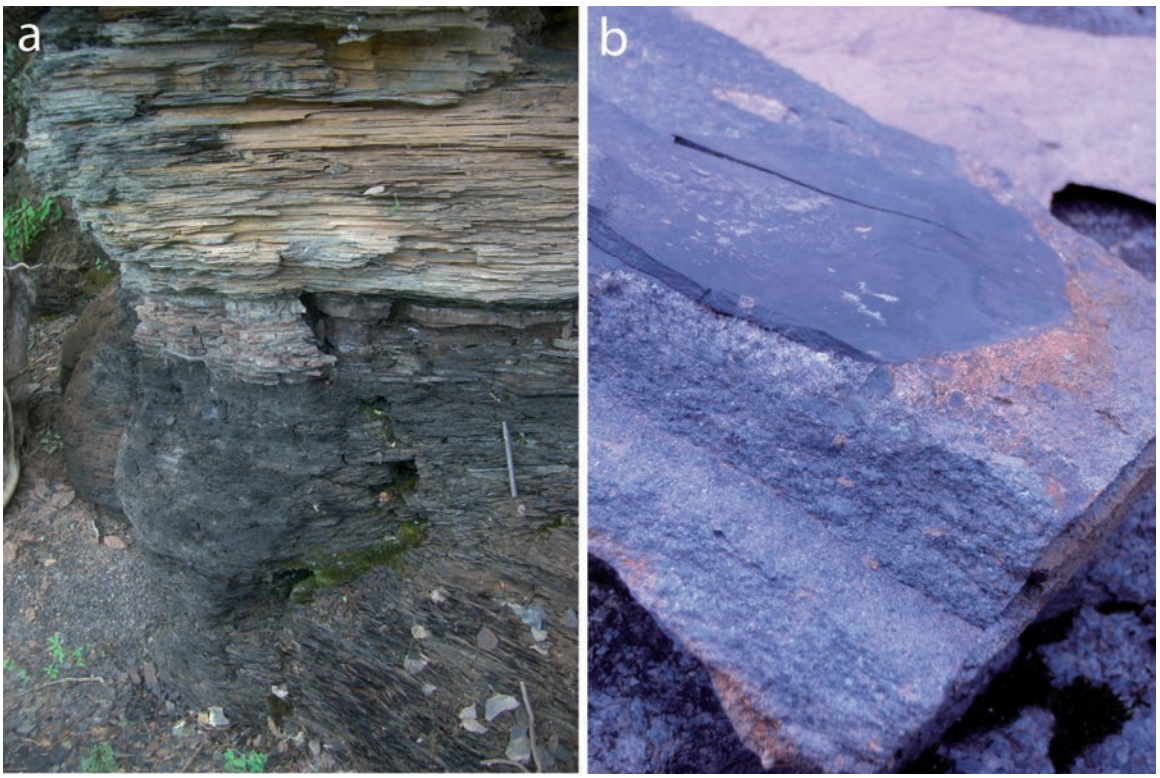


Figure 7.9: Summary of sedimentological structures at outcropping on the shore of the Kaministiquia River. (a) eastern shore, and (b) western shore.

7.2.2.9 Kaministiquia River Western Shore

Location: N48°24'17.4" W089°37'45.1" (Figure 7.1, locality b)

Within the Kakabeka Falls Provincial Park, upstream of the falls themselves and on the western shore of the river, accessible through the Fern's Edge campsite, is a bedding plane outcrop of shales, volcaniclastic material and chert, representing one of the tuffaceous shale facies within the Upper Gunflint member of Fralick & Barrett (1995). Only around 30 cm of stratigraphic thickness is exposed, but the bedding plane reaches around 70 m^2 in total.

The bulk of the rock is made up of fine, planar laminated grey pyritic shale with minor glauconite, similar to that seen upstream and up section on the eastern shore. A number of laterally discontinuous features are evident on this bedding plane, including a patchy thin veneer of chert, and thin laterally discontinuous lenses of volcanic grainstone embedded in a cherty matrix. Over the surface of the bedding plane the areas covered by cherty veneer show no observable pattern, but the bound grainstone appears to occupy channels that cut down through the shales, as well as forming discontinuous laminae. This grainstone comprises volcaniclastic grains of mostly quenched volcanic glass, pumice, and scoria of basaltic composition, and the chert that binds them is cryptocrystalline and poikiloblastic. Grains are well rounded and some are coated by rims of carbonate, iron oxides and phosphate.

Depositional setting for the lithofacies is similar to that of the overlying shales of the eastern shore outcrop: deep quiescent and bathyal. Cherty veneers may form locally where changes in water chemistry permit it. The volcanic material contained within the grainstone is evidence of a volcanic sediment source nearby, but its processing into a grainstone necessitates an oscillating current action as may be generated in a mobile grainstone bar. That bar is not preserved here, but instead slumps and infilling channels have formed from destabilisation of that bar. From the overall direction of crosscutting channels, the grainstone bar could be expected to lie to the east or the west of this outcrop.

7.2.3 Revised palaeoenvironmental interpretations

Using the small-scale sedimentological data collected from those accessible outcrops of the Gunflint Formation in Ontario, it is possible to reconstruct an idealised basin

environment in which they were deposited.

Figure 7.10 illustrates such an idealised basin. Sedimentation and chemical precipitation occurs in a variety of peritidal settings, affected by variations in topography or water depth which bring about tidal or wave-dominated features. Away from the shoreface, sediment deposition and processing continues to occur in association with an ephemeral and laterally mobile grainstone bar, supplied with clastic and chemical material from the peritidal environment as well as nearby volcanic sources. The grainstone bar supplies material inshore and offshore during storms or as a result of slope destabilisation. Fine clastic, volcanic and occasionally chemical sediments accumulate in quiescent offshore settings unaffected by either tidal or wave action.

The general basin structure detailed above is similar to that proposed by Fralick & Barrett (1995), but differing substantially in the inclusion of the grainstone bar. This revised interpretation is necessary to explain the sedimentological and petrographical observations of heavily processed and rounded grains in nearshore, otherwise laminar sediments, as well as in deep offshore, usually quiescent settings. Such granular sediment could be formed as a result of oscillating nearshore currents, but the lack of any substantial grainstone lithofacies in the localities studied implies a more ephemeral source. The periodic supply of grainstone and no other carbonate or chert material to fine deep sediments, as at the Kaministiquia River western shore outcrop, requires that the grainstone source be closer to this deep setting than the shoreface sediments, corroborating the interpretation of an offshore bar.

The inclusion of the grainstone bar in a revised depositional basin for the Gunflint Formation may also help to explain the distribution of chemical sediments among the different lithofacies. Iron-rich chert-carbonate alternations are observed in nearshore shelf environments. The precipitation of stratiform chert in particular is paradoxical, as without a hydrothermal source of silica, and before the metazoan concentration of silica into tests or spicules, the chert must form from supersaturation-driven precipitation. Although silica concentrations of the Palaeoproterozoic are projected to be higher than today (Siever 1992), this alone cannot be sufficient to initiate precipitation, as evidenced by the absence of stratiform cherts in deeper water sediments. But if an offshore grainstone bar is inferred for the supply of granular material, then it may also help to explain local supersaturation conditions through the creation of

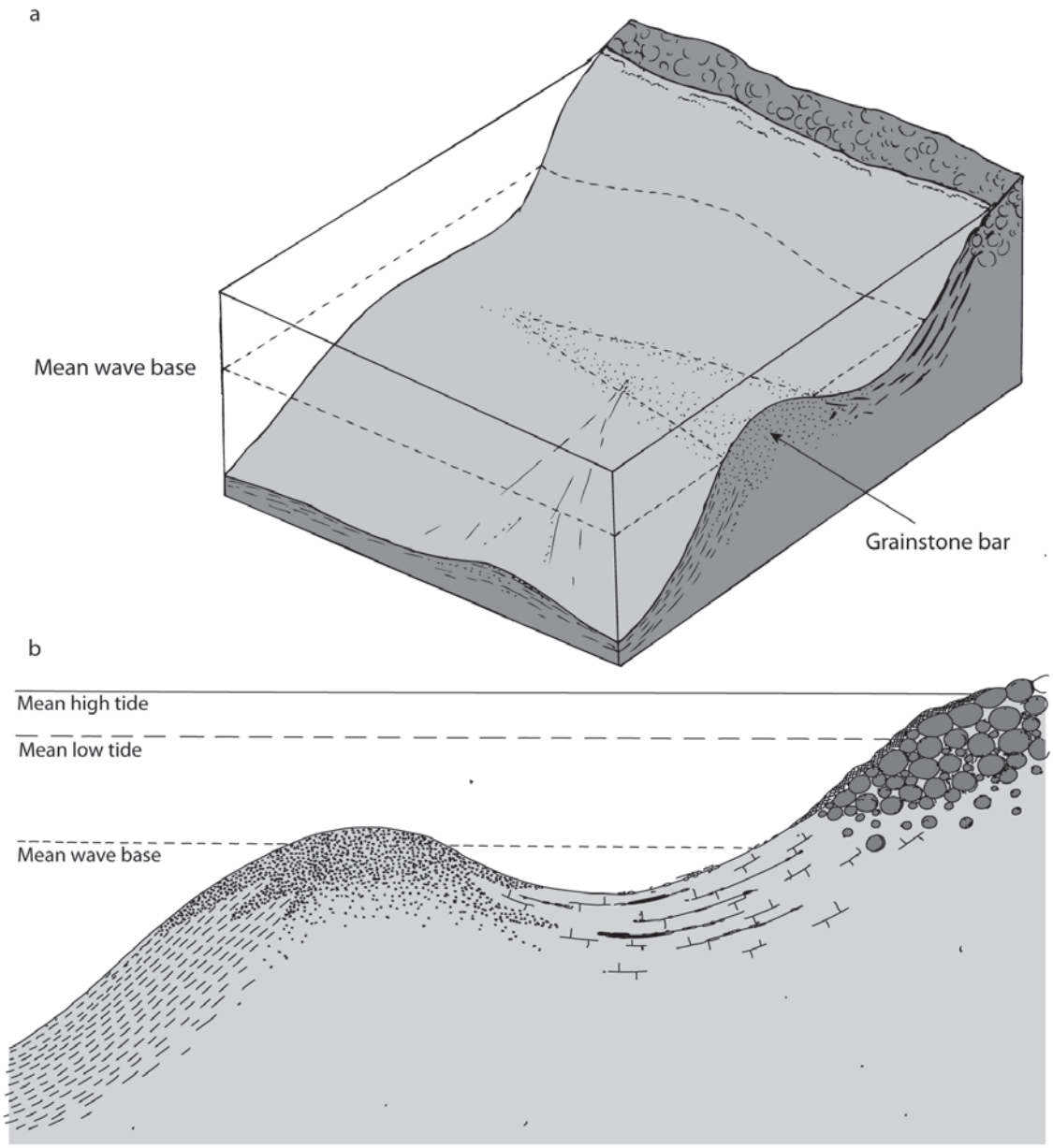


Figure 7.10: Schematic reconstruction of an idealised depositional basin for the Gunflint Formation lithofacies, incorporating the disparate depositional environments of individual outcrops, and stratigraphic variations in lithology. (a) Idealised block model, incorporating laterally discontinuous and temporally mobile grainstone barriers. (b) Simplified transect from upper intertidal to deep bathyal conditions represented by the Gunflint lithofacies.

a semi-restricted environment similar to today's back-reef lagoons. In this environment, restriction of incoming water by bar migration and evaporation of water within the lagoon would elevate silica concentrations sufficiently to initiate precipitation. Alternations with carbonate and siderite may represent periodic influxes of seawater more dilute with respect to silica, and the resumption of 'normal' chemical carbonate sedimentation. Supersaturation alone may not be sufficient to explain precipitation of the range of chemical sediments of the Gunflint, and their formation will be revisited at the end of this chapter.

The basin topography and chemistry described above is an idealised one for the Gunflint Formation, and cannot be reconstructed perfectly from the present day outcrop, as is possible with the Torridon Group (Chapter 2).

The lithofacies reviewed from the accessible outcrops in Ontario represent the entire sequence of the Gunflint Formation, in contrast to the single confined basin of the Diabaig Formation in Scotland. The deposition within the Gunflint is unconstrained in all directions, and as well as recording lateral variation in facies, deposited in the same time period (e.g., as with Frustration Bay and Pass Lake), will also record stratigraphic changes related to transgressions and regressions, as clearly recorded at Centennial Park and Boulevard Lake. Thus, while individual lithofacies can be related to the overall model, present day locations in which they occur may be preserving fundamentally different time periods, or a stratigraphic transect through them. As mentioned above, the fragmentary nature of the Gunflint outcrop has precluded reconstruction of a clear continuous stratigraphy. While the sedimentological observations presented here serve to revise the overall depositional setting of the Gunflint Formation, they cannot 'fill in the gaps' and provide any more complete a stratigraphic picture than previous works (Fralick & Barrett 1995, Goodwin 1956). Laterally diachronous transgressions and regressions within the basinal environment may bring about non-linear alternations between lithofacies, which cannot be decoded until a full regional stratigraphy is built up, perhaps through borehole studies.

7.3 Microbiota

7.3.1 Background

The Gunflint Iron Formation has become synonymous with the classic microbiota that it was found to contain. In fact, in relation to the extent and variety of lithofacies

within the Formation, microfossils have been described from relatively few localities. Elso Barghoorn and Stanley Tyler worked on the deposits from Schreiber beach between 1952 and 1958 (private communications, now held at the Department of Earth Sciences, University of Oxford), resulting in their initial report of a novel assemblage of microfossils dating to almost 2 Ga (Barghoorn & Tyler 1965). Their findings have been added to in numerous subsequent studies (Awramik & Barghoorn 1977, Knoll et al. 1978, Schelble et al. 2004) and while the affinity of many of the forms remains unresolved (e.g. Krumbein 2010), they are still taken to represent the oldest diverse assemblage of demonstrably biogenic microfossils.

Particularly characteristic of the Gunflint assemblage are septate trichomes of *Gunflintia* spp., spheroidal and ovoid coccoids of *Huroniospora* spp., and more complex forms of unresolved affinity: *Eosphaera* sp., *Eoastrion* sp., *Kakabekia* sp., and *Archaeorestis* sp., among others (Awramik & Barghoorn 1977, Barghoorn & Tyler 1965, Knoll et al. 1978, Schelble et al. 2004). Similar assemblages have been recognised across the world at approximately this time period: including microbiotas from the Duck Creek Dolomite of north west Australia (Knoll & Barghoorn 1974); the Frere Formation, Nabberu Basin, Western Australia (Tobin 1990); and Belcher Islands, North West Territories, Canada (Hofmann 1976). It has been proposed that the characteristic morphotypes be used for biostratigraphic correlation for the Labradorian period of 2.0 to 1.6 Ga (Sergeev 2009).

7.3.2 Fossil recovery and biogenicity

Revisiting the Gunflint Iron Formation nearly 50 years after the first reports (Barghoorn & Tyler 1965), and with an awareness of the full diversity of the characteristic Gunflint assemblage, it is of interest to conduct higher resolution investigations on those microfossils, that may help to resolve some of the unanswered questions of the Gunflint microbiota and its palaeoenvironmental context.

For this micropalaeontological study, material collected by the author is used in combination with samples collected by members of the Oxford Working Group. Samples are housed in the Department of Earth Sciences; sample numbers given in Appendix B.

7.3.2.1 Identifiable fossils

Petrographic thin sections of cherts, carbonates and siliciclastic rocks from all studied lithofacies were examined by optical microscopy to identify organic-walled microfossils. Only three localities yielded assemblages of identifiable microfossils: Schreiber Channel, Kakabeka Car Park, and Frustration Bay. Of the 22 taxa taxonomically described from the Gunflint Formation, only 12 were observed in these samples, and this is perhaps testament to the extreme rarity of those taxa of *incertae sedis* that were initially described from just one specimen (e.g. *Xenothrix inornata* Awramik & Barghoorn 1977).

The stromatolitic domes of Schreiber Channel yielded by far the richest assemblage of microfossils, with multiple specimens of each taxon observed in various states of degradation. The assemblages of Kakabeka Car Park and Frustration Bay are poorer in comparison, containing representatives of just three and four taxa respectively. Those taxa that do occur are the simplest filamentous and coccoidal forms of *Gunflintia* and *Huroniospora*, which are also the most abundant in the Schreiber Channel assemblage.

7.3.2.2 Biogenicity

As discussed in Chapter 3, multiple lines of evidence are required to verify the age and biogenicity of organic structures in ancient rocks. Within the Gunflint Formation, the preservation of three-dimensional microfossils by complete chert occlusion, and imaging of these fossils by petrographic thin section, is sufficient to demonstrate that they are native to the chert, not contaminants. Establishing a biological origin of the organic structures is more of a challenge, especially in these chemical sediments where multiple phases of crystal growth and recrystallisation may have occurred and disrupted biological and non-biological material in unpredictable ways. In particular, it is important to distinguish true biological structures from pseudofossils. One notable type of pseudofossil is discussed below: carbon-containing microspheres.

The stratiform cherts at Kakabeka Car Park are rich in carbon. This carbon is mostly disseminated through the siliceous matrix with no identifiable microfossil structure. In certain horizons, however, there are dense concentrations of microscopic

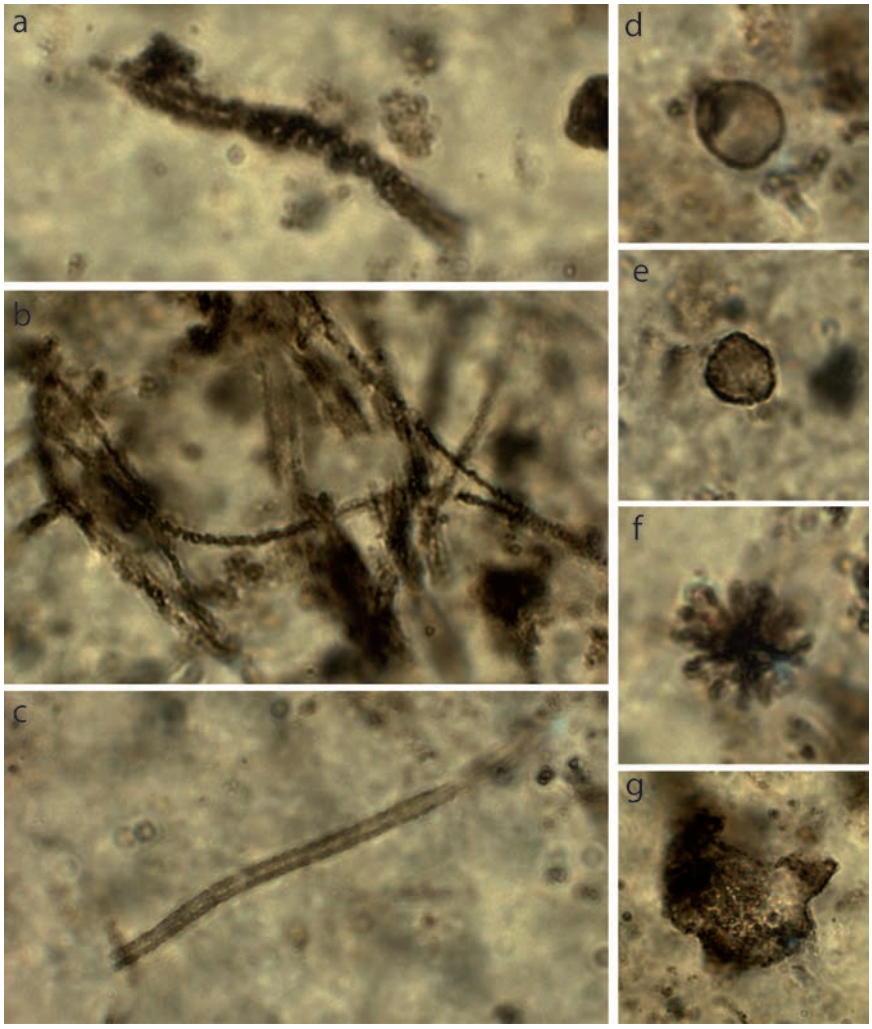


Figure 7.11: Organic walled microfossils identified from resampled cherts of the Gunflint Formation. (a) Wide tubular structures identified as *Gunflintia grandis*. (b) Networks of narrow filamentous structures identified as *Gunflintia minuta*. (c) Hollow smooth-walled tubular structure identified as *Siphonophycus inornatum* (d) Thin walled coccoid structure identified as *Huroniospora psilata*. (e) Thick and finely reticulate-walled coccoid identitifed as *Huroniospora microreticulata*. (f) Radiating stellar filaments identified as *Eoastrion simplex*. (g) Irregularly lobate structure formed from disseminated organic particles, but with a clear perimeter, tentatively identified as *Archaeorestis magna*. Scale bars: a-f, 10 μm; g, 100 μm. All fossils figured from sample SC5-05 from Schreiber Channel. Not shown here are *Huroniospora macroreticulata*, *Kakabekia umbellata*, *Eoastrion bifurcatum*, *Animikea septata*, and *Corymbococcus*, owing to difficulty in imaging.

	Schreiber Beach	Kakabeka Road Cut	Frustration Bay
Gunflintia grandis	x	x	x
Gunflintia minuta	x	x	x
Huroniospora microreticulata	x		
Huroniospora macroreticulata	x	x	x
Huroniospora psilata	x		
Kakabekia umbellata	x		
Eosphaera tyleri			
Eoastrion simplex	x		
Eoastrion bifurcatum	x		
Animikea septata	x		x
Enterosphaeroides amplus			
Archaeorestis schreiberensis			
Archaeorestis magna	x		
Corymbococcus hodgekissii	x		
Xenothrix inornata			
Thymos halis			
Exobrachium triangulum			
Galaxiopsis melanocentra			

Table 7.1: Summary of previously described Gunflint taxa, and their recovery from three fossiliferous sections in this study.

spherules 40-60 μm across, made from carbonate material, in which carbon is especially concentrated (Figure 7.12). At first appearances, these have the appearance of coccoid organic-walled microfossils, and may easily be misinterpreted as such. Several clues point to the abiogenic origin of these structures however.

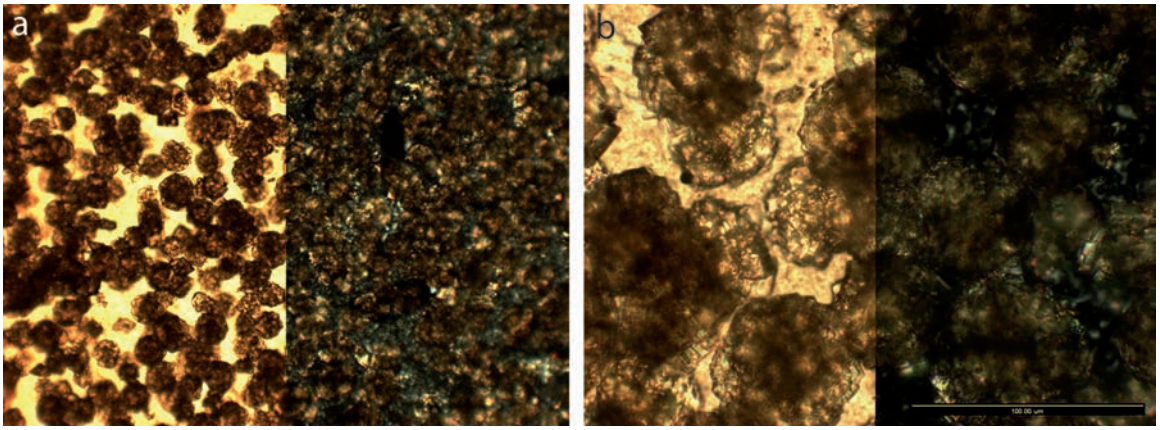


Figure 7.12: Carbon-containing carbonate microspheres, identified here as pseudofossils. (a) General view of dense packing of identical microspheres within a single layer. Left hand side, plane polarised light; right hand side, crossed polarised light. Scale bar 1 mm (b) Higher magnification view of carbonate microspheres, showing their angular crystalline edge and carbon concentrated at the edges. Left hand side, plane polarised light; right hand side, crossed polarised light. Scale bar 100 μm. Both images from sample KCP-03 from chert-carbonates at Kakabeka Car Park.

Firstly, the spheres themselves are of extremely uniform size and shape, where true biological structures will be subject to ontogenetic variations in their size as well as taphonomic or mutational changes to their preserved morphology, and so could be expected to show more considerably more variation than this. Secondly, the relationship of the carbon to the carbonate is constant and characteristically abiogenic. Carbon confined only to the angular crystal boundaries of these spherules, when combined with the observation of disseminated carbon throughout the matrix, indicates that the organic compounds were swept along by a crystallisation front as carbonate formed with the chert, and are found today where that crystallisation ended around the edges of the spherules. Finally, at high magnification, the edges of the carbonate crystallites do not appear smooth and rounded, as would be seen in coherent organic-walled vesicles. They appear jagged, as radiating crystals that make up the spherules have grown to approximately the same length, but this regularity breaks down at higher magnification.

7.3.3 Applying taphospace

The concept of taphospace introduced in Chapter 4 can be applied to the organic walled microfossils preserved in the cherts of the Gunflint Formation, to characterise the taphonomic environment in these lithofacies, and to provide some perspective on the differing assemblages in each.

Figure 7.13 illustrates the taphospace plots for the three lithofacies from which microfossils were recovered. In the following discussions, the qualitative plots are visually compared, however future refinements of the taphospace scheme may enable more robust statistical comparison.

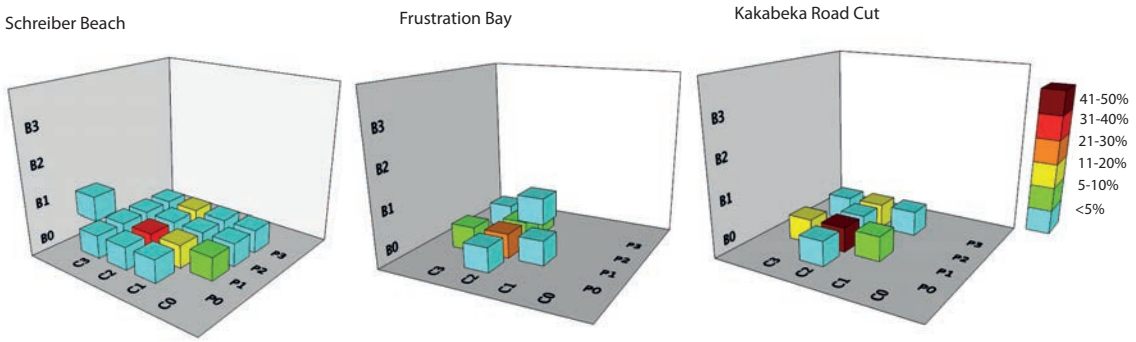


Figure 7.13: Taphospace plots for organic-walled microfossils recovered from three Gunflint lithofacies. a) Schreiber Channel. N=100. From sample SC5-05; (b) Kakabeka Car Park. N=50. From sample KCP-03b; c) Frustration Bay. N=50. From sample FBY-10. Sampled taxa for each lithofacies are shown in Table 7.1 For explanation of degradational indices, see Chapter 4.

The Schreiber Channel assemblage preserves taphonomic grades ranging through all levels of chemical degradation, but with the majority (91%) of fossils having undergone at least some chemical changes (Figure 7.13). Carbon flocculation of the wall is common (55%), and carbon dissemination, while observed (9%), may be underrepresented here, owing to the typical loss of identifiable structure at this stage of chemical degradation and the large amount of particulate carbon observed in the chert matrix. The degree of physical damage is quite low (32% at grades P2 and P3), and is likely due to the fact that these fossils have not been transported far, and are preserved where they grew, in stable stromatolitic mats. Almost no biological degradation is preserved, and this may also be due to the rapid *in-situ* occlusion of the microbiota—there is little chance of bacterial heterotrophy before older generations

of microorganisms are occluded and entombed in chert.

Both the Kakabeka Car Park and Frustration Bay taphospace plots appear very similar, with degradation being dominated by chemical flocculation of the cell wall (74% at the Kakabeka Car Park, and 90% at Frustration Bay)(Figure 7.13). As with the Schreiber Channel assemblage, much carbon is disseminated within the matrix of the chert, and is concentrated into dark organic-rich laminae; these features may represent the disseminated remains of microorganisms that have since lost their characteristic morphology and so underrepresentation of carbon dissemination is inferred. The narrower range and higher taphonomic grade compared with the Schreiber Channel assemblage is related to the differing habits of the cherts between the two lithofacies. Stratiform chert carbonates are likely to be more slowly and cyclically precipitating than the stromatolitic cherts, probably owing to the less active biological component of the sediment here. This allows more time for considerable chemical degradation of the organic matter, and concentration of it into discrete laminae before lithification of the sediments. The poor representation of biological degradation here may be due to the intense chemical alteration, masking potential biological signals. Alternatively, the absence of microbial heterotrophic characters may indicate an absence of heterotrophs themselves, implying incomplete ecological recycling at this time. This could only be verified by a systematic absence of biological decay, in an otherwise relatively pristine assemblage.

The high taphonomic grades of the stratiform chert facies help to explain the differences between the taxa preserved in these and the stromatolitic chert lithofacies. Only the morphologically simple and more robust taxa were unequivocally identified in the Kakabeka Car Park and Frustration Bay assemblages, and it is likely that these were the taxa more able to resist the considerable chemical attack which evidently occurred during formation of the cherts. Those taxa which were rare (e.g.*Archaeorestis magna*) or delicate (e.g. *Huroniospora psilata*) to begin with, would be the most susceptible to taphonomic attack, and so most likely to be lost from the assemblage. Given this high degree of taphonomic loss, it is not possible to accurately assess any original differences in composition between the different assemblages.

Understanding the taphonomic alterations occurring within the Gunflint cherts also helps to shed further light on some of the formally described taxa of the Gunflint assemblage, in particular those for which only the holotype exists. While their

antiquity and biogenicity may have been demonstrated, taxa such as *Exobrachium triangulum*, *Xenothrix inconcreta* and *Thymos halis* may not deserve attention as individual species and may instead represent advanced taphonomic variants of other taxa. Such an inference cannot be conclusive without recourse to the original material and its associated taphonomic grade, but caution should be taken before interpreting individual fossils as new pristine taxa, when taphonomy in this environment is clearly such a powerful modifier.

7.4 Macroscopic Structures

A complete palaeontological study of the Gunflint Formation should not be limited to the preserved microbiota, as it is now understood that colonies of microscopic organisms can create macroscopic features visible not only as stromatolites, but also in clastic rocks (Noffke 2010 and Chapter 5). Stromatolites have long been recognised from the classic Schreiber Channel locality of the Lower Gunflint Member, but it may be possible to recognise other biogenic macrostructures elsewhere in the other lithofacies. Microbially-induced sedimentary structures (MISS) as defined by Noffke (2010) are expressly defined to describe those structures in siliciclastic environments, and so direct translation of these techniques to the predominantly chemical sediments of the Gunflint Formation is not straightforward. There are some siliciclastic environments however, such as the tuffaceous shales, which may be assessed for MISS, and shallow-water granular carbonates behave in similar ways to clastic sediments, so some application of the term and the biogenetic principles is possible, and is here attempted.

7.4.1 Stromatolites and stratiform lamination

Domal stromatolites have been reported from the classic Gunflint microfossil locality at Schreiber Channel, and are accepted as biogenic owing largely to their similarity in morphology and construction to modern day stromatolites such as those at Shark Bay, Australia. The comparison is a close one, with the 2 Ga-old Gunflint examples exhibiting many features observed in modern day structures: millimetre-scale laminations defined by micro-scale changes in mineralogy, microdigitate columnar structures within the domes themselves, nucleation on topographic highs in the substrate, and the preservation of microfossils within the rapidly lithifying substrate (Figure 7.14). One major difference between the Palaeoproterozoic and modern structures is their mineralogy: being formed of chert and calcium carbonate respectively. Although

there is some evidence to suggest that some of the Gunflint cherts had carbonate precursors (Sommers et al. 2000), this difference may also be due to fundamentally different water chemistries in the Precambrian and the Phanerozoic oceans (e.g. Siever 1992).

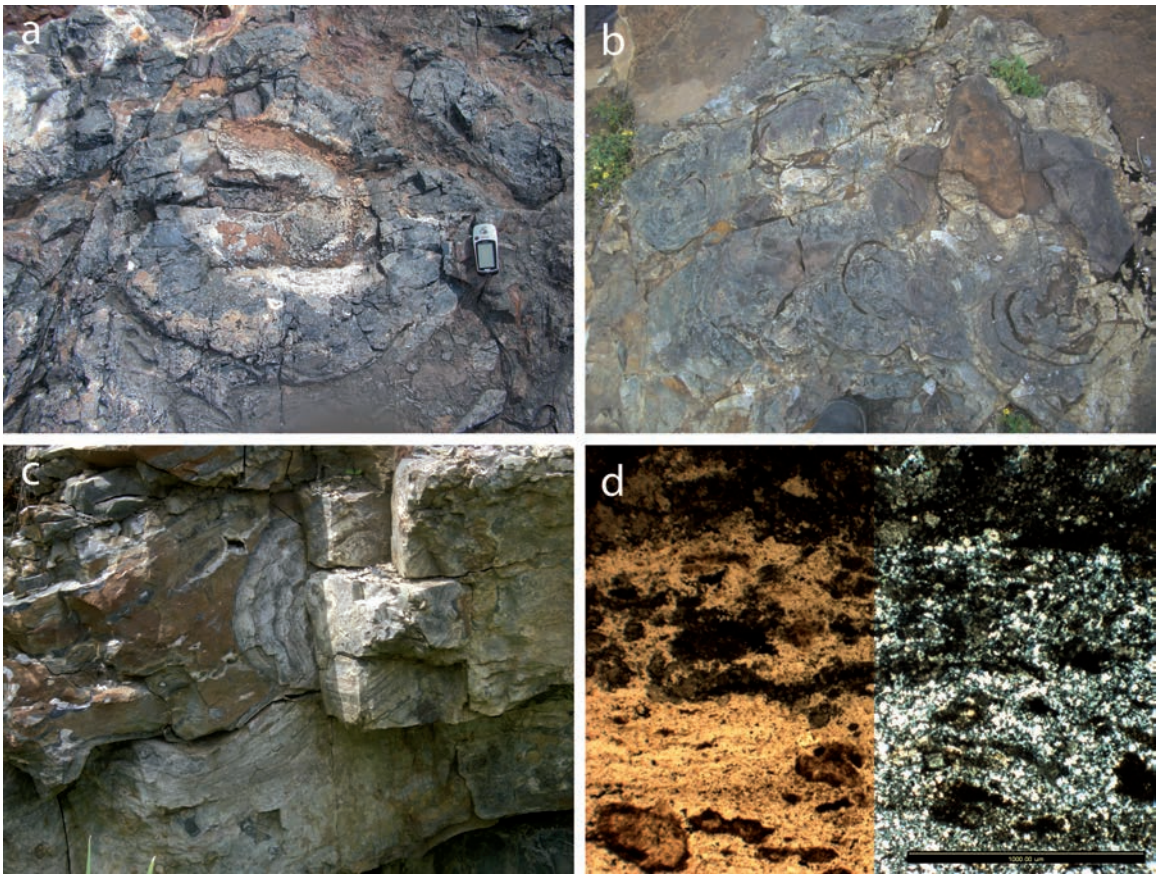


Figure 7.14: Summary of stromatolitic structures in various Gunflint lithofacies, and potentially biogenic lamination within stratiform cherts. (a) Parallel cross section through domal stromatolites at Schreiber Channel. (b) Parallel cross section though domal stromatolites at Boulevard Lake. Field of view approx. 2 m. (c) Perpendicular cross section through stromatolite dome outcropping at Kakabeka Road Cut. Field of view approx. 2 m. (d) Wispy organic laminations in stratiform cherts from Frustration Bay. Scale bar 1 mm.

Stromatolitic cherty domes are also present in other lithofacies of the Gunflint Formation: in the lower chert-carbonate sections at Boulevard Lake; and within the layered iron-rich cherts at Kakabeka Road Cut. Both of these examples preserve interacting dome-shaped structures up to 70 cm across, with laminations of alternating mineralogy, and microdigitate columns or undulations. Their mode of formation is

inferred to be identical to the Schreiber Channel domes, in similar intertidal depositional settings.

Identifying stromatolitic layering in cherts becomes more problematic in the stratiform lithofacies of the formation. Without the direct comparison to dome-forming microorganisms today, and lacking digitate structures of any scale, lamination within planar-bedded cherts is difficult to distinguish as biological or physical in origin. In addressing this problem, one criterion defined by Noffke (2010) may be applied: organic binding mat microfabrics. When viewing these stratiform cherts and their associated grainstone carbonates in petrographic thin section cut perpendicular to bedding, densely packed organic layers may indicate the presence of an endobenthic or epibenthic microbial mat. Such undulating, wispy laminations were observed in abundance, in particular in sections from Frustration Bay, and Kakabeka Car Park. Similar structures were seen in the shales in the upper part of the Boulevard Lake outcrop, but were pyritic in mineralogy. The pyritisation of once organic laminae may be brought about by the creation and maintenance of reducing conditions in the sediment, the mechanism and consequences of which are discussed below.

7.4.2 Non-stromatolitic macroscopic structures

In searching for potentially biogenic macroscopic features in the Gunflint sediments, more is to be gained by studying the bedding plane surfaces for ordered wrinkle structures, such as those identified in the Torridon rocks (Chapter 5). Such anomalous structures were identified at three localities, and their morphology and likely biogenicity is here presented and discussed.

7.4.2.1 Kaministiquia River Eastern Shore

On the surfaces of the fine siliciclastic shales of this lithofacies, a number of different structures were observed, that can be split into two distinct categories: shale-displacing protrusions, and networks.

Shale displacing protrusions occur in a spectrum of surface morphologies, ranging from isolated nodes up to 1 cm across and 0.5 cm high (Figure 7.15a), through chain-like structures of up to ten nodes in a linear pattern around 7 cm long, 1 cm wide and 0.5 cm high (Figure 7.15b), to smooth tubular structures up to 10 cm long and much

thicker, reaching up to 2 cm high (Figure 7.15c). While these three morphologies are quite distinct, together they form a transition from isolated nodes, fusing into linear 'chains', and subsequently growing into a larger structure. Transverse section reveals all of these structures to contain from pale-blue chalcedonic quartz with a more or less homogenous structure. These chalcedony nodules displace the shales above and below, and their morphology is impressed in negative hyporelief and positive epirelief on their top surface, and positive hyporelief and negative epirelief on their lower surface.

These are striking features within the otherwise planar-laminated shales, and alone, the surface expressions of the nodules may be postulated as biological in origin, owing to their sporadic regularity. But the chert nodules themselves show no sign of being confined to biological structures, and the range of morphologies they display are at times profoundly non-biological. When searching for an explanation as to their presence, organic particles may be invoked as nucleation sides for the chalcedony, but no trace of these or any other grains were found in the interior of these nodules. The structures must therefore be regarded as abiogenic until additional information can prove otherwise.

Also within these shales are network structures in positive epirelief, with corresponding 'elephant skin'-type patterns in negative hyporelief on the counterpart, superficially resembling the networks described from the Torridon sediments (Callow et al. 2011 and Chapter 5). Two typical morphologies of these networks are shown in Figure 7.15f and g: nodal networks with polygonal structure (Figure 7.15f), and sinusoidal ridges without nodes (Figure 7.15g).

While tempting to observe these structures' superficial resemblance to the Torridon wrinkle mats and apply the same logic to argue for their biogenicity, there are important differences between the two, which call the Gunflint examples into question. Firstly, the apparently nodal network in Figure 7.15f frames rectangular domains, created by four-way, and occasionally T-shaped junctions at nodes with 90 degree angles rarely seen in the biogenic structures of the Torridon. On closer inspection, these nodes and their connecting ridges are made from subtly coarser silty material, and the structure takes on the appearance of intersecting cracks. Such cracks may form during dewatering or sediment equilibration (Plummer & Gostin 1981), but there is no sedimentological evidence for sealing by organic mats (Noffke

2010). The second morphology, formed of intersecting sinusoidal ridges, does not have the nodal characteristic of most wrinkle structures described from the Torridon (Chapter 5), and are also formed from material coarser than the surrounding sediment. Thus for these structures, an abiogenic mode of formation through dewatering fracturing seems the most parsimonious.

7.4.2.2 Centennial Park

At Centennial Park, macroscopic patterns of pits and protrusions can be observed on the bedding surfaces of the deep, laminar bedded shales marking the first transgressions of this sequence. Irregularly distributed across the bedding surfaces, they are often concentrated in patches up to 50 cm across. Occurring as both positive (pustulae) and negative (pits) epirelief on the top surfaces of exposed bedding planes, individual features are up to 2 cm across. Single concentrated patches will contain only either pits or protrusions, but this varies laterally across single bedding planes and between beds.

These irregular features superficially resemble some of the degradational structures from the Avalonian rocks of Newfoundland, informally named 'pizza disks', but in the absence of identifiable undegraded body fossils and considering the great age of the Gunflint rocks, the comparison must end there. Transverse sections reveal that, as at the eastern shore of Kaministiquia river, the pits and protrusions are formed from shales displaced around pale blue chalcedonic nodules, which in this outcrop have remained isolated, even when densely packed. As with those previously described features, it is possible that these nodules nucleated from degrading biological matter—and the lateral discontinuity of these features across the bedding planes may corroborate such an interpretation—but no such organic matter was found in or around the chalcedonic nodules.

Rarely occurring on a few bedding planes are very fine network-like reticulate structures, that appear to be constructed from pointed nodes and short connecting limbs (Figure 7.15h), as described from the Torridon rocks. The extremely fine scale of these networks makes the geometry and consistency of the structure difficult to resolve, and too few examples were observed to collect adequate measurements.

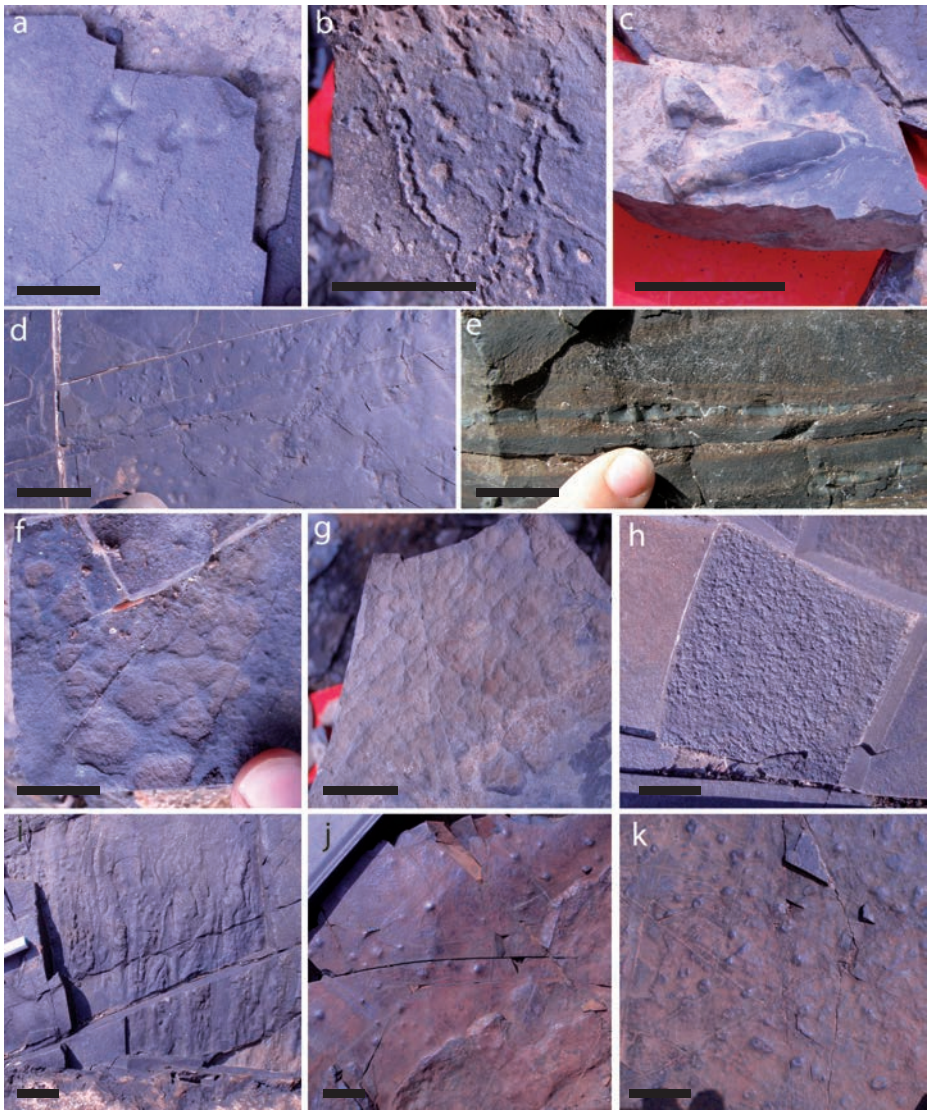


Figure 7.15: Candidate microbially induced macrostructures in various Gunflint lithofacies. (a-c, f-g) from shales on Kaministiquia eastern shore; (d-e, h) from deep water shales of Centennial Park; (i-k) from pyritic shales at Boulevard Lake. (a) Isolated protrusions in positive epirelief, irregularly distributed but locally concentrated. Scale bar 2 cm. (b) Chain-like structure in negative epirelief, formed of linearly merging pits. Scale bar 5 cm. (c) Thick tubular structure containing pale blue chalcedonic quartz displacing the shale above and below. Scale bar 5 cm. (d) Irregularly disitributed pits and ridges across adjacent bedding surfaces. Scale bar 10 cm. (e) Perpendicular section of shales, showing pale blue chalcedonic quartz displacing shale above and below. Scale bar 2 cm. (f) Nodes and connecting ridges with 90 angles in positive epirelief. Scale bar 1 cm. (g) Sinusoidal ridges with no nodes in positive epirelief. Scale bar 1 cm. (h) Very fine wrinkled structure with pointed nodes and short connections. Scale bar 1 cm. (i) Arumberia-like linear structures with flat-topped protrusions in sandy material. Scale bar 1 cm. (j) Sharply rounded protrusions in positive epirelief in pyritic shales. Scale bar 1 cm. (k) Ring shaped protrusions with central depression, in positive epirelief in pyritic shales. Scale bar 1 cm.

Their resemblance to the Torridon wrinkle structures is noted, but their overall similarity and therefore their biogenicity cannot be confirmed until further samples are discovered.

7.4.2.3 Boulevard Lake

The pyritic shales at the top of the section exposed at Boulevard Lake, in addition to the putatively microbial layering visible in transverse section, also contain macroscopic structures more convincingly biogenic than any observed in other Gunflint lithofacies.

Irregularly distributed across the bedding surfaces, where slightly coarser material is exposed, are sub-parallel linear ridges, occasionally bifurcating, up to 0.5 cm across and several millimetres high. Similar structures have been described from a range of Proterozoic deposits as the microbial fabric 'Arumberia' (McIlroy & Walter 1997), and are thought to represent folds in a coherent microbial mat formed by current action (Callow & Brasier 2009)(Figure 7.15i). Set within the low relief areas of this fabric, are dense concentrations of flat-topped, rounded protrusions around 0.5 cm across and 1-2 mm high.

Rounded protrusions also occur in the finer portions of pyritic shale, laterally discontinuous across the bedding surfaces and densely concentrated in places. Protrusions range from 3 mm to 15 mm in diameter, and are of two distinct morphologies: with sharply rounded tops (Figure 7.15j), and with central depressions forming a ring of positive relief (Figure 7.15k).

The protrusions in the shale and coarser material here differ considerably from those observed in the Kaministiquia eastern shore and Centennial Park lithofacies. Transverse section reveals them to be infilled with clastic material, rather than nodular chalcedony, so their formation is likely synchronous with sediment deposition. Two possibilities can be considered for their formation. Firstly, an abiogenic interpretation, that the structures represent gas bubbles escaping from the sediment. Secondly, that they represent megascopic colonies of prokaryotic organisms, similar to modern day *Nostoc* balls, that have since decayed away. There is little sedimentological evidence that can distinguish between these two possibilities, as both gas bubbles and microbial colonies would have consistent size ranges, potentially collapse to form ring structures, and be concentrated in specific areas. Parsimony favours the abiogenic

interpretation, all else being equal. For gas bubbles to form, however, some temporary sealing of the sediment is necessary, and here the putative biogenic origin of the pyritic laminae may be invoked to fulfil this role. Thus, even an abiogenic interpretation for these structures is intimately linked with the likely microbial colonisation of the sediment surface or sub-surface.

7.5 Phosphate

Search for phosphate in the Gunflint Formation was carried out in collaboration with MESci student Sean McMahon (McMahon 2010). In the following section, all field observations were made by the author, laboratory analysis and imaging were carried out together, and all interpretations are the author's own.

7.5.1 Previous work

While the Gunflint is well known for its characteristic associations of chert, iron oxides and carbonate, formed in a predominantly chemical setting, reports of phosphate minerals have been scarce. To the author's knowledge, the only previously reported finding was of apparently 'common' apatite crystallites among the white chert in stromatolites of Schreiber Channel (Mojzsis & Arrhenius 1998). Despite extensive subsequent search in petrographic thin section and under SEM, this finding could not be repeated, and so remains unverified. If phosphate does exist in these rocks at this locality, it must be confined to small scale microenvironments unrepresentative of the depositional area as a whole.

7.5.2 Phosphate in the Gunflint Formation

After undertaking a renewed sedimentological and petrological search, phosphate was found within several other lithofacies of the Gunflint Formation, occurring in varying habits and mineral assemblages. This discovery was made by the author in collaboration with Sean McMahon as part of a research project in support of a MESci qualification from Department of Earth Sciences, University of Oxford. In the following sections, analyses were conducted collaboratively, and some images have been reproduced from the report submitted for that work (McMahon 2010).

7.5.2.1 New findings

Phosphate was actively sought amongst the chemical cherts and carbonates of the Gunflint at all of the localities visited and detailed above. Identification of phosphate in the field proved especially problematic, as many of the black cherts have a waxy lustre elsewhere characteristic of phosphate. The presence of phosphate within samples was tested for using ammonium molybdate (for test procedure see Appendix A), in combination with optical and scanning electron microscopy and EDX mapping. Although the qualitative ammonium molybdate testing suggested phosphate in 10 of the 20 candidate samples, just four localities were found to contain measurable amounts of phosphatic material that could be identified, imaged and quantified. They are detailed below, ordered by increasing phosphate content: Kakabeka Falls Car Park; Frustration Bay, Kaministiquia River Western Shore, and Boulevard Lake.

Kakabeka Falls Car Park Phosphate in this lithofacies is not common, not evident in the field and identified through ammonium molybdate testing only within the dark black cherty laminae. EDX mapping revealed it to be confined to small amorphous patches and as individual miniscule crystals of apatite spread diffusely through particular laminae (Figure 7.16). Phosphatic minerals appear most abundant here in cherty domains rich in carbon, and in association with carbon-rich siliceous microspheres. Where carbon forms undulating laminae, phosphate is present but is diffuse around those laminae, both above and below. Amorphous patches of phosphate found with no associated carbon may represent small scale reworking of the original diffuse phosphatic laminae.

Frustration Bay Although phosphate in this lithofacies is generally fairly scarce, isolated apatite-rich grains up to 1 mm across occur within the microbial cherts and as isolated clasts among the breccia embedded in the carbonate grainstone (Figure 7.17). These are commonly sub-angular to rounded, and host ellipsoidal or irregular siliceous inclusions around 5-10 μm across. The grains' large size, competence, and lack of internal structure implies that they were formed as part of a larger structure such as a phosphatic hardground, that has since been reworked during the many periods of pervasive brecciation. The sedimentological structures and associated glauconite grains at this locality would suggest a setting with low net deposition that would favour formation of such a hardground, but no such structure was identified in the field or in petrographical study. Although not impossible that phosphatic hardgrounds could be completely destroyed by a reworking event, leaving only these scattered

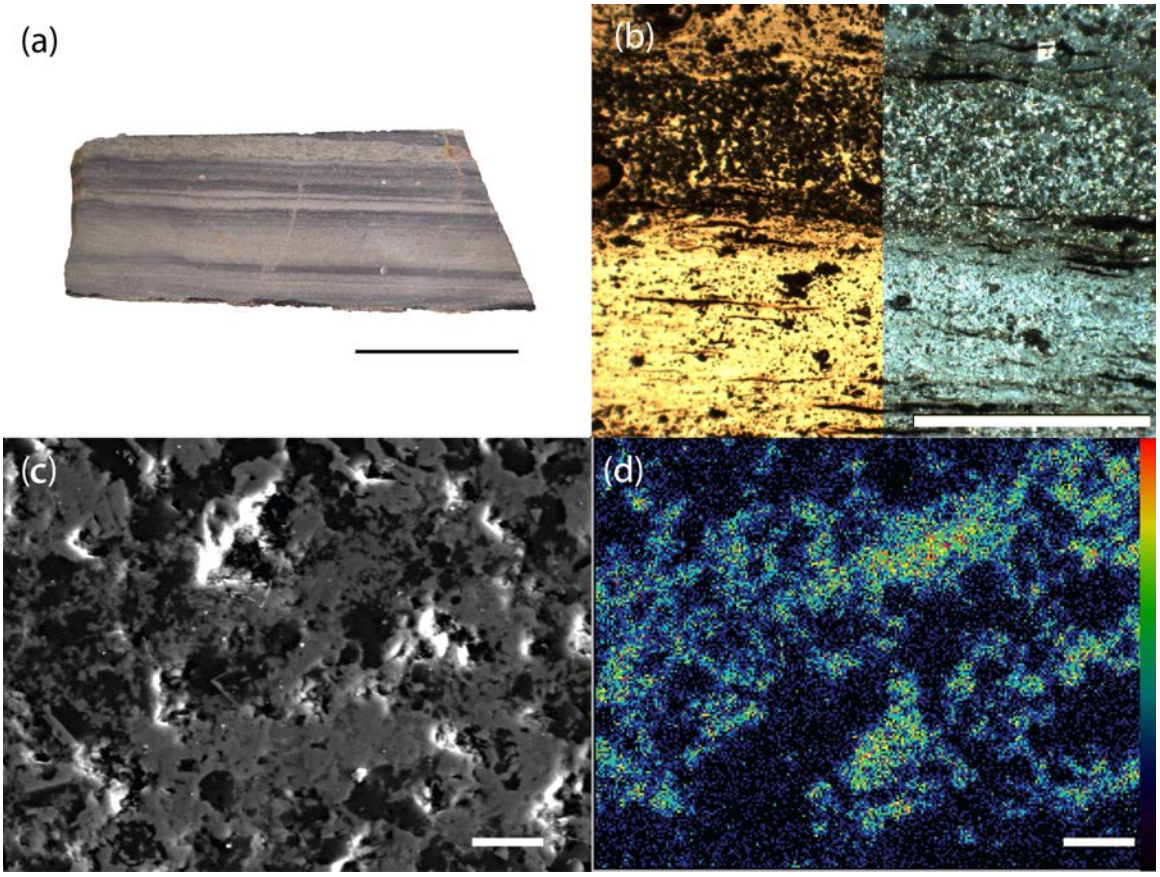


Figure 7.16: Plate illustrating occurrence of phosphate in the ferruginous banded chert-carbonate at the parking lot of Kakabeka falls. a, Cut hand sample image illustrating alternating layers of cherty material and carbonate. Scale bar 3 cm. b, Optical photomicrograph (plane polarised light on the left, cross polarised light on the right) illustrating enigmatic spheroids in a cherty matrix. Scale bar 1 mm. c, BSE narrowfield image of polished thin section surface. Scale bar 10 μm. d, EDX phosphorus map of field of view shown in (c). Brighter colours indicate higher concentrations. Phosphorus is concentrated in small crystal domains which define a broad banding, not visible in the BSE image. Scale bar 10 μm. Sample KCP-03.

clasts, there is also the possibility that the phosphate is allochthonous to this setting, being secondarily washed in during rare storms which may be invoked to explain the brecciation.

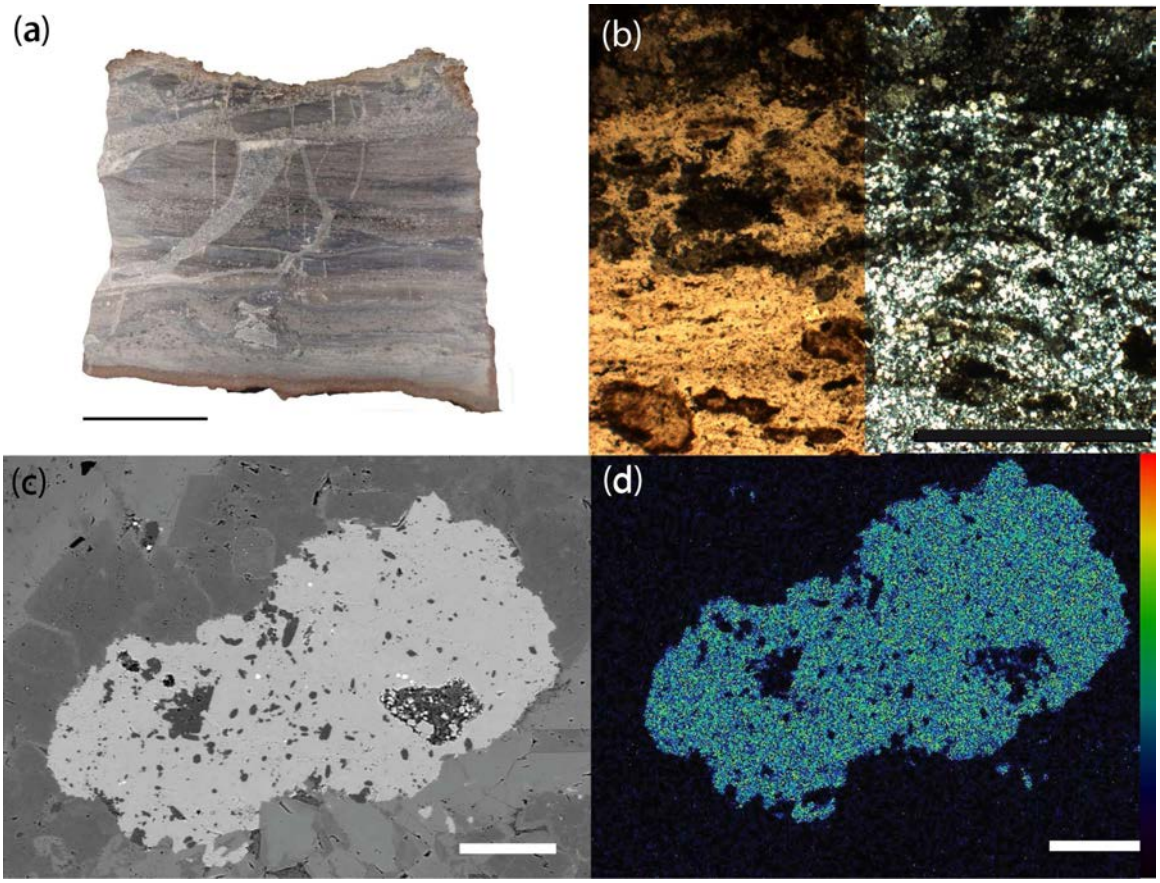


Figure 7.17: Plate illustrating phosphate occurrence in the grainy and banded chart-carbonates at Frustration Bay. a, Cut hand sample image showing brecciation of the laminate cherts and carbonates. Scale bar 3 cm. b, Optical photomicrograph (plane polarised light on the left, cross polarised light on the right) illustrating a cherty groundmass with carbonate bands and domains, especially prominent towards the top of the image. Scale bar 1 mm. c, BSE image of polished thin section surface. Scale bar 100 μm. d, EDX phosphorus map of field of view shown in (c). Brighter colours indicate higher concentration. Phosphate is clearly concentrated within the intraclast. Scale bar 100 μm. Sample FBY-10 from Frustration Bay.

Kaministiquia River Western Shore There is a small, but quantifiable amount of phosphate present in this unit. Ammonium molybdate testing yielded a weakly positive result within the pyritic shales, consistent with rare small grains of apatite in association with detrital clays and rutile. A much stronger positive result was

achieved when testing the volcaniclastic grainstone, and optical and scanning electron microscopy identified the characteristic distribution of phosphate minerals in this lithology (Figure 7.18). EDX maps reveal that calcium phosphate is concentrated into euhedral crystals that line the insides of vesicles of certain volcanic clasts. These crystals are all of a fairly consistent size range, between 2 and 4 μm, and are present in all the vesicles in any particular clast, so that some smaller pores are filled entirely by phosphate mineral. Larger vesicles contain just one layer of phosphatic crystals in contact with the volcanic glass, followed by further layers of carbonate or silica, or void filling microcrystalline chert.

The rounded nature of the volcanic grains making up the grainstone at this locality, as well as the cross-cutting channel relationships of the grainstone units through the shales, suggests that the grains are allochthonous to this setting. The occurrence of phosphate minerals in only some of the vesicular volcanic grains is consistent with this interpretation, implying these grains were derived from a specific, different location, or that phosphate formed in a local zone within a broad region subsequently reworked into these allochthonous deposits.

Boulevard Lake Phosphate was recovered from the pyritic shales and their interbedded grainstones at the top of this succession. These sediments are by far the most phosphate-rich of those observed within the Gunflint Formation. Phosphate here occurs in four identifiable characters (Figure 7.19).

Firstly, as finely disseminated sub-micron-sized crystals occur within the sediment in the spaces between pyritic laminae in the shales themselves (Figure 7.19g, h). The pyritic laminae undulate and appear wispy on a fine scale, draping rare detrital clasts. Phosphate-rich zones are confined especially to where these laminae are densely packed, and are likely to be autochthonous and authigenic. It is clear that the co-occurrence of the pyrite and the phosphate is of some significance.

Secondly, fine coatings and partial replacement of siliceous grains are seen within the grainstone layers of the shales (Figure 7.19e, f). The degree of phosphatic lining or replacement is not consistent between grains, and varies from sub-micron-thick discontinuous coatings, to almost complete replacement of siliceous grains by amorphous calcium phosphate. The formation of these grains by phosphatic replacement is interpreted from the observed spectrum of increasing phosphatic content, from none to

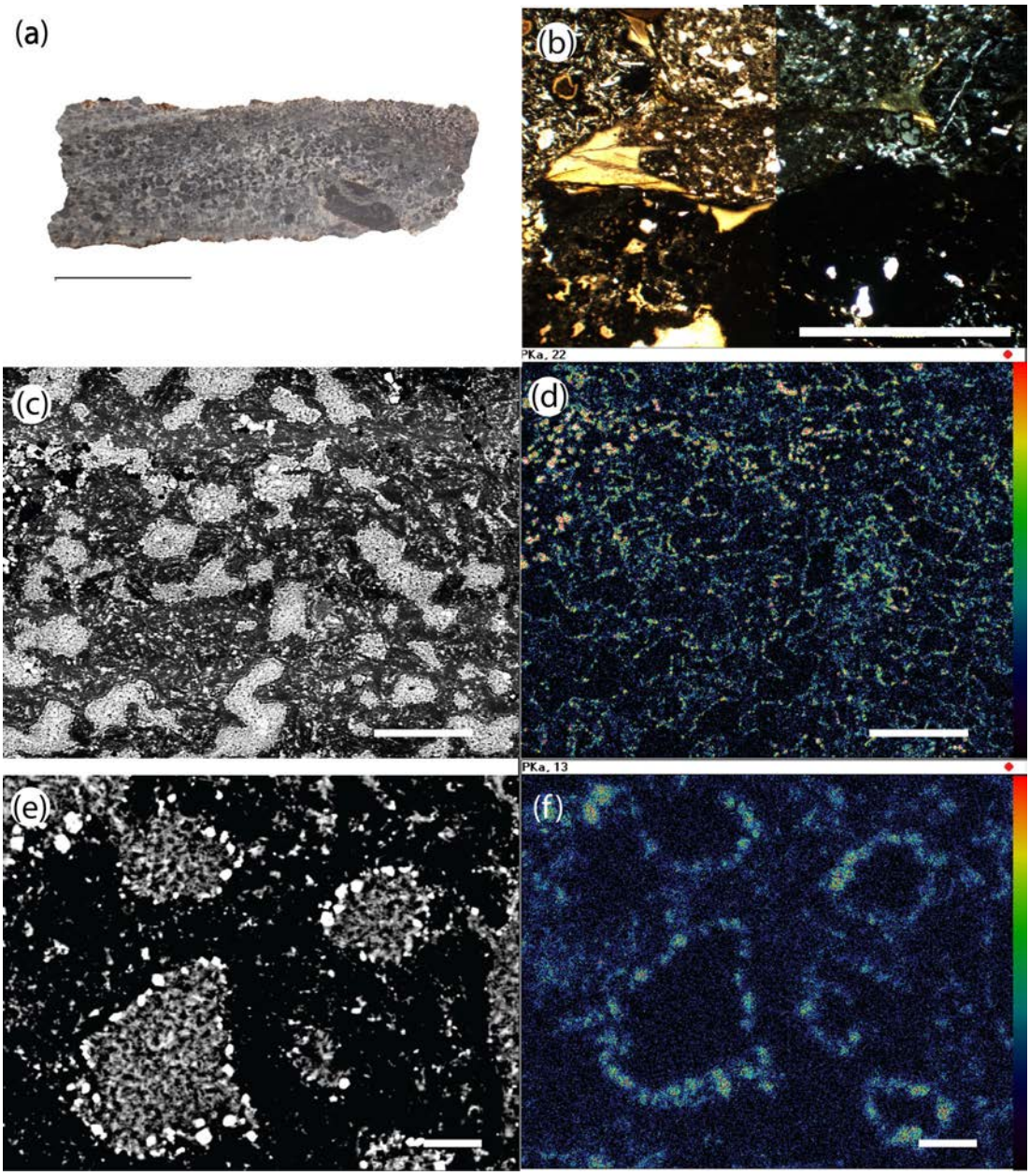


Figure 7.18: Plate illustrating phosphate occurrence in the volcaniclastic shale upstream of Kakabeka Falls. a, Cut hand-sample image showing granular nature of volcaniclastic material. Scale bar 3 cm. b, Optical photomicrograph (plane polarised light on the left, cross polarised light on the right) illustrating several vesicular volcaniclastic grains. Scale bar 1 mm. c, BSE image of polished thin section showing a vesicular volcaniclastic material with infillings. Scale bar 100 μm. d, EDX phosphorus map of field of view shown in (c), showing rimming phosphates. Brighter colours indicate higher concentrations of phosphorus. Scale bar 100 μm. e, BSE image of polished thin section, showing vesicles at a higher magnification. Scale bar 10 μm. f, EDX phosphorus map of field of view shown in (e), showing equant crystals concentrated in phosphorus. Brighter colours indicate higher concentrations of phosphorus. Scale bar 10 μm. Sample KRP-5 from western shore of Kaministiquia river.

approximately 90%, always penetrating from the outer surface of the grain. Grains that are approximately 50% replaced are clearly visible in the top right corner of Figure 7.19f.

Thirdly, reworked grains of phosphate occur concentrated along particular horizons within the grainstone layers (Figure 7.19c, d). These may represent siliceous grains that have undergone complete replacement by phosphate, but they differ considerably from the habit described above, in that they are often much more irregularly shaped, with a low sphericity, and they are commonly annealed together into a more consolidated horizon. Thus, a different mode of formation is hypothesised for these grains: authigenic precipitation of amorphous phosphate followed by a reworking event before full lithification, allowing plastic deformation and annealing of grains.

Finally, disseminated apatite grains, up to 500 μm in diameter, occur, particularly concentrated in certain shaley laminae, and seem to be associated with minor reworked grains. These grains probably owe their origin to similar authigenic precipitation as the annealed layers, but have undergone more significant reworking and transportation, mixing them with other reworked grains and depositing them amongst shales. A degree of lateral discontinuity in energy levels and sediment processes is likely, based on these observations.

7.5.2.2 Environments of phosphogenesis

The occurrence of phosphate at a limited number of lithofacies within the Gunflint Formation suggests that some non-cosmopolitan factors are at work at this time, driving the localised precipitation of this mineral.

Figure 7.20 illustrates the likely environmental settings of those phosphate-bearing lithofacies, within the idealised basin structure proposed above. The small amounts of dispersed phosphate at Kakabeka Falls Car Park occurs among stratiform chert-carbonates which are interpreted to have formed in a shallow lagoonal environment beneath the mean wave base. Frustration Bay has intraformationally brecciated, wave rippled cherts and carbonates that formed and were reworked in an intertidal setting with low net sedimentation; phosphate clasts are reworked amongst these sediments, but could also possibly have an allochthonous origin. Phosphate at the outcrop on the western shore of Kaministiquia River is more or less entirely confined to the rims and linings of the volcaniclastic grainstone, so although it is now found in rocks that

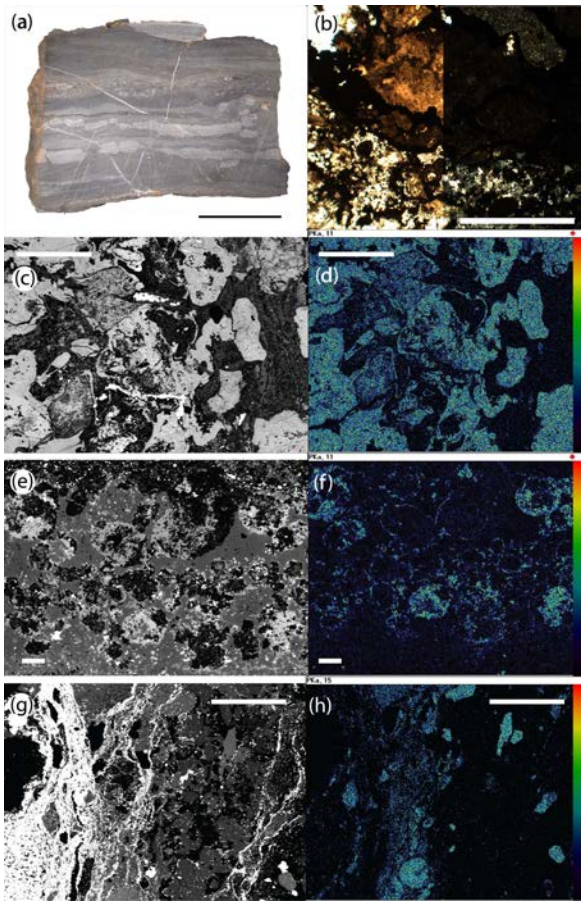


Figure 7.19: Plate illustrating phosphate occurrence in the ferruginous phosphatic chert-carbonate at Boulevard Lake. a, Cut hand-sample image of phosphate-bearing rock at this locality, showing brecciated bedding and 'crinkly' laminated structures. Scale bar 3 cm. b, Optical photomicrograph (plane polarised light on the left, cross polarised light on the right) illustrating iron oxide-rich laminae with both cherty (bottom) and phosphatic-rich (top) groundmasses. Scale bar 1 mm. c, e, g, BSE images of polished thin section. d, f, h, EDX phosphorus maps of field of view shown in c, e, and g, respectively. Brighter colours indicate higher concentrations of phosphate. c, Granular portion of rock. Image illustrates a range of mineralogies, including phosphate and pyrite. Scale bar 1 mm. d, Image shows phosphate to be considerably concentrated in the granular fabric. Scale bar 1 mm. e, Matrix supported granular fabric. Scale bar 100 μm. f, Image shows phosphorus concentrated in thin coatings of the grains and occasionally penetrating some way into selected grains. Scale bar 100 μm. g, Crinkly laminated fabric that also incorporates a fine granular texture. Scale bar 1 mm. h, Image shows phosphorus to be enriched within certain grains of the granular fabric. Scale bar 1 mm. All images from sample CBL-13 from Boulevard Lake.

formed in a deep bathyal setting, its authigenic growth probably occurred within an oscillating grainstone bar at shallower water depths. Finally, the abundant phosphatic minerals found within the pyritic shale at Boulevard Lake likely formed in deep waters beneath the wave base, although their preferential association with the coarser interbeds and small zones of reworking suggest that their growth occurred under more energetic and possibly shallower-water conditions.

There is considerable variation in phosphogenic environment in the Gunflint basin, ranging from deep siliciclastic to shallow subtidal zones dominated by chert formation. But phosphate minerals do not occur commonly with the chemical sediments, so phosphogenesis itself is not a cosmopolitan phenomenon in the basin. It may be that microenvironments conducive to phosphatisation are not readily identifiable in the sedimentological record, or that phosphate can form under a wide range of conditions. These ideas will be explored in the following section.

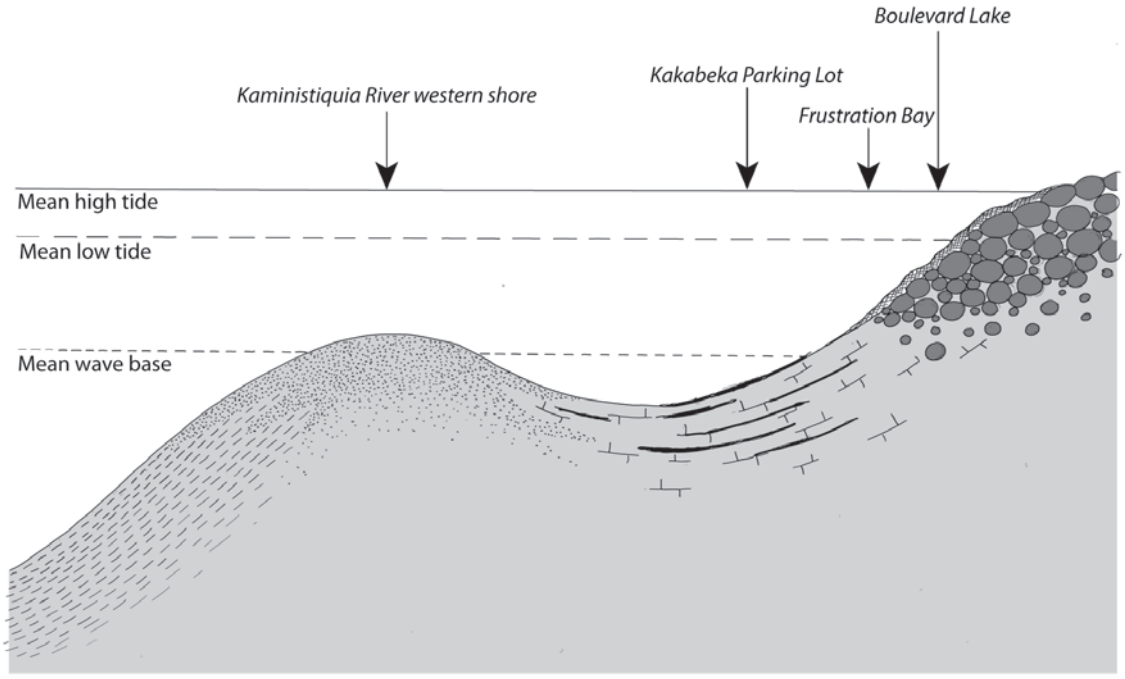


Figure 7.20: Likely loci of phosphogenesis within Gunflint sediments, in relation to the idealised, generalised, basin transect from Figure 7.10

7.5.3 Phosphatisation and Biota

Studies of the individual lithofacies of the Gunflint Formation has provided an extensive database of sedimentological characters which, when combined with the small occurrences of phosphate found in these rocks, can offer insight into the formation of the chemical sediments.

The predominance of phosphatic mineralisation in areas with low clastic input, and corresponding hardground and chert formation suggests a mechanism which depends on limited sediment dilution.

In the absence of metazoans, which concentrate phosphate minerals in Phanerozoic sediments, growth of authigenic calcium phosphate is most likely to be initiated by supersaturation of PO_4^{2-} at a suitable locus for phosphatisation at or below the sediment-water interface. Given that the ambient waters themselves are not supersaturated with respect to PO_4^{2-}, there are two ways in which this may be achieved: by active concentration and precipitation of phosphate in the EPS of certain microbial mats (e.g. Papineau 2010); or by redox-driven desorption of phosphatic groups from iron hydroxides already present within the sediment (Shaffer 1986). The former of these mechanisms is favoured for the sporadic occurrence of phosphate minerals in the Gunflint Formation.

An active microbial component to the chemical system would be expected to leave some trace within the chemical sediments, in the form of organic or iron-mineralised microfossils, or macroscopic sedimentary structures. Although microfossils and biogenic macrostructures have been described from other lithofacies of the formation, features in association with the phosphate are limited to wispy pyritic and organic putatively microbial laminations (at Frustration Bay and Boulevard Lake), and a few dispersed and degraded microfossils (at Frustration Bay). Certainly no microfossils are found within the amorphous phosphate grains, as seen in the Torridon Group, and as may be expected if phosphate-precipitating microbes were to entomb themselves. Large quantities of disseminated organic matter within the chert-carbonates at Kakabeka Car Park, the confinement of disseminated phosphate between organic and pyritic layers at Boulevard Lake, and the high levels of taphonomic degradation in those microfossils recovered from Frustration Bay however, provide strong evidence for the close interrelationship of organic and phosphatic material.

Redox pumping of phosphatic ions to and from iron and manganese hydroxide mineral surfaces is a well-documented phenomenon, and one that has been used previously to explain phyllocrystalline and nodular phosphate occurrences (Föllmi 1996). The overall absence of particulate iron-oxides within the Gunflint chemical sediments renders this mechanism unlikely to concentrate large quantities of phosphate. Thus the ultimate degradation of organic carbonaceous material is indication of the microbial modifying component of the sediment and seston layer, promoting supersaturation and phosphate precipitation. This purely biological mechanism requires a high flux of phosphate-sequestering organic matter from overlying waters to maintain supersaturation long enough to initiate and maintain precipitation. The limited distribution of phosphate in this basin may therefore be related to those limited areas where there is an active flux of biogenic material, in addition to low clastic dilution to the sediment.

During the Proterozoic, while microbial action near the sediment surface may help to concentrate phosphate ions to the point of supersaturation, it is the rate of supply of phosphorus to the basin that controls primary production on a longer time scale. The principal source of phosphorus in water bodies is weathering of continental and volcanic surfaces, rather than hydrothermal output (Föllmi 1996). For this reason, the relatively limited extent of phosphate in the Gunflint chemical sediments may be explained by the absence of any significantly weathered ancestral continent in the region of the Gunflint basin (Goodwin 1956).

7.6 Summary

A synthesis of the sedimentological, micropalaeontological and petrological observations confirm and add to the modern view of the Gunflint Formation as being composed of complex and laterally discontinuous lithofacies. The basin comprises shallow marine depositional settings with previously unidentified quickly shifting grainstone barriers creating short lived isolated lagoons. It is in these quiescent and isolated environments that the sedimentary phosphate is able to form, when input concentrations are high enough and perhaps when the conditions are conducive to a microbial bloom and concentration.

Reviewing the microbial component and assemblages of the Gunflint rocks, and applying novel techniques to interpret taphonomy, has shown the dominance of chemical

degradation in this setting. Such knowledge is invaluable in assessing the use of classical taxonomy, and suggests that some formally described taxa, especially those rare forms, or 'species' defined by varying surface ornament, may simply be taphomorphs of one another. Microbially induced sedimentary structures have been described from the clastic portions of the Gunflint basin for the first time. These observations in addition to the stromatolitic structures in the cherts, while still requiring additional study and verification, go some way to tying together the preserved microbiota, and the non-uniformitarian chemical sediments of the Gunflint Formation.

Chapter 8

Major transitions: the End-Proterozoic in Newfoundland

8.1 Introduction

Approaching the Precambrian-Cambrian boundary, the biosphere and physical environments undergo major change (Knoll & Walter 1992), switching from a dominantly microbial world to a macroscopic one, with major ramifications for biological, chemical and physical processes in all environments.

The beginning of this revolutionary period is marked by two severe glacial events, termed 'snowball' glaciations as palaeomagnetic and sedimentological data seem to locate ice deposits near to the equator (Hoffman et al. 1998). Although some of these data have been subsequently questioned, undermining interpretations of ice extent (Condon et al. 2002, Meert & van der Voo 1994, Rieu et al. 2007), the Marinoan (dated 650-560 Ma) and Sturtian (dated 730-716 Ma) glaciations are associated with extreme variations in sea level and seawater isotope excursions (Christie-Blick et al. 1995, Kaufman & Knoll 1995).

Within the biosphere, the appearance of the enigmatic Ediacaran biota is a macroscopic precursor to the evolution of recognisable animal phyla during the Cambrian explosion. These first diverse macroscopic forms are accompanied by an increase in microbial diversity, as reflected by diversification of acanthomorphic acritarchs and other megaspheroidal forms during the early Ediacaran (Cohen et al. 2009). This increase in diversity is thought to be driven in part by increases in evolutionary tempo in the terminal Neoproterozoic (Knoll 1995), and culminates in a mass extinction of characteristic Ediacaran macrofossils and acritarchs around 560 Ma (Cohen et al.

2009).

The appearance of macroscopic forms at the beginning of the Cambrian, and in particular the invention of trophic tiering at this time (McIlroy & Logan 1999), give rise to fundamental biochemical changes and differing biology-sediment interactions. The jump in oxygenation of the atmosphere and water bodies between 850 and 540 Ma, caused by gas build-up in the absence of terrestrial sinks (Holland 2006), means that bottom waters of late Precambrian and Cambrian basins are less susceptible to anoxia. This limits the distribution of microbiota that make use of anoxia at this time, as well as inhibiting physicochemical reactions that take place under reducing conditions. In addition, the advent of vertical burrowing that marks the beginning of the Cambrian (Narbonne et al. 1987) disrupts sealing sedimentary laminae, and results in deeper penetration of oxygen beneath the sediment-water interface. This in turn drives the redox boundary down through the sediment, and with it the zone of phosphogenesis and optimum loci for chemotrophic microbial metabolisms (Brasier & Callow 2007).

It is to be expected that these fundamental changes in the terminal Neoproterozoic will be reflected in changes in fossil preservation and mineralisation. Some of these have been documented by Brasier & Callow (2007), but it is of interest in this study to investigate fossil preservation and phosphogenesis, for comparison with the newly described deposits from the 1 Ga-old Torridon of northwest Scotland, and the 2 Ga-old Gunflint Formation of Ontario, Canada.

The type section for the Precambrian-Cambrian boundary in the Avalon Peninsula of Newfoundland (Narbonne et al. 1987) is chosen for this study, as rocks from a variety of depositional settings are preserved across the boundary itself, as well as through part of the terminal Proterozoic. Sedimentary successions are well exposed with interbedded volcanic units for precise dating, and well-studied macrofossils to provide biological context (e.g. Droser et al. 2006, Narbonne 2005).

8.2 Global context

In the terminal Proterozoic, the Avalon terrane formed within a volcanic arc setting on the southern margin of Gondwana, likely adjacent to the northern margin of West

Africa, around 38°S (McNamara et al. 2001). Sedimentary rocks and volcanic and volcaniclastic units are deposited in a basin experiencing two-phase tectonic evolution. First, between 630 and 590 Ma, deposition took place in a fore-arc basin, locally affected by arc volcanism, followed by, between 590 and 540 Ma, the subduction of the spreading centre and a switch to strike-slip motion and deposition in rifting pull-apart basins (Murphy et al. 1999). Through these changes, a progressive coarsening and shallowing trend prevails, outcropping today on the Avalon Peninsula of eastern Newfoundland, with deep turbiditic sequences at the base, through to shallow terrestrial sediments at the top of the Proterozoic sequence.

On the Burin peninsula and elsewhere, the Placentian period, between 542 and 516 Ma, is also represented (Landing et al. 1989), containing the type section for the Precambrian-Cambrian boundary (Narbonne et al. 1987), but disconformable with the underlying Neoproterozoic deposits. Deposition takes place within a local extensional regime as Avalonia splits from Gondwana, recording several episodes of onlap and offlap indicating periodic sea level change (Landing et al. 1989).

8.3 Geology

The geological successions of eastern Newfoundland span the terminal Proterozoic and Lower Cambrian, but not in a continuous sequence. Two stratigraphic regimes are recognised: the Avalonian Succession from a maximum of 631 Ma to around 560 Ma (King et al. 1988), outcropping on the Avalon Peninsula, and the Placentian Series of the Burin Peninsula and elsewhere, from around 542 to 516 Ma (Landing et al. 1989). In the following geological reviews, these two successions are described separately.

8.3.1 Avalonian Succession

Figure 8.2 illustrates the generalised stratigraphic succession of terminal Proterozoic rocks from the Avalon Peninsula, after King et al. (1988).

Lowermost volcanics of the Harbour Main group are dated at 631±2 Ma (Krogh et al. 1988), providing a maximum age for this sedimentary succession. Unconformably overlying rocks of the Conception, St Johns, and Signal Hill groups follow a

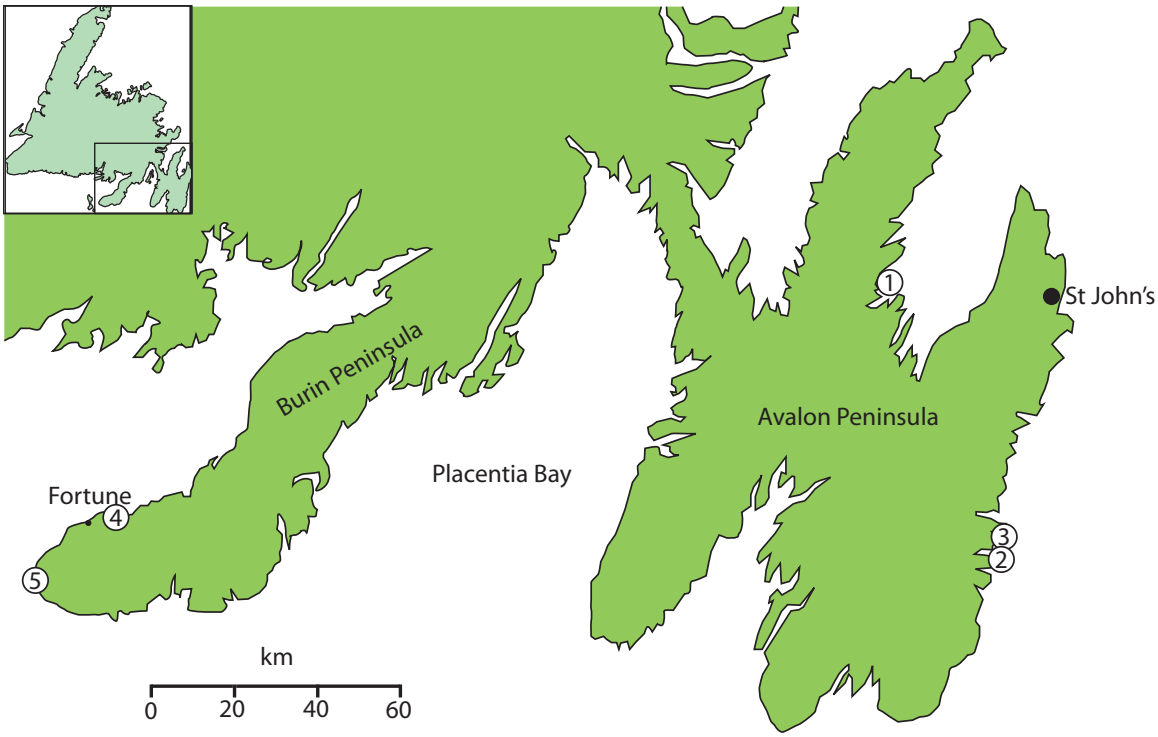


Figure 8.1: Map of the Avalon and Burin Peninsulas, eastern Newfoundland. Localities in this study: 1, Spaniards Bay South; 2, Silos Cove; 3, Ferrylands Head; 4, Grand Bank Head; Little Dantzic Cove.

general coarsening and shallowing upwards trend (Myrow 1995, Williams et al. 1995).

Within the lowermost Conception Group, the Mall Bay Formation contains turbiditic and other deep-water units that were deposited in basin plain and delta fan fringe settings (Gardner & Hiscott 1988). Overlying this, the Gaskiers Formation comprises a diamictite with striated clasts, likely deposited by a subaqueous density flow between 50 and 600 km distant from the glacial margin (Eyles & Eyles 1989). The Drook Formation and, above it, the Briscal Formation contain multiple packages of turbidite deposits, interbedded with distal mudstones and ashes, formed around submarine fan lobes (Gardner & Hiscott 1988, Williams & King 1979). The Mistaken Point Formation, at the top of the Conception Group, has become synonymous with the intricately preserved macroscopic biota within it, and is dated to 565±3 Ma (Benus 1988). Together with the overlying Trepassey Formation, at the base of the St John's Group, it comprises extensive turbidites and debris flows with interbedded volcanic units, which were deposited on a southeast-facing slope (Wood et al. 2003).

The shallowing trend begins mid-way through the St John's group, following the deep-deposited turbidites of the Trepassey Formation. The overlying Fermeuse Formation contains sediments that were deposited in a delta front or slope setting, and show extensive large-scale slumping (Gehling et al. 2000, King et al. 1988). Upwards, the Renews Head Formation comprises coarser, shallower shoaling delta deposits, which are exposed to above the storm wave base, and possibly even subaerially (Williams & King 1979). The top of the St John Group is separated from the Signal Hill Group by a local disconformity.

Shallow and terrestrial deposits dominate the Signal Hill Group. The lowermost unit, the Cappahayden Formation, comprises sandstones deposited in a subtidal delta front to prodelta setting, marking a slight reversal in the overall shallowing trend (King et al. 1988, Narbonne et al. 2001). Shallowing returns, however, with the overlying Gibbet Hill Formation, which consists of sandstones from a shallow distributary mouth-bar setting, with small and large-scale sedimentary features indicating current flow to the south or southwest (King et al. 1988). Upwards, the Ferryland Head Formation comprises several upward shallowing successions ranging from delta front to delta plain, ultimately shallowing from a distributary mouth-bar to subaerially exposed delta plains (Narbonne et al. 2001). The top of the Signal Hill Group, marked by the Cape Ballard Formation and several other small formations, is interpreted as

fully proximal, consisting of deposition on terrestrial alluvial plains (King et al. 1988).

8.3.2 Placentian Series

Figure 8.2 illustrates a generalised stratigraphy through the Placentian of the Avalon Peninsula, after Landing et al. (1989). There is no overall trend observed in this basin, as in the Avalonian succession, but instead a number of transgression-regression sequences are recorded by successive onlap and offlap of sedimentary units (Landing et al. 1989).

Deposition within this basin begins with the unconformity bounded Rencontre Formation, which is uppermost Precambrian in age. It comprises red coloured sandstones that were deposited in fluvial, marginal marine, and open marine settings within an extensional fault bounded basin (Smith & Hiscott 1984). Overlying this, the Chapel Island Formation is classically divided into five members, each with differing depositional characters (Myrow 1987, 1988): lowermost Member 1 is peritidal; Member 2 is storm-influenced; Member 3 sediments are deep and distal; Member 4 shows a return to peritidal conditions; and Member 5 was deposited on a storm-dominated sandy shelf (Landing et al. 1989). Overall, the sediments record a transition from marginal marine through a shallowing delta front which then deepens before shallowing again to the top of the formation. The Precambrian-Cambrian boundary stratotype is located near the base of Member 2 of the Chapel Island Formation, specifically where it outcrops at Fortune Head (Narbonne et al. 1987). Above the Chapel Island Formation, the Random Formation consists primarily of quartz arenites from a storm-influenced macrotidal setting, marking a transgression to platformal conditions with interbedded shales and minor carbonates (Hiscott 1982, Smith & Hiscott 1984). The unit is correlated with the Tommotian (Anderson 1981) and is truncated at its upper extent by an unconformity, marking uplift and erosion.

Above this unconformity, the Petley Formation and the West Centre Cove Formation record a transgressional return to deep-water deposition, followed by rapid shoaling, in an onlap-offlap cycle (Brasier et al. 1992). Upwards, the Cuslett Formation preserves strikingly pink nodular limestones and red shales that are onlapped, recording transgressive deepening through the deposition of these inner shelf deposits. The overlying Fosters Point, or locally the Smith Point Limestone, displays the corresponding offlap in shoaling from subtidal to peritidal environments. The rocks here

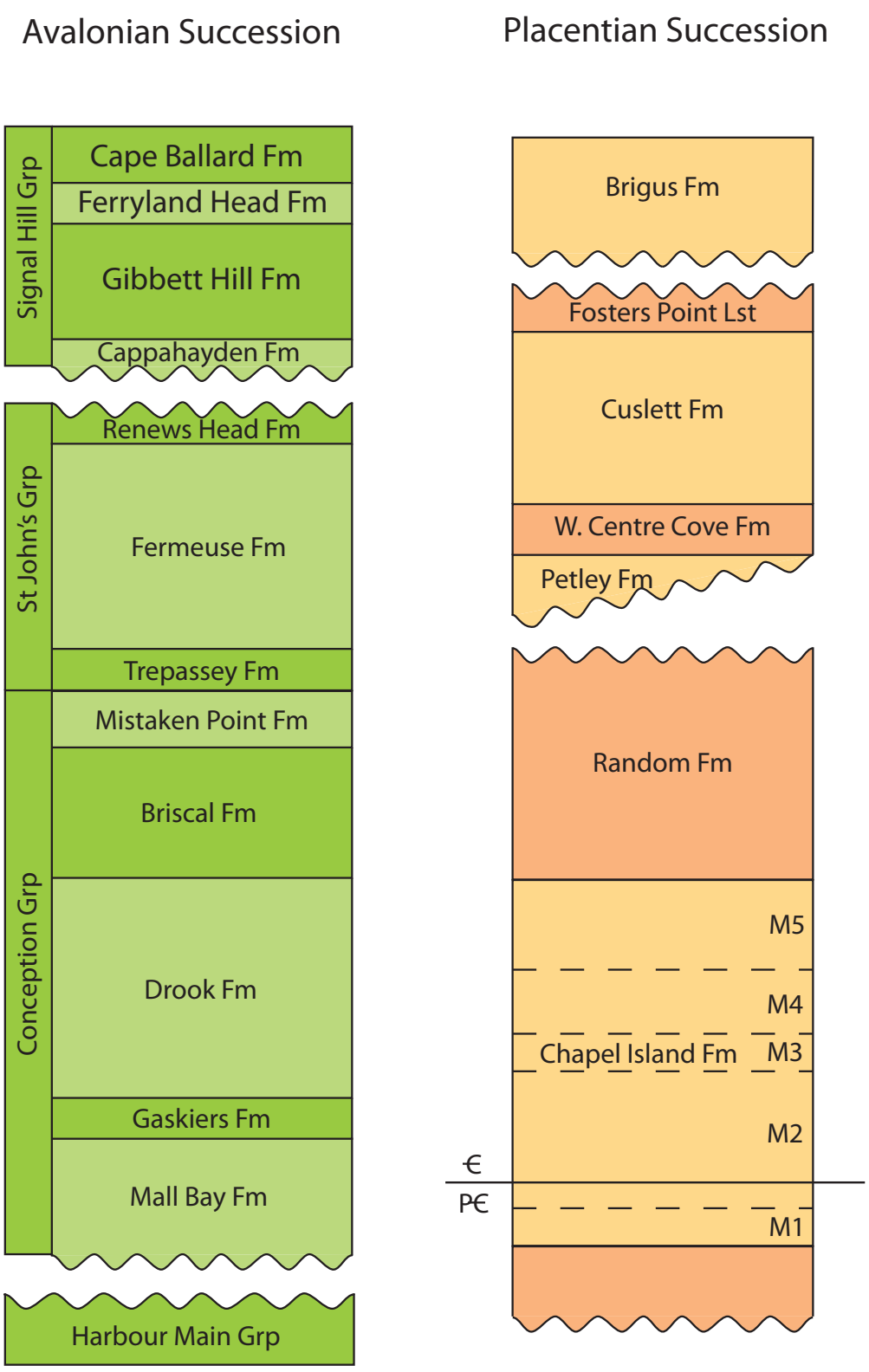


Figure 8.2: Generalised stratigraphy for the Avalonian succession, outcropping on the Avalon Peninsula, and for the Placentian series, outcropping on the Burin Peninsula and elsewhere.

are pink nodular and fossiliferous limestones and ferruginous stromatolites (Benus 1988), and are truncated by a further erosional unconformity.

The Brigus Formation is the youngest unit of the Placentian series, and is seen onlapping the underlying unconformity with pink limestones and manganese-rich carbonates of likely microbial origin, interbedded with inner shelf red shales, but showing signs of occasional emergence (Landing et al. 1989). Trilobites appear in this succession for the first time, marking the end of the sub-trilobitic period of the Lower Cambrian (Bullock & Morris 2011).

8.4 Microbiota

8.4.1 Introduction

In comparison to the majority of the Proterozoic, the Ediacaran microfossil record is astonishingly diverse. The appearance and diversification of so-called 'Large Ornamented Ediacaran Microfossils' (LOEMs) from around 635 Ma (Cohen et al. 2009) are broadly coeval with the appearance of Ediacaran macrofauna and other uniquely Ediacaran fossils interpreted by some as embryos (Xiao & Knoll 2000, Xiao et al. 1998). The correlation of this global diversification event with the termination of the last major Neoproterozoic glaciation suggests a potential causation, perhaps through renewed liberation of nutrients, or a increase in optimum shelf habitats through post-glacial transgression. Alternative hypotheses may be proposed for this period of advanced evolution and apparent burst in dynamic macroevolution (cf. Butterfield 2007), involving genomic revolutions in sexual reproduction or homeobox body plan organisation (Kumar & Hedges 1998). Such revolutions may themselves be triggered by the optimum post-glacial conditions, but without them the Ediacaran radiations and the subsequent Cambrian explosion of animal phyla might not have been possible.

The large acanthomorphic acritarchs characteristic of this diversification period have been interpreted as early animal resting cysts (Cohen et al. 2009), but their sudden disappearance in a microbial extinction event around 560 Ma suggests a more primitive, perhaps experimental phase that was not subsequently repeated. The sudden microbial extinction can be broadly correlated with the appearance of diverse macroscopic Ediacaran organisms, and it may be supposed that the nutrient demands

of motile creatures, or metabolic actions of these newly evolved macroorganisms contributed to the acritarchs' demise.

8.4.2 Organic-Walled Microfossils

In Newfoundland, organic walled microfossils have been recovered from throughout the Avalonian succession by Hoffman and others (1979), where they described a poorly preserved, low-diversity assemblage comprising non-septate sheaths of *Taeniatum* sp. and some relatively simple acritarchs. Despite the low diversity of this assemblage, it is generally consistent with global diversity at this time (Knoll & Walter 1992), preceding the large-scale diversification of LOEMs (Cohen et al. 2009). Other reviews have noted but not imaged the densely colonial microfossil *Bavlinella* Shepeleva in samples from the Fermeuse and Renews Head Formations (Anderson et al. 1982, Timofeyev et al. 1980); it was also found amongst the diamictic sediments of the Gaskiers Formation (Hofmann et al. 1979).

Despite sampling of clastic and phosphatic material from several likely horizons within the Avalonian succession and Placentian Series, no identifiable structured microfossils were recovered that met the established biogenicity criteria (Chapter 3). Disseminated carbon was observed in thin sections of phosphatic nodules, but this was fine and particulate, indicating heavily degraded carbonaceous matter. Without structural-organic microfossils, it is impossible to properly assess diversity or taphonomic grade, but the high concentrations of disseminated organic matter within sediments and phosphatic cements tentatively places the Avalonian taphonomic environment at the extreme scale of chemical degradation, excluding resolution of any further details.

The sediments do, however, host a number of pseudobiological structures that justify further analysis and consideration.

8.4.3 Pyrite Strings

Within shales and phosphates sampled from the Fermeuse Formation of Silos Cove, short strings of pyrite framboids occur, which have some characters that recommend

them for a biological interpretation (Figure 8.3a).

The sediments here comprise finely laminated dark grey shales and occasional thin phosphatic bands, which are tectonically and locally slumped into chaotic bedding formations. Examination of thin sections perpendicular to bedding through the shales and phosphates reveal short strings subparallel to bedding, made up of black opaque pyrite framboids that are uniserially or complex-multiserially arranged. Strings are of limited length, reaching a maximum of around 200 μm, and are typically of a common thickness around 10 μm. In places, framboids are packed densely into tubular structures with straight orthogonal boundaries. The strings differ from other occurrences of pyrite within the Avalonian succession in their close string-like or tubular associations and limited length. Pyrites seen in abundance in the Trepassey Formation at Melrose on the Bonavista Peninsula are loosely associated throughout particular laminae, not linked into strings, and often concentrated in amorphous patches or made up of euhedral crystals.

It is clear that the pyrite strings observed at Silos Cove are substantially different from dispersed pyrite occurrences elsewhere within the Avalonian or Placentian successions, and their constrained morphologies are directly appealing to a biogenic interpretation. Similar uniserial structures have been formally described as *Ferrimonilis variabile*, from the 1600-1400 Ma Barney Creek Formation, but without sufficient demonstration of biogenicity, this taxon's validity is in doubt.

Characters of these pyrite strings that support a biogenic interpretation are as follows: they are a consistent shape and size, suggesting that something is constraining their dimensions; and the morphologies and size ranges seen are similar to those described from organic-walled fossil filaments and living filamentous bacteria; the strings are almost always oriented sub-parallel to bedding, indicating that they formed synchronously with formation of layers and did not precipitate indiscriminately at a later date; they are also found dispersed widely among laminae in both the phosphate and the shale, and are not confined to a particular horizon, as would be expected for a short-lived mineralogical phenomenon; pyrite framboids are considered by some (Passier et al. 1997) to be a biological signature, and the strings are made up entirely of rounded framboids with no euhedral crystals present. Framboids here are also found only in strings and almost never as isolated individuals.

While the above observations provide good evidence for a biological origin for these pyrite strings' formation, such a conclusion is far from conclusive. An absence of carbonaceous matter in association with the structures in most cases undermines the interpretation of an organic sheath template. Also, while bacteria that utilise iron within their metabolisms are known to encrust their sheaths with pyrites or iron oxides (e.g. Schelble et al. 2004), no modern analogies are known that form uniserial chains like those seen here.

Optical and scanning electron microscopy cannot provide any further resolution or information that can resolve the issue of biogenicity for these structures. Further information may be sought from higher resolution FIB-TEM imaging that may identify diaphanous organic matter, or from sulphur isotope studies on the pyrites that may demonstrate extreme biological fractionation (cf. Chambers & Trudinger 1979).

8.4.4 Ambient Inclusion Trails

Phosphatic material from the Trepassey Formation at Spaniards Bay South (for more detail see phosphate discussion below), contains enigmatic starburst-like structures partially made up of carbonaceous material, which are here described as ambient inclusion trails (AITs; Figure 8.3b).

The structures are generally variable in shape and size, ranging from broadly equidimensional with a total diameter of 20 μm, or elongate and up to 100 μm long and 30 μm wide. They comprise a central amorphous and irregularly shaped carbonaceous body, from which apparently hollow tubes or fibres radiate irregularly. Tubes are approximately 5 μm thick and up to 50 μm long, and radiate out, curving or bending irregularly in all directions. When elongated, the carbonaceous body is oriented subparallel to bedding, but the tubular threads crosscut bedding indiscriminately.

This description, and the appearance of the structures in transmitted light, can be closely compared with previously described and defined AITs from Proterozoic rocks (e.g. Knoll & Barghoorn 1974, Lepot et al. 2011, Tyler & Barghoorn 1963), despite superficial resemblance to filamentous microfossils. AITs are typically defined as trails left by metal- or carbon-rich inclusions as they are propelled through a lithified substrate such as chert. They have been observed from a range of lithologies

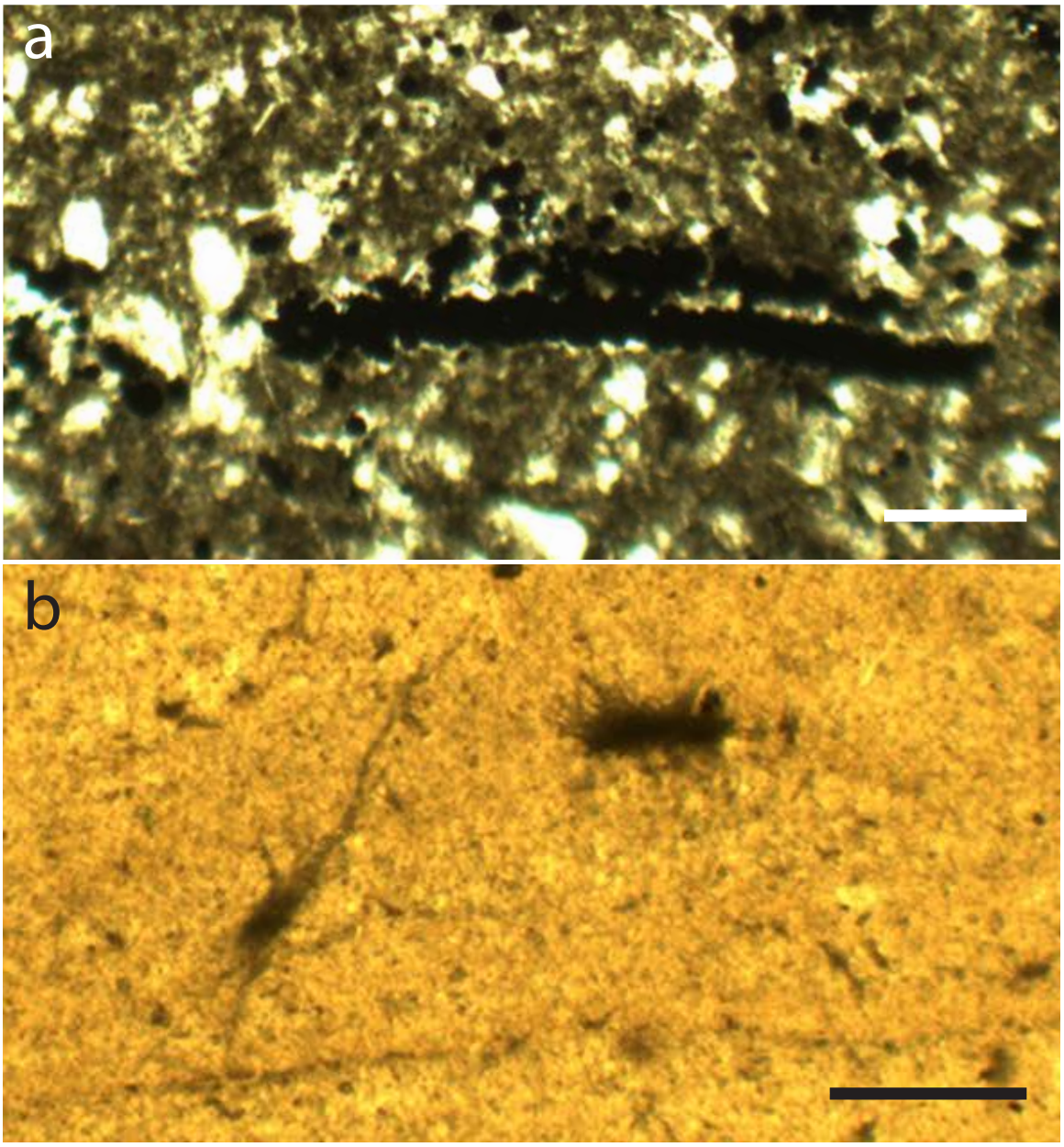


Figure 8.3: Pseudofossils or fossils from the Avalonian of eastern Newfoundland. a) Short, laterally confined tubular filamentous structures made up of complex multiserial arrangements of pyrite framboids. Scale bar 10 μm. b) Starburst-like arrangements of hollow tubular features radiating from a central carbonaceous body, interpreted here as ambient inclusion trails. Scale bar 100 μm.

and ages, including but not limited to cherts of the 2700 Ma Fortescue Group (Knoll & Barghoorn 1974) and permineralising phosphates of the Doushantuo Formation (Xiao & Knoll 1999). In the first general review of these structures Wacey and others (2008) defined several specific criteria for identifying AITs in thin section: that they contain a mineral grain at their distal end; they bear longitudinal striations along their length; they typically have a polygonal cross section; tracks propagate in multiple directions; tracks form a starburst-like structure around organic matter; tracks are curved and twisted, or have sharp angular turns, crosscutting one another; and tracks may bear smaller side branches. Potential AITs need not possess all of these features, but a combination of some within a likely lithology should be taken as good evidence for an AIT affinity.

The structures found in the Trepassey phosphates meet some of these criteria, specifically those of multidirectional propagation of tracks, overall starburst-like morphology and sharp angular turns within track directions. Optical microscopy does not confer sufficient resolution to establish whether a mineral grain is present in the distal end, or whether the tracks possess a polygonal cross section or longitudinal striae. As yet, these structures have evaded imaging by electron microscopy, as they reside beneath the surface of the slide, but SEM- or FIB-TEM would allow imaging of the finer scale structures.

Given that these features are AITs, they can be considered alongside previous reports to elucidate their significance. In an early report, Knoll & Barghoorn (1974) proposed that AITs in the middle Precambrian cherts of Western Australia were formed by "pressure solution initiated by gas evolution from organic matter attached to pyrite", but the mechanism by which this occurs has yet to be tested. Wacey and others (2008) proposed a more detailed hypothesis for their formation, involving a four-stage process that, with few variations, can produce any AIT texture yet seen in the geologic record. First, rapid lithification of a substrate traps pyrite and organic matter within it, before the organic matter has fully decayed. Secondly, the organic carbon begins to degrade within the rock, producing gases that apply pressure to pyrite or carbonaceous grains, which is facilitated by local dissolution of the substrate by resident microbial communities, resulting in the movement of that grain. Thirdly, further heating and burial intensifies these reactions, causing further movement of the grain and development of a long track. Finally, in a stage that may or may not be present, later replacement of the surrounding substrate can serve to

obscure the original AIT texture somewhat, and alter the mineralogy of the propelled grain (Wacey et al. 2008).

Despite the notable lack of pyrite in the Avalonian examples, if their formation conforms to this model, they are not only adding to the growing database of described AITs from the geological record, but they may also be used as a proxy for specific petrological and biological phenomena. The presence of AITs implies that the cryptocrystalline phosphate in which they are found formed and lithified rapidly, and trapped relatively undecayed organic matter present at the time. In addition, it implies that degradation of the organic matter continued after lithification of the host rock, perhaps in response to burial heating and metamorphism, thereby suggesting rapid post-diagenetic alteration of the rocks.

Without experimental data or modern analogy for the formation of AITs however, these conclusions must remain tentative, as the model is a speculative one based on geological observations alone. It may be that the AITs represent structures induced by a certain kind of microbial metabolism, or as-yet unknown physical process. These newly described structures from the Avalonian succession of Newfoundland add richness to the known data and may in future assist in decoding the formation and significance of AITs.

8.5 Phosphate

8.5.1 Previous reports

Across the Proterozoic-Cambrian transition vast phosphorite deposits are seen globally, especially across Australia and central Asia (for review see Cook & Shergold 1986). It is therefore surprising that phosphates have been scarcely described from the Avalonian or Placentian rocks of Newfoundland. Christie & Sheldon (1986) allude to minor occurrences within Cambrian beds of eastern Newfoundland, but dismiss them on the basis of their small concentration of P_2O_5. As a result, phosphatic deposits are here described for the first time from the Avalonian and Placentian successions of the Avalon Peninsula.

8.5.2 New Findings

A comprehensive search for phosphatewas carried out through classically exposed strata of the Avalonian and Placentian successions on the Avalon Peninsula. Sedimentological data were compiled and potentially phosphatic material collected to be prepared as petrographic thin sections and imaged by optical microscopy and SEM-EDX analysis. Phosphate was recovered from five localities and stratigraphic levels, and is described below in order of decreasing age.

8.5.2.1 Spaniards Bay South

N 47° 36' 43.1" W 053° 16' 15.8"
On the southern shore of the promontory to the south of Spaniards Bay, medium grained orange-coloured sandstones are interbedded with dark muddy shales with undulating lamination and irregular lenses of coarser sandy carbonate. Small phosphatic nodules occur within the shaley portions, disturbing lamination locally. The rocks here belong to the Neoproterozoic Trepassey Formation, and in their lower portion contain impression fossils of Ediacaran morphotypes including *Charniodiscus* sp. and *Fractofusus* sp. (cf. Gehling & Narbonne 2007, LaFlamme et al. 2004).

Microscopic examination of the phosphates here reveal them to be large disrupted and somewhat reworked lenses, more or less *in-situ*, and surrounded by fine undulating laminae rich in carbonaceous material. It has a generally granular appearance, showing continuous carbonaceous laminae in cross section (Figure 8.4). In places, phosphate is poorer in carbon and clastic material, appearing pure and cryptocrystalline and containing sparsely distributed large amorphous patches of carbon and ambient inclusion trails (see above). As with the Torridon phosphates, crystals of apatite here are too small to resolve by optical or scanning electron microscopy, but SEM-EDX reveals the elemental association of calcium and phosphate with iron, aluminium and silicon, suggesting finely intergrown iron-rich clays making up the granular texture. In places, stellar or spherulitic structures are seen, similar to those observed in the granular phosphates of Lower Diabaig in the Torridon Group (Figure 6.3). These spherules are typically composed of radially arranged blade-like crystals of apatite, and are sparsely and randomly distributed through the phosphate-clay matrix, sometimes crosscut by laminae. In contrast to the Torridon examples, there is no halo of organic matter associated with these structures and they are not readily visible

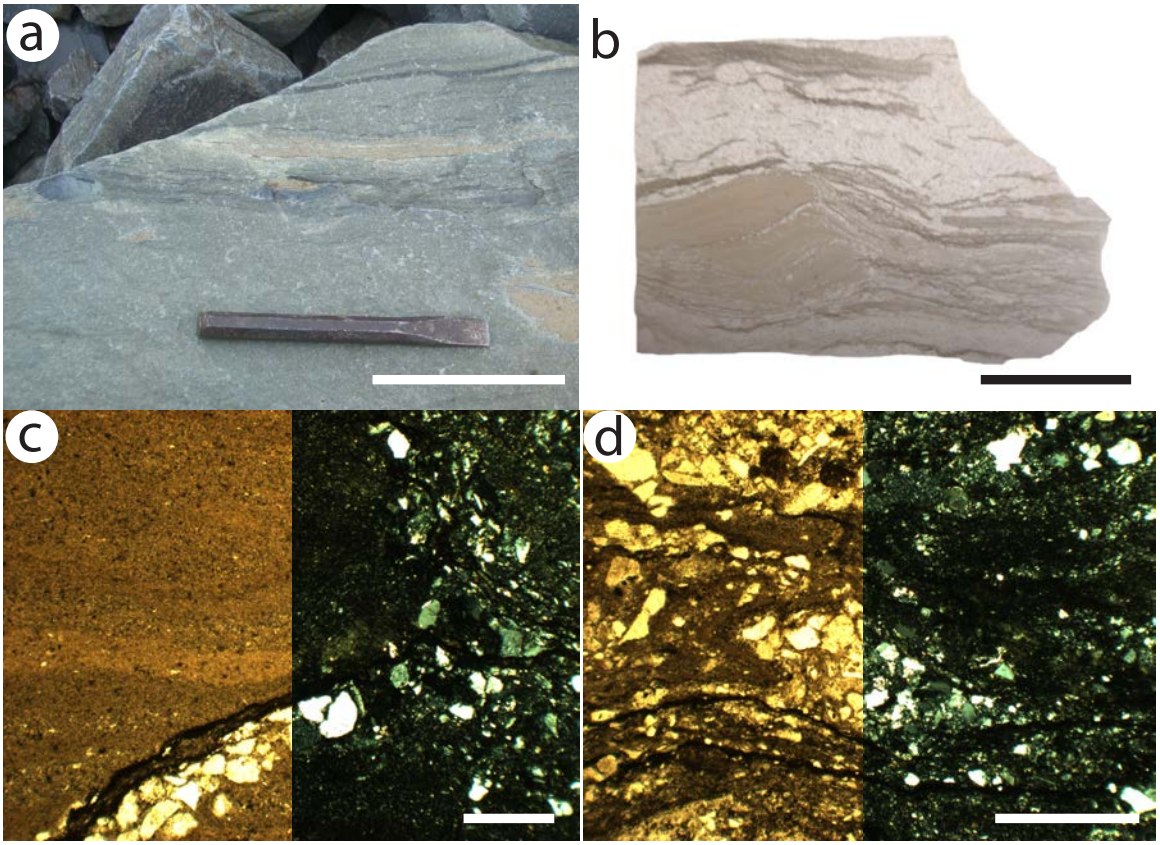


Figure 8.4: Phosphate sedimentology, petrology and mineralogy at Spaniards Bay South. a) Sedimentological setting for phosphate. Laminae and enlarged nodules are found in fine to medium grained sandstone beds, often with associated sandy carbonate lenses. Scale bar 10 cm. b) Thin section texture , illustrating microscale alternations of carbonaceous laminae, and somewhat disturbed phosphatic nodules. Scale bar 5 mm. c) Optical photomicrograph of edge of granular phosphate nodule, with dense carbonaceous material at boundary. Plane polars left hand side, cross polars right hand side. Scale bar 500 μm. d) Optical photomicrograph of phosphate-carbonaceous layers in sandy matrix. Plane polars left hand side, cross polars right hand side. Scale bar 500 μm. Sample SPB-2a from Spaniards Bay South, Trepassey Formation.

with transmitted light. It is likely, therefore, that they precipitated and replaced secondarily the phosphate-clay matrix, perhaps as a result of late-stage degradation of organic matter trapped within.

Texture and associations of phosphate at this deep water locality appear broadly similar to that seen in the lacustrine Torridon siltstones: granular intergrowths of phosphate and iron-rich clay closely associated with carbonaceous layers. Caution must be taken before drawing too close a comparison between these differing ages and environments, but the petrology remains strikingly similar.

8.5.2.2 Silos Cove

N 47° 00' 38.2" W 052° 53' 36.4"
To the south of Ferryland Head on the east coast of the Avalon Peninsula, Silos Cove exposes slumped and faulted rocks of the Fermeuse Formation. The rocks here comprise dark grey laminated shales that are broadly planar bedded but heavily deformed. Shales consist of fine-scale alternations between silicon and calcium-rich clays, and phosphate occurs occasionally as indurated resistant bands conformable with bedding and containing faint planar laminations.

Sections through the dark resistant bands within the shale show them to be composed of dominantly finer material than seen elsewhere within the siltstones, incorporating clays and carbonaceous material into fine indistinct layers that are optically dark. Within these layers uniserial and complexly multiserial pyrite strings are common (see above). Elemental mapping by SEM-EDX reveals that the finer layers are composed of a mixture of amorphous apatite and fine calcium-bearing clay phases (Figure 8.5). Within the coarser silty layers, apatite occurs only as rare detrital grains.

Thus, it can be seen that in this deep-water environment, phosphate is associated only with deposition of fine clays and therefore, by extension, during quiescent periods of low deposition. Its association with the enigmatic pyrite strings is to be noted, implying some correlation between iron reducing activity, possibly microbial, and phosphate formation at this locality.

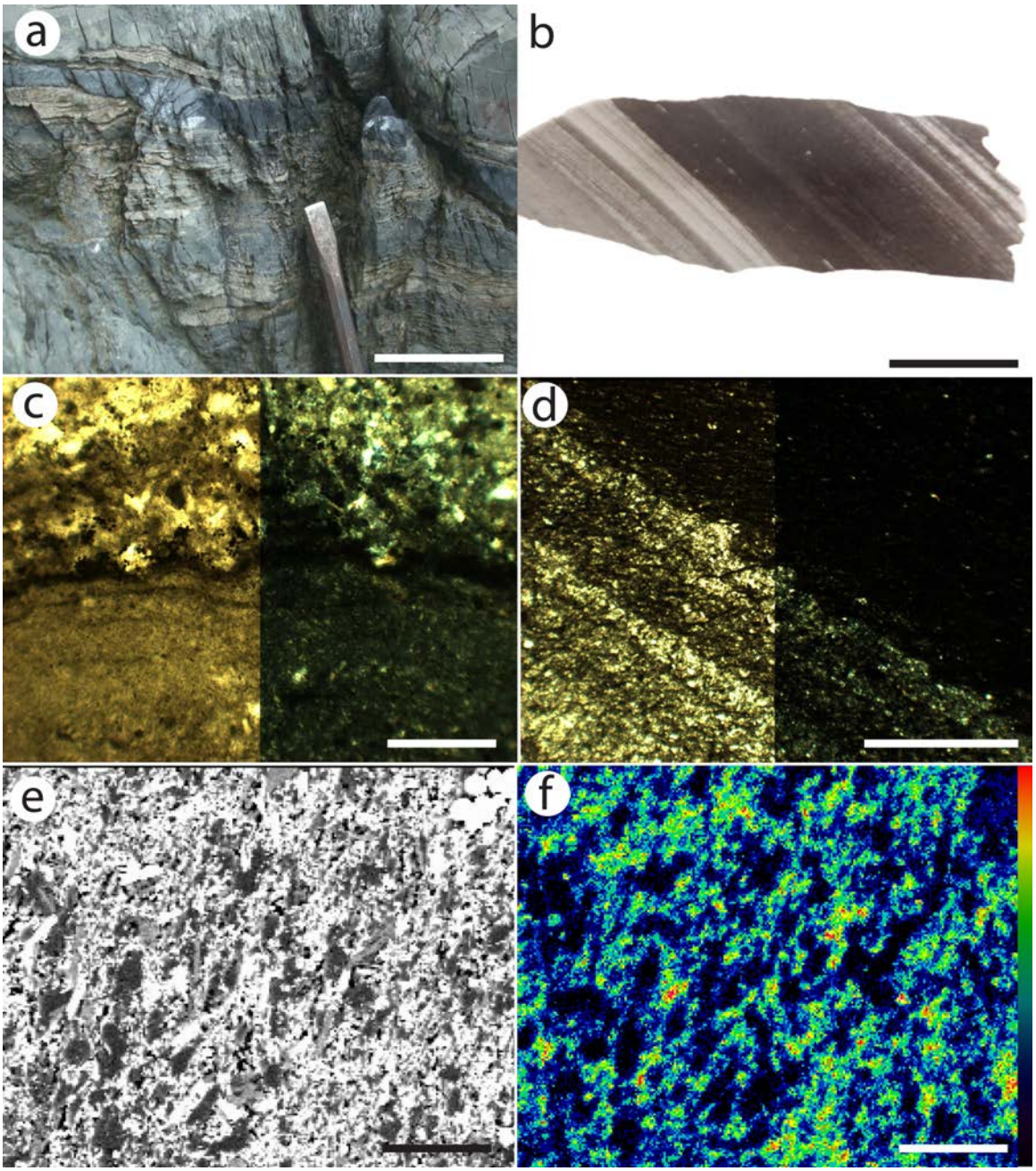


Figure 8.5: Phosphate sedimentology, petrology and mineralogy at Silos Cove. a, Sedimentological setting for phosphate. Thick dark bands occur amidst sheared and disrupted laminae in grey shales. Scale bar 10 cm. b, Thin section texture, illustrating laminar banding in shales and concordant phosphatic material. Scale bar 5 mm. c, Optical photomicrograph of carbonaceous-rich edge to phosphatic band. Plane polars left hand side, cross polars right hand side. Scale bar 300 μm. d, Optical photomicrograph of sheared carbon-rich layers within the siltstone matrix. Plane polars left hand side, cross polars right hand side. Scale bar 1 mm. e, SEM-BSE image of phosphate texture within phosphatic band. Scale bar 10 μm. f, SEM-EDX phosphorus map of field of view in (e). Scale bar 10 μm. Sample SIL-1a from Silos Cove, Fermeuse Formation.

8.5.2.3 Ferrylands Head

N 47° 01' 06.1" W 052° 51' 31.7"
At the tip of Ferrylands Head at the base of the lighthouse, the Ferrylands Head Formation represents the marginal marine and terrestrial facies of the Avalonian succession. Here, green and red sandstones form repetitive packets characteristic of channel migration and flood plain deposition in a meandering river system. Phosphate is identifiable here as thin, white-weathering crusts amongst the fine-laminated red portions representing quiescent overbank deposition in this facies.

Microscopically, phosphate occurs in two habits at this locality. Firstly, it occurs as discrete concentrated bands on the surface of thin centimetre-bedded red units. Its lower margin is sharp, and it has a granular texture, appearing optically dark but massive with a moderate amount of disseminated carbon. Calcium and phosphorus are densely concentrated in these bands and absent from the underling sandstone (Figure 8.6). Secondly, within red sandy units, phosphate makes up an interstitial cement, conferring a resistance and induration to these units, not seen elsewhere. SEM-EDX reveals apatite to be highly concentrated within red layers, and less abundant in adjacent green units. No intergrown clay phases are observed in any notable abundance.

Phosphate in this shallow water terrestrial facies is closely associated with oxidised red beds, as opposed to those finer, reduced units. This suggests its formation under oxidising and possibly even emergent conditions in contrast to most observed occurrences and phosphogenic models. The thin carbon-rich phosphate layers may hold a clue to phosphate distribution, having the appearance of colonising epibenthic mats, which may act to concentrate high levels of phosphate delivered locally by fluvial input.

8.5.2.4 Grand Bank Head

N 47° 06' 34.5" W 055° 46' 14.1"
On the Burin Peninsula to the west of Avalonia, phosphate is found in lowermost Cambrian strata of Chapel Island Formation, Member 2, at Grand Bank Head. Here, thin tabular rip-up clasts of phosphate are found within sandy beds that are also host to the boundary defining ichnofossil *Phycodes pedum* (cf. Dzik 2005). Sandstones here

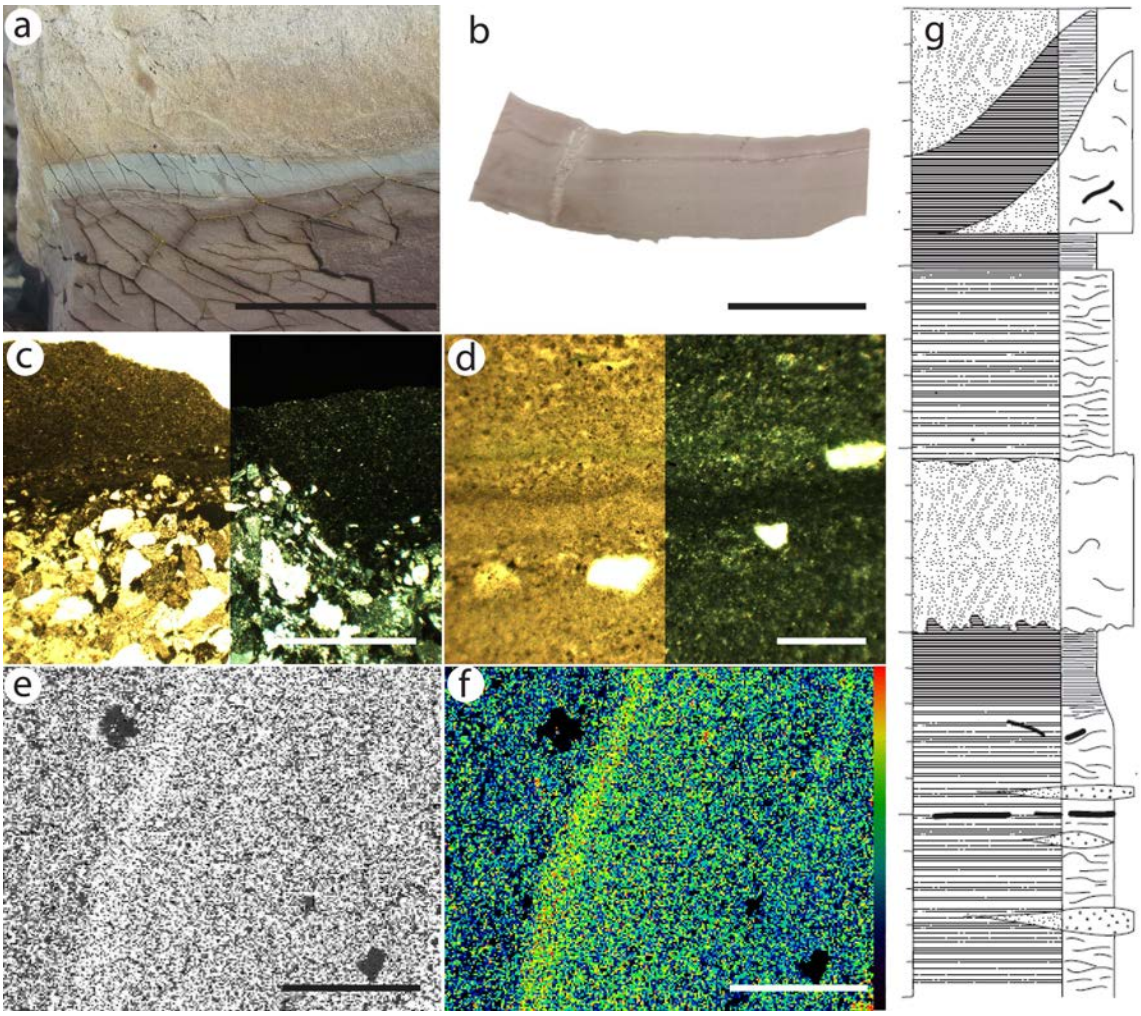


Figure 8.6: Phosphate sedimentology, petrology and mineralogy at Ferrylands Head Formation. a, Sedimentological setting for phosphate. Bands and thin layers occur primarily within red areas characteristic of overbank deposition. Scale bar 10 cm. b, Thin section texture, fine red sandstone with no notable nodular structure. Scale bar 1 cm. c, Optical photomicrograph of thin disrupted granular phosphate band on clastic material. Plane polars left hand side, cross polars right hand side. Scale bar 1 mm. d, Optical photomicrograph of layered pure and granular phosphatic material in sandstone matrix. Plane polars left hand side, cross polars right hand side. Scale bar 1 mm. e, SEM-BSE image of layered phosphate. Scale bar 10 μm. f, SEM-EDX phosphorus map of field of view in (e). Scale bar 10 μm. Sample FLH-3b from Ferrylands Head, Ferrylands Head Formation. g, Sedimentary log from sedimentary rocks at Ferrylands Head. Small markers every 10 cm.

formed in a periodically storm-affected shelf setting.

The microscopic character of the rounded rip-up clasts varies on a small scale. They include phosphate-rich mineralogies, which are zoned with respect to their clastic content, as well as purer gelatinous phosphate supporting large quartzose or polymictic iron-bearing grains (Figure 8.7). There are also siliceous clasts that are rounded and deformed in a similar manner.

The rounded nature of these grains indicates a reworking event while they were still plastic, and the apparent concentric zonation of some clasts may indicate rolling or subsequent remineralisation of the emplaced grain. Different phosphatic textures imply a source area of originally complex, presumably layered, mineralogy, that incorporated pure apatitic material amongst a variety of detrital mineralogies, as well as accompanying early-stage growth of siliceous material. The occurrence of these textures only as rip-up clasts however precludes further interpretation of the stratigraphic ordering or other associations, implying only that these early-semi-lithifying minerals formed under more quiescent conditions that were subsequently thoroughly reworked into massive sandy beds.

8.5.2.5 Little Dantzic Cove

N 46° 56' 57.8" W 055° 58' 58.2"
At the western tip of the Burin Peninsula, exposure at Little Dantzic Cove is allied to the uppermost Random Formation, of Tommotian age. Large-scale yellow sandstone beds occur, with erosional tops and redeposited phosphatic and lithic clasts in their basal portions. Deposition of this unit occurred within a storm-influenced, macrotidal shelf setting.

As at Grand Bank Head, composition of the rip-up clasts is varied. They range from granular carbon-rich phosphatic textures with variable amounts of clastic material, to pure gelatinous material that appears to coat quartzose grains and fill interstitial spaces (Figure 8.8). In addition, rip up clasts comprising iron-rich grains within a fine calcium-rich matrix occur throughout. The sandstone surrounding these rip-ups is bound by a sparry calcite cement.

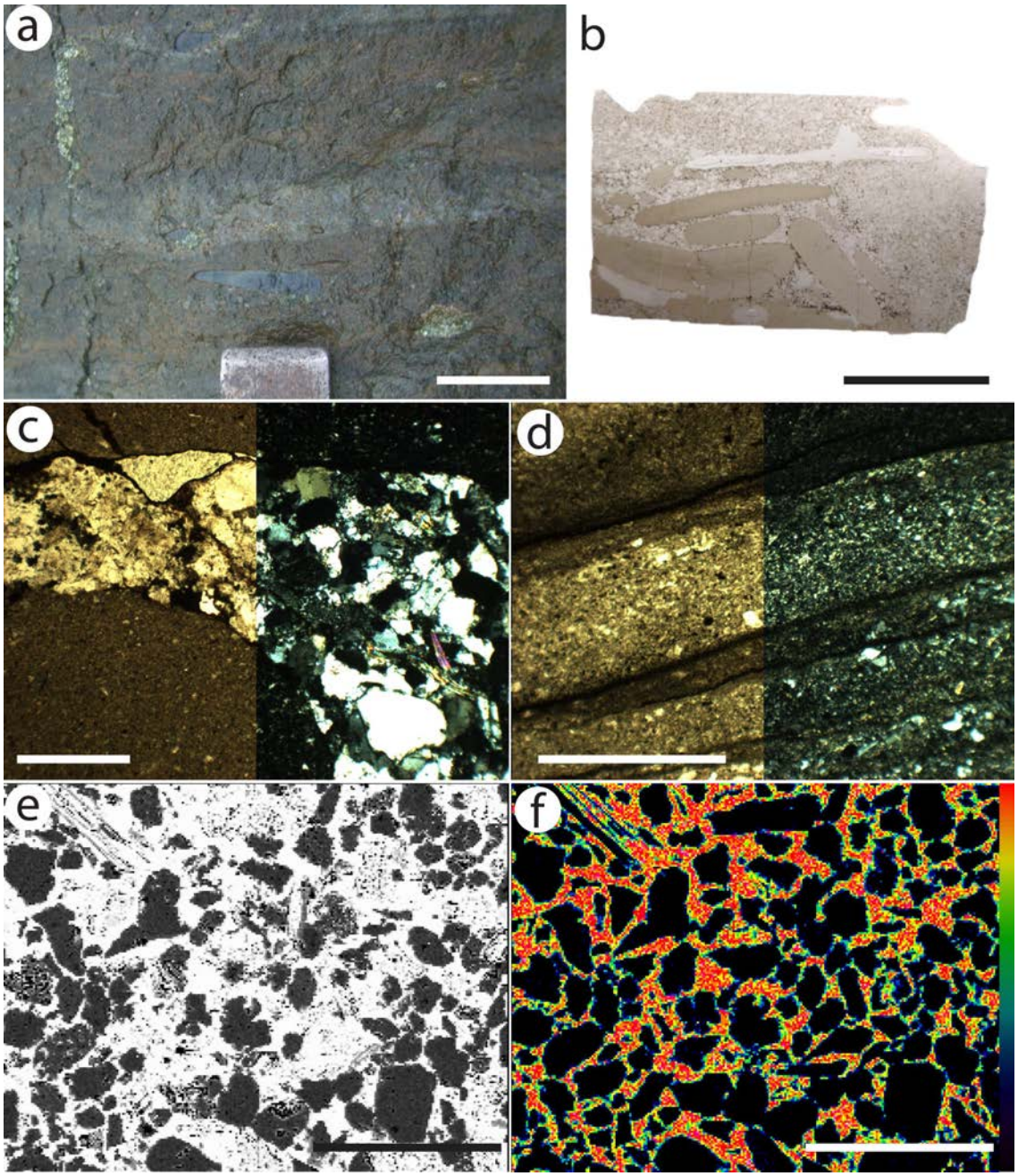


Figure 8.7: Phosphate sedimentology, petrology and mineralogy at Grand Bank Head. a) Sedimentological setting for phosphate. Phosphatic (and other) nodules are somewhat energetically ripped up and reposited. Scale bar 10 cm. b) Thin section texture, illustrating flattened rounded rip-up clasts with darkened outer margins. Scale bar 1 mm. c) Optical photomicrograph of dark granular phosphate with sharp, carbonaceous edges. Plane polars left hand side, cross polars right hand side. Scale bar 1 mm. d) Optical photomicrograph of carbonaceous layering within granular phosphate and clastic material. Plane polars left hand side, cross polars right hand side. Scale bar 1 mm. e) SEM-BSE image of dense interstitial phosphate texture. Scale bar 10 μm. f) SEM-EDX phosphorus map of field of view in (e). Scale bar 10 μm. Sample GBH-1a from Grand Bank, Chapel Island Formation.

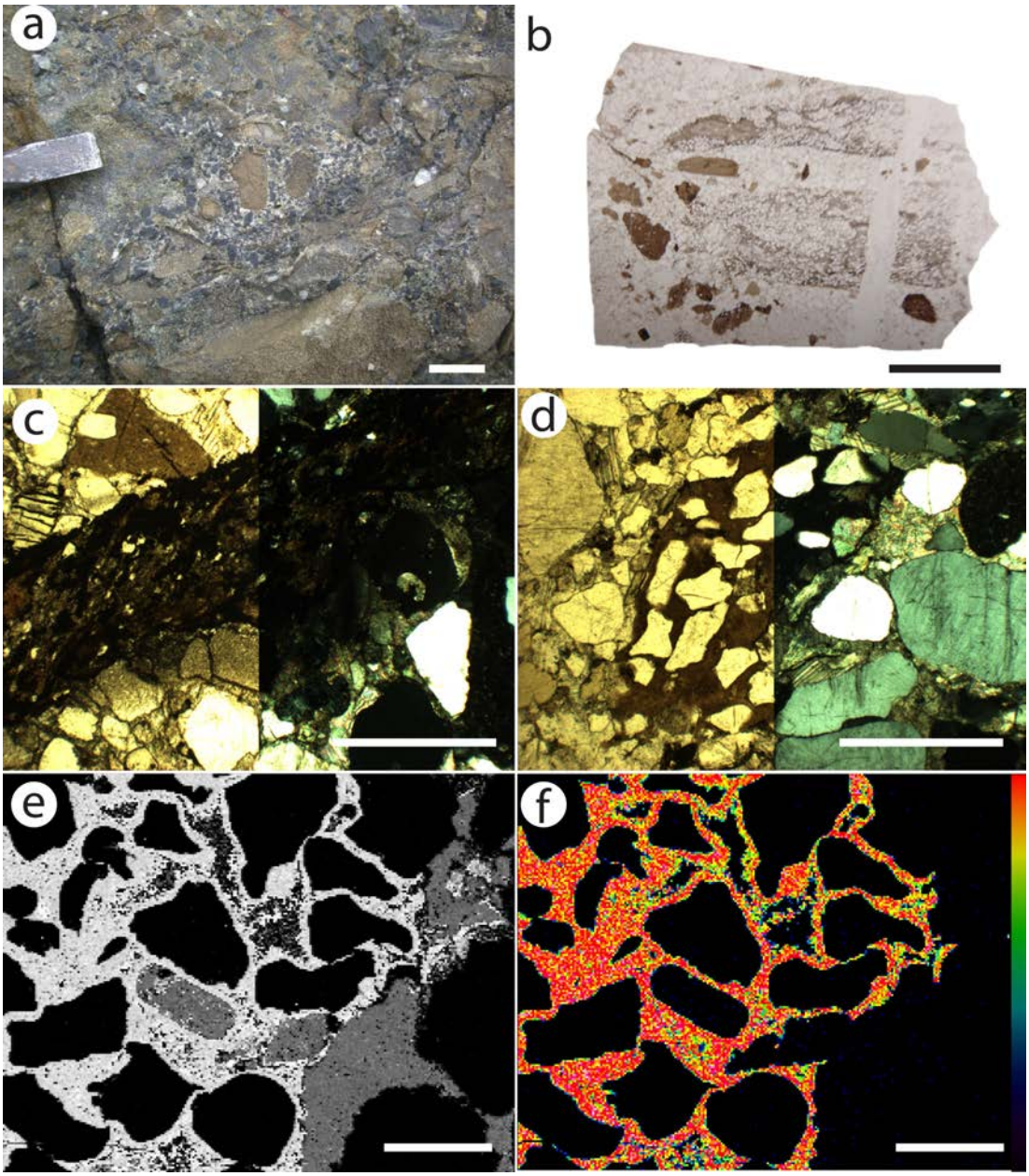


Figure 8.8: Phosphate sedimentology, petrology and mineralogy at Little Dantzic Cove. a) Sedimentological setting for phosphate. Coarse conglomeratic reworked texture, incorporating phosphatic, sandy and carbonate clasts. Scale bar 2 cm. b) Thin section texture, illustrating rip-up clasts of varying appearance and mineralogy. More diffuse areas in the matrix may represent secondary mineralisation. c) Optical photomicrograph of sheared phosphate-carbononaceous layers within the siltstone matrix. Plane polars left hand side, cross polars right hand side. Scale bar 100 μm. d) Optical photomicrograph of gelatinous, rimming and interstitial pure phosphate. Plane polars left hand side, cross polars right hand side. Scale bar 100 μm.e) SEM-BSE image of rimming and interstitial phosphate texture. Scale bar 10 μm. f) SEM-EDX phosphorus map of field of view in (e). Scale bar 10 μm. Sample LDC-1a from Little Dantzic Cove, Random Formation.

Similar to Grand Bank Head, the association of different phosphatic and non-phosphatic lithologies in these sandy beds implies sampling from a succession of primary early lithifying textures. The pure interstitial phosphatic material gives some indication of its formation, in initially rimming clasts before filling pore spaces. This suggests a similar mode of formation to that proposed by Pufahl & Grimm (2003) for phosphatic grainstones and coated grains. Cryptocrystalline granular phosphate is broadly comparable to that seen elsewhere in the Avalonian succession and in the Torridon Group, but without *in-situ* data, it is not possible to resolve textural associations into a model of phosphogenesis. It is likely, however, that all phosphate textures, and presumably those calcium-rich portions, formed under more quiescent periods that were subsequently eroded and reworked.

8.6 Modes of Formation and Perspective

The vast differences in age between units of the Avalonian and Placentian successions, and the wide variation in depositional setting through evolving tectonic regimes, precludes synthesis of these phosphatic occurrences into a unified model for phosphogenesis at this time. Instead, individual occurrences have been assessed in isolation, with respect to their particular sedimentological settings.

It is possible to draw broad comparisons between some of these occurrences and other phosphates observed in this study, from the 1 Ga-old Torridon Group. Especially in the Ediacaran Avalonian succession, the presence of granular phosphate textures intimately associated with carbonaceous layers and carbon enrichments, at Spaniards Bay South and Ferrylands Head, or with putative microbial structures as at Silos Cove, suggests local biological interactions with the sediment implicated in phosphate formation. In addition, the abundance of iron-bearing minerals in all of these sediments suggests that the iron pump and shuttle would have also been a viable mechanism for concentrating phosphate. In contrast to older phosphatic deposits, however, Avalonian phosphates are distributed across a wide range of depositional settings, from likely euxinic turbiditic deposits of the Fermeuse Formation at Silos Cove, to the oxygenated fluvial units of the Ferryland Head Formation at Ferrylands Head. This perhaps reflects elevated global concentrations of available phosphate, which contributes to the large-scale phosphorite deposits elsewhere at

this time, meaning supersaturation-induced authigenic growth of apatite is more easily achieved in a range of palaeoenvironments.

Recovery of phosphatic material only in reworked strata of the Placentian series frustrates complete understanding of its formation in Phanerozoic rocks. These rip-up textures are, however, indication that phosphatic mineralogies formed much more rarely, and apparently during depositional hiatuses prior to subsequent erosion. The low abundance of authigenic phosphate may be in part due to lower global concentrations as newly evolved energy-demanding motile metazoans sequester it in metabolic and structural molecules. Changes in the chemistry of the sediment profile as a result of bioturbation-derived oxygenation are thought to deepen the redox boundary (Brasier & Callow 2007), along with the optimum loci of phosphogenesis and other authigenic mineral growth. As a result, the conjunction of phosphate yielding material and optimum precipitation conditions is likely to happen more rarely, or only under localised microenvironments, further contributing to the minerals' rarity. The generally low concentrations of carbonaceous material in these rip-up textures further corroborates this hypothesis, implying phosphate formation occurred at a depth in the sediment where all carbonaceous material had degraded and been recycled.

In summary, these first detailed reports of sedimentary phosphate in the terminal Neoproterozoic and Proterozoic-Cambrian boundary rocks of eastern Newfoundland add important perspective to the emerging picture of phosphatic evolution through time. Avalonian occurrences appear broadly similar in texture and mineralogical associations to deposits seen deeper in the Proterozoic, whereas abundances and textures are fundamentally different following the Precambrian-Cambrian boundary biological and chemical revolution. Further efforts should be made to explore coeval strata worldwide, even in areas without economic-scale phosphorite deposits, to enrich the database of phosphate occurrences, and help in more fully understanding biochemical interactions and evolution at this time.

Chapter 9

Context and Perspectives

The newly described microbiota and phosphate deposits of the Torridon Group in northwest Scotland are dated to a crucial, revolutionary time within the Proterozoic (cf. Knoll et al. 2007); second only to the Cambrian explosion that marks its termination. For this reason, comparative sections from the older Gunflint Formation of Ontario, Canada, and the younger boundary strata of the Avalonian and Placentian of eastern Newfoundland have also been analysed, so as to place the Torridon sedimentological and biological phenomena in context.

The discoveries made within these three sections, and the novel analyses carried out, add information to the growing knowledge of life, geology and chemistry in the Proterozoic. Specific context that they provide in the fields of microbiology, phosphate chemistry and astrobiology are here presented with wider-ranging perspective for the rest of the Proterozoic and beyond.

9.1 Microbiota

9.1.1 Fossil Affinities

The exceptional preservation of microfossils in the Torridon phosphates allows observation and study not only of large, well preserved, recalcitrant acritarchs, but also much else within the ecological assemblage, including the taphonomic spectrum arising from physicochemical and biological degradation. For this reason, and the fact that a lacustrine depositional environment approaches a closed system, we may interpret the assemblage of phosphate-hosted microfossils as having the potential to encapsulate more of the Torridon lake microbiota than has previously been documented.

Owing to the morphological simplicity and evolutionary antiquity of many of the Torridonian (and indeed all Proterozoic) microfossils, it is probably not prudent to attempt to relate them directly to modern genera or families. In addition, it is possible that the major algal and bacterial divisions had not acquired their characteristic derived crown group features at this time, further hindering taxonomic allocation. It should be possible, however, to make preliminary assessments into whether individual microfossils are of prokaryotic or eukaryotic affinity, and thereby determine the relative abundances of these fundamentally different domains and ways of life. This is not a simple process. Since prokaryotes have a more ancient evolutionary heritage which undoubtedly predates the Torridonian rocks (e.g. Awramik & Barghoorn 1977), then it may be logical to assume that any fossil observed is prokaryotic, until proven otherwise. Multiple lines of evidence thus become necessary to suggest a eukaryotic, rather than a prokaryotic affinity, especially given the large size and morphological complexity of certain bacteria (Bailey et al. 2006).

Features that may be consistent with eukaryotic affinity include a combination of a large ($\sim$60 μm) size plus the presence of a complex wall ultrastructure which may take the form of ornamentation of the outer wall, or median splits or circular pylomes as excystment structures (Javaux et al. 2003, 2001, 2004, Knoll et al. 2006, Strother et al. 2011). It should be noted that none of these characteristics, when seen independently, necessarily imply a eukaryotic affinity. For example, the recent findings of Javaux et al. (2010) of large (300 μm diameter) spherical organic-walled vesicles within the 3.2 Ga Moodies Group of South Africa demonstrates the extreme size that ancient prokaryotes or their sheaths may achieve.

On the basis of these requirements, several forms from the Torridon rocks may be interpreted as fossil eukaryotes. While these, and other forms contained with the phosphate and described from acid maceration of the shales by Strother et al. (2011), may be assigned a eukaryotic affinity, it is clear from the statistical survey of the Torridonian form taxa (Chapter 3) that the dominant morphologies comprise simple, small, spherical and ellipsoidal coccoids, of likely prokaryotic affinity. Similarly, the abundant clusters of coccoids and filamentous morphotypes may best be regarded as benthic mat-forming prokaryotes.

Distribution of the fossil forms within the phosphate does not give much clue as to the likely planktonic or benthic affinity of the fossil organisms. All individuals recovered are distributed equally and randomly thoughout the fossiliferous nodules, without the stratal or lateral clustering or concentration expected from *in-situ* benthic organisms. Even when filamentous forms are recovered, thet are almost always found secondarily worked into bunches or patches of a few intertwined filaments. Thus, inference of the Torridon fossils as planktonic or benthic is done so on the basis of modern distributions of such morphotypes, whereas their deposition and preservation most likely occurred in a somewhat disturbed seston layer at the sediment-water interface.

When the overall dominance of prokaryotic forms, the presence of eukaryotes, and the taphonomic evidence is taken into account, the assemblage can be argued to preserve a community including bacterial and likely algal primary production together with an accompanying heterotrophic bacterial component.

9.1.2 Diversity

The newly described Torridon phosphate- and shale-hosted microfossil deposit (Chapter 3 and 4) contains 17 formally described genera and 25 species, 8 of which are new. The resultant assemblage is considerably more diverse than previously appreciated (Cloud & Germs 1971, Downie 1962, 1984, Peat & Diver 1982, Zhang 1982), with representatives of benthic filamentous bacteria, coccoid algae and bacteria, and planktonic forms, both prokaryotic and eukaryotic, as well as a previously unrecognized heterotrophic component. The Torridon rocks contain fossils recognised elswhere in Proterozoic assembages of this age, including examples of *Valeria* (Figure 3.16i-k), *Pterospermopsimorpha* (Figure 3.16h), and *Dictyosphaera* (Strother et al. 2011), as well as leiospheres with median split excystment structures. In comparison with the worldwide microfossil diversity at this time, however, the Torridon assemblage has a number of notable deficiencies.

Several deposits date to around 1000 Ma ago, including the Hector Formation of southwestern Alberta, Canada (Moorman 1974), the Bangemall Group of northwestern Australia (Buick & Knoll 1999), and probably also several Russian and Chinese deposits that have poor age constraints (e.g. the Billyakh Group of the Anbar uplift, Russia (Sergeev et al. 1995)). Within these deposits, specific morphotypes have been

described that are assigned to major revolutions in the biosphere. *Bangiomorpha pubescens* Butterfield, for example, has multi-celled arrangements and differentiated cells, being allied to the red algae (Butterfield 2000). Similarly, the appearance of stalked cyanobacteria *Polybessarus bipartitus* Schopf is suggested to reflect a new phase in prokaryotic evolution (Sergeev 2009).

In a global biostratigraphic review of the Proterozoic, Sergeev (2009) recognised two characteristic assemblages of Mesoproterozoic-Neoproterozoic rocks, which he names the Turukhanian unit, between 1.2 and 1.03 Ga, and the Uchuromayan unit, between 1.03 and 0.85 Ga. Characteristic taxa of these units are *Bangiomorpha pubescens* Butterfield and *Polybessarus bipartitus* Schopf for the former, and spine bearing *Trachyhystrichosphaera* sp. and *Prolatoforma* sp. for the latter. Yet the Torridon assemblage, which dates to the beginning of the Uchuromayan unit, despite its moderate diversity, does not contain any of these taxa.

There may be numerous reasons for the absence of these hallmark Mesoproterozoic-Neoproterozoic forms in the Torridon rocks, despite its overall moderately high diversity. It may be that the early, experimental forms that are found in some coeval marine strata had yet to make the transition to terrestrial environments, and may even be unable to do so. Colonisation of lacustrine waters presumably requires some element of wind dispersal of spores or hardy vegetative forms, and larger eukaryotic or complex forms may not have been capable of such transport. Alternatively, the non-marine lacustrine waters may present an unsuitable environment, which is prohibitive to certain taxa newly evolved in marine waters. Differing water chemistries or the local stresses posed by episodic desiccation or eutrophication may preclude colonization by organisms adapted for fundamentally different environments.

Previously, it may have been argued that the absence of certain taxa from an assemblage like the Torridon was due to taphonomic biases imposed in that environment. Detailed study of the preservation of these microfossils using high-resolution techniques, and objective assessment of the taphonomic biases imposed on those preserved fossils however, give a clearer picture of likely degradational losses. In the case of the Torridon, extremely high fidelity of preservation of even the most diaphanous membranes, conferred by preservation in phosphate and iron-rich clay minerals (Chapter 6), as well as a taphonomic profile that is dominated by moderate physical and chemical decay, suggests that any taphonomic biases are likely to be very

minor. Thus, the complete absence of a particular taxon is most likely to represent a primary absence, for at least one of the reasons detailed above.

Studies are now starting to provide growing support for a Precambrian land based biota in the form of palaeosols (Brasier 2011, Retallack & Mindszenty 1994); stromatolites (Awramik & Buchheim 2009, Buick 1992); microbially induced sedimentary structures (Prave 2002); molecular ages (Raven & Edwards 2001); and carbon isotope signatures (Knauth & Kennedy 2009). Until recently, few body fossils have been recognised (Cloud & Germs 1971, Downie 1962, 1984, Naumova & Pavlovsky 1961, Peat & Diver 1982, Zhang 1982). The exceptionally preserved ecological assemblage in the Torridon phosphates may therefore help to develop this picture of a verdant Proterozoic landscape.

9.1.3 Taphonomy

The Torridon phosphate-hosted microfossils described herein are arguably the best preserved assemblage yet known from non-marine conditions in the Proterozoic. They reveal the exciting and previously unrecognised potential of sedimentary phosphate for the fine preservation of cellular and ultrastructural details in such ancient rocks, as well as preserving a complete taphonomic spectrum from pristine organic microfossils to well-dispersed kerogen. Such rich information allows an assessment of the broad taxonomic affinities of the microorganisms, with implications for our understanding of the ecosystem structure and nutrient recycling in 1 Ga-old lakes.

For the first time, it has been possible to objectively assess the taphonomic grade of an organic-walled microfossil deposit in the biological, physical and chemical domains, through application of the herein devised taphospace classification. The utility of this classification has been demonstrated in both the 1 Ga Torridon assemblages, and the 2 Ga Gunflint Formation. It allows comparison of taphonomic alteration within and between deposits, which previous taphonomic indices (Bartley 1996, Grey & Willman 2009) have failed to do.

The taphospace classification and three-dimensional plot are useful tools for semi-quantitatively assessing and visualizing the nature of the preservational environment and, by extension, preservation potential of different types (e.g. vegetative cells versus

resistant cysts) or organic-walled microfossil. Such visualizations may be characteristic for certain environments or preservational lithologies, and it may be possible to trace transitions through taphospace as biological and taphonomic environments evolve together through the Proterozoic and Phanerozoic. They may also help to understand the degree of information loss within an assemblage, for example if tearing or fragmentation is common in an assemblage, delicate structures or features may be more easily abraded away, leaving only the more robust taxonomic representatives. Similarly, it will help in assessing the degree of morphological alteration within an assemblage that may be used, given sufficient comparative data, to retro-deform or retro-decay microfossils to give a more accurate view of assemblage diversity and disparity.

During the compilation of the Proterozoic taxonomic atlas (Appendix D), and review of all accessible monographs describing Proterozoic microfossil taxa, it is clear that many formally described morphotypes are delineated solely on the basis of taphonomic artifacts. As a result, treatment of these different morphotypes as distinct formal taxa will result in a gross overestimation of taxonomic richness.

For example, the Gunflint assemblage genus of small isolated coccoids, *Huroniospora* Barghoorn and Tyler 1965, has 4 species, each differentiated by the ornamentation of their wall. In this case, however, the ornamentation refers largely to differing scales of granulation, which is often irregular and morphologically indistinguishable to the wall flocculation and dissemination that occurs during chemical degradation. Similarly, the Neoproterozoic spheromorphic genus *Kildinosphaera* comprises 4 species, the majority of which are defined on the basis of the structure of compressional folds and shape of the flattened vesicle.

Taphonomic artifacts may be characteristic of a certain kind of fossil in a certain environment, for example, the response of a rigid vesicle to shale-like compaction. Therefore, classification on the basis of these taphonomic features is of some use within that deposit. Differing taphonomic conditions between different environments may produce markedly different morphotypes, however, given the same original organism.

If Proterozoic taxa should be treated solely as taphomorphic variants, as some authors have implied, then their binomial, Linnaean names and descriptions, as well

as the frequent assignation to higher, modern taxa (e.g. the genus *Siphonophycus* assigned to the Class Hormogonaceae (Schopf 1968)), is misleading and inappropriate. A reconsideration of formal taxonomy, taking taphonomy into account, will be more valuable in the long term, although more technically challenging.

Carrying out this taxonomic reconsideration is beyond the scope of the present study, but it is hoped that taphospace classification will be valuable in differentiating between primary and taphonomically induced morphologies in varying depositional environments. Using taphospace to qualitatively 'retro-decay' previously described Proterozoic taxa may see a significant reduction in diversity, and it will be of interest to see new patterns that may develop in taxonomic richness and taphonomic alteration throughout the Proterozoic. Such a process, using the qualitative taphonomic characters herein used to define the taphospace, would neccessarily be imprecise. It will likely require comparison between many individuals in a fossil assemblage, and a thorough understanding of each mode of decay. Nevertheless, even an imprecise removal of taphonomic overprints is likely to result in changes in the observed diversity.

Future descriptions of new organic-walled microfossil taxa need not be frustrated by the possibility of including taphonomic features in the diagnosis. High-resolution imaging and analysis techniques such as FIB-TEM are becoming more widespread in the study of fossils (Javaux et al. 2004, Marshall et al. 2005, 2007, Moczydlowska et al. 2011, 2010, Moczydlowska & Willman 2009), and the ability to resolve fossil wall structures on a very fine scale should enable easy distinction between intrinsic structural components of a wall, and local disruptions. Where possible, these techniques should be employed in the descriptions of all new microfossil taxa, heralding a new, high-tech age of palaeobiology.

9.2 Phosphate

9.2.1 Preservation in Phosphate

The rocks of the billion-year-old Torridon Group of northwest Scotland are unique in hosting carbonaceous fossils within shales and phosphatic nodules, preserved with exceptional fidelity. No other well-preserved microfossils have been described from cryptocrystalline phosphate, and the fine scale preservation seen in three dimensions within the phosphatic nodules is mirrored to some extent in the preservation of the

same material, albeit compressed, in the shales. In a similar vein, from the extensive phosphorite and minor phosphatic deposits worldwide from the Proterozoic and lower Cambrian, no such microfossil preservation has ever been recorded, despite the common occurrence of disseminated carbonaceous material. Thus, it follows that the Torridon preservation stands alone in its quality, and some reason for this can be sought in an examination of associated mineralogy.

High-resolution *in-situ* elemental analysis techniques (FIB-TEM and FIB-SEM-EDX) reveal the close association between phosphatic and iron-rich clay phases within the cryptocrystalline precipitate, corroborated by SEM-EDX elemental maps of phosphate from several different lithofacies. In places, these associations seem to be zoned in the vicinity of preserved microfossils, comprising clays oriented sub-parallel to cell walls, and in some cases an infilling potassium-rich phase. As these iron-rich clays are also observed in the finer, non-phosphatic portions of the Torridon Group, it is therefore suggested that their presence is intimately linked to, if not necessary for the fine scale preservation of these deposits.

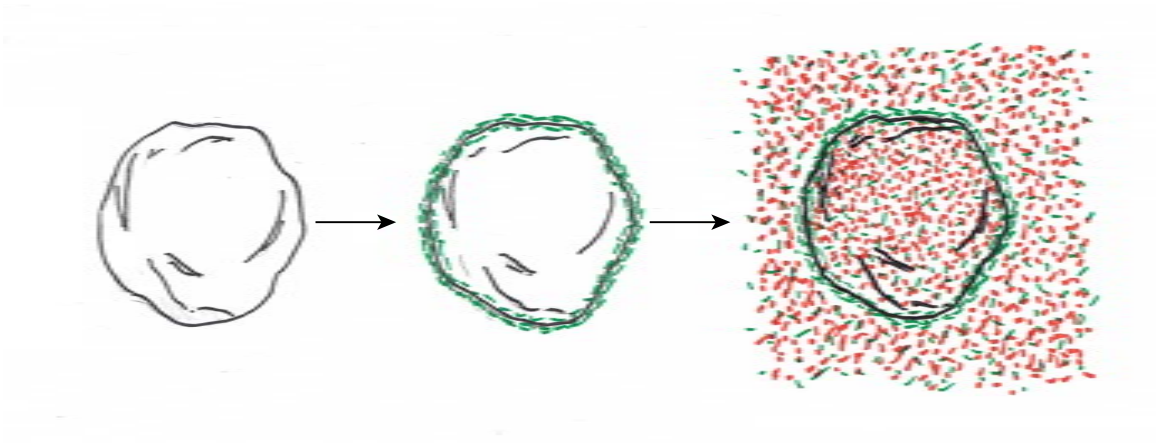


Figure 9.1: Schematic illustrating the hypothesised mode of preservation for the Torridon fossils. Organic structures are deposited in the zone of phosphatisation, having recieved some degree of degradation or deformation. The first minerals to form are tabular clay minerals (green), that use the organic membrane as a template and draw ions for their growth directly from the decay microenvironment. Supersaturation-driven precipitation in the remainder of the seston layer proceeds more slowly, and these mixed crystallites of apatite and iron-rich clay subsequently infill voids and interstita.

The clay minerals must be relatively early-forming, using the organic walls as templates for their authigenic growth (Figure 9.1). As a result, they rapidly occlude

the microbes, preventing further biological or chemical decay, and preserving them in the state in which they were deposited. Subsequent rapid formation of an intermixed precipitate of clays and phosphate within a seston layer or beneath the sediment-water interface maintains the spatial relationships of the assemblage.

It is not immediately clear why these iron-rich clays form alongside phosphate and within shales of the Torridon, nor why their authigenic growth precedes that of the phosphate around organic-walled microfossils. It may be that the localized conditions of the Torridon lakes provided elevated concentrations of iron and aluminium, or that the action of microbial metabolisms concentrates these ions locally to permit supersaturation-induced authigenic growth. The kinetics and cycling of these clays are, as yet, poorly understood, but their close association with apatite and carbonaceous material in the Torridon points to interrelated mechanisms of formation, perhaps related to the iron pump and shuttle (Shaffer 1986), or to the unique and understudied chemistries of the seston layer.

9.2.2 Phosphate in context

This study has reported sedimentary phosphate for the first time from the 2 Ga Gunflint Formation, and the Precambrian-Cambrian deposits of eastern Newfoundland, as well as describing in detail the fossiliferous phosphates of the Torridon Group. These minor deposits add information about the distribution and associations of phosphate within Proterozoic rocks, that can assist in further understanding its formation in a premetazoan non-uniformitarian world.

Economic-grade phosphorite deposits have been well reported from Proterozoic and early Cambrian strata, but their significance only noted in terms of volumetric abundance and concentration (e.g. review in Cook & Shergold 1986). Patterns in phosphatisation throughout the Precambrian show long periods of phosphate scarcity, interrupted by large-scale phosphogenic events that result in the deposition of economic phosphorites. Three such events are recognized in the Proterozoic (Papineau 2010): around 2 Ga, resulting in the formation of Jatuli-type formations of Finland (Äikäs 1980, Laajoki & Saikkonen 1977) and the Jhamarkotra Formation, Aravalli Supergroup, India (Banerjee 1971, Chauhan 1979), amongst others; around 1 Ga, with phosphates seen in Bambuí Group, Brazil (Dardenne et al. 1986), and elsewhere; and at the Precambrian-Cambrian boundary, where worldwide phosphorite deposits occur, including those in the Amadeus basin and Adelaide Geosyncline in

Australia (Howard 1986, Wells et al. 1970).

Thus, the three minor phosphate deposits described here broadly correlate with these Proterozoic events, but their small phosphate concentrations represent phosphogenesis in non-optimal basins. Nevertheless, the sedimentological and petrological detail contained within these occurrences help to build a picture of changing phosphate chemistries and associations accompanying biochemical revolutions throughout the Proterozoic.

9.2.2.1 Torridon

Phosphate within the lacustrine rocks of the Torridon group may be considered enigmatic, as its occurrence was previously thought to be a solely marine phenomenon (Föllmi 1996). The small quantities of phosphate present here, however, indicate that non-cosmopolitan factors are at work to concentrate and precipitate cryptocrystalline phosphate in select locations where conditions are favourable, thus avoiding the non-marine problem.

The exceptional preservation of fossils in the Torridon hints at the factors controlling phosphogenesis. Evidence from fossil distribution and taphonomy, the co-occurrence of macroscopic wrinkle structures and microbially induced sedimentary structures, sedimentological data, and petrographic associations all indicate a heavily biologically-controlled system. In combination with a biologically induced iron redox pump, these factors drive phosphate and associated ions to local supersaturation and induce precipitation within the flocculent seston layer at the sediment surface and to shallow depths within the sediment.

This model has general applicability to other Proterozoic phosphate deposits. Ever since the evolution of bacterial ecosystems, variations in the input of phosphorus into an aquatic system will prompt an accompanying reaction in primary bacterial production rates. The modifying and concentrating action of microbial blooms results in the formation of nodular and banded phosphate throughout the Precambrian, adding weight to the understudied hypothesis of microbially controlled cycling of nutrients on the early Earth (Krajewski et al. 1994). In all aquatic systems, microbes may have represented a significant biomass, but their structural lability permitted more rapid degradation and efficient recycling of nutrient and wall components back into the

water column. Thus, taking only the fossil record of microbes and the carbonaceous component of sediments into account, the living biomass may be underappreciated. By extension, their effect on biogeochemical cycling may also be underappreciated, and small-scale, information-rich deposits like the Torridon indicate their powerful influence on sedimentary and biochemical dynamics.

The large-scale phosphogenic events that occur in the Proterozoic at 2 Ga and 1 Ga (Papineau 2010), and again at the Precambrian-Cambrian boundary (Cook & Shergold 1986) are likely to have some global driver that increases amount of available phosphate in the oceans, or increases the available loci for phosphate formation. The long-term periodicity of the events is evidence for some plate tectonic or orogenic control on the net flux of phosphate to the oceans. An alternative, biological, explanation may influence temporal concentrations of phosphate in the oceans around one billion years ago.

Fossil evidence suggests the evolution and diversification of eukaryotes occurred towards the end of the Mesoproterozoic (e.g. Butterfield 2000, Javaux et al. 2004). The more efficient intracellular machinery and metabolisms of these eukaryotes would have led to their ecological dominance in favourable water bodies. In isolated systems, or even globally, nitrogen will become biolimiting, as non-nitrogen fixing eukaryotes outcompete heterocyst-bearing cyanobacteria for space and other bioavailable nutrients. For a short time, nitrogen biolimitation will result in a decrease in biomass, and thus an increase in aquatic phosphate concentrations. Globally elevated phosphate will make sediments more susceptible to supersaturation and precipitation, allowing the formation of large-scale phosphorite deposits. This phenomenon is likely to be short lived before nitrogen-fixing cyanobacteria rise to dominance and equilibrium is established in the ecosystem.

The 'nitrogen-crisis' hypothesis for the formation of phosphate deposits is currently untested, but evidence in its support may lie in the fine scale changes in diversity and ecological dominance recorded in fossiliferous material at this time. It is possible that a similar crisis occurred at the Precambrian-Cambrian boundary, following the evolution of metazoans with high nitrogen demands.

9.2.2.2 Gunflint Formation

The formation of the chemical cherts, carbonates, iron formations and the phosphates in the Gunflint Formation is a process that cannot be explained by simple uniformitarian models. Such sediments do not form together in shallow water environments today, or for much of the Phanerozoic. The thermodynamics and kinetics of the chemical sediments make their precipitation purely as a result of supersaturation unlikely (Jarvis et al. 1994). Thus, some authors (e.g. Konhauser & Ferris 1996) have suggested that microbes played an active or passive part in precipitating not only phosphate, but all Proterozoic chemical sediments.

The observations of phosphate in the Gunflint Formation lend support to the idea of a microbially-induced chemical environment. As Figure 9.2 shows, a typical cross section through a modern bacterial mat contains aerobic and anaerobic photoautotrophs at the top, followed by aerobic and anaerobic heterotroph groups. Beneath this, differing cellular metabolisms predominate, utilising differing compounds as electron donors with increasing depth and decreasing pore water oxygen content: nitrate or nitrite; iron; sulphur or sulphate; and methane (Armstrong & Brasier 2005, Konhauser 2006). The redox state of the sediment governs the dominance of oxidising or reducing ecosystem components. This is a simplified picture and these zones are not, in fact, well defined, with different metabolisms thriving under differing temporally controlled microconditions (Baumgartner et al. 2006, Visscher et al. 2000). All of the chemical sediments in the Gunflint can be passively associated with one or more of the members of this typical, but alterable, microbial mat. Photosynthesisers contribute to the growth of carbonate and chert stromatolites (although there is good petrological evidence to suggest that some of the cherty structures had carbonate precursors (Sommers et al. 2000)). Iron oxidation and reduction will assist in fixing iron into the sediments, in some cases mineralising the bacteria that precipitate it (Schelble et al. 2004). The bacterial groups that are known to concentrate phosphate in large quantities (e.g. *Beggiatoa*, *Thioploca*, and *Thiomargarita* cf. Papineau (2010)) are all recognised sulphide oxidisers. Thus, fluctuating environmental conditions may cause temporary dominance of one community from the mat ecosystem, and thus bring about a changing or cyclic alternation of predominant chemical sediment.

Caution is needed before interpreting all the chemical sediments of the Gunflint and other Proterozoic deposits as being directly influenced or controlled by bacteria. In the Gunflint, other supporting evidence for a strong biological component to

the system is relatively scarce. Verifiably biogenic organic or iron-mineralised fossils are not present in all sections or facies; and the extent of microbially induced sedimentary structures *sensu* Noffke (2010) and classic stromatolites is limited. Thus, interpretation of the microbial involvement in the precipitation of all Gunflint chemical sediments must necessarily remain tentative.

9.2.2.3 Newfoundland

The process of microbial concentration and release of phosphate at or below the sediment–water interface during the Proterozoic will be fundamentally altered approaching the Precambrian-Cambrian transition, where more efficient eukaryotic and heterotrophic ecosystems, and ultimately the grazing of metazoans, limit the extent and tenacity of microbial mats and seston concentrations (Brasier & Callow 2007).

This transition is seen to some extent in the minor phosphate deposits of the Avalonian and Placentian series, where phosphate textures switch from carbon-rich and granular, indicating formation at a shallow depth within the sediment, to carbon-poor and reworked, suggesting rarer phosphate formation at depositional hiatuses and potentially at some depth within the sediment column.

The change in locus of phosphogenesis is likely to be largely due to the increase in penetration of bioturbation at the beginning of the Cambrian, oxygenating the upper layers of the sediment column and pushing the redox boundary and its associated microbial metabolisms to a greater depth (Brasier & Callow 2007)(Figure 9.2). As a result, carbonaceous material that settles and is deposited at the sediment water interface is more aggressively, oxygenically degraded, and its constituent nutrients are released directly back into the water column or bound to sediment particles in low concentrations. The fluctuations in redox chemistry that are so common in the undisturbed and poorly oxygenated Proterozoic sediments are too deeply buried to affect the fresh influx of carbonaceous material, and by the time they are buried to an appropriate depth, any ionic compounds will have been lost. Thus, the mode of phosphogenesis shifts upon entering the Phanerozoic, to supersaturation-driven precipitation that is derived from direct supply of metazoan and skeletonised material with high phosphate concentrations to the sediment surface (Krajewski et al. 1994). As a result, global loci of phosphogenesis are limited to areas of upwelling or similar eutrophic concentration, where these organisms can thrive (Föllmi 1996).

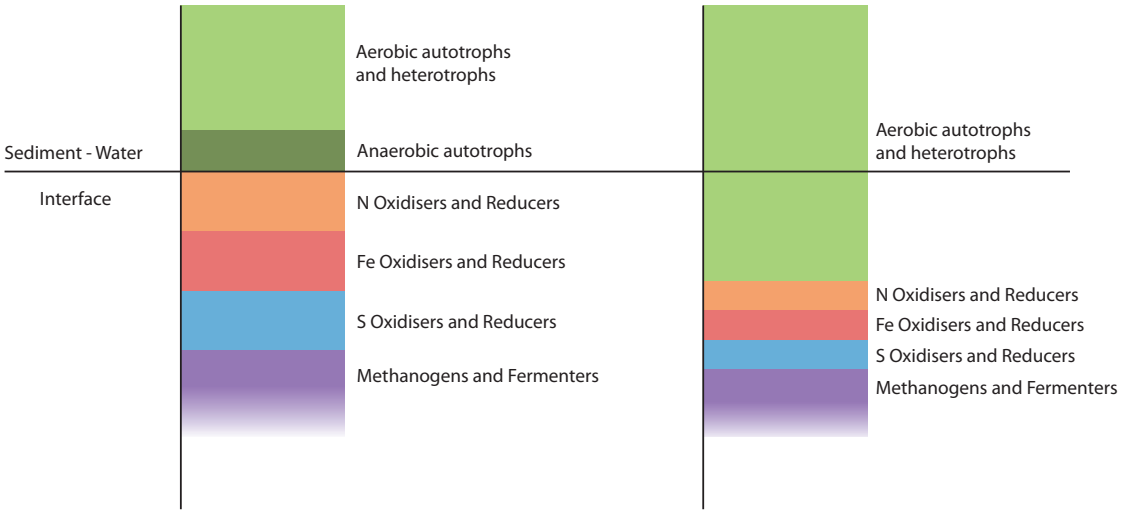


Figure 9.2: Profiles through microbial mats with varying metabolisms as different electron donors become dominant with depth. Two profiles on the left and right represent differing states during the Proterozoic and the Phanerozoic respectively. Increasing biological tiering and bioturbation across the Precambrian-Cambrian boundary drives the redox boundary deeper in the sediment, pushing the chemotrophs away from regions of fresh flux of material. Thus, the zones of early diagenetic mineralisation, like phosphogenesis, are lost.

9.3 Astrobiology

The studies of microfossils from the Torridon, as well as their taphonomy and preservation allow better understanding of Proterozoic evolution and environmental interactions. They are also useful to astrobiological research, informing on the search for life in space by guiding investigations as to where to look, how to look, and what to expect of extraterrestrial life.

Understanding the early record of life on Earth gives perspective on the rates of evolution and diversification in different environments, and the reaction of life to changing conditions. These perspectives may be extrapolated to other planetary environments, to inform on the expected evolutionary advancement of potential extraterrestrial organisms. Such comparisons are increasingly used in astrobiological applications, as out knowledge of planetary biology is currently limited to the single data point of Earth. For example, studies of 1 Ga-old fossil assemblages show that, approximately 2500 million years after the likely appearance of life on Earth, complex eukaryotic cells were thriving, the oceans were displaying the beginnings of algal multicellularity, and terrestrial water bodies were colonized by diverse eukaryotic and prokaryotic ecosystems. Extrapolating these advancements to relic habitable environments elsewhere gives an indication of the maximum evolutionary stage achieved before habitability was lost, and therefore helps guide search directions and instrumentation.

Investigation into the Torridon rocks has shown that one billion years ago, life thrived in lakes, forming diverse ecosystems with interacting populations that were able to adapt to adverse conditions. Similar analogous environments may be sought extraterrestrially, especially in the solar system where bodies classically viewed as uninhabitable may in fact host small, habitable refugia. Thus, the search for extraterrestrial life need not be limited to Earth-like oceanic planets, but can be extended to places where isolated or ephemeral water bodies exist. Such environments may be found in, for example, seasonally ephemeral melt pools on or just below the surface of Mars (Mckay & Davis 1991); closed subsurface oceans on Europa (Gaidos et al. 1999); or the methane lakes on Titan (McKay & Smith 2005). In the latter case, the replacement of water by methane would necessitate a fundamentally non-terrestrial chemistry (Schulze-Makuch & Grinspoon 2005), but the physiodynamic interactions

of life with its environment would be the same.

These potentially habitable refugia may be current or relic fossil environments. The study and understanding of degradation and fossilization on Earth allows informed expectation of what organisms may be preserved in certain environments, and the amount of morphological alteration likely. By extension this will guide not only the kinds of deposits that are likely to host fossil life, but also the most appropriate instrumentation to study it. For example, in remote exploration of the surface of Mars, clay minerals in craters and delta deposits (Ehlmann et al. 2008) may be targeted for organic-walled microfossils like those preserved by phosphate and clay in the Torridon, and the surfaces of apparently barren siliciclastic rocks may be scanned for ordered macroscopic wrinkle structures caused by colonizing microbial mats. Mineralogical proxies for life may be identified in the absence of structural fossils: as the precipitation of phosphate of a specific given cryptocrystalline texture in the Proterozoic seems largely biologically induced, its presence in extra-terrestrial environments may be indicative of present or past life.

Chapter 10

Future directions

In describing in detail the microfossils and phosphate from the Torridon rocks of northwest Scotland, this study has contributed to the growing picture of colonized terrestrial environments in the Proterozoic. Further discoveries and description of phosphate from the Palaeoproterozoic Gunflint Formation and the Avalonian and Placentian successions of the Precambrian-Cambrian boundary in eastern Newfoundland have contributed sedimentological and petrological data to global perspective of biogeochemical evolution on the early Earth. These discoveries and analyses have answered some outstanding questions for the Proterozoic, but have also raised new avenues for further research and investigation.

10.1 Geology

The relatively undeformed rocks of the Torridon Group offer a unique opportunity for studying and reconstructing ancient fluvial catchment areas and lacustrine basins. This has been achieved here for the first time for such a lacustrine environment, but continued geological and sedimentological investigation of similar rocks of all ages may lead to the discovery of more preserved lakes. With a larger dataset, it will be possible to make comparisons between lacustrine environments of different ages and of different continental settings.

In analyzing the lake basins of the Torridon Group and, to some extent, the fault bounded Sleat Group, studies of the geology of the underlying Stoer Group have been neglected. The Stoer basins contain carbonates and sedimentary structures indicative of a lagoonal or marginal marine environment, and thus represent a preceding marine phase of Torridonian deposition. It will be of interest to investigate the sedimentological relations here, as well as to compare any contistuent micro- or macrobiota.

In addition, the Stoer Group contains deposits from a bolide impact within the Stac Fada Formation (Amor et al. 2008), the regional geological and biological effects of which require further study.

10.2 Microbiota

These information-rich Torridon phosphates still hold many questions for future study. Continued high-resolution analysis of the full range of morphotypes represented in the Torridon will allow for extensive testing for eukaryocity through ultrastructural criteria (Javaux 2007, Javaux et al. 2003, 2001, Knoll et al. 2006), as well as resolving the full range of microbial morphotypes on a small scale. Three dimensional spatial reconstructions using serial SEM or synchrotron slice data will the reveal the relationships between different members of the seston consortia or microbial mat construction. This work is underway in collaboration with Manchester University and the Diamond Light Source in Oxfordshire.

Modern experimental studies may be used to constrain the criteria used in classification of taphonomic profiles, and application of the taphospace criteria and plots to other Proterozoic assemblages will allow the characterization of different taphonomic environments throughout the Precambrian. Using these semi-quantitative visualisations of degradational effects will allow reassessment of diversity in previously described and newly discovered assemblages. In addition, changes in taphonomic style can be traced through different palaeoenvironments and time periods, leading to a fuller understanding of biogeochemical evolution.

In summary, clays seem to play an important role in preserving fine details of organic-walled microfossils in the Torridon. It would be of interest to investigate the extent of thier involvement in other fine preservational schemes, within the Torridon, elsewhere in association with phosphate, and in other preservational regimes (e.g. in preserving details of the Burgess Shale macrofauna (Orr et al. 1998, We 1996). This study has demonstrated the utility of high-resolution techniques to resolve small-scale associations of clays and other minerals, and continued development and application of these techniques can potentially reveal much about this preservational system.

Reports of organic-walled microfossils from the Torridon phosphates and shales can be further supported by chemical studies into these rocks. Analyses of organic

biomarkers may help to constrain the representative species present, and the occluding nature of the sedimentary phosphate provides a relatively pristine environment for these studies, as they preclude penetration by contaminating organisms. This work is underway in collaboration with Imperial University. Similarly, isotope studies on the carbonaceous material or the sulphides associated with the Torridon microfossils may help to confirm a biological origin or influence. This work is underway in collaboration with the University of Glasgow.

Finally, the discovery of an extraordinarily well-preserved ecological assemblage, both in previously undescribed sedimentary phosphates, and within a rare and ambient lacustrine setting, should prompt renewed exploration into Proterozoic sedimentary rocks. Recognition of eukaryotic and prokaryotic members of an assemblage, as well as complete taphonomic spectra (often ignored by authors seeking the best preserved fossils), can add considerable weight and context to an understanding of the Proterozoic biosphere.

10.3 Microbially induced macrostructures

Wrinkle structures have been described in detail from the siliciclastic rocks of the Diabaig Formation, Torridon Group of northwest Scotland. While such structures have been noted and allied with other microbially-induced sedimentary structures (Gehling 1999, Noffke 2010), their sedimentological and palaeoenvironmental relationships have yet to be fully resolved. Torridonian wrinkle structures show some palaeoenvironmental dependence, but it is suggested that a thorough search beyond the Torridon sediments will enable the build-up of a rich database of variable wrinkle structures. In combination with modern experimental studies of their formation and preservation, global characterization of these biological structures can provide important indicators of biological activity where organic-walled microfossils may be lacking.

10.4 Phosphate

Discovery of phosphatic deposits in the Gunflint Formation, Torridon Group, and Precambrian-Cambrian boundary rocks of eastern Newfoundland are volumetrically minor when compared with large-scale phosphorites, but they contain important sedimentological and petrological information that provides context to phosphate evolu-

tion on the early Earth.

Future studies should further strive to better understand non-economic deposits of phosphate to help identify the local or global variables that bring about its formation on short and long timescales. It is expected that many more minor phosphate deposits are overlooked in the Proterozoic, and their discovery and documentation can fill in holes in current understanding and test hypotheses of their formation.

Modern experimentation is also valuable in future investigations. Fossil evidence indicates that phosphate must form over short timescales of days to months, and thus the precipitation and fossilization processes should be replicable under laboratory conditions. Carrying out this work would constrain the palaeochemistry and palaeoenvironments under which phosphates can form, and may tie in certain microbial consortia, thereby linking biochemical cycling with sedimentary petrology on the early Earth. This work is underway in collaboration with NASA Ames.

Finally, renewed searches in similar environments to the Torridon may reveal other fossil-bearing phosphatic rocks, providing further data to the interpretations of preservational processes and biochemical interactions that have been intrinsically inferred from the isolated Torridon example.

Many future avenues of investigation have resulted from study and documentation of a uniquely preserved microfossil deposit in northwest Scotland and comparative deposits. The Proterozoic period is no longer a distant mysterious time period, but a well-documented one, which is still revealing its secrets in the face of increasingly advanced technologies. Fossils and phosphates of the Torridon Group add a valuable dimension to this understanding, helping to construct a picture of Proterozoic terrestrial colonization and authigenic mineral evolution in a non-uniformitarian world.

References

Abramov, O. & Mojzsis, S. J. (2009), 'Microbial habitability of the Hadean Earth during the late heavy bombardment', *Nature* **459**(7245), 419–422.

Äikäs, O. (1980), Uraniferous phosphorite and apatite-bearing gneisses in the proterozoic of finland, *in* J. Ferguson & A. B. Goleby, eds, 'Uranium in the Pine Creek Geosyncline', International Atomic Energy Agency, Vienna, pp. 675–681.

Allwood, A. C., Walter, M. R. & Marshall, C. P. (2006), 'Raman spectroscopy reveals thermal palaeoenvironments of c. 3.5 billion-year-old organic matter', *Vibrational Spectroscopy* **41**, 190–197.

Amor, K., Hesselbo, S. P., Porcelli, D., Thackrey, S. & Parnell, J. (2008), 'A precambrian proximal ejecta blanket from Scotland', *Geology* **36**(4), 303–306.

Anderson, M. (1981), 'The Random Formation Of Southeastern Newfoundland - A Discussion Aimed At Establishing Its Age And Relationship To Bounding Formations', *American Journal Of Science* **281**(6), 807–830.

Anderson, M. M., Choubert, G., Faure-Muret, A. & Timofeev, B. V. (1982), 'Les couches bavlinella de part et d'autre de l'atlantique', *Bull. Soc. Gèol. Fr* **2**, 389–392.

Armstrong, H. A. & Brasier, M. D. (2005), *Microfossils*, 2nd edn, Blackwell.

Awramik, S. M. & Barghoorn, E. S. (1977), 'The gunflint microbiota', *Precambrian Research* **5**(2), 121–142.

Awramik, S. M. & Buchheim, H. P. (2009), 'A giant, late archean lake system: The meentheena member (Tumbiana Formation; Fortescue Group), western australia', *Precambrian Research* **174**(3-4), 215–240.

Bailey, J. V., Joye, S. B., Kalanetra, K. M., Flood, B. E. & Corsetti, F. A. (2006), 'Evidence of giant sulphur bacteria in neoproterozoic phosphorites', *Nature* **445**(7124), 198–201.

Bambach, R. K., Bush, A. M. & Erwin, D. H. (2007), 'Autecology and the filling of ecospace: Key metazoan radiations', *Palaeontology* **50**(Part 1), 1–22.

Banerjee, D. M. (1971), 'Precambrian stromatolitic phosphorites of Udaipur, Rajasthan, India', *Geological Society of America Bulletin* **82**(8), 2319–2329.

Barghoorn, E. S. & Tyler, S. A. (1965), 'Microorganisms from the Gunflint chert', *Science* **147**, 563–577.

Bartley, J. (1996), 'Actualistic taphonomy of cyanobacteria: Implications for the precambrian fossil record', *Palaios* **11**(6), 571–586.

Battison, L. & Brasier, M. D. (2012), 'Remarkably preserved prokaryote and eukaryote microfossils within 1 Ga-old lake phosphates of the Torridon Group, NW Scotland', *Precambrian Research* **196**, 204–217.

Baumgartner, L. K., Reid, R. P., Dupraz, C., Decho, A. W., Buckley, D. H., Spear, J. R., Przekop, K. M. & Visscher, P. T. (2006), 'Sulfate reducing bacteria in microbial mats: Changing paradigms, new discoveries', *Sedimentary Geology* **185**(3-4), 131–145.

Benton, M. J. & Donoghue, P. C. J. (2007), 'Paleontological evidence to date the tree of life', *Molecular Biology And Evolution* **24**(1), 26–53.

Benus, A. P. (1988), Sedimentological context of a deep-water Ediacaran fauna (Mistaken Point Formation, Avalon Zone, eastern Newfoundland), *in* E. Landing, G. M. Narbonne & P. Myrow, eds, 'Trace Fossils, Small Shelly Fossils and the Precambrian-Cambrian Boundary', Vol. 463, New York State Museum Bulletin.

Bény-Bassez, C. & Rouzaud, J. N. (1985), 'Characterization of carbonaceous matter by correlated electron and optical microscopy and raman microspectrometry', *Scanning Electron Microscopy* **1**, 119–132.

Berner, R. A. (1980), *Early Diagenesis - A theoretical approach*, Princeton University Press.

Brasier, A. T. (2011), 'Searching for travertines, calcretes and speleothems in deep time: Processes, appearances, predictions and the impact of plants', *Earth-Science Reviews* **104**(4), 213–239.

Brasier, M., Anderson, M. & Corfield, R. (1992), 'Oxygen And Carbon Isotope Stratigraphy Of Early Cambrian Carbonates In Southeastern Newfoundland And England', *Geological Magazine* **129**(3), 265–279.

Brasier, M. D. (1990), 'Phosphogenic events and skeletal preservation across the Precambrian-Cambrian boundary interval', *Geological Society, London, Special Publications* **52**(1), 289–.

Brasier, M. D. & Antcliffe, J. B. (2009), 'Evolutionary relationships within the Avalonian Ediacara biota: new insights from laser analysis', *Journal Of The Geological Society* **166**, 363–384.

Brasier, M. D. & Callow, R. H. T. (2007), 'Changes in the patterns of phosphatic preservation across the Proterozoic-Cambrian transition', *Memoirs of the Association of Australasian Palaeontologists* **34**, 377–389.

Brasier, M. D., Green, O. R., Jephcoat, A. P., Kleppe, A. K., Kranendonk, M. J. V., Lindsay, J. F., Steele, A. & Grassineau, N. V. (2002), 'Questioning the evidence for earth's oldest fossils', *Nature* **416**(6876), 76–81.

Brasier, M. D., Green, O. R., Lindsay, J. F., McLoughlin, N., Steele, A. & Stoakes, C. (2005), 'Critical testing of earth's oldest putative fossil assemblage from the ˜3.5 ga apex chert, chinaman creek, western australia', *Precambrian Research* **140**, 55–102.

Brasier, M. D., Jonathan, B. A. & Richard, H. T. C. (2010), *Evolutionary Trends in Remarkable Fossil Preservation Across the Ediacaran-Cambrian Transition and the Impact of Metazoan Mixing*, Springer, pp. 519–568.

Brasier, M. D., McLoughlin, N., Green, O. R. & Wacey, D. (2006), 'A fresh look at the fossil evidence for early archaean cellular life', *Philosophical Transactions of the Royal Society B: Biological Sciences* **361**(1470), 887–902.

Brasier, M., Green, O., Lindsay, J. & Steele, A. (2004), 'Earth's oldest (similar to 3.5 Ga) fossils and the 'Early Eden hypothesis': Questioning the evidence', *Origins Of Life And Evolution Of The Biosphere* **34**(1-2), 257–269.

Brasier, M. & Lindsay, J. (1998), 'A billion years of environmental stability and the emergence of eukaryotes: New data from northern Australia', *Geology* **26**(6), 555–558.

Briggs, D. E. G. & Wilby, P. R. (1996), 'The role of the calcium carbonatecalcium phosphate switch in the mineralization of soft-bodied fossils', *Journal of the Geological Society of London* **153**, 665–668.

British Geological Survey (1976), '1:50,000 solid and drift, Broadford'.

Brocks, J. J. & Summons, R. E. (2004), Sedimentary hydrocarbons, biomarkers for early life, *in* H. D. Holland & K. K. Turekian, eds, 'Biogeochemistry', Vol. 8 of *Treatise on Geochemistry*.

Brocks, J., Logan, G., Buick, R. & Summons, R. (1999), 'Archean molecular fossils and the early rise of eukaryotes', *Science* **285**(5430), 1033–1036.

Brocks, J., Love, G., Summons, R., Knoll, A., Logan, G. & Bowden, S. (2005), 'Biomarker evidence for green and purple sulphur bacteria in a stratified Palaeoproterozoic sea', *Nature* **437**(7060), 866–870.

Brody, R., Edwards, H. & Pollard, A. (2001), 'A study of amber and copal samples using FT-Raman spectroscopy', *Spectrochimica Acta Part A-Molecular And Biomolecular Spectroscopy* **57**(6), 1325–1338.

Brugnoli, E. & Farquhar, G. D. (2000), Photosynthetic fractionation of isotopes, *in* T. D. Sharkey & S. Caemmerer, eds, 'Photosynthesis, physiology and metabolism', Kluwer Academic Publishers, The Netherlands, pp. 399–434.

Buchan, K. L., Mertanen, S., Park, R. G., Pesonen, L. J., Elming, S. A., Abrahamsen, N. & Bylund, G. (2000), 'Comparing the drift of laurentia and baltica in the proterozoic: the importance of key palaeomagnetic poles', *Tectonophysics* **319**(3), 167–198.

Buick, R. (1992), 'The antiquity of oxygenic photosynthesis: evidence from stromatolites in sulphate-deficient archaean lakes', *Science* **255**(5040), 74–78.

Buick, R. & Knoll, A. (1999), 'Acritarchs and microfossils from the Mesoproterozoic Bangemall Group, northwestern Australia', *Journal Of Paleontology* **73**(5), 744–764.

Bullock, R. J. & Morris, J. R. amd Selby, D. (2011), 'New findings of body and trace fossils in the st. bride's area, cape st. mary's peninsula, newfoundland', *Current Research, Newfoundland and Labrador Department of Natural Resources* **11-1**, 241–252.

Butterfield, M. J., Knoll, A. H. & Swett, K. (1994), Paleobiology of the Neoproterozoic Svanbergfjellet Formation, Spitsbergen, Vol. 34 of *Fossils and Strata*, Wiley-Blackwell, p. 84pp.

Butterfield, N. J. (2000), 'Bangiomorpha pubescens n. gen., n. sp.: implications for the evolution of sex, multicellularity, and the Mesoproterozoic/Neoproterozoic radiation of eukaryotes', *Paleobiology* **26**(3), 386–399.

Butterfield, N. J. (2007), 'Macroevolution and macroecology through deep time', *Palaeontology* **50**(Part 1), 41–55.

Callow, R. H. T., Battison, L. & Brasier, M. D. (2011), 'Diverse microbially induced sedimentary structures from 1 Ga lakes of the Diabaig Formation, Torridon Group, northwest Scotland', *Sedimentary Geology* **239**(3-4), 117–128.

Callow, R. H. T. & Brasier, M. D. (2009), 'Remarkable preservation of microbial mats in Neoproterozoic siliciclastic settings: Implications for Ediacaran taphonomic models', *Earth-Science Reviews* **96**(3), 207–219.

Chambers, L. A. & Trudinger, P. A. (1979), 'Microbiological fractionation of stable sulfur isotopes: A review and critique', *Geomicrobiology Journal* **1**, 249–293.

Chauhan, D. S. (1979), 'Phosphate-bearing stromatolites of the Precambrian Aravalli phosphorite deposits of the Udaipur region, their environmental significance and genesis of phosphorite', *Precambrian Research* **8**(1-2), 95–126.

Christie-Blick, N., Dyson, I. & Vonderborch, C. (1995), 'Sequence stratigraphy and the interpretation of neoproterozoic earth history', *Precambrian Research* **73**(1-4), 3–26.

Christie, R. L. & Sheldon, R. P. (1986), Proterozoic and cambrian phosphorites - regional review: North america, *in* P. J. Cook & J. H. Shergold, eds, 'Phosphate deposits of the world: Proterozoic and Cambrian phosphorites', Cambridge University Press, pp. 101–106.

Cloud, P. & Germs, A. (1971), 'New Pre-Paleozoic nannofossils from the stoer formation (Torridonian), northwest scotland', *Geological Society of America Bulletin* **82**(12), 3469–3474.

Cocks, L. R. M. & Torsvik, T. H. (2006), European geography in a global context from the Vendian to the end of the Palaeozoic, *in* Gee, DG and Stephenson, RA, ed., 'European Lithosphere Dynamics', Vol. 32 of *Geological Society Memoirs*, pp. 83–95.

Cohen, P. A., Knoll, A. H. & Kodner, R. B. (2009), 'Large spinose microfossils in Ediacaran rocks as resting stages of early animals', *Proceedings Of The National Academy Of Sciences Of The United States Of America* **106**(16), 6519–6524.

Condon, D., Prave, A. & Benn, D. (2002), 'Neoproterozoic glacial-rainout intervals: Observations and implications', *Geology* **30**(1), 35–38.

Cook, P. J. & Shergold, J. H. (1986), *Phosphate deposits of the world: Proterozoic and Cambrian phosphorites*, Cambridge University Press.

Cota, G., Pomeroy, L., Harrison, W., Jones, E., Peters, F., Sheldon, W. & Weingartner, T. (1996), 'Nutrients, primary production and microbial heterotrophy in the southeastern Chukchi Sea: Arctic summer nutrient depletion and heterotrophy', *Marine Ecology-Progress Series* **135**(1-3), 247–258.

Cowie, J. & McNamara, K. J. (1978), 'Olenellus (Trilobita) from the lower cambrian strata of north-west scotland', *Palaeontology* **21**(3), 615–634.

Dacks, J. & Roger, A. (1999), 'The first sexual lineage and the relevance of facultative sex', *Journal Of Molecular Evolution* **48**(6), 779–783.

Dardenne, M. A., Trompette, R., Magalhaes, L. F. & Soares, L. A. (1986), Proterozoic and cambrian phosphorites—regional review: Brazil, *in* P. J. Cook & J. H. Shergold, eds, 'Phosphate deposits of the world: Proterozoic and Cambrian phosphorites', Cambridge University Press, pp. 116–131.

Dauphas, N., Robert, F. & Marty, B. (2000), 'The late asteroidal and cometary bombardment of Earth as recorded in water deuterium to protium ratio', *Icarus* **148**(2), 508–512.

De Paolo, D. (1981), 'Neodymium Isotopes In The Colorado Front Range And Crust-Mantle Evolution In The Proterozoic', *Nature* **291**(5812), 193–196.

Delsemme, A. (1999), 'The deuterium enrichment observed in recent comets is consistent with the cometary origin of seawater', *Planetary And Space Science* **47**(1-2), 125–131.

Des Marais, D. & Walter, M. (1999), 'Astrobiology: Exploring the origins, evolution, and distribution of life in the Universe', *Annual Review Of Ecology And Systematics* **30**, 397–420.

Donoghue, P. C. J. (2007), 'Palaeontology - Embryonic identity crisis', *Nature* **445**(7124), 155–156.

Douzery, E., Snell, E., Bapteste, E., Delsuc, F. & Philippe, H. (2004), 'The timing of eukaryotic evolution: Does a relaxed molecular clock reconcile proteins and fossils?', *Proceedings Of The National Academy Of Sciences Of The United States Of America* **101**(43), 15386–15391.

Downie, C. (1962), So-called spores from the torridonian, *in* 'Proceedings of the Geological Society, London', Vol. 1600, pp. 127–128.

Downie, C. (1984), *Acritarchs in British Stratigraphy*, Blackwell Scientific Publications, Oxford.

Droser, M., Gehling, J. & Jensen, S. (2006), 'Assemblage palaeoecology of the Ediacara biota: The unabridged edition?', *Palaeogeography Palaeoclimatology Palaeoecology* **232**(2-4), 131–147.

Dutkiewicz, A., Volk, H., George, S., Ridley, J. & Buick, R. (2006), 'Biomarkers from Huronian oil-bearing fluid inclusions: An uncontaminated record of life before the Great Oxidation Event', *Geology* **34**(6), 437–440.

Dutkiewicz, A., Volk, H., Ridley, J. & George, S. (2003), 'Biomarkers, brines, and oil in the Mesoproterozoic, Roper Superbasin, Australia', *Geology* **31**(11), 981–984.

Dzik, J. (2005), 'Behavioral and anatomical unity of the earliest burrowing animals and the cause of the "Cambrian explosion"', *Paleobiology* **31**(3), 503–521.

Ehlmann, B. L., Mustard, J. F., Fassett, C. I., Schon, S. C., Head, III, J. W., Marais, D. J. D., Grant, J. A. & Murchie, S. L. (2008), 'Clay minerals in delta deposits and organic preservation potential on Mars', *Nature Geoscience* **1**(6), 355–358.

Eyles, N. & Eyles, C. (1989), 'Glacially-Influenced Deep-Marine Sedimentation Of The Late Precambrian Gaskiers Formation, Newfoundland, Canada', *Sedimentology* **36**(4), 601–620.

Fettes, D. J., Mendum, J. R., Smith, D. I., Survey, B. G. & Watson, J. V. (1992), *Geology of the Outer Hebrides: memoir for 1:100000 (solid edition) geological sheets, Lewis, and Harris, Uist and Barra (Scotland)*, Natural Environment Research Council.

Föllmi, K. B. (1996), 'The phosphorus cycle, phosphogenesis and marine phosphate-rich deposits', *Earth Science Reviews* **40**(1-2), 55–124.

Fralick, P., Davis, D. W. & Kissin, S. A. (2002), 'The age of the Gunflint Formation, Ontario, Canada: single zircon U-Pb age determinations', *Canadian Journal of Earth Sciences* **39**, 1085–1091.

Fralick, P. W. (1988), Microbial Bioherms, lower Proterozoic Gunflint formation, Thunder Bay, Ontario, *in* H. H. J. Geldsetzer, N. P. James & G. E. Tebbut, eds, 'Reefs, Canada and Adjacent Areas', Vol. 13, pp. 24–29.

Fralick, P. W. & Barrett, T. J. (1995), *Depositional controls on iron formation associations in Canada*, Special Publication 22, International Association of Sedimentologists, pp. 137–156.

Francis, S., Margulis, L. & Barghoorn, E. S. (1978), 'On the experimental silicification of microorganisms II. on the time of appearance of eukaryotic organisms in the fossil record', *Precambrian Research* **6**(1), 65–100.

Franklin, J. M. (1991), Proterozoic geology of the thunder bay to marathon area, *in* J. M. Franklin, B. R. Schneiders & E. R. Koopman, eds, 'Mineral deposits in the western Superior Province, Ontario. Field Trip 9', Geological Survey of Canada, Ottowa, Open File Report 2164, pp. 105–110.

Gaidos, E. J., Nealson, K. H. & Kirschvink, J. L. (1999), 'Life in ice-covered oceans', *Science* **284**(5420), 1631–1633.

Gardner, S. & Hiscott, R. (1988), 'Deep-Water Facies And Depositional Setting Of The Lower Conception Group (Hadrynian), Southern Avalon Peninsula, Newfoundland', *Canadian Journal Of Earth Sciences* **25**(10), 1579–1594.

Gehling, J. (1999), 'Microbial mats in terminal Proterozoic siliciclastics: Ediacaran death masks', *Palaios* **14**(1), 40–57.

Gehling, J. G. & Narbonne, G. M. (2007), 'Spindle-shaped Ediacaran fossils from the Mistaken Point assemblage, Avalon Zone, Newfoundland', *Canadian Journal Of Earth Sciences* **44**(3), 367–387.

Gehling, J., Narbonne, G. & Anderson, M. (2000), 'The first named Ediacaran body fossil, Aspidella terranovica', *Palaeontology* **43**(Part 3), 427–456.

Geikie, A. (1900), 'Summary of progress of the geological survey of great britain for 1899'.

Glenn, C., Follmi, K., Riggs, S., Baturin, G., Grimm, K., Trappe, J., Abed, A., Galliolivier, C., Garrison, R., Ilyin, A., Jehl, C., Rohrlich, V., Sadaqah, R., Schidlowski, M., Sheldon, R. & Siegmund, H. (1994), 'Phosphorus And Phosphorites - Sedimentology And Environments Of Formation', *Eclogae Geologicae Helvetiae* **87**(3), 747–788.

Goodwin, A. M. (1956), 'Facies relations in the Gunflint iron formation (Ontario)', *Economic Geology* **51**(6), 565–595.

Gostling, N. J., Dong, X. & Donoghue, P. C. J. (2009), 'The role of the calcium carbonatecalcium phosphate switch in the mineralization of soft-bodied fossils', *Palaeontology* **52**, 169–186.

Gostling, N. J., Thomas, C. W., Greenwood, J. M., Dong, X., Bengtson, S., Raff, E. C., Raff, R. A. & Degnan, B. M. (2008), 'Deciphering the fossil record of early bilaterian embryonic development in light of experimental taphonomy', *Evolution and Development* **10**, 339–349.

Grey, K. (1999), 'A modified palynological preparation technique for the extraction of large neoproterozoic acanthomorph acritarchs and other acid insoluble microfossils', *Geological Survey of Western Australia, Record* **199/10**, 1–23.

Grey, K. (2005), *Ediacaran palynology of Australia*, Vol. 31, Association of Australian Paleontologists Memoir.

Grey, K. & Willman, S. (2009), 'Taphonomy Of Ediacaran Acritarchs From Australia: Significance For Taxonomy And Biostratigraphy', *Palaios* **24**(3-4), 239–256.

Hedges, S. B., Chen, H., Kumar, S., Wang, D. Y.-C., Thompson, A. S. & Watanabe, H. (2001), 'A genomic timescale for the origin of eukaryotes', *Bmc Evolutionary Biology* **1**.

Hiscott, R. (1982), 'Tidal Deposits Of The Lower Cambrian Random Formation, Eastern Newfoundland - Facies And Paleoenvironments', *Canadian Journal Of Earth Sciences* **19**(10), 2028–2042.

Hoffman, P., Kaufman, A., Halverson, G. & Schrag, D. (1998), 'A Neoproterozoic snowball earth', *Science* **281**(5381), 1342–1346.

Hofmann, H. (1976), 'Precambrian microflora, Belcher islands, Canada - Significance and Systematics', *Journal of Paleontology* **50**(6), 1040–1073.

Hofmann, H. J., Hill, J. & King, A. F. (1979), 'Late precambrian fossils, southeastern newfoundland', *Geological Survey of Canada Papers* **79-1B**, 83–98.

Hofmann, H., Narbonne, G. & Aitken, J. (1990), 'Ediacaran Remains From Intertillite Beds In Northwestern Canada', *Geology* **18**(12), 1199–1202.

Holland, H. D. (2006), 'The oxygenation of the atmosphere and oceans', *Philososphical Transactions of the Royal Society B* **361**, 903–915.

Horodyski, R. & Donaldson, J. (1980), 'Micro-Fossils From The Middle Proterozoic Dismal Lakes Group, Arctic Canada', *Precambrian Research* **11**(2), 125–159.

Hough, J. L. (1958), 'Fresh water environment of deposition of Precambrian banded iron formations', *Journal of Sedimentary Petrology* **28**, 414–492.

Howard, P. (1986), Proterozoic and cambrian phosphorites - regional review: Australia, *in* P. J. Cook & J. H. Shergold, eds, 'Phosphate deposits of the world: Proterozoic and Cambrian phosphorites', Cambridge University Press, pp. 101–106.

Isley, A. E. (1995), 'Hydrothermal plumes and the delivery of iron to banded iron formation', *The Journal of Geology* **103**, 169–185.

Jarvis, I., Burnett, W., Nathan, Y., Almbaydin, F., Attia, A., Castro, L., Flicoteaux, R., Hilmy, M., Husain, V., Qutawnah, A., Serjani, A. & Zanin, Y. (1994), 'Phosphorite Geochemistry - State-Of-The-Art And Environmental Concerns', *Eclogae Geologicae Helvetiae* **87**(3), 643–700.

Javaux, E. J. (2007), Patterns of diversification in early eukaryotes, *in* P. Steemans & E. Javaux, eds, 'Recent Advances in Palynology', Vol. 2007/1 of *Notebooks on Geology, Memoir*.

Javaux, E. J., Knoll, A. H. & Walter, M. (2003), 'Recognizing and interpreting the fossils of early eukaryotes', *Origins of Life and Evolution of Biospheres* **33**(1), 75–94.

Javaux, E. J., Knoll, A. H. & Walter, M. R. (2001), 'Morphological and ecological complexity in early eukaryotic ecosystems', *Nature* **412**(6842), 66–69.

Javaux, E. J., Knoll, A. H. & Walter, M. R. (2004), 'TEM evidence for eukaryotic diversity in mid-Proterozoic oceans', *Geobiology* **2**(3), 121–132.

Javaux, E. J., Marshall, C. P. & Bekker, A. (2010), 'Organic-walled microfossils in 3.2-billion-year-old shallow-marine siliciclastic deposits', *Nature* pp. 934–U108.

Jehlicka, J., Urban, O. & Pokorny, J. (2003), 'Raman spectroscopy of carbon and solid bitumens in sedimentary and metamorphic rocks', *Spectrochimica Acta Part A-Molecular And Biomolecular Spectroscopy* **59**(10), 2341–2352.

Johnston, D. T., Wolfe-Simon, F., Pearson, A. & Knoll, A. H. (2009), 'Anoxygenic photosynthesis modulated Proterozoic oxygen and sustained Earth's middle age', *Proceedings Of The National Academy Of Sciences Of The United States Of America* **106**(40), 16925–16929.

Jones, K. & Blake, S. (2003), *Mountain building in Scotland*, Open University Worldwide.

Jordan, H. & Keyes, P. (1964), 'Aerobic, gram-positive, filamentous bacteria as etiologic agents of experimental periodontal disease in hamsters', *Archives of oral biology* **9**(4), 401–413.

Kaufman, A. & Knoll, A. (1995), 'Neoproterozoic Variations In The C-Isotopic Composition Of Seawater - Stratigraphic And Biogeochemical Implications', *Precambrian Research* **73**(1-4), 27–49.

Kempe, A., Wirth, R., Altermann, W., Stark, R., Schopf, J. & Heckl, W. (2005), 'Focussed ion beam preparation and in situ nanoscopic study of Precambrian acritarchs', *Precambrian Research* **140**(1-2), 36–54.

King, A. F., Anderson, M. M. & Benus, A. P. (1988), Late precambrian sedimentation and related orogenesis of the avalon peninsula, eastern avalon zone, *in* P. Davenport, R. N. Hiscott, P. P. O'Neill & L. W. Nolan, eds, 'Geological Association of Canada Annual Meeting, Field Trip Guidebook, Trip, A4'.

Kirschvink, J., Gaidos, E., Bertani, L., Beukes, N., Gutzmer, J., Maepa, L. & Steinberger, R. (2000), 'Paleoproterozoic snowball Earth: Extreme climatic and geochemical global change and its biological consequences', *Proceedings Of The National Academy Of Sciences Of The United States Of America* **97**(4), 1400–1405.

Knauth, L. (2005), 'Temperature and salinity history of the Precambrian ocean: implications for the course of microbial evolution', *Palaeogeography Palaeoclimatology Palaeoecology* **219**(1-2), 53–69.

Knauth, L. P. & Kennedy, M. J. (2009), 'The late precambrian greening of the earth', *Nature* **460**(7256), 728–732.

Knoll, A. (1995), Proterozoic and early Cambrian protists: Evidence for accelerating evolutionary tempo, *in* Fitch, WM and Ayala, FJ, ed., 'Tempo And Mode In Evolution: Genetics And Paleontology 50 Years After Simpson', Natl Academy Press, pp. 63–83.

Knoll, A. (2003), *Life on a young planet: the first three billion years of evolution on earth*, Princeton University Press.

Knoll, A. & Barghoorn, E. (1974), 'Ambient Pyrite In Precambrian Chert - New Evidence And A Theory', *Proceedings of the National Academy of Sciences of the United States of America* **71**(6), 2329–2331.

Knoll, A. H., Barghoorn, E. S. & Awramik, S. M. (1978), 'New Microorganisms from Aphebian Gunflint Iron Formation, Ontario', *Journal of Paleontology* **52**(5), 976–992.

Knoll, A. H., Javaux, E. J., Hewitt, D. & Cohen, P. (2006), 'Eukaryotic organisms in proterozoic oceans', *Philosophical Transactions of the Royal Society B: Biological Sciences* **361**(1470), 1023–1038.

Knoll, A. H., Summons, R. E., Waldbauer, J. R. & Zumberge, J. E. (2007), The geological succession of primary produces in the oceans, *in* 'Evolution of Primary Producers in the Sea', Academic Press, pp. 133–163.

Knoll, A. & Walter, M. (1992), 'Latest Proterozoic Stratigraphy And Earth History', *Nature* **356**(6371), 673–678.

Kodner, R. B., Summons, R. E. & Knoll, A. H. (2009), 'Phylogenetic investigation of the aliphatic, non-hydrolyzable biopolymer algaenan, with a focus on green algae', *Organic Geochemistry* **40**(8), 854–862.

Konhauser, K. O. (2006), *Introduction to Geomicrobiology*, 1st edn, Wiley-Blackwell.

Konhauser, K. O. & Ferris, F. G. (1996), 'Diversity of iron and silica precipitation by microbial mats in hydrothermal waters, Iceland: Implications for Precambrian iron formations', *Geology* **24**, 323–326.

Kopp, R., Kirschvink, J., Hilburn, I. & Nash, C. (2005), 'The paleoproterozoic snowball Earth: A climate disaster triggered by the evolution of oxygenic photosynthesis', *Proceedings Of The National Academy Of Sciences Of The United States Of America* **102**(32), 11131–11136.

Krajewski, K., Van Cappellen, P., Trichet, J., Kuhn, O., Lucas, J., Martinalgarra, A., Prevot, L., Tewari, V., Gaspar, L., Knight, R. & Lamboy, M. (1994), 'Biological Processes And Apatite Formation In Sedimentary Environments', *Eclogae Geologicae Helvetiae* **87**(3), 701–745.

Krogh, T. E., Strong, D. F., O'Brien, S. J. & Papezik, V. S. (1988), 'Precise U-Pb zircon dates from the Avalon Terrane in Newfoundland', *Candian Journal of Earth Sciences* **25**, 442–453.

Krumbein, W. E. (2010), Gunflint chert microbiota revisited—neither stromatolites, nor cyanobacteria, *in* J. Seckbach & A. Oren, eds, 'Microbial Mats: Modern and Ancient Microorganisms in Stratified Systems', Vol. 14 of *Cellular Origin, Life in Extreme Habitats and Astrobiology*, Springer Science, pp. 53–70.

Kudryavtsev, A., Schopf, J., Agresti, D. & Wdowiak, T. (2001), 'In situ laser-Raman imagery of Precambrian microscopic fossils', *Proceedings Of The National Academy Of Sciences Of The United States Of America* **98**(3), 823–826.

Kumar, S. & Hedges, S. (1998), 'A molecular timescale for vertebrate evolution', *Nature* **392**(6679), 917–920.

Laajoki, K. & Saikkonen, R. (1977), 'On the geology and geochemistry of the Precambrian iron formations in Väyrylänkylä, South Puolanka area, Finland', *Geological Survey of Finland Bulletin* **292**, 1–137.

LaFlamme, M., Narbonne, G. & Anderson, M. (2004), 'Morphometric analysis of the ediacaran frond Charniodiscus from the mistaken point formation, Newfoundland', *Journal Of Paleontology* **78**(5), 827–837.

Lammer, H., Bredehöft, J. H., Coustenis, A., Khodachenko, M. L., Kaltenegger, L., Grasset, O., Prieur, D., Raulin, F., Ehrenfreund, P., Yamauchi, M. et al. (2009), 'What makes a planet habitable?', *Astronomy and Astrophysics Review* **17**(2), 181–249.

Landing, E., Myrow, P., Benus, A. & Narbonne, G. (1989), 'The Placentian Series - Appearance Of The Oldest Skeletalized Faunas In Southeastern Newfoundland', *Journal Of Paleontology* **63**(6), 739–769.

Lane, N. (2009), *Life Ascending: The Ten Great Inventions of Evolution*, W. W. Norton.

Lepot, K., Benzerara, K. & Philippot, P. (2011), 'Biogenic versus metamorphic origins of diverse microtubes in 2.7 gyr old volcanic ashes: Multi-scale investigations', *Earth and Planetary Science Letters* **312**, 37–47.

Lespade, P., Aljishi, R. & Dresselhaus, M. (1982), 'Model For Raman-Scattering From Incompletely Graphitized Carbons', *Carbon* **20**(5), 427–431.

Li, Z. X., Bogdanova, S. V., Collins, A. S., Davidson, A., De Waele, B., Ernst, R. E., Fitzsimons, I. C. W., Fuck, R. A., Gladkochub, D. P., Jacobs, J., Karlstrom, K. E., Lu, S., Natapov, L. M., Pease, V., Pisarevsky, S. A., Thrane, K. & Vernikovsky, V. (2008), 'Assembly, configuration, and break-up history of Rodinia: A synthesis', *Precambrian Research* **160**(1-2), 179–210.

Lindsay, J. & Brasier, M. (2000), 'A carbon isotope reference curve for ca. 1700-1575 Ma, McArthur and Mount Isa Basins, northern Australia', *Precambrian Research* **99**(3-4), 271–308.

Lineweaver, C. H., Fenner, Y. & Gibson, B. K. (2004), 'The galactic habitable zone and the age distribution of complex life in the Milky Way', *Science* **303**(5654), 59.

Linossier, A., Gajardo, M. & Olavarria, J. (1996), 'Paleomicrobiological study in dental calculus: Streptococcus mutans', *Scanning Microscopy* **10**, 1005–1013.

Liu, A. G., Mcilroy, D., Antcliffe, J. B. & Brasier, M. D. (2011), 'Effaced preservation in the Ediacara biota and its implications for the early macrofossil record', *Palaeontology* **54**(Part 3), 607–630.

Lougheed, M. S. (1983), 'Origin of Precambrian iron-formations in the Lake Superior region', *Geological Society of Americal Bulletin* **94**, 325–340.

Macdonald, F. A., Schmitz, M. D., Crowley, J. L., Roots, C. F., Jones, D. S., Maloof, A. C., Strauss, J. V., Cohen, P. A., Johnston, D. T. & Schrag, D. P. (2010), 'Calibrating the Cryogenian', *Science* **327**(5970), 1241–1243.

Manning, C. E., Mojzsis, S. J. & Harrison, T. M. (2006), 'Geology, age and origin of supracrustal rocks at Akilia, West Greenland', *American Journal Of Science* **306**(5), 303–366.

Margulis, L. & Sagan, D. (1986), *Origins of Sex*, Yale University Press.

Marshall, C. P., Javaux, E. J., Knoll, A. H. & Walter, M. R. (2005), 'Combined micro-Fourier transform infrared (FTIR) spectroscopy and micro-Raman spectroscopy of proterozoic acritarchs: A new approach to palaeobiology', *Precambrian Research* **138**(3-4), 208–224.

Marshall, C. P., Leuko, S., Coyle, C. M., Walter, M. R., Burns, B. P. & Neilan, B. A. (2007), 'Carotenoid analysis of halophilic archaea by resonance Raman Spectroscopy', *Astrobiology* **7**(4), 631–643.

Mawson, D. (1949), 'A third occurrence of glaciation evidenced in the adelaide system', *Transactions of the Royal Society of South Australia* **73**, 117–121.

McIlroy, D. & Logan, G. (1999), 'The impact of bioturbation on infaunal ecology and evolution during the Proterozoic-Cambrian transition', *Palaios* **14**(1), 58–72.

McIlroy, D. & Walter, M. (1997), 'A reconsideration of the biogenicity of *Arumberia banksii* Glaessner & Walter', *Alcheringa* **21**(1-2), 79–80.

Mckay, C. & Davis, W. (1991), 'Duration Of Liquid Water Habitats On Early Mars', *Icarus* **90**(2), 214–221.

McKay, C. P. & Smith, H. D. (2005), 'Possibilities for methanogenic life in liquid methane on the surface of titan', *Icarus* **178**(1), 274–276.

McKerrow, W., Mac Niocaill, C. & Dewey, J. (2000), 'The Caledonian Orogeny redefined', *Journal Of The Geological Society* **157**(Part 6), 1149–1154.

McMahon, S. (2010), Deciphering a Palaeoproterozoic nutrient cycle: New evidence from phosphate in the 1.9 Ga Gunflint Formation, Canada, Master's thesis, University of Oxford.

McNamara, A., Mac Niocaill, C., van der Pluijm, B. & Van der Voo, R. (2001), 'West African proximity of the Avalon terrane in the latest Precambrian', *Geological Society Of America Bulletin* **113**(9), 1161–1170.

Meert, J. & van der Voo, R. (1994), 'The Neoproterozoic (1000-540 Ma) Glacial Intervals - No More Snowball Earth', *Earth And Planetary Science Letters* **123**(1-4), 1–13.

Moczydlowska, M., Landing, E. D., Zang, W. & Palacios, T. (2011), 'Proterozoic Phytoplankton And Timing Of Chlorophyte Algae Origins', *Palaeontology* **54**(Part 4), 721–733.

Moczydlowska, M., Schopf, J. W. & Willman, S. (2010), 'Micro- and nano-scale ultrastructure of cell walls in Cryogenian microfossils: revealing their biological affinity', *Lethaia* **43**(2), 129–136.

Moczydlowska, M. & Willman, S. (2009), 'Ultrastructure of cell walls in ancient microfossils as a proxy to their biological affinities', *Precambrian Research* **173**(1-4), 27–38.

Mojzsis, S., Arrhenius, G., McKeegan, K., Harrison, T., Nutman, A. & Friend, C. (1997), 'Evidence for life on Earth before 3,800 million years ago ', *Nature* **386**(6626), 738.

Mojzsis, S. J. & Arrhenius, G. (1998), 'Phosphates and carbon on mars: Exobiological implications and sample return considerations', *Journal of Geophysical Research* **103**, 28495–28511.

Moorman, M. (1974), 'Microbiota of late Proterozoic Hector formation, southwestern Alberta, Canada', *Journal of Paleontology* **48**(3), 524–539.

Moreau, J. & Sharp, T. (2004), 'A transmission electron microscopy study of silica and kerogen biosignatures in-1.9 Ga gunflint microfossils', *Astrobiology* **4**(2), 196–210.

Morey, G. B. (1983), Animikie Basin, Lake Superior Region, USA., *in* A. F. Trendall & R. C. Morris, eds, 'Iron-Formation: Facts and Problems', Elsevier, Amsterdam, pp. 13–68.

Morey, G. B., Southwick, D. L. & Schottler, S. P. (1991), *Manganiferous zones in Early Proterozoic iron formation in the Emily district, Cuyuna range, east-central Minnesota.*, Vol. 39, Minnesota Geological Survey, Report of Investigations.

Murphy, J., Keppie, J. & Nance, R. (1999), 'Fault reactivation within Avalonia: plate margin to continental interior deformation', *Tectonophysics* **305**(1-3), 183–204.

Myrow, P. (1995), 'Neoproterozoic Rocks Of The Newfoundland Avalon Zone', *Precambrian Research* **73**(1-4), 123–136.

Myrow, P. M. (1987), Sedimentology and depositional history of the Chapel Island Formation (Late Precambrian-Early Cambrian), southeast Newfoundland, PhD thesis, Memorial University, Newfoundland.

Myrow, P. M. (1988), Storm-shelf and tidal deposits of the chapel island and random formations, burin peninsula: facies and trace fossils, *in* P. Davenport, R. N. Hiscott, P. P. O'Neill & L. W. Nolan, eds, 'Geological Association of Canada Annual Meeting, Field Trip Guidebook, Trip, A4', p. 108.

Nagovitsin, K. (2009), 'Tappania-bearing association of the siberian platform: Biodiversity, stratigraphic position and geochronological constraints', *Precambrian Research* **173**(1-4), 137–145.

Narbonne, G. (2005), 'The ediacarabiota: Neoproterozoic origin of animals and their ecosystems', *Annual Review Of Earth And Planetary Sciences* **33**, 421–442.

Narbonne, G. M., Dalrymple, R. W. & G., G. J. (2001), *Neoproterozoic fossils and environments of the Avalon Peninsula, Newfoundland*, Geological Association of Canada, Mineralogical Association of Canada, Joint Annual Meeting, St Johns 2001, Field Trip Guidebook B5.

Narbonne, G., Myrow, P., Landing, E. & Anderson, M. (1987), 'A Candidate Stratotype For The Precambrian Cambrian Boundary, Fortune Head, Burin Peninsula,

Southeastern Newfoundland', *Canadian Journal Of Earth Sciences* **24**(7), 1277–1293.

Naumova, S. N. & Pavlovsky, E. V. (1961), 'The discovery of plant remains (spores) in the torridonian shales of scotland', *Akad. Nauk SSSR Doklady* **141**, 181–182.

Noffke, N. (2009), 'The criteria for the biogeneicity of microbially induced sedimentary structures (miss) in archean and younger, sandy deposits', *Earth Science Reviews* **96**, 173–180.

Noffke, N. (2010), *Geobiology: Microbial Mats in Sandy Deposits from the Archean Era to Today*, 1st edn, Springer.

Noffke, N., Eriksson, K., Hazen, R. & Simpson, E. (2006), 'A new window into Early Archean life: Microbial mats in Earth's oldest siliciclastic tidal deposits (3.2 Ga Moodies Group, South Africa)', *Geology* **34**(4), 253–256.

Noffke, N., Gerdes, G., Klenke, T. & Krumbein, W. (2001), 'Microbially induced sedimentary structures - A new category within the classification of primary sedimentary structures', *Journal Of Sedimentary Research* **71**(5, Part a), 649–656.

Noffke, N., Hazen, R. & Nhleko, N. (2003), 'Earth's earliest microbial mats in a siliciclastic marine environment (2.9 Ga Mozaan Group, South Africa)', *Geology* **31**(8), 673–676.

Noffke, N. & Paterson, D. (2008), 'Microbial interactions with physical sediment dynamics, and their significance for the interpretation of Earth's biological history', *Geobiology* **6**(1), 1–4.

Oehler, J. & Logan, R. (1977), 'Microfossils, Cherts, And Associated Mineralization In Proterozoic Mcarthur (HYC) Lead-Zinc-Silver Deposit', *Economic Geology* **72**(8), 1393–1409.

Ojakangas, R. W. (1983), Tidal deposits in the early Proterozoic basin of the Lake Superior region—The Palms and Pokegama Formations: Evidence for subtidal shelf deposition of Superior-type banded iron formations., *in* L. G. Madaris Jr., ed., 'Early Proterozoic Geology of the Great Lakes Region', Vol. 160, pp. 49–66.

Orr, P. J., Briggs, D. E. G. & Kearns, S. L. (1998), 'Cambrian burgess shale animals replicated in clay minerals', *Science* **281**, 1173–1175.

Papineau, D. (2010), 'Global Biogeochemical Changes at Both Ends of the Proterozoic: Insights from Phosphorites', *Astrobiology* **10**(2), 165–181.

Papineau, D., Walker, J., Mojzsis, S. & Pace, N. (2005), 'Composition and structure of microbial communities from stromatolites of Hamelin Pool in Shark Bay, Western Australia', *Applied And Environmental Microbiology* **71**(8), 4822–4832.

Park, R. G., Stewart, A. D. & Wright, D. T. (2003), *The Hebridean terrane*, Geological Society of London, London, pp. 45–61.

Parnell, J., Boyce, A. J., Mark, D., Bowden, S. & Spinks, S. (2010), 'Early oxygenation of the terrestrial environment during the mesoproterozoic', *Nature* **468**(7321), 290–293.

Parnell, J., Mark, D., Fallick, A. E., Boyce, A. & Thackrey, S. (2011), 'The age of the Mesoproterozoic Stoer Group sedimentary and impact deposits, NW Scotland', *Journal of the Geological Society* **168**(2), 349–.

Passier, H., Middelburg, J., deLange, G. & Bottcher, M. (1997), 'Pyrite contents, microtextures, and sulfur isotopes in relation to formation of the youngest eastern Mediterranean sapropel', *Geology* **25**(6), 519–522.

Pasteris, J. & Wopenka, B. (2003), 'Necessary, but not sufficient: Raman identification of disordered carbon as a signature of ancient life', *Astrobiology* **3**(4), 727–738.

Peach, B. N., Horne, J., Gunn, W., Clough, C. T., Hinxman, L. W. & H., J. J. (1907), *The Geological Structure of the NW Highlands of Scotland*, Memoirs of the Geological Survey of Great Britain.

Pearson, D. L. (1984), Pollen/spore colour "standard", *in* 'Phillips Petroleum Company', Bartlesville, OK, p. 2.

Peat, C. J. & Diver, W. L. (1982), 'First signs of life on earth', *New Scientist* **95**, 776–781.

Peters, K. E., Walters, C. C. & Moldowan, J. M. (2005), *The Biomarker Guide: Biomarkers and Isotopes n the Environment and Human History*, Vol. 1, Cambrigde University Press.

Peterson, K., Lyons, J., Nowak, K., Takacs, C., Wargo, M. & McPeek, M. (2004), 'Estimating metazoan divergence times with a molecular clock', *Proceedings Of The National Academy Of Sciences Of The United States Of America* **101**(17), 6536–6541.

Planavsky, N., Rouxel, O., Bekker, A., Shapiro, R., Fralick, P. & Knudsen, A. (2009), 'Iron-oxidizing microbial ecosystems thrived in late paleoproterozoic redox-stratified oceans', *Earth and Planetary Science Letters* **286**, 230–242.

Playford, P. E. & Cockbain, A. E. (1976), Modern algal stromatolites at Hamelin Pool, a hypersaline barred basin in Shark Bay, Western Australia, *in* M. R. Walter, ed., 'Stromatolites', Elsevier, Amsterdam, pp. 389–411.

Plummer, P. & Gostin, V. (1981), 'Shrinkage Cracks - Desiccation Or Synaeresis', *Journal Of Sedimentary Petrology* **51**(4), 1147–1156.

Polat, A. & Kerrich, R. (1999), 'Formation of an Archean tectonic melange in the Schreiber-Hemlo greenstone belt, Superior Province, Canada: Implications for Archean subduction-accretion process', *Tectonics* **18**(5), 733–755.

Poulton, S., Fralick, P. & Canfield, D. (2004), 'The transition to a sulphidic ocean similar to 1.84 billion years ago', *Nature* **431**(7005), 173–177.

Prager, E. J. & Ginsburg, R. N. (1989), 'Carbonate nodule growth on floridas outer shelf and its implications for fossil interpretations', *Palaios* **4**, 310–317.

Prave, A. R. (2002), 'Life on land in the Proterozoic: Evidence from the Torridonian rocks of northwest Scotland', *Geology* **30**(9), 811–814.

Pufahl, P. & Grimm, K. (2003), 'Coated phosphate grains: Proxy for physical, chemical, and ecological changes in seawater', *Geology* **31**(9), 801–804.

Raff, E. C., Schollaert, K. L., Nelson, D. E., Donoghue, P. C. J., Thomas, C.-W., Turner, F. R., Stein, B. D., Dong, X., Bengtson, S., Huldtgren, T., Stampanoni, M., Chongyu, Y. & Raff, R. A. (2008), 'Embryo fossilization is a biological process mediated by microbial biofilms', *Proceedings Of The National Academy Of Sciences Of The United States Of America* **105**(49), 19360–19365.

Raff, E., Villinski, J., Turner, F., Donoghue, P. & Raff, R. (2006), 'Experimental taphonomy shows the feasibility of fossil embryos', *Proceedings Of The National Academy Of Sciences Of The United States Of America* **103**(15), 5846–5851.

Raven, J. A. & Edwards, D. (2001), 'Roots: evolutionary origins and biogeochemical significance', *Journal of Experimental Botany* **52**(Special Issue), 381–401.

Retallack, G. J. & Mindszenty, A. (1994), 'Well preserved late precambrian paleosols from northwest scotland', *Journal of Sedimentary Resarch* **64**(2a), 264–281.

Riding, R. (1975), 'Girvanella And Other Algae As Depth Indicators', *Lethaia* **8**(2), 173–179.

Rieu, R., Allen, P. A., Ploetze, M. & Pettke, T. (2007), 'Climatic cycles during a Neoproterozoic "snowball" glacial epoch', *Geology* **35**(4), 299–302.

Rodd, J. & Stewart, A. (1992), 'Geochemistry, Weathering And Diagenesis Of The Diabaig Formation (Torridon Group) In NW Scotland', *Scottish Journal Of Geology* **28**(Part 1), 27–35.

Rogers, J. K. & Keevers, R. E. (1976), Lady Annie-Lady Jane phosphate deposits, Georgina Basin, Queensland, *in* C. L. Knight, ed., 'Economic Geology of Australia and Papua New Guinea, 4. Industrial Minerals and Rocks', Monograph series 8. Australasian Institute of Mining and Metallurgy, Melbourne, pp. 251–261.

Runnegar, B. & Fedonkin, M. A. (1992), Proterozoic metazoan body fossils, *in* J. W. Schopf & C. Klein, eds, 'The Proterozoic Biosphere', Cambridge University Press, pp. 369–388.

Sagan, L. (1967), 'On the origin of mitosing cells', *Journal of Theoretical Biology* **14**, 225–274.

Samuelsson, J., Dawes, P. & Vidal, G. (1999), 'Organic-walled microfossils from the Proterozoic Thule Supergroup, Northwest Greenland', *Precambrian Research* **96**(1-2), 1–23.

Sansom, R. S., Gabbott, S. E. & Purnell, M. A. (2010), 'Non-random decay of characters causes bias in fossil interpretation', *Nature* **463**, 797–800.

Schelble, R. T., Westall, F. & Allen, C. C. (2004), '∼1.8 Ga iron-mineralised microbiota from the Gunflint Iron Formation, Ontario, Canada: implications for Mars', *Advances in Space Research* **33**, 1268–1273.

Schidlowski, M. (1988), 'A 3,800-Million-Year Isotopic Record Of Life From Carbon In Sedimentary-Rocks', *Nature* **333**(6171), 313–318.

Schieber, J. (2007), *Atlas of Microbial Mat Features Preserved Within the Siliciclastic Rock Record*, Elsevier.

Schiffbauer, J. D. & Xiao, S. (2009), 'Novel Application Of Focused Ion Beam Electron Microscopy (FIB-TEM) in Preparation And Analysis Of Microfossil Ultrastructures: A New View Of Complexity in early eukaryotic organisms', *Palaios* **24**(9-10), 616–626.

Schopf, J. (2006), 'Fossil evidence of Archaean life', *Philosophical Transactions Of The Royal Society B-Biological Sciences* **361**(1470), 869–885.

Schopf, J. W. (1968), 'Microflora of the bitter springs formation, late precambrian, central australia', *Journal of Paleontology* **42**(3), 651–688.

Schopf, J. W. (1993), 'Microfossils of the Early Archean Apex chert: new evidence of the antiquity of life', *Science* **260**(5108), 640–646.

Schopf, J. W. & Blacic, B. M. (1971), 'New microorganisms from the Bitter Springs Formation (Late Precambrian) of the north-central Amadeus Basin, central Australia', *Journal of Paleontology* **45**, 925–960.

Schopf, J. W. & Klein, C. (1992), *The Proterozoic biosphere: a multidisciplinary study*, Cambridge University Press.

Schopf, J. W., Kudryavtsev, A. B., Agresti, D. G., Wdowiak, T. J. & Czaja, A. D. (2002), 'Laser-Raman imagery of earth's earliest fossils', *Nature* **416**(6876), 73–76.

Schulze-Makuch, D. & Grinspoon, D. (2005), 'Biologically enhanced energy and carbon cycling on Titan?', *Astrobiology* **5**(4), 560–567.

Schweizer, M. K. (2008), Molecular taphonomy of major evolutionary lagerstätten: a critical appraisal of fossils from the Messel, Chengjiang, Rhynie and Doushantuo biotas, PhD thesis, University of Oxford.

Scotese, C. R. (2001), *Atlas of Earth History*, The PALEOMAP Project, Arlington, Texas.

Scott, C., Lyons, T. W., Bekker, A., Shen, Y., Poulton, S. W., Chu, X. & Anbar, A. D. (2008), 'Tracing the stepwise oxygenation of the Proterozoic ocean', *Nature* **452**(7186), 456–U5.

Seilacher, A., Grazhdankin, D. & Legouta, A. (2003), 'The dawn of animal life in the shadow of giant protists', *Paleontological Research* **7**, 43–54.

Sergeev, V. N. (2009), 'The distribution of microfossil assemblages in Proterozoic rocks', *Precambrian Research* **173**(1-4), 212–222.

Sergeev, V. N., Knoll, A. H. & Grotzinger, J. P. (1995), 'Paleobiology of the mesoproterozoic billyakh group, anabar uplift, northeastern siberia', *Paleontological Society Memoir* **39**, 1–37.

Shaffer, G. (1986), 'Phosphate Pumps And Shuttles In The Black-Sea', *Nature* **321**(6069), 515–517.

Sherlock, S. C., Jones, K. A. & Park, R. G. (2008), 'Grenville-age pseudotachylite in the Lewisian: laserprobe $^{40}Ar/^{39}Ar$ ages from the Gairloch region of Scotland (UK)', *Journal of Geological Society* **165**(1), 73–86.

Siever, R. (1992), 'The Silica Cycle In The Precambrian', *Geochimica Et Cosmochimica Acta* **56**(8), 3265–3272.

Simonson, B. M. (1985), 'Sedimentological constraints on the origins of Precambrian iron-formations', *Geological Society of America Bulletin* **96**, 244–252.

Skorokhod, A., Gamulin, V., Gundacker, D., Kavsan, V., Muller, I. & Muller, W. (1999), 'Origin of insulin receptor-like tyrosine kinases in marine sponges', *Biological Bulletin* **197**(2), 198–206.

Smith, S. & Hiscott, R. (1984), 'Latest Precambrian To Early Cambrian Basin Evolution, Fortune Bay, Newfoundland - Fault-Bounded Basin To Platform', *Canadian Journal Of Earth Sciences* **21**(12), 1379–1392.

Sommers, M. G., Awramik, S. M. & Woo, K. S. (2000), 'Evidence for initial calcite-aragonite composition of Lower Algal Chert Member ooids and stromatolites, Paleoproterozoic Gunflint Foromation, Ontario, Canada', *Canadian Journal of Earth Sciences* **37**, 1229–1243.

Soufiane, A. & Achab, A. (2000), 'Upper Ordovician and Lower Silurian chitinozoans from central Nevada and Arctic Canada', *Review Of Palaeobotany And Palynology* **113**(1-3), 165–187.

Staplin, F. L. (1982), Determination of thermal alteration index from color of exinite (pollen, spores), *in* F. L. Staplin, ed., 'How to Assess Maturation and Paleotemperatures', Vol. 7, SEPM Short Course, pp. 7–11.

Stewart, A. D. (1969), Torridonian rocks of scotland reviewed, *in* M. Kay, ed., 'North Atlantic-Geology and Continental Drift', Vol. 12, Memoir of the American Association of Petroleum Geologists, pp. 595–608.

Stewart, A. D. (2002), *The later Proterozoic Torridonian rocks of Scotland: their sedimentology, geochemistry and origin*, Geological Society Pub House.

Stewart, A. D. & Parker, A. (1979), 'Palaeosalinity and environmental interpretation of red beds from the late precambrian ('Torridonian') of scotland', *Sedimentary Geology* **22**(3-4), 229–241.

Strother, P. K., Battison, L., Brasier, M. D. & Wellman, C. D. (2011), 'Earth's earliest Non-Marine eukaryotes', *Nature* **473**, 505–509.

Summons, R., Jahnke, L., Hope, J. & Logan, G. (1999), '2α-Methylhopanoids as biomarkers for cyanobacterial oxygenic photosynthesis', *Nature* **400**(6744), 554–557.

Summons, R. & Walter, M. (1990), 'Molecular Fossils And Microfossils Of Prokaryotes And Protists From Proterozoic Sediments', *American Journal Of Science* **290A**, 212–244.

Tan, P. H., Dimovski, S. & Gogotsi, Y. (2004), 'Raman scattering of non-planar graphite: arched edges, polyhedral crystals, whiskers and cones', *Philosophical Transactions of the Royal Society of London, A.* **362**, 2289–2310.

Tappan, H. (1976), 'Possible Eukaryotic Algae (Bangiophycidae) Among Early Proterozoic Microfossils', *Geological Society Of America Bulletin* **87**(4), 633–639.

Teall, J. J. H. (1907), *The Petrography of the Torridonian Formation*, Memoirs of the Geological Survey of Great Britain, pp. 278–290.

Timofeyev, B., Choubert, G. & Fauremuret, A. (1980), 'Acritarchs Of The Precambrian In Mobile Zones', *Earth-Science Reviews* **16**(2-3), 249–255.

Tobin, K. J. (1990), 'The paleoecology and significance of the Gunflint-type microbial assemblages from the Frere Formation (Early Proterozoic), Nabberu Basin, Western Australia', *Precambrian Research* **47**, 71–81.

Tollo, R. P., Corriveau, L., McLelland, J. & Bartholomew, M. J. (2004), Proterozoic tectonic evolution of the Grenville orogen in North America: An introduction, *in* Tollo, RP and Corriveau, L and McLelland, J and Bartholomew, MJ, ed., 'Proterozoic Tectonic Evolution Of The Grenville Orogen In North America', Vol. 197 of *Geological Society of America Memoir*, pp. 1–18.

Tomitani, A., Knoll, A., Cavanaugh, C. & Ohno, T. (2006), 'The evolutionary diversification of cyanobacteria: Molecular-phylogenetic and paleontological perspectives', *Proceedings Of The National Academy Of Sciences Of The United States Of America* **103**(14), 5442–5447.

Torsvik, T. (2003), 'The Rodinia jigsaw puzzle', *Science* **300**(5624), 1379–1381.

Trent, J., Embaye, T., Buckwalter, P., Richardson, T.-M., Kagawa, H., Reinsch, S. & Martis, M. (2010), 'Offshore membrane enclosures for growing algae (omega): A system for biofuel production, wastewater treatment, and co2 sequestration', *NASA Technical Reports Server* pp. 1–4.

Turnbull, M., Whitehouse, M. J. & Moorbath, S. (1996), 'New isotopic age determinations for the Torridonian, NW Scotland', *Journal of the Geological Society* **153**(6), 955–964.

Tyler, S. A. & Barghoorn, E. S. (1963), 'Ambient pyrite grains in precambrian cherts', *Americal Journal of Science* **261**, 424–432.

Upfold, R. L. (1984), 'Tufted microbial (cyanobacterial) mats from the Proterozoic Stoer Group, Scotland', *Geological Magazine* **121**(04), 351–355.

Versteegh, G. J. M. & Blokker, P. (2004), 'Resistant macromolecules of extant and fossil microalgae', *Phycological Research* **52**(4), 325–339.

Visscher, P. T., Reid, R. P. & Bebout, B. M. (2000), 'Microscale observations of sulfate reduction: Correlation of microbial activity with lithified micritic laminae in modern marine stromatolites', *Geology* **28**(10), 919–922.

Volkman, J. (2003), 'Sterols in microorganisms', *Applied Microbiology And Biotechnology* **60**(5), 495–506.

Vorob'eva, N. G., Sergeev, V. N. & Knoll, A. H. (2009), 'Neoproterozoic microfossils from the margin of the East European Platform and the search for a biostratigraphic model of lower Ediacaran rocks', *Precambrian Research* **173**(1-4), 163–169.

Wacey, D., Kilburn, M. R., McLoughlin, N., Parnell, J., Stoakes, C. A., Grovenor, C. R. M. & Brasier, M. D. (2008), 'Use of NanoSIMS in the search for early life on Earth: ambient inclusion trails in a c.3400 Ma sandstone', *Journal of the Geological Society* **165**, 43–53.

Wacey, D., Kilburn, M. R., Saunders, M., Cliff, J. & Brasier, M. D. (2011), 'Microfossils of sulphur-metabolizing cells in 3.4-billion-year-old rocks of Western Australia', *Nature Geoscience* **4**(10), 698–702.

Walter, M. R. (1972), *Stromatolites and the biostratigraphy of the Australian Precambrian and Cambrian*, Vol. 11, Special Papers in Palaeontology.

We, K. M. T. (1996), 'Fossil preservation in the burgess shale', *Lethaia* **29**(1), 107–108.

Wells, A. T., Forman, D. J., Ranford, L. C. & Cook, P. (1970), 'Geology of the amadeus basin, central australia', *Australian Bureau of Mineral Resources, Bulletin* **100**, 222.

Westall, F., de Vries, S. T., Nijman, W., Rouchon, V., Orberger, B., Pearson, V., Watson, J., Verchovsky, A., Wright, I., Rouzaud, J.-N., Marchesini, D. & Severine, A. (2006), The 3.466 Ga "Kitty's Gap Chert" an early Archean microbial ecosystem, *in* Reimold, WU and Gibson, RL, ed., 'Processes On The Early Earth', number 405 *in* 'Geological Society of America Special Papers', pp. 105–131.

Williams, G. E., Gostin, V. A., McKirdy, D. A. & Preiss, W. V. (2008), 'The elatina glaciation, late Cryogenian (Marinoan Epoch), South Australia: Sedimentary facies and palaeoenvironments', *Precambrian Research* **163**(3-4), 307–331.

Williams, H. & King, A. F. (1979), 'Trepassey map area, Newfoundland', *Geological Survey of Canada Memoirs* **389**, 24.

Williams, H., O'Brien, S., King, A. & M.M., A. (1995), Geology of the appalachian-caledonian orogen in canada and greenland, avalon zone-newfoundland, *in* H. Williams, ed., 'Geology of North America', pp. 226–237.

Willman, S. & Cohen, P. A. (2011), Ultrastructural approaches to the microfossil record: Assessing biological affinities by use of transmission electron microscopy, *in* M. Laflamme, J. D. Schiffbauer & S. Q. Dornbos, eds, 'Quantifying the Evolution of Early Life', Vol. 36 of *Topics in Geobiology*, Springer Netherlands, pp. 301–320.

Wood, D., Dalrymple, R., Narbonne, G., Gehling, J. & Clapham, M. (2003), 'Paleoenvironmental analysis of the late Neoproterozoic Mistaken Point and Trepassey formations, southeastern Newfoundland', *Canadian Journal Of Earth Sciences* **40**(10), 1375–1391.

Xiao, S. & Knoll, A. (1999), 'Fossil preservation in the Neoproterozoic Doushantuo phosphorite Lagerstatte, South China', *Lethaia* **32**(3), 219–240.

Xiao, S. & Knoll, A. (2000), 'Phosphatized animal embryos from the Neoproterozoic Doushantuo Formation at Weng'An, Guizhou, South China', *Journal Of Paleontology* **74**(5), 767–788.

Xiao, S., Knoll, A., Yuan, X. & Pueschel, C. (2004), 'Phosphatized multicellular algae in the Neoproterozoic Doushantuo Formation, China, and the early evolution of florideophyte red algae', *American Journal Of Botany* **91**(2), 214–227.

Xiao, S. & Laflamme, M. (2009), 'On the eve of animal radiation: phylogeny, ecology and evolution of the Ediacara biota', *Trends In Ecology & Evolution* **24**(1), 31–40.

Xiao, S., Zhang, Y. & Knoll, A. H. (1998), 'Three-dimensional preservation of algae and animal embryos in a neoproterozoic phosphorite', *Nature* **391**(6667), 553–558.

Yueyan, L. (1986), Proterozoic and cambrian phosphorites - regional review: China, *in* P. J. Cook & J. H. Shergold, eds, 'Phosphate deposits of the world: Proterozoic and Cambrian phosphorites', Cambridge University Press, pp. 42–62.

Zhang, Y., Yin, L., Xiao, S. & Knoll, A. (1998), 'Permineralized fossils from the terminal Proterozoic Doushantuo Formation, south China', *Journal Of Paleontology* **72**(4, S), 1–52.

Zhang, Z. (1982), 'Upper Proterozoic microfossils from the Summer Isles, NW Scotland', *Palaeontology* **25**(3), 443–460.

Zhao, G., Cawood, P., Wilde, S. & Sun, M. (2002), 'Review of global 2.1-1.8 Ga orogens: implications for a pre-Rodinia supercontinent', *Earth-Science Reviews* **59**(1-4), 125–162.

Zhao, G., Sun, M., Wilde, S. & Li, S. (2004), 'A Paleo-Mesoproterozoic supercontinent: assembly, growth and breakup', *Earth-Science Reviews* **67**(1-2), 91–123.

Zukerkandl, E. & Pauling, L. B. (1962), Molecular disease, evolution, and genetic heterogeneity, *in* M. Kasha & B. Pullman, eds, 'Horizons in Biochemistry', Academic Press, New York, pp. 189–225.

Appendix A

Methods

A.1 Preparation

A.1.1 Ammonium molybdate

Samples of candidate material were tested qualiatively for presence of phosphate using an acidified vandate-molybdate solution, after the technique of Green (2001). An acidic molybdate solution is made up by dissolving 10 g ammonium molybdate ($(NH_4)_6MO_7O_24.4H_2O$ in 100ml of distilled water. A vandalomolybdate solution is made up by dissolving 0.3 g of ammonium metavanadate (NH_4VO_3) in 60 g of distilled water, and adding 40 ml of concentrated nitric acid (HNO_3), before being mixed with the ammonium molybdate.

A small amount of the sample to be tested is crushed, a small amount of acidic vanadate-molybdate solution is added, and the reaction observed. The presence of phosphate in the sample is indiccated by the formation of a yellow preciptate from the solution. No attempt was made at quantitative analysis by this method.

A.1.2 Thin Section

Rocks were mounted and sectioned for optical and electron microscopy by the standard method, at the Department of Earth Sciences, University of Oxford. Surfaces of interest were prepared to an appropriate size by cutting with diamond saw. If small, broken, or friable, rock samples were first embedded in epoxy resin. After smoothing, the sliver is mounted onto a glass slide and cut, ground and lapped down to a thickness of 30 μm, or in some cases 100 μm to preserve large fossils within the phosphate. Once the correct thickness, sections are polished to allow SEM imaging.

A.1.3 Acid Maceration

Palynological samples were prepared at the Department of Animal and Plant Sciences, University of Sheffield, using conventional acid maceration techniques. Following HCl-HF-HCl acid maceration, the residues were sieved using a 10μ mesh. They were then treated to a heavy liquid separation using zinc chloride, followed by further sieving at 10μ. The organic residues were mounting directly onto glass slides using epoxy resin.

A.1.4 FIB extraction of ultrathin TEM lamellae

Study samples were standard polished 30 μ-thick geological thin sections. Prior to FIB milling the thin sections were examined by optical microscopy and SEM in order to gain a preliminary understanding of the microfossil distributions and morphologies, and to select the most appropriate targets for detailed study. Of great importance in the field of palaeobiology is that FIB preparation of TEM sections allows features just below the surface of the thin sections to be targeted, thus eliminating the risk of surface contamination (for example during diamond polishing) producing artifacts. The preliminary SEM work was performed using a Zeiss Supra 1555 and the optical microscopy was performed using Nikon Optiophot-2 and Optiophot-pol microscopes. A dual-beam FIB system (FEI Helios NanoLab) at Adelaide Microscopy, The University of Adelaide was used to prepare the TEM lamellae from the polished thin sections. Regions of interest (ROI) were located and monitored within the dual-beam FIB using electron beam imaging. The top surface of each ROI was protected with a strip of platinum (Pt) that was somewhat larger than the required ROI (generally $\sim$25 μ long, $\sim$2 μm wide and $\sim$1 μm thick). The Pt was deposited within the instrument using a built-in gas injection source. Material on either side of the Pt strip was then removed by an energetic Gallium (Ga) ion beam operating at 30 KV with a beam current of $\sim$9 nA. This resulted in two stepped troughs either side of a wedge shaped sample. The sample then underwent a primary cleaning and thinning process. During this process the ion-beam-damaged material on the outer edges of the wedge (resulting from the initial high energy milling) was removed by applying sequentially smaller ion beam currents (e.g., 2.8 nA, 0.9 nA, 0.3 nA), and the sample thinned to ¡ 1μm. The resulting milled section (now $\sim$20 μm long, ¡1 μm wide, and $\sim$ 5 μm deep) was cut free along one side and along the bottom using a 0.3 nA beam at 52°

tilt angle leaving the section attached along one side only. An in-situ micromanipulator was then attached to the top of the section via a Pt connector strip. The one remaining side of the section was freed from the rock matrix, again using a 0.3 nA beam, and the micromanipulator was used to transfer the section to an Omniprobe copper TEM sample holder, where it was attached using two Pt connector strips. Once the micromanipulator was freed from the section, final thinning and cleaning could be performed on the section. Sections were thinned to ∼100 nm using beam currents of 0.3 nA, then 93pA operating alternately on each side of the section at 50° (top side) and 54° (bottom side) tilt angles. Redeposited dust, generated during processing, was removed from the surfaces of the final lamella by line scanning of the ion beam at low KV and low beam current. The Cu sample holder was removed form the dual-beam instrument and stored in a standard grid box until TEM analysis.

A.2 Imaging and Analysis

A.2.1 Optical Microscopy

Imaging of thin sections was carried out using Nikon Optiphot-Pol and Nikon Optiphot-2 compound microscopes with x4, x10, x20, x40 and x100(immersion) lenses, at the Department of Earth Sciences, University of Oxford.

Images were captured with Q-imaging USB camera, and processed with Synchroscopy imaging software (Acquis, Auto-Montage, and Montage Explorer). Post processing was carried out in Adobe Photoshop.

Photographs of hand samples and thin sections, as well as field photos, were captured with an Olympus μTough-8000 12 MP digital camera. Post processing carried out in Adobe Photoshop.

A.2.2 SEM-BSE, SE and EDX

SEM analysis was carried out at the Department of Earth Sciences, University of Oxford, on a JEOL JSM-840A SEM, with Oxford INstruments Isis 300 ED system. Quantitative ED analyses are performed by measurement against element oxide and well-characterised silicate standards, using proprietary software, and correcting by routine ZAF method.

BSE analysis carried out with Oxford Instruments Tetra detector, SE images captured with JEOL equipment.

A.2.3 Raman spectroscopy

Laser Raman analyses were carried out at the University of Bergen using a Horiba LabRAM HR800 integrated confocal Raman system and LabSpec5 acquisition and analysis software. Samples were standard uncovered geological thin sections allowing optical and chemical maps to be superimposed. The laser was focused c. 2 μm below the surface of the thin sections to avoid surface polishing effects. Since the thin sections were c. 30 μm thick there was no possibility of obtaining a signal from the mounting resin. All analyses were carried out using a 514.5 nm laser, 100 μm confocal hole, 1800 grating and x50 objective lens. For mineral identification from Raman spectra, dual acquisitions were taken from each analysis point, each with an acquisition time of 4 s. Raman maps were acquired with a 1.5 μm spatial resolution. Quartz maps were produced using the $\sim$ 465 cm^{-1} Raman quartz peak, carbon G maps using the $\sim$ 1600 cm^{-1} Raman carbon peak, carbon D maps using the $\sim$ 1350 cm^{-1} Raman carbon peak, and apatite maps using the $\sim$ 960 cm^{-1} Raman apatite peak.

A.2.4 TEM analysis of FIB-milled wafers

TEM data were obtained using a JEOL 2100 LaB6 TEM equipped with a Gatan Orius CCD camera and Tridiem energy filter operating at 200kV, and a JEOL 3000F FEGTEM equipped with a Gatan Imaging Filter, Oxford Instruments INCA EDS system and Bright Field and High-Angle Annular Dark Field (HAADF) STEM operating at 300kV. Both instruments were located in the Centre for Microscopy, Characterisation and Analysis (CMCA) at The University of Western Australia. Energy-filtered TEM elemental maps were obtained using the conventional three-window technique (Brydson, 2001), with energy windows selected to provide optimum signal-to-noise. Selected area electron diffraction (SAED) was performed using an aperture that selected a 200 nm diameter area of the sample.

A.2.5 FIB-SEM nano-tomography

Sequential FIB milling and SEM imaging was performed on the FEI Helios NanoLab dual-beam instrument at Adelaide Microscopy, and on a Zeiss Neon 40 dual-beam instrument at the Naval Postgraduate School, Monterey, California. Although two

different instruments were used, the protocol for achieving high quality images was very similar. The protocol for the Helios NanoLab instrument was as follows. Regions of interest (ROI) were located (from the preliminary Zeiss Supra 1555 SEM images) using electron beam imaging. A protective ∼1 μm-thick Pt layer was then deposited over the entire rectangular ROI and a trench was milled using a ∼9 nA ion beam at the leading edge of the ROI, much like in the initial stage of TEM foil preparation. This trench must be around 20 μm wider in the x direction than the ROI, and must have sufficient depth in both y and z directions so that clear images of the face of interest can be subsequently obtained using the electron beam. Two further narrow trenches (∼10 μm each side) were milled along the two sides of the ROI. These are required to collect the debris sputtered from the ROI by the ion beam milling process. The front and side faces of the ROI were then cleaned (with sequentially reduced ion beam currents), repositioned, refocused and imaged using the electron beam. Subsequent milling and imaging was fully automated and key parameters were optimized by trial and error. It was found that an electron beam of 800 V, ion beam current of 2.8 nA, step size of 200 nm per slice, and image capture time of ∼30 seconds per frame produced images of sufficient spatial resolution, minimized charging effects, and was not too time consuming. For example, milling and imaging a ROI of 35 μm x 20 μm x 10 μm at 200 nm step size (i.e., 100 sequential images) under these conditions took approximately six hours. Using the Zeiss Neon instrument, sample charging was less problematical so larger electron beam currents could be used for imaging, and smaller step sizes (75 nm and 150 nm) were used to obtain greater spatial resolution in the y direction.

A.2.6 3D volume rendering

FIB-SEM images contained 2048 x 1536 pixels with pixel sizes in the x and y directions varying between 18.5 nm and 47 nm dependent on the width of the ROI. The pixel size in z was dependent on the FIB-milling step size and varied from 75 nm to 200 nm. In preparation for further visual analysis, the reconstructed 3d image-stacks were post-processed (aligned and in some cases cropped) using FIJI v1.45j (Walter et al., 2010). Final volumetric datasets were generated by resampling the images stacks at 1:1 voxel / spatial resolution. Background noise was removed using an edge-preserving bilateral filter (spatial radius = 4.0, value range = 150), and intensity ranges were normalised to 0.0 ->1.0. The resulting files were exported and loaded into ParaView to generate the 3d volume renderings (Cedilnik et al., 2006). Two types of visualizations were

generated to provide a comparative view of the microstructures present in the FIB-slice-based volumetric reconstructions. The first type uses standard direct volume rendering to showcase the cellular structures present in a dataset using a 1d opacity transfer function. The second type modulates the scalar density values using the 1st-order and 2nd-order differentials of the volume, providing a better emphasis and isolation of curvature (Kindlmann and Durkin, 1998), and has been shown to be particularly beneficial for the investigation of cellular tissue (Sato et al., 2000). For all the visualizations, the transfer functions were specifically designed to isolate the dark carbonaceous particles and bands present in each of the FIB-slice images, and provide an unobstructed view of the denser regions of the slice material. To avoid confusion for color-deficient viewers, a diverging color-space was chosen to provide a perceptual linear, unbiased presentation of the density fields (Moreland, 2009).

Appendix B

Materials

Samples used in this study are listed here for easy reference. Some are referenced and figured in the main text and all were prepared explicitly for this study.

Samples are curated in the Department of Earth Sciences, University of Oxford, with the exception of Torridon Group samples TOR08/45, and T11/109, which belong to Professor Charles Wellman, and are housed at the Deparment of Animal and Plant Sciences, University of Sheffield.

Microscopic section samples:

Torridon Group: 74 sections, 25 coated for SEM-BSE and SEM-EDX analysis, 2 analysed by FIB-TEM and FIB-SEM, and 2 analysed by Laser Raman

Gunflint Formation: 19 sections, all coated for SEM-BSE and SEM-EDX analysis

Avalonian and Placentian successions: 27 section, 10 coated for SEM-BSE and SEM-EDX analysis

Microscopic samples from the Torridon Group and Sleat Group, northwest Scotland

Sample Number	Formation	Locality	Preparation, analysis
CAI-2a	Cailleach Head	Cailleach Head	Polished section
CAI-2b	Cailleach Head	Cailleach Head	Polished section, TEM sectioning
CAI-2c	Cailleach Head	Cailleach Head	Polished section, TEM sectioning
CAI-2d	Cailleach Head	Cailleach Head	Polished section
CAI-2e	Cailleach Head	Cailleach Head	Polished section
CAI-2f	Cailleach Head	Cailleach Head	Polished section, carbon coated
CAI-7a	Cailleach Head	Cailleach Head	Polished section, carbon coated
CAI-7b	Cailleach Head	Cailleach Head	Polished section
CAI-10a	Cailleach Head	Cailleach Head	Polished section
CAI-16a	Cailleach Head	Cailleach Head	Polished section, carbon coated
DIA-1a	Diabaig	Lower Diabaig	Polished section, carbon coated
DIA-2a	Diabaig	Lower Diabaig	Polished section
DIA-3a	Diabaig	Lower Diabaig	Polished section
DIA-4a	Diabaig	Lower Diabaig	Polished section, carbon coated
DIA-5a	Diabaig	Lower Diabaig	Polished section
DIA-6a	Diabaig	Lower Diabaig	Polished section, Laser Raman
DIA-7a	Diabaig	Lower Diabaig	Polished section
DIA-10a	Diabaig	Lower Diabaig	Polished section, carbon coated
DIA-13a	Diabaig	Lower Diabaig	Polished section
DIA-13b	Diabaig	Lower Diabaig	Polished section
DIA-13c	Diabaig	Lower Diabaig	Polished section
DIA-13d	Diabaig	Lower Diabaig	Polished section, carbon coated
DIA-13e	Diabaig	Lower Diabaig	Polished section, carbon coated
DB1-0.6a	Diabaig	Lower Diabaig	Polished section
DB1-0.65a	Diabaig	Lower Diabaig	Polished section
DB1-0.8a	Diabaig	Lower Diabaig	Polished section, carbon coated
DB1-4.95ppr	Diabaig	Lower Diabaig	Polished section, carbon coated
DB1-4.95ppa	Diabaig	Lower Diabaig	Polished section
DB1-4.95sha	Diabaig	Lower Diabaig	Polished section
DIA-CR-TS	Diabaig	Lower Diabaig	Polished section
DIA-CR-LS	Diabaig	Lower Diabaig	Polished section, carbon coated
BAD-4a	Diabaig	Badachro	Polished section
BAD-5per	Diabaig	Badachro	Polished section, carbon coated
BAD-5pa	Diabaig	Badachro	Polished section
FFA1-0.7	Diabaig	North Shieldaig (Fish Farm)	Polished section
FFA1-0.9a	Diabaig	North Shieldaig (Fish Farm)	Polished section
FFA1-0.9b	Diabaig	North Shieldaig (Fish Farm)	Polished section, Laser Raman
FFA1-1.45a	Diabaig	North Shieldaig (Fish Farm)	Polished section, carbon coated
FFA1-1.45b	Diabaig	North Shieldaig (Fish Farm)	Polished section
FFA1-2.5a	Diabaig	North Shieldaig (Fish Farm)	Polished section
FFA1-2.6a	Diabaig	North Shieldaig (Fish Farm)	Polished section
FFA1-2.6b	Diabaig	North Shieldaig (Fish Farm)	Polished section

SHI-6a	Diabaig	Sheildaig Peninsula	Polished section, carbon coated
FLA-1a	Diabaig	Fladday	Polished section
FLA-2a	Diabaig	Fladday	Polished section, carbon coated
FLA-3a	Diabaig	Fladday	Polished section
FLA-5a	Diabaig	Fladday	Polished section, carbon coated
FLA-5b	Diabaig	Fladday	Polished section
FLA-6a	Diabaig	Fladday	Polished section, carbon coated
FLA-7a	Diabaig	Fladday	Polished section
BRO-1	Diabaig	Brochel Castle	Polished section
BRO-4	Diabaig	Brochel Castle	Polished section, carbon coated
BRO-4pl	Diabaig	Brochel Castle	Polished section
BRO-4Pa	Diabaig	Brochel Castle	Polished section
BRO-4Pb	Diabaig	Brochel Castle	Polished section
SLE-2a	Kinloch	Kinloch	Polished section
SLE-3a	Kinloch	Kinloch	Polished section, carbon coated
SLE-3b	Kinloch	Kinloch	Polished section
SLE-4a	Kinloch	Kinloch	Polished section
SLE-4b	Kinloch	Kinloch	Polished section
SLE4c	Kinloch	Kinloch	Polished section
KIN01a	Kinloch	Kinloch	Polished section, carbon coated
KIN01b	Kinloch	Kinloch	Polished section
BRO01a	Diabaig	Brochel Castle	Polished section
BRO01b	Diabaig	Brochel Castle	Polished section
BRO02a	Diabaig	Brochel Castle	Polished section, carbon coated
BRO02b	Diabaig	Brochel Castle	Polished section
BRO02c	Diabaig	Brochel Castle	Polished section
BRO04a	Diabaig	Brochel Castle	Polished section
KOL01a	Kinloch	Kyle of Lochalsh	Polished section, carbon coated
KOL01b	Kinloch	Kyle of Lochalsh	Polished section, carbon coated
KOL02a	Kinloch	Kyle of Lochalsh	Polished section
KOL02b	Kinloch	Kyle of Lochalsh	Polished section
KOL03a	Kinloch	Kyle of Lochalsh	Polished section
KOL03b	Kinloch	Kyle of Lochalsh	Polished section
DB-lum	Diabaig	Lower Diabaig	Polished section
UD1-04	Diabaig	Upper Diabaig	Polished section
LD1-03	Diabaig	Lower Diabaig	Polished section, carbon coated
LD1-05	Diabaig	Lower Diabaig	Polished section
SHB-03	Diabaig	Sheildaig Bay	Polished section
CAI7mac	Cailleach Head	Cailleach Head	residues of phosphate maceration
DIA13mac	Diabaig	Lower Diabaig	residues of phosphate maceration
TOR08/45	Cailleach Head	Cailleach Head	residues of shale maceration
T11/109	Diabaig	Lower Diabaig	residues of shale maceration

Microscopic samples from the Gunflint Formation, Ontario, Canada

Sample Number	Formation	Locality	Preparation, analysis
CBL09	Lower Gunflint Member	Boulevard Lake	Polished section, carbon coated
CBL10	Lower Gunflint Member	Boulevard Lake	Polished section, carbon coated
CBL13a	Lower Gunflint Member	Boulevard Lake	Polished section, carbon coated
CBL13b	Lower Gunflint Member	Boulevard Lake	Polished section, carbon coated
CCP10	Lower Gunflint Member	Centennial Park	Polished section, carbon coated
SBS04	Lower Gunflint Member	Schrieber Beach	Polished section, carbon coated
FBY01	Upper gunflint Member	Frustration Bay	Polished section, carbon coated
FBY07	Upper gunflint Member	Frustration Bay	Polished section, carbon coated
FBY09a	Upper gunflint Member	Frustration Bay	Polished section, carbon coated
FBY09b	Upper gunflint Member	Frustration Bay	Polished section, carbon coated
FBY10	Upper gunflint Member	Frustration Bay	Polished section, carbon coated
KRC03	Lower Gunflint Member	Kakabeka Road Cut	Polished section, carbon coated
KRC08a	Lower Gunflint Member	Kakabeka Road Cut	Polished section, carbon coated
KRC08b	Lower Gunflint Member	Kakabeka Road Cut	Polished section, carbon coated
KSC08	Lower Gunflint Member	Kaministiquia River Western Shore	Polished section, carbon coated
KSC11	Lower Gunflint Member	Kaministiquia River Western Shore	Polished section, carbon coated
KCP03a	Lower Gunflint Member	Kakabeka Car Park	Polished section, carbon coated
KCP03b	Lower Gunflint Member	Kakabeka Car Park	Polished section, carbon coated
KCP03c	Lower Gunflint Member	Kakabeka Car Park	Polished section, carbon coated

Microscopic samples from the Avalonian and Placentian successions, southeastern Newfoundland

Sample Number	Formation	Locality	Preparation, analysis
FLH1a	Ferryland Head	Ferryland Head Formation	Polished section, carbon coated
FLH1b	Ferryland Head	Ferryland Head Formation	Polished section
FLH2a	Ferryland Head	Ferryland Head Formation	Polished section
FLH2b	Ferryland Head	Ferryland Head Formation	Polished section, carbon coated
SPB2a	Spaniards Bay South	Trepassey Formation	Polished section, carbon coated
SPB2b	Spaniards Bay South	Trepassey Formation	Polished section
LDC1a	Little Dantzic Cove	Random Formation	Polished section, carbon coated
LDC1b	Little Dantzic Cove	Random Formation	Polished section
LOC1a	Long Cove	Fosters Point Limestone	Polished section, carbon coated
LOC1b	Long Cove	Fosters Point Limestone	Polished section
LOC1c	Long Cove	Fosters Point Limestone	Polished section
SIL1a	Silos Cove	Fermeuse Formation	Polished section, carbon coated
SIL1b	Silos Cove	Fermeuse Formation	Polished section
SIL2a	Silos Cove	Fermeuse Formation	Polished section, carbon coated
SIL2b	Silos Cove	Fermeuse Formation	Polished section
SIL3a	Silos Cove	Fermeuse Formation	Polished section
SIL3b	Silos Cove	Fermeuse Formation	Polished section
FHR1a	Fortune Head River	Brigus Formation	Polished section
STM1a	St Mary's	Gaskiers Formation	Polished section, carbon coated
GBH1a	Grand Bank Head	Chapel Island Formation	Polished section, carbon coated
GBH4a	Grand Bank Head	Chapel Island Formation	Polished section
LCA1a	Little Catalina	Trepassey Formation	Polished section
LCA1b	Little Catalina	Trepassey Formation	Polished section
MEL1a	Melrose	Trepassey Formation	Polished section, carbon coated
MEL1b	Melrose	Trepassey Formation	Polished section
MEL2a	Melrose	Trepassey Formation	Polished section
MEL2b	Melrose	Trepassey Formation	Polished section

Macroscopic samples from the Diabaig Formation, Torridon Group, northwest Scotland

Sample	Locality	Type of Mat	Relief
SHM01	Sheildaig Peninsula	Loose network and stellar nodes	Negative
SHM02	Sheildaig Peninsula	Elephant skin	Negative
SHM03	Sheildaig Peninsula	Elephant skin	Negative
SHM04	Sheildaig Peninsula	Loose network and stellar nodes	Positive
SHM05	Sheildaig Peninsula	Cracks/polygonal network	Negative
SHM06	Sheildaig Peninsula	Stellar nodes and filaments	Positive
SHM07	Sheildaig Peninsula	Network	Positive
SHM08	Sheildaig Peninsula	Elephant skin	Negative
SHM09	Sheildaig Peninsula	Swirling ridges/Arumberia	Positive
SHM10	Sheildaig Peninsula	Network and stellar nodes	Positive
SHM11	Sheildaig Peninsula	Pustules/protrusions	Positive
SHM12	Sheildaig Peninsula	Nodes and stellar nodes	Positive
SHM13	Sheildaig Peninsula	Elephant skin	Negative
SHM14	Sheildaig Peninsula		
SHM15	Sheildaig Peninsula	Irregularpitted	Negative
SHM16	Sheildaig Peninsula	Elephant skin	Negative
SHM17	Sheildaig Peninsula	Protrusions and miroreticulate network	Positive
SHM18	Sheildaig Peninsula	Elephant skin	Negative
SHM19	Sheildaig Peninsula	Microreticulate network	Positive
SHM20	Sheildaig Peninsula	Cracks/polgonal network	Negative
SHM21	Sheildaig Peninsula		
SHM22	Sheildaig Peninsula	Protrsions and network	Positive
SHM23	Sheildaig Peninsula	Curved ridges/Arumberia	Positive
DBM01	Lower Diabaig	Microreticulate network and ridges	Positive
DBM02	Lower Diabaig	Broad ridges	Positive
DBM03	Lower Diabaig	Stellar nodes	Postive
DBM04	Lower Diabaig	Nodes and microreticulate network	Positive
DBM05	Lower Diabaig	Network	Positive
DBM06	Lower Diabaig	Network and stellar nodes	Positive
DBM07	Lower Diabaig	Microreticulate network	Positive
DBM08	Lower Diabaig	Network	Positive
DBM09	Lower Diabaig	Irregular pustulate?	Positive
DBM10	Lower Diabaig	Ridges/arumberia	Positive
DBM11	Lower Diabaig	Network	Positive
DBM12	Lower Diabaig	Network	Positive
DBM13	Lower Diabaig	Loose network	Positive
DBM14	Lower Diabaig	Pustular, and micropitting	Positive and negative
DBM15	Lower Diabaig	Network	Positive
DBM16	Lower Diabaig	Network	Positive
DBM17	Lower Diabaig	Grooves	Negative
DBM18	Lower Diabaig	Ridges/arumberia, and network	Positive
DBM19	Lower Diabaig	Microreticualte network?	Positive

DRM20	Lower Diabaig	Network	Positive
DRM21	Lower Diabaig	Irregular pustulae and grooves	Positive and negative
DRM22	Lower Diabaig	Fine pustulae and parallel grooves	Negative
DRM23	Lower Diabaig	Elephant skin	Negative
DRM24 bottom	Lower Diabaig	Elephant skin/polygonal network	Negative
DRM24 top	Lower Diabaig	Phosphatic pustulae/microreticulate network	Positive
DRM25	Lower Diabaig	Microreticulate network	Positive
DRM26	Lower Diabaig	Phosphatic pustulae	Positive
DRM27	Lower Diabaig	Elephant skin	Negative
DRM28	Lower Diabaig	Network	Negative
DRM29	Lower Diabaig	Network	Positve
DRM30	Lower Diabaig	Network	Positive
DRM31	Lower Diabaig	Network and stellar nodes	Positive
DRM32	Lower Diabaig	Micropitting?	Negative
DRM33	Lower Diabaig	Network/stellar nodes	Positive
FFM01	Fish Farm	Irregular pustulae	Positive
FFM02	Fish Farm	Elephant skin	Neagtive
FFM03	Fish Farm	Ladders	Positive
FFM04	Fish Farm	Elephant Skin	Negative
FFM05	Fish Farm	Network	Positive
FFM06	Fish Farm	Elephant Skin	Negative
FFM07	Fish Farm	Network	Negative
FFM08	Fish Farm	Elephant Skin/Network	Negative
FFM09	Fish Farm	Ladders	Negative
DRM01	Upper Diabaig	Elephant Skin	Negative
DRM02	Upper Diabaig	Network	Positive
DRM03 bottom	Upper Diabaig	Trails	Negative
DRM03 top	Upper Diabaig	Microreticulate network	Positive
DRM04	Upper Diabaig	Network	Positive
DRM05	Upper Diabaig	Sparse ridges	Positive
DRM06	Upper Diabaig	Elongated network	Positive
DRM07	Upper Diabaig	Sparse ridges	Positive
DRM08	Upper Diabaig	Sparse ridges/elongated network	Positive
DRM09	Upper Diabaig	Elongated network/Ladders	Positive
DRM10	Upper Diabaig	Pustulae/sparse grooves	Positive and negative
DRM11	Upper Diabaig	Loose network/stellar nodes	Positve
DRM12	Upper Diabaig	Microreticulate network	Positive
DRM13	Upper Diabaig	Broad ridges	Positive
BRM41	Brochel Castle	Microreticulate network	Positive
BRM42	Brochel Castle	Ridges/Arumberia	Positive
BRM43	Brochel Castle	Ridges/Arumberia	Positive
BRM44	Brochel Castle	Ridges/Arumberia	Positive
BRM45	Brochel Castle	Network/Ladder	Positive

BRM46	Brochel Castle	Ladder	Positive
BRM47	Brochel Castle	Ladder	Positive
BRM48	Brochel Castle	Ladder/Network	Positive
BRM49	Brochel Castle	Ladder	Positive
BRM50	Brochel Castle	Network/Ladder	Positive
BRM51	Brochel Castle	Ladder	Positive
BRM52	Brochel Castle	Ladder	Positive
BRM53	Brochel Castle	Ladder	Positive
BRM54	Brochel Castle	Network	Positive
BRM55	Brochel Castle	Microreticulate network/stellar nodes?	Positive
BRM56	Brochel Castle	Network	Positive
BRM57	Brochel Castle	Elephant skin	Negative
BRM58	Brochel Castle	Broad ridges/arumberia	Positive
BDM01	Badachro	Grooves and stellar nodes	Negative and positive
BDM02	Badachro	Irregular pitting	Negatice
BDM03 bottom	Badachro	Trails	Negative
BDM03 top	Badachro	Trails, ridges	Negative and positive
BDM04	Badachro	Irregular pustulae/ridges	Positive
BDM05	Badachro	Creases	Positive
BDM06	Badachro	Microreticulate network/ridges?	Positive
BDM07	Badachro	Irregular fine pustulate	Positive
BDM08	Badachro	Irregular pustulate	Positive
BDM09	Badachro	Microreticulate network	Positive
BDM10	Badachro	Trails and micropitting	Negative
BDM11	Badachro	Ridges and Irregular pustulae	Positive
BDM12	Badachro	Creases	Positive
BDM13	Badachro	Creases	Positive
BDM14	Badachro	Micropitting/Microprotrusions	negative and positive
BDM15	Badachro	Microreticulate network	Positive
BDM16	Badachro	Creases	Positive
BDM17	Badachro	?Ridges	Positive
BDM18	Badachro	Creases	pOsitive
BDM19	Badachro	Creases/ridges	Positive
BDM20	Badachro	Rough ridges/arumberia	Positive
BDM21	Badachro	Rough grooves/arumberia	Negative
BDM22	Badachro	Ridges/arumberia	Positive
BDM23	Badachro	Microreticulate network	Positive
BDM24	Badachro	Irregular pustulae	Positive
BDM25	Badachro	Patches of pustulae	Positive
BDM26	Badachro	Ridges/arumberia	Positive
BDM27	Badachro	Grooves/arumberia	Negative
BDM28	Badachro	Grooves/arumberia	Negative
BDM29	Badachro	Aligned creases	Positive
BDM30	Badachro	Aligned grooves	Negative

BDM31	Badachro	Creases	Positive
BDM32	Badachro	Irregular pustulae	Positive
BDM33	Badachro	Regular pustulae	Positive
BAL-R01	Balgay River	Network	Positive
BAL-R02	Balgay River	Network	Positive
BAL-R03 bottom	Balgay River	Elephant skin	Negative
BAL-R03 top	Balgay River	Network	Positive
BAL-R04	Balgay River	Network	Positive
BAL-S01	Balgay Shore	Ridges	Positive
BAL-S01	Balgay Shore	Elephant skin	Negative
BRO-07	Brochel	Network	Positive
LD1-01	Lower Diabaig	Rounded protrusions	Positive
LD1-02	Lower Diabaig	Rounded protrusions	Positive
LD1-03	Lower Diabaig	Open Network	Positive
LD1-04	Lower Diabaig	Tight Network	Positive
LD1-05	Lower Diabaig	Network	Positive
LD1-06	Lower Diabaig	Aligned short grooves	Negative
SHB-01	Sheildaig Bay	Short ridges	Positive
SHB-02	Sheildaig Bay	Tight network	Positive
SHB-03	Sheildaig Bay	Tight netowrk	Positive
UDI-01	Upper Diabaig	Trails/Irregular grooves	Negatice
UDI-02	Upper Diabaig	Network	Positive
UDI-03	Upper Diabaig	Network	Positive
UDI-04	Upper Diabaig	Network	Positive

Appendix C

Publications

Full copies of published papers can be found on included flash drive, or by following the QR code below.



Remarkably preserved prokaryote and eukaryote microfossils within 1 Ga-old lake phosphates of the Torridon Group, NW Scotland. Battison, L. and Brasier, M. D., 2012. *Precambrian Research*, 196, 204-217.

Abstract: The 1000 Ma Torridon Group of northwest Scotland are here shown to contain a rich diversity of organic walled microfossils preserved in exceptional detail within sedimentary phosphate. The phosphatic nodules and bands in which they occur are autochthonous, as are the organic fossils they contain. The associated sedimentology of this phosphate is shown to be consistent with a lacustrine setting. Informal taxonomic treatment of the microfossils allows statistical assessment of the relative abundances of different morphotypes across a range of lacustrine environments. Exceptional preservation of pristine organic-walled eukaryotes and prokaryotes, together with a taphonomic spectrum in both physicochemical and biological degradational conditions allows a picture to be built of the earliest lacustrine ecological communities.

Diverse microbially induced sedimentary structures from 1 Ga lakes of the Diabaig Formation, Torridon Group, northwest Scotland. Callow, R. H. T., **Battison, L.** and Brasier, M. D., 2011. *Sedimentary Geology*, 239, 117-128.

Abstract: The siliciclastic lacustrine rocks of the similar to 1000 Ma Diabaig Formation, northwest Scotland, contain a remarkable diversity of macroscopic structures on bedding planes that can be compared with various kinds of microbially induced sedimentary structures (MISS). Field sedimentological investigations, combined with laboratory analysis of bedding planes and petrographic study of thin sections have allowed us to characterise a range of depositional environments and document the spectrum of biological structures. MISS are reported from frequently subaerial environments, through commonly submerged facies, and down to permanently sub-wavebase settings. Palaeoenvironmental conditions (water depth, exposure, hydrodynamic energy) control the distribution of MISS within these facies. This demonstrates that mat-forming microbial communities were arguably well adapted to low light levels or periodic exposure. Some MISS from the Diataig Formation are typical of Precambrian microbial mats, including reticulate fabrics and 'old elephant skin' textures. In addition to these, a number of new and unusual fabrics of putative microbial origin are described, including linear arrays of ridges and grooves (cf. 'Arumberia') and discoidal structures that are comparable with younger Ediacaran fossils such as Beltanelliformis. These observations indicate that benthic microbial ecosystems were thriving in freshwater lake systems similar to 1000 Ma, and indicate how microbially induced sedimentary structures may be applied as facies indicators for Proterozoic lacustrine environments. The discovery of structures closely resembling Ediacaran fossils (cf. Beltanelliformis) also serves to highlight the difficulty of interpreting simple discoidal bedding plane structures as metazoan fossils.

Niche Habitats for Extra-Terrestrial Life: The Potential for Astrobiology on the Moons of Saturn and Jupiter. Battison, L., 2011. *Journal of Cosmology*, 13, 3790-3799.

Abstract: Astrobiology today has a strong anticipatory focus, and efforts are concentrated on determining the factors behind the potential presence, type, and distribution of life in our solar system and beyond. The critical requirements for life: a liquid solvent, and electron acceptors and donors for metabolism, guide the search, and is a central concept to the location and extent of circumstellar habitable zones. For our own solar system, however, the search can be widened beyond this narrow band of earth-like conditions, and our increasing knowledge of the capabilities of life,

as well as higher resolution imaging and analysis of solar system bodies, warrants the application of a more expansive habitable niche approach. The Saturnian and Jovian satellite systems are ideal for the application of this concept, and are here used to demonstrate how a collection of system characteristics may be used to assess the potential for individual bodies to harbour life. Europa, Callisto, and Ganymede in the Jovian system, and Enceladus, Titan, Hyperion, Iapetus, and Hyperion in the Saturnian system all possess characters that could make them conducive to the origin or maintenance of life upon or within them. The possibility of some of these bodies containing extraterrestrial life is reflected in future explorative missions.

Earth's earliest non-marine eukaryotes. Strother, P. K., **Battison, L.**, Brasier, M. D., and Wellman, C. H. 2011. *Sedimentary Geology*, 239, 117-128.

Abstract: The existence of a terrestrial Precambrian (more than 542 Myr ago) biota has been largely inferred from indirect chemical and geological evidence associated with palaeosols(1,2), the weathering of clay minerals(3) and microbially induced sedimentary structures in siliciclastic sediments(4). Direct evidence of fossils within rocks of nonmarine origin in the Precambrian is exceedingly rare(5,6). The most widely cited example comprises a single report of morphologically simple mineralized tubes and spheres interpreted as cyanobacteria, obtained from 1,200-Myr-old palaeokarst in Arizona(5). Organic-walled microfossils were first described from the non-marine Torridonian (1.2-1.0 Gyr ago) sequence of northwest Scotland in 1907(7). Subsequent studies(8-10) found few distinctive taxa-a century later, the Torridonian microflora is still being characterized as primarily nondescript"leiospheres"(11). We have comprehensively sampled grey shales and phosphatic nodules throughout the Torridonian sequence. Here we report the recovery of large populations of diverse organic-walled microfossils extracted by acid maceration, complemented by studies using thin sections of phosphatic nodules that yield exceptionally detailed three-dimensional preservation. These assemblages contain multicellular structures, complex-walled cysts, asymmetric organic structures, and dorsiventral, compressed organic thalli, some approaching one millimetre in diameter. They offer direct evidence of eukaryotes living in freshwater aquatic and subaerially exposed habitats during the Proterozoic era. The apparent dominance of eukaryotes in non-marine settings by 1 Gyr ago indicates that eukaryotic evolution on land may have commenced far earlier than previously thought.

Appendix D

Atlas of Proterozoic Microfossils

To compliment the description of a novel assemblage of organic-walled microfossils from the Proterozoic of northwest Scotland, in this study, a more through review of Proterozoic taxonomy has been carried out.

Despite the field of Proterozoic palaeontology being enriched with deposits, described particularly in the last 50 years, a thorough synthesis of reported morphotypes and taxa has yet to be done. This complicates the field unnecessarily for young researchers, as much literature is available only from copyright, or international libraries, and often in foreign languages. It is the authors intention to compile currently known taxa, synonomies, and known spatial and temporal ranges for all described Proterozoic organic-walled microfossils, into an interactive searchable database available to researchers. The full scale of this task is beyond the scope of this current study, but a preliminary atlas of over 500 taxa has bee compiled, and is here presented in digital form.

Each atlas entry lists taxon name, synonomies, monograph authors and references, as well as genus and species diagnoses, and time and place where first recorded. Where images are available from the original monograph, they have been included.

The systematic palaeontology presented at the end of Chapter 3 was completed with the aid of this atlas, demonstrating its immediate utility in the description of new deposits. It is hoped that future pursuit of rare and distributed manuscripts will enrich this atlas and make it a valuable resource in the future study of Precambrian palaeontology.

The atlas may be found on the included flash drive, or by following the QR code below.

